Theses and Dissertations--Electrical and Computer Engineering

Electrical and Computer Engineering

2016

INCORPORATING MACHINE VISION IN PRECISION DAIRY FARMING TECHNOLOGIES

Anthony N. Shelley
University of Kentucky, anshel2@uky.edu
Digital Object Identifier: http://dx.doi.org/10.13023/ETD.2016.147

STUDENT AGREEMENT:

I represent that my thesis or dissertation and abstract are my original work. Proper attribution has been given to all outside sources. I understand that I am solely responsible for obtaining any needed copyright permissions. I have obtained needed written permission statement(s) from the owner(s) of each third-party copyrighted matter to be included in my work, allowing electronic distribution (if such use is not permitted by the fair use doctrine) which will be submitted to UKnowledge as Additional File.

I hereby grant to The University of Kentucky and its agents the irrevocable, non-exclusive, and royalty-free license to archive and make accessible my work in whole or in part in all forms of media, now or hereafter known. I agree that the document mentioned above may be made available immediately for worldwide access unless an embargo applies.

I retain all other ownership rights to the copyright of my work. I also retain the right to use in future works (such as articles or books) all or part of my work. I understand that I am free to register the copyright to my work.

REVIEW, APPROVAL AND ACCEPTANCE

The document mentioned above has been reviewed and accepted by the student's advisor, on behalf of the advisory committee, and by the Director of Graduate Studies (DGS), on behalf of the program; we verify that this is the final, approved version of the student's thesis including all changes required by the advisory committee. The undersigned agree to abide by the statements above.

<div align="right">

Anthony N. Shelley, Student

Dr. Daniel Lau, Major Professor

Dr. Caicheng Lu, Director of Graduate Studies

</div>

INCORPORATING MACHINE VISION IN PRECISION DAIRY FARMING
TECHNOLOGIES

DISSERTATION

A dissertation submitted in partial fulfillment of the
requirements for the degree of Doctor of Philosophy in the
College of Engineering
at the University of Kentucky

By

Anthony Neal Shelley

Lexington, Kentucky

Director: Dr. Daniel Lau, Professor of Electrical Engineering

Lexington, Kentucky

2016

ABSTRACT OF DISSERTATION

INCORPORATING MACHINE VISION IN PRECISION DAIRY FARMING
TECHNOLOGIES

The inclusion of precision dairy farming technologies in dairy operations is an area of increasing research and industry direction. Machine vision based systems are suitable for the dairy environment as they do not inhibit workflow, are capable of continuous operation, and can be fully automated. The research of this dissertation developed and tested 3 machine vision based precision dairy farming technologies tailored to the latest generation of RGB+D cameras. The first system focused on testing various imaging approaches for the potential use of machine vision for automated dairy cow feed intake monitoring. The second system focused on monitoring the gradual change in body condition score (BCS) for 116 cows over a nearly 7 month period. Several proposed automated BCS systems have been previously developed by researchers, but none have monitored the gradual change in BCS for a duration of this magnitude. These gradual changes infer a great deal of beneficial and immediate information on the health condition of every individual cow being monitored. The third system focused on automated dairy cow feature detection using Haar cascade classifiers to detect anatomical features. These features included the tailhead, hips, and rear regions of the cow body. The features chosen were done so in order to aid machine vision applications in determining if and where a cow is present in an image or video frame. Once the cow has been detected, it must then be automatically identified in order to keep the system fully automated, which was also studied in a machine vision based approach in this research as a complimentary aspect to incorporate along with cow detection. Such systems have the potential to catch poor health conditions developing early on, aid in balancing the diet of the individual cow, and help farm management to better facilitate resources, monetary and otherwise, in an appropriate and efficient manner. Several different applications of this research are also discussed along with future directions for research, including the potential for additional automated precision dairy farming technologies, integrating many of these technologies into a unified system, and the use of alternative, potentially more robust machine vision cameras.

Anthony Shelley_____
Student's Signature

4-26-16_____
Date

INCORPORATING MACHINE VISION IN PRECISION DAIRY FARMING
TECHNOLOGIES

By

Anthony Neal Shelley

Dr. Daniel Lau_____
  Director of Dissertation

Dr. Caicheng Lu_____
  Director of Graduate Studies

4-26-16_____

TABLE OF CONTENTS

LIST OF TABLES

LIST OF FIGURES

viii

CHAPTER I: INTRODUCTION

Many attempts at making whole or partial farming operations fully automated have been conducted in recent years to promote production quantity, efficiency, and quality, in both plant and animal resources. In the arena of livestock, dairy and beef cattle have been significantly examined relative to other livestock. Part of this pursuit includes technologies that can make it possible to monitor specific biometrical data of individual dairy cow. The research of this dissertation was conducted solely utilizing machine vision based approaches in order to address specific biometric monitoring needs of precision dairy farming.

1.1 Dairy Industry Overview

The structure of dairy farming in the United States is ever changing. For the most part, the number of dairy cattle in the United States has been fairly constant over the past century while the amount of milk production expected of the individual cow continues to increase. According to the USDA, the number of milk cow operations continues to decline in the United States. There were 65,000 milk cow operations in 2009 compared to 97,460 in 2001, a decline of 33 percent. Despite the large decrease in milk cow operations during this time period, both milk production and milk cow numbers have been on the rise. Milk production increased 15 percent, from 165,332 million pounds in 2001 to 189,320 million pounds in 2009. Milk cow inventory showed a smaller increase of 1 percent, from 9.10 million head in 2001 to 9.20 million head in 2009 [1]. From the USDA, we can see that in 2015 there were approximately 9.315 million head of dairy cattle producing 208.5 billion pounds of milk, or averaging 22,383 pounds of milk per cow. [2] Most notable to this research is the fact that while the number of dairy cattle

remains near constant and the number of dairy operations decreases, the average dairy operation size has continued to increase as well as the annual milk production per cow. This means that more milk production is being expected and realized from a near constant dairy cattle population. This also means that the number of smaller operations is continuing to decrease as larger operations increase.

Large commercial farms have several advantages over small farms, including access to skilled labor, market knowledge, technical knowledge, finance and capital, risk management, access to markets, and product traceability and quality assurance.[3] According to Winsten[4] the major concerns that smaller scale producers have include the profit level and financial progress of their dairy as well as their anxiety and stress levels associated with operating the dairy. In their study, mean milk production per cow on large, modern confinement farms was 21% greater than on traditional dairy farms and 45% greater than on management-intensive grazing farms. The large, modern confinement farms were more likely to be using production technologies and services.[4] According to Tauer[5] many believe that small dairy farms cannot survive because costs of production per cwt (or per 100 pounds) of milk are thought to be higher than the cost of production per cwt of milk on larger farms. In their study of New York dairy farms, it was determined that efficient small dairy farms can be competitive with larger dairy farms in producing milk at comparable costs per unit. The frontier cost of production for a 50-cow farm was $13.61 per cwt, which was only slightly over 4% more than costs for a 500-cow farm which saw frontier cost of production at $13.03 per cwt. In a study by Hadley et al.[6] which observed the managerial and financial implications of dairy farm expansions in Michigan and Wisconsin, it was noted that as herd size increased, labor

efficiency improved because of labor saving technology adoption, specialization, and economies of size. Most expansion experienced a significant improvement in labor and management expense per cwt. Those who did not improve labor expense either failed to adopt technology to improve labor efficiency or faced an extremely competitive labor environment.[6] Research by Bewley et al.[7] observing an overview of experiences of Wisconsin dairy farmers who modernized their operations indicates that producers who modernized their operations had positive feelings about their expansion experiences, accompanied by increased production and improved profitability and quality of life. As herd size increased, milk production, labor efficiency, and satisfaction with herd performance, profitability, and quality of life increased.[7]

Facilities improvements have been able to aid in increasing dairy efficiency, but the major factor in dairy production is still the individual animal. Although genetics is a major reason for increased milk production of individual cow, proper individual cow management is also critical to enable the modern high-producing cow to meet her production potential.[8] Individual cow monitoring is hard enough for small operations where labor intensive visual inspections are done, but being able to monitor operations on a cow by cow basis is practically impossible with larger operations which tend to range in size from 500 to 2,000 cows and increasing.[1] In the past, dairy producers have relied upon experience and personal judgment to address individual animal needs. These skill sets are valuable to the industry as the management decisions ultimately rely upon the end judgments of these seasoned experts, but such skills are limited in their ability to accurately diagnose, treat, or even notice issues as they arise. Often, by the time the producer is able to accurately identify that there is a health or production issue with an

3

individual animal, it is too late to effectively remedy the situation as most of these cues are based upon what the producer sees. Many times, the issue begins as an internal physiological process, which cannot be seen readily by the human eye. The use of technology in the dairy industry can aid in detecting and intervening sooner in such cases.

1.2 Precision Dairy Farming Overview

The use of individual animal biometric monitoring technologies in dairy operations falls into a category known as *precision dairy farming*. Precision dairy farming is the use of technologies to measure physiological, behavioral, and production indicators on individual animals to improve management strategies and farm performance.[10] Current examples of precision dairy farming include processes such as daily milk yield monitoring and daily body weight monitoring. Other processes such as monitoring feeding behavior or feed intake, respiration and heart rates, and automated BCS scoring are fairly new applications to the industry. The main objectives of precision dairy farming are maximizing individual animal potential, detecting disease earlier, and minimizing the use of medication through preventive health measures.[10]

As previously stated, the number of dairy cattle remains near constant while the demand for milk derived products continues to increase. This has caused producers to selectively breed out those cattle that do not viably produce enough milk while continuing to breed higher yield cattle. This is the only way to meet the demands of production and to make the most profit possible on what resources are available.[11,12,13,14,15] Precision dairy farming practices realize this need and are so formatted to continue to aid in increasing the per cow yield while minimizing the added stress to the animal. Monitoring the cow during pregnancy enables the producer to be

able to act if a problem arises due to pregnancy complications. Using precision dairy farming aids in producing the healthiest calf possible so that it is able to grow faster and stronger than previous generations. Making the most out of offspring is the best way to ensure the continuing progresses in the dairy industry, especially as milk product demands continue to increase globally. The better head start the next generation of dairy cattle can achieve, the better off the industry as a whole will be.

The loss of individual heads of cattle due to stress or disease is of serious concern to the producer as each individual is worth a few thousand dollars alone, not considering the loss of milk yield per day that the cow is sick or deceased.[16,17,18,19,20] Being able to detect the onset of a sickness is essential to maintaining not just the health of the individual but of the entire herd as well. In the worst case scenario, an entire herd can be lost due to illness if not contained or remedied in time. With the aid of precision dairy farming, the ability to detect the early onset of any symptoms in the individual or the herd can aid in preventing sickness, death, or loss in daily yield. For smaller producers the threat is even more so than for larger producers as the percentage of income is higher on a per head basis. Precision dairy farming practices realize this and are aimed at not just helping large scale commercial operations but family owned, smaller operations, too.

If any precision dairy farming technology used is to be truly viable, it must be cost effective for any size operation.[21,22] The ability to have a veterinarian on hand can become costly and time consuming for any size operation, but more so for the smaller operator. So, the necessity of automated systems that can aid in detecting some of the symptoms of an onset of a problem without the immediate need of a veterinarian is met by many of the proposed applications of precision dairy farming.[23,24,25,26]

The easiest way to lose money besides having a sick cow is having one that cannot be milked because of medication concerns.[18,27,28] Sometimes, the cow may not be allowed to be milked due to the medication in its system. Other times, the cow may even be over-dosing or under-dosing on medications which can impede its return to a healthy state. Precision dairy farming addresses these issues by again monitoring for the onset of sickness, but also monitoring during the recovery period.[29,30] A veterinarian cannot practically watch over every cow individually whereas an automated system can. The day by day health can be monitored to determine if the medication or health recovery process being used is working, if the dosage or other therapy needs to be increased or decreased, and finally can give an accurate reading to the producer as to when the cow is healthy enough to resume full production capabilities.

The use of precision dairy farming technologies is not limited to ill cows. In fact, the majority of available technologies on the market are aimed at primarily monitoring healthy cow. The purpose of these technologies is to provide data to the producer, veterinarians, researchers, and other interested parties which can guide the dairy operation in better understanding individual dairy cow behavior which in turn leads to maximized individual animal production.[31,32,33,34] Examples of easily adjusted cow comfort include lying comfort, ambient temperature control, and water and feed access. Comfortable cows are able to devote more of their resources towards milk production instead of working just to maintain their health. Precision dairy farming allows for the detection of the early onset of stressors or previously unnoticed stressors which affect cow performance. Often, only simple adjustments need be made to alleviate or remove

these stressors, such as providing better access to comfortable bedding, cooling fans, or water and feed.

1.3 Machine Vision Based Precision Dairy Farming

The majority of precision dairy farming technologies provide tactile equipment which must be attached to the cow in some manner in order to monitor their specified metric. The major pitfall to these technologies is that such tactile placement of equipment can lead to broken or lost components. If these components cannot monitor their respective metric because they have lost contact with the cow, then they have lost their benefit of use. In the research of this dissertation, we propose various machine vision based precision dairy farming systems which remove this mandatory tactile data acquisition method. Machine vision is the use of imaging-based approaches for automatic inspection and analysis applications.[35,36,37] The benefits of using machine vision include the fact that such systems do not inhibit normal workflow, can be fully automated, and the camera's contact with potentially damaging effects can be minimized by placing the system at a distance from the scene or object of interest and within a ruggedized enclosure.

There are many methods of machine vision which require image processing of the image data acquired by the system. These image processing methods include registration, filtering, thresholding, segmentation, edge detection, pattern recognition, object detection, and object recognition. For each of these image processing methods, there are also numerous, specialized sub-methods that can be utilized. The systems of this dissertation research each aim to address a specific precision dairy farming need. In doing so, each system combines different image processing methods in order to obtain

the desired output solely based upon the input imaging data. The specific image processing methods utilized are outlined in their respective chapters addressing each machine vision system developed.

Automated systems, such as those developed in this research, are an ideal solution to the problem of individual animal biometrics monitoring. Such systems can handle any size herd and have the capability to monitor metrics on a daily, per milking, or other time scale basis as needed. With increased metrics monitoring of individual dairy cow, the health of each cow can be monitored to adjust for matters such as feed intake, monitor for health concerns and pregnancy, and better manage quality facility production. These technologies are not meant to replace the human component but to merely aid in decision making and provide a supplementary tool in resolving issues as they arise as well as a consultation tool to make better, more informed choices.

1.4 Range Imaging Cameras

There exist several options when it comes to deciding upon a camera to use for a machine vision application and each has its own unique set of qualifications that make it best suited for the job. In our research, the main consideration must be the environment in which the camera must work first and foremost. Because this system can potentially be exposed to the natural elements for an indefinite amount of time, it must be able to withstand the changes in temperature throughout the year, withstand possible light water exposure, operate at a distance from the scene which can range from a single meter up to 5 meters, and maintain real-time data rates at potentially large distances of over 40 meters.

The second vital consideration for our choice of machine vision camera depends upon what we are trying to observe. In each of our systems, the main goal was to monitor either a change in shape or identify a specific shape. There are several camera technologies which are used for observing shape, the majority of which rely upon range imaging data. Range imaging is used to describe 2D cameras which use sensor technology in order to determine the distance to points in the camera scene respective to each pixel of the 2D camera array, thereby creating a pseudo-3D, or also referred to as a 2.5D, depth mapping of the camera scene. Example range imaging cameras include time-of-flight, stereovision, and structured light. These different sensors utilize either passive or active lighting architecture. In passive systems, the lighting of the scene is from ambient light. In active systems, the lighting of the scene is controlled by the system itself. Ambient light may remain in the scene with an active system, but it is not the dominant source of scene illumination.

The third most important consideration in camera choice must be the cost. In order for such a precision dairy farming system to be adopted, it must be economically viable for the dairy operation. A system which incorporates a camera that cost significantly less than an equal alternative will have a much higher chance of being utilized. Therefore, this research only considered budget conscious options which could still afford proficient range imaging data acquisition and resolution. Pixel resolution was an important factor as well since our systems would have to operate at a distance from the scene. The camera's sensitivity to changing ambient light was also a factor since the system would be expected to work in areas where lighting may be inconsistent due to the

9

dynamic nature of the camera scene. In order for our system to run at real-time data rates, the frame rate of the camera must be at least 30fps.

The rapid development of range imaging devices for the home computer gaming console industry has provided several sensor devices which can be engineered into machine vision applications. The Microsoft™ Kinect™ is a prominent example of such a device, which incorporates the use of RGB+D. The RGB aspect provides the scene color information while the depth (D) provides the range sensing information of the same scene for 2.5D scene reconstruction. RGB+D makes the removal of background clutter that we are not interested in easy because the depth channel can act as a green screen. Because such gaming console sensors are mass produced, the cost of the sensor is rather inexpensive at a range of $100 to $200 per unit where a traditional machine vision sensor may range from $300 to $1,200 or up to $5,000 for a smart camera.

In terms of how these range imaging sensors operate, there are several methods available with each device having its own unique method of operation. Besides the RGB+D setup already discussed, there also exists active and passive stereovision, structured light illumination, and time-of-flight systems. Each range imaging method is designed to address a set of unique circumstances depending upon the operating environment of the system. The aim is to select the range imaging method that best meets the needs and goals of the machine vision application being studied and optimizes the accuracy and precision of the results.

Stereovision

Passive stereovision systems are relatively cheap, can be stationary, and can collect image data in a short period of time. In our case, we refer more directly to it as

passive computer stereovision. Passive stereovision works much like the human visual process, but with two cameras. It takes a vantage of a scene from two differing perspectives or angles and then creates a 3D image based upon the disparities of objects in the two images due to depth information differences. Any distortions in the field of view must be removed, such as barrel distortion. The images collected by both cameras must also be reflected back to a common plane for comparison in a process known as image rectification. The displacement, or disparity, of features in the images is measured to create a disparity map, which gives rise to the 3D nature of this imaging technique. While an excellent tool in 3D imaging, it does have some small error in not always being able to find the corresponding points for all points between images. The limitation of accuracy using passive stereovision is minimal, but must always be considered as several small errors can lead to inaccurate data or results.

Structured Light Illumination (SLI)

The resolution and accuracy of stereovision systems can be improved upon by reducing the stereometric system to just one camera and a projector in a system architecture known as structured light illumination (**SLI**). By using an active stereovision SLI system instead of a passive two camera stereovision setup, the costs are further decreased, image data collection timing is faster, and resolution and accuracy of the scan are improved. SLI systems work on the basis of projecting a light pattern, typically a set of stripes or a constellation of points, across the scene being observed in order to create depth and surface information from the deformation of the known projected pattern. The accuracy of SLI systems comes from their ability to resolve the pixel correspondence matching problem that other systems encounter and they allow for

error detection and correction. SLI systems are also more precise because they can capture the entire field of view at once instead of one point at a time.

The PrimeSense™ Carmine 1.08 RGB+Depth sensor (PrimeSense™, Tel Aviv, Israel) is an example of a single pattern SLI range imaging device. This camera is the same as is used in the Microsoft™ Kinect™ (Microsoft Corporation, Redmond, Washington). This device works on the principle of structured light illumination by projecting a pseudo-random dot pattern from a near-infrared (**NIR**) laser illuminator that codes the scene. The distorted light pattern then returns to a NIR CMOS image sensor that uses various algorithms to triangulate the coded light from the scene in the system in order to extract the 3D depth data. The position of these constellations within the camera's field of view determines how far the target surface is from the sensor. A second CMOS image sensor is included in the system that obtains the visible light, or RGB color, information of the scene.

The disparity-depth model utilized by the PrimeSense™ Carmine 1.08 for range imaging derives the depth value of an object as shown in Equation 1.1, where Z_r is the distance of the reference plane from the baseline, f is the focal length of the NIR camera, b is the triangulation base length separation between the NIR emitter and the NIR camera, and d is the observed disparity in the image space between the reference plane and the object plane.[38]

$$Z_0 = \frac{Z_r}{(1 + \frac{Z_r}{fb}d)} = \frac{1}{(\frac{1}{Z_r} + \frac{d}{fb})} \tag{1.1}$$

The Intel® RealSense™ R200 (Intel Corporation, Santa Clara, California) is an example of a multiple pattern SLI range imaging device that also incorporates dual

camera stereovision in its system architecture. The active lighting architecture utilizes multiple light patterns projected from a NIR laser projector to code the scene and 2 NIR cameras for depth data collection. Because the NIR cameras are located on either side of the NIR laser projector, the system can also be viewed in a stereoscopic sense as the depth data is computed from the disparity between the 2 NIR cameras using triangulation. A third camera is included in the system that obtains the visible light, or RGB color, information of the scene.

Time-of-Flight (TOF)

Time-of-flight (**TOF**) range imaging sensors work on the principle of determining the amount of time it takes for an emitted light pulse to bounce off of the scene and return to the sensor. Because the speed of light is a constant, the time elapsed for this process allows for every independent pixel to be able to sense the distance between the pixel and the reflected object surface in the scene. TOF systems utilize an active lighting system architecture constructed with a laser range finder or a flash-like light source in order to detect the distance to a point. TOF systems are limited by the number of data points that they can capture at a given time and their relatively limited field of view. Therefore, TOF systems can lead to accuracy errors. TOF sensors have traditionally been much more expensive than comparable range imaging devices, but since the research of this study began, the cost associated with manufacturing newer TOF devices has markedly dropped while the imaging components behind TOF range imaging have improved in performance.

The latest range sensor developed by Microsoft™ is their Kinect™ V2. The Microsoft™ Kinect™ V2 sensor provides more imaging data streams to work with and a

greater pixel resolution and image size for image frames. The single best feature update with this sensor is the use of a TOF sensor for depth data instead of a SLI based system architecture. This TOF system utilizes the principle of continuous modulation defined in Equation 1.2.[39,40]

$$c(\tau) = r \otimes s = \lim_{T \to \infty} \int_{-T/2}^{T/2} r(s) \times s(t + \tau) dt \qquad (1.2)$$

The pixels of the NIR camera are able to directly correlate the incident light signal *r(t)* with the reference signal *s(t)*. τ in Equation 1.2 is a phase offset used to sample the correlation function at different positions. The depth distance returned by the TOF signal can be calculated using Equation 1.3 where ϕ is the phase offset of the returned signal due to the round-trip time of the light and λ_m is the modulated wavelength.

$$d = \frac{\lambda_m}{4\pi} \phi \qquad (1.3)$$

The Microsoft™ Kinect™ V2 acquires three samples of the correlation function *c(τ)* for use in deriving the phase offset ϕ which Microsoft™ claims in their patent reduces the effects of varying temperature, ambient lighting, the influence of an imperfect modulation signal, and the variation of the components of the device over time.[41]

A tabulated comparison of the different features available with these 3 different range imaging camera technologies currently available on the market can be seen in Table 1.1. With the research systems presented in this dissertation, all of the range imaging data collection was conducted with the same PrimeSense™ Carmine 1.08 device. The PrimeSense™ Carmine 1.08 has been openly available on the market since 2010, which is also the same year that this dissertation research and the search for a range

imaging device began. The Micorsoft® Kinect™ V2 has only become available to software developers and consumers since 2014. The Intel® RealSense™ R200 has only been available to software developers and consumers since 2015. Because these other devices have only been recently developed for consumers, they were not accessible at the time of initial data collection. Therefore, future precision dairy farming research studies incorporating machine vision are strongly encouraged to utilize the Microsoft™ Kinect™ V2 and the Intel® RealSense™ R200 devices.

Table 1.1 – Comparison table of various range imaging devices[1]

	PrimeSense™ Carmine 1.08	Kinect™ V2	Intel® RealSense™ R200
Color image resolution	640 x 480 pixels	1,920 x 1,080 pixels	1,920 x 1,080 pixels
Color image FOV	~62 x 49 degrees (~10 x 10 pixels/degree)	~84 x 54 degrees (~22 x 20 pixels/degree)	~70 x 43 degrees (~27 x 25 pixels/degree)
Depth image resolution	320 x 240 pixels	512 x 424 pixels	480 x 360 pixels
Depth image FOV	~57 x 43 degrees (~5 x 5 pixels/degree)	~70 x 60 degrees (~7 x 7 pixels/degree)	~59 x 46 degrees (~8 x 8 pixels/degree)
USB Standard	2.0	3.0	3.0
Supported OS	Windows 7 or later	Windows 8 or later	Windows 8.1 or later
Range Imaging System	SLI – Single pattern	TOF	SLI – Multiple patterns

[1]*All values are shown with horizontal direction/dimension first and then the vertical direction/dimension.*

1.5 Dissertation Outline

The goal of this dissertation is to pioneer the application of 3D video sensors to precision dairy farming for fully autonomous biometric monitoring of animals. To do this, we will demonstrate the use of inexpensive RGB+D cameras to perform the tasks of (1) monitoring feed intake in terms of volume instead of mass; (2) reporting each animal's body condition score over a period of nearly seven months, taking measurements twice daily; (3) anatomical labeling of the animal in terms of tailhead and

hips when viewed from above; and (4) identifying each animal based on its body markings. The main reason that these topics were chosen was because they are all interrelated.

Feed intake is directly responsible for the body condition of the cow, just as the body condition is a reflection on the amount of feed intake. The use of animal detection and recognition are necessary if a machine vision system is to be designed to determine if and where a cow is present in the image frame as well as determining who the cow is. This is important because the accuracy of precision dairy farming requires the monitoring of individual animal metrics. In this manner, animal detection and recognition can be further incorporated into either a feed intake or body condition monitoring system in order for the system to be able to run completely autonomously and automatically in storing accurate metric data for every individual. In the course of our research, each topic was researched independently so that no one topic could directly influence the outcomes of another.

Unlike other approaches to monitoring individual dairy cow welfare, we postulate that the use of machine vision in precision dairy farming systems has the capability to increase metric measurement accuracy and reduce dairy personnel workload. As well, such systems are capable of working efficiently and effectively in an autonomous manner, will not inhibit workflow, and can boost dairy farm profits by minimizing daily operational costs and increasing individual animal performance. In the research of this dissertation, we address the incorporation of machine vision based technology in three methods of precision dairy farming practices. In this manner, the research conducted will be able to demonstrate not only the applicability of machine vision, but also its

adaptability and complexity with which it can address diverse problems while utilizing the same instrumental components.

In Chapter 2, we address the potential for the application of machine vision in individual dairy cow feed intake monitoring. The system developed for this research tested various imaging approaches for the potential use of machine vision in automated dairy cow feed intake monitoring. The incorporation of such a system in a dairy operation has the ability to provide detailed and timely insight into the health condition of each individual dairy cow in a herd based upon changes in feed consumption as well as possibly financially benefiting the dairy operation by reducing the amount of feed wasted. Though the feed tested by the system was done so in a controlled manner and with a small sample size, it provides a great deal of insight into the use of such a system in future work concerning the monitoring of dairy cow feed consumption in open feed bunks and controlled individual feeders alike.

In Chapter 3, we address the potential for the application of machine vision in monitoring the gradual change in dairy cow BCS over time. The system developed in this study monitored 116 individual dairy cow over a period of nearly 7 months in order to monitor the gradual changes in BCS. Several proposed automated BCS algorithms and systems have been previously developed by researchers, but none have monitored the change in BCS with such an automated system for a duration of this magnitude. By monitoring the change in BCS over this timeframe, we are able to test the ability of an automated BCS system to capture the gradual changes in body condition on a per cow basis. These gradual changes in BCS, whether higher or lower, infer a great deal of beneficial and immediate information on the health condition of every individual cow

being monitored. Such information has the potential to catch poor health conditions developing early on, aid in balancing the diet of the individual cow, and help farm management to better facilitate resources, monetary and otherwise, in an appropriate and efficient manner.

In Chapter 4, we address the potential for the application of machine vision in the automation of dairy cow detection and identification. Two approaches were tested independently in this study. The first approach was to use Haar cascade classifiers designed to detect distinct anatomical features of dairy cow in a feature detection based approach. These features include the tailhead region, hips region, and rear region of the cow body. The features chosen are done so in order to aid machine vision applications in determining if and where a cow is present in an image or video frame. Such an automation in dairy cow presence detection is critical in allowing precision dairy farming machine vision based applications to be left to operate capably and automatically on their own with no user input for an indefinite and uninterrupted period of operational time. The second approach was to use an optical flow based system in order to determine the identification of the individual cow in the imaging frame of the system. All precision dairy farming systems must be able to maintain accurate information for each individual in the herd. This requires a robust method of identification in order to determine which cow is present in the working area of the metric monitoring system. By deriving an imaging based approach for cow detection and recognition, we are able to verify the presence and identification of the cow returned by other methods, such as RFID, which may already be incorporated in the dairy operation.

Finally, in Chapter 5, we summarize the contributions of this dissertation research and provide an outlook for the continued proliferation of machine vision in precision dairy farming technologies. Several different applications of this research are also discussed along with future directions for research. Integrating many of these technologies together into a unified system will be a major advancement that will greatly benefit both the technology being used and the dairy operation utilizing it. Also, integrating existing precision dairy farming technologies with those proposed in this study will help to ensure that the systems proposed are not seen as being conflictive in nature, but instead as cohesive advancements that greatly improve the reliability and performance of such autonomously operating systems.

In order for us to develop and test our systems, a sample dairy had to be chosen which would accurately represent a typical small to mid-size dairy operation in the United States. The University of Kentucky Coldstream Dairy Research Farm is located about 8 miles north of the main University of Kentucky campus. This dairy operation was the base for testing and validating each of the machine vision based precision dairy farming systems developed. The University of Kentucky Coldstream Dairy Research Farm was originally constructed in the 1960's and has been continually updated and used as a research facility.

Among the various components of the complex are a free stall barn with 108 stalls for the milking herd; a tie-stall barn with 36 stalls, used primarily for cows in research trials that require individual feeding; a small free stall barn with 18 stalls and Calan™ (American Calan, Inc., Northwood, New Hampshire) individual feeders, used primarily for nutrition research; a milking parlor that holds eight cows (essentially 2 "double 2"

parlors); replacement heifer, dry cow, and maternity facilities; and a management building that includes an office, teaching facilities, and laboratory space. The animals located at the farm that were used in this study consist of a dairy cow herd of approximately 100 Holsteins at a given time. The average annual milk yield production is approximately 24,000 lbs. for the Holsteins.[9] The farm can be seen in Figure 1.1 with the offices in the building on the left side of the image, the milking and walkway areas in the middle building of the image, and the individual feeding stalls located in the arched barn seen at the right side of the image.

Figure 1.1 – *3D mapped image of the University of Kentucky Coldstream Dairy Research Farm showing (red dot) environmentally controlled office, (blue dot) milking parlor and walkway, and (green dot) individual feed stalls.*

All of the cows exit the milking parlor by proceeding through the same walkway. The walkway is enclosed with a concrete slab floor, concrete block walls, and a roof. This enclosed walkway was chosen for our cow image data collection needs in order to keep the cameras and other equipment free from the natural elements, away from the influence of changing sunlight exposure in the image, and to have the best control environment. The feed used in testing the feed intake system also originated from this

facility, though it was tested off site in a laboratory space back on the University of Kentucky campus. Once the precision dairy farming topics were chosen, the herd for observation selected, and the site selected for data collection, the research was then able to move forward to determining which camera technology and machine vision processes would work best in developing plausible, suitable, efficient, and economically viable systems for individual animal welfare monitoring.

To summarize, machine vision based approaches have the potential to be utilized in monitoring several performance metrics of the individual dairy cow. The use of machine vision is already well established in maximizing the efficiency and profits of several businesses in the manufacturing industry, so there is no reason not to reap those same benefits in the dairy industry. The major benefit that machine vision based technologies have over the majority of current precision dairy farming technologies is that they are non-tactile systems which have a much lower risk of being broken or otherwise damaged by the cow as it is placed out of reach and in a sturdy, secure location. The results of the different research studies conducted herein greatly expand the knowledge of the use of machine vision based applications within the realm of precision dairy farming. Incorporation of these precision dairy systems into existing dairy facilities has the potential to increase individual animal management and welfare, the production capacity and capabilities of each individual animal, the profitability and efficiency of the individual dairy, and the well-being of the individual dairy producer and laborer.

CHAPTER II: POTENTIAL FOR AUTOMATED MONITORING OF DAIRY COW FEED INTAKE

Feed is the greatest expense for milk production [42] while feed intake is a major determinant of energy intake and consequently of milk production [43]. According to Bernard and Montgomery, lactating dairy cows must consume large quantities of dry matter to provide the nutrients needed to maintain high levels of milk production. The consequences of low DMI are lower peak milk yields, lower total milk production, excessive loss of body weight, and poor reproductive performance. Research shows a 0.91 kg increase in milk production for each 0.45 kg increase in DMI, and as milk production continues to increase, management of DMI becomes more critical.[44]

Monitoring dairy cow feed intake can simply utilize human visual inspection, such as the research conducted by Bach et al.[45], but the difficulty in manually collecting data at the time of feeding limits the extent of this type of monitoring [46]. Several nutrition models have also been developed to attempt to predict feed intake, but even the best models have only been able to account for no more than 70% of the variation in intake [47] and all of the models under-predict actual observed DMI [48].

An automated feed monitoring system has the potential to electronically monitor individual cow feed intake. Radio frequency identification (**RFID**) is the typical means used in automated identifications of individual cow for the purpose of monitoring individual cow behavior, such as monitoring their feed intake. An RFID transponder located on the cow, typically in an ear tag or collar, interacts with an RFID reader located at the feeding area for traceability of an individual animal. Example RFID based systems include GrowSafe™ (GrowSafe Systems, Ltd., Airdrie, Canada) and Calan™ gates..

Most of the previous work with RFID systems are more interested in monitoring feeding behavior than feed intake.[49,50,51,52,53]

Research conducted by A. Bach et al.[45] used weighing scales to monitor both feeding behavior and feed intake. This research required that the system automatically detect cow presence at the feed bunk and then monitored the amount of feed consumed at each presence detection. The system did have occasions where the system computer failed to recognize the presence of cow, and therefore any feed consumed during that time was not recorded. This study also reaffirmed the inability of human observers to keep track of feed intake as there were at least 96 occasions where the human observers did not detect cow presence at the feed bunk but the computer did.[45]

The Insentec™ (Insentec™, Marknesse, the Netherlands) monitoring system allows for loose-housed cows to freely access a number of feeding and drinking stations; which also allows researchers to collect continuous feeding and drinking behavioral data. The basis of this system is an RFID identification coupled with an automated barrier between the cow and the feed and water. The Insentec™ monitoring system performed well in the study by Chapinal et al.[51], but it still interfered with the natural feeding behaviors of the cow as a physical barrier was placed between the cow and the feed. The fact that the number of cows that can feed at any time is reduced by such individual feed intake monitoring systems also plays a role in feed intake. It has been suggested that lower feed intake by cows, utilizing such systems may be due to the fact that the visual stimulation associated with food is removed, and the lack of competition that exists with individual feeding compared to group feeding.[54]

None of these systems analyze the feed intake on a dry matter basis, which is where most of the nutritional value comes from the feed. These systems instead work on an as-fed basis where the average noisture content of the feed is approximately half of the volume of the feed. Another concern with using such systems is that they were built to fit local conditions, namely being suitable for closed, free, or tied stall barns. The system utilized needs to be able to be exposed to harsh, uncontrolled, and changing environmental conditions and must perform reliably under the variable daily working conditions of a dairy. The ideal system measures, controls, and monitors individual feed intake of the free-housed dairy cow while not interfering with feeding habits and not introducing additional work or inhibiting workflow on the farm.[55]

The basis of the feed intake monitoring research conducted in this dissertation relies upon the ability to determine the volumetric mass density of a TMR simply by determining how much mass of the TMR can be contained within a known volumetric container; in this research, measured as kg/m^3. Since TMR are not solid but instead contain air pockets due to the particulate nature of the TMR, bulk density is the preferred volumetric basis. Given the implied link between feed volume and matter density as they relate to mass, an initial test was performed to determine how moisture content of feed changed over time and what effect this change might have on weight. An example of this testing conducted by Shelley[56] can be seen in Figure 2.1 where a dry matter and moisture content analysis was conducted on samples of the feed delivered to the dairy cows from each day of feeding over the course of 20 days. The Koster testing method [57, 58] was utilized by the farm management in order to determine the dry matter and

moisture content percentages of the feed samples. As can be seen, the moisture content remained fairly constant over the duration of the samples tested.

Date Sampled	Dry Matter (%)	% Moisture Content	Date Tested
1/7/2013	49	51	1/11/2013
1/8/2013	51.5	48.5	1/11/2013
1/9/2013	50	50	1/11/2013
1/10/2013	49.5	50.5	1/11/2013
1/11/2013	51	49	1/14/2013
1/12/2013	55	45	1/14/2013
1/13/2013	49	51	1/14/2013
1/14/2013	51	49	1/17/2013
1/15/2013	50	50	1/17/2013
1/16/2013	49.5	50.5	1/17/2013
1/17/2013	51	49	1/23/2013
1/18/2013	50	50	1/23/2013
1/19/2013	48	52	1/23/2013
1/20/2013	53	47	1/23/2013
1/21/2013	52	48	1/23/2013
1/22/2013	53	47	1/23/2013
1/23/2013	54	46	1/28/2013
1/24/2013	48	52	1/28/2013
1/25/2013	49	51	1/28/2013
1/26/2013	48.5	51.5	1/28/2013

Figure 2.1 – Feed samples tested for moisture content.[56]

The moisture content was also tested on orts samples to see how the moisture content changed between the time of feed offering and feed removal. It was determined that since the moisture content of the feed offered to the cow changed by less than 1% over a 24-h period, it had a negligible effect on the feed's weight and was, therefore, not monitored in this study. Typical TMR feedings situations do not incur large changes in temperature or pressure, nor does the TMR undergo major changes in air or water content, and therefore the relative density of the TMR remains near unity between the times of TMR offering and orts disposal. Since the physical properties and moisture

content of a TMR change negligibly over a 24 h period, using the volumetric shape of the TMR can be utilized in directly determining the weight of the feed. For these same reasons, a single TMR was tested with each experimental setup. The dry matter content of the TMR used in the first experimental setup is shown in the second column of Table 2.1, and the dry matter content of the TMR used in the second and third experimental setups is shown in the third column of Table 2.1. By knowing any two of the three variables of density, volume, and mass, the third can be directly calculated.

Table 2.1 - Ingredient and dry matter content of the TMR tested in the experimental setups[1]

Composition	TMR 1	TMR 2
	(% of DM)	
Corn silage	44.6	34.3
Alfalfa silage	25.6	12.7
Cottonseed whole	2.8	5.8
Alfalfa hay	2.8	4.9
Grain mix	24.2	42.3

[1]*TMR 1 was tested in the first experimental setup. TMR 2 was tested in the second and third experimental setups.*

The objective of this study was to assess the proof of concept usefulness of an inexpensive 3D video camera for measuring individual dairy cow feed intake by scanning and recording feed volume, from which we indirectly derive feed weight. For the system to be deemed successful at measuring feed intake in terms of weight, it must perform well regardless of how the feed lays in the bin. For instance, if after feeding, the bulk of feed lines the bin on one side only, then the camera system must handle this equally as well as other cases for this same weight of feed, such as when the feed is evenly distributed across the bin or lined along the opposing side. The overall procedure of this study was to record 3D scans of a feed bin at various fill levels, and from the resulting scale weight versus feed volume, derive a single mapping from volume to weight. The resulting

26

mapping was then used to compare the weight of feed derived from the volume to the actual weight measured by a digital scale. The differences between these two values were analyzed by regression analysis.

Simple regression analysis was conducted on all experimental setups tested. The choice of regression analysis was made as the objective was to determine if a strong correlation existed between the camera sensor depth measurement values of the feed surface in a bin and the scale measured weight values of feed in a bin. A linear correlation was assumed, but a quadratic correlation was utilized to expose inherent sensor error when the camera was positioned from the feed at or below the lower optimal operating range. This sensor noise at close range has been previously studied and can be modelled as a quadratic relationship as outlined in the work by Nguyen et al.[59].

For the purpose of establishing a data set of weights and volumes, the same plastic feed bin used in controlled research feeding at the University of Kentucky Coldstream Dairy Research Farm was used in this research. The bin was a Rubbermaid® 3501 Food/Tote Box (Rubbermaid Commercial Products, LLC., Winchester, VA) with dimensions of 66.0 cm in length, 45.7 cm in width, and 38.1 cm in depth for a total volume capacity of 81.4 L or 0.29 m^3 and a maximum weight capacity of 23.98 kg. A digital scale, ROYAL™ 17016G 315-lb freight scale (Royal Consumer Information Products, Inc., Bridgewater, New Jersey), which measures weight with an accuracy of within 0.0045 kg was employed for obtaining feed weight measurements. For measuring volume, we employed a PrimeSense™ Carmine 1.08 RGB+depth sensor. Positioning the sensor over the feed bin then creates an opportunity to measure the feed in the bin simulating the times before and after a cow has fed from the bin.

As with any machine vision system, no camera can make measurements occluded from its view, such as feed that may be hidden at the bottom of a bin when imaged from the side. For this reason, measuring feed volume must either be done using a scanning process of sweeping the camera over the feed to ensure that no portion of the feed is occluded from the camera, such as the first and second experimental setups, or the camera must be placed directly above the feed bin to ensure no portion of the bin occludes the feed, such as the third experimental setup. The first and second experimental setups allowed for observing the effects of sensor range and sensor noise given that placing the sensor further away allows the camera to see more of the bin in a camera frame but with potentially less depth accuracy, surface definition, and sensor noise than at close distances. The third experimental setup allowed for comparing the ability of a single image capture system to derive values equivalent to those observed in the merged scanning process of the first two experimental setups.

In the first and second experimental setups, the entire feed bin was captured as a 3D model of merged meshes. This required multiple images to be captured from differing perspectives around the feed bin in order to create the 3D model of the entire feed bin. Figure 2.2A-D shows the image capture of the feed bin shown from the perspective of the camera. Several points of occlusion from both the feed and the bin existed in a single image capture of the scene. Therefore, multiple image captures around the feed bin not only facilitated creating a 3D merged mesh model, but also eliminated these points of occlusion observed in single image captures. We recorded successive images at different positions around the bin, such as in Figure 2.2A-D, where the perspective is kept the same as in the first image captured but with the camera and data

collection at different positions around the scene. Figure 2.2A is the initial image capture position for every test bin. This initial image capture is taken at an angle perpendicular to the left side of the feed bin and in line with the viewpoint of the observer of the image. Image capture with the camera located at the rear side of the bin where the camera is to the right of the observer is shown in Figure 2.2B. Image capture with the camera perpendicular to the right side of the bin and with the camera positioned opposite the observer is shown in Figure 2.2C. Image capture with the camera at the front side of the bin with the camera positioned to the right of the observer is shown in Figure 2.2D. The final merged image and data point cloud is shown in Figure 2.2E, which shows little to no points of data occlusion. The system architecture and setup are shown in Figure 2.2F with the arm of the frame and camera extended outwards at full length. The camera arm in this position is perpendicular to the front side of the feed bin. Markers were placed on the floor to ensure the same placement of the bin for every image capture.
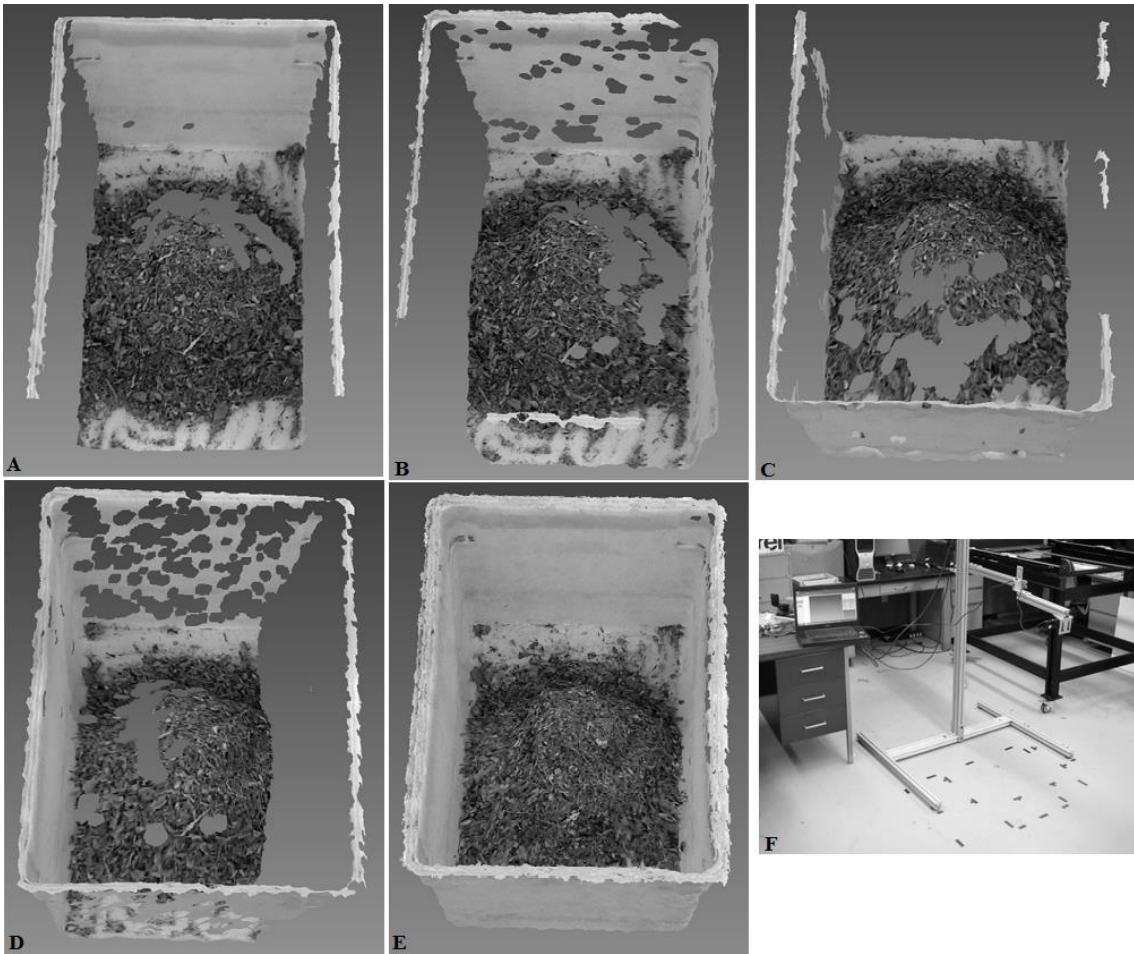
*Figure 2.2 – Data collection from different camera positions shown in **A**, **B**, **C**, and **D**. The final merged image and data point cloud for a sample is shown in **E**. The system architecture and setup are shown in **F**.*

Merging these disparate views allowed the system to scan the feed surface without occlusion. In order to create an accurate scan model of the feed bin, there must exists enough overlapping data in the images captured to accurately align them. The more input data overlap that exists, the greater the precision of the output merged image data. Eventually, a point of diminishing returns will be realized where the amount of time, data, and other resources used to collect the next image in the sequence outweighs the benefit of the newly added data information. Therefore, in order to recreate a 3D surface with sufficient precision, a determination must be made as to the minimum amount of

data collection necessary to avoid occlusions as well as the maximum amount of data collected before reaching diminishing returns.

KScan3D™ (LMI Technologies, Inc., Delta, British Columbia, Canada) was used for image capture and to merge images in real-time. In order to use the PrimeSense™ camera and the KScan3D™ software to capture an accurate scan model of the feed bin, it was determined that a series of 14 successive images were to be collected of the feed surface and bin. The final result is a 3D surface recreation of the feed bin such as in Figure 2.2E. More or less frames could have been captured during this process. Less frames captured would not have made it possible for the KScan3D™ software to automatically align the scans as there was limited overlapping data from one image to the next. More frames would have provided only a slight improvement on image merging and data overlap, but would overall not have been necessary.

The sensor was installed onto an 80/20® aluminum frame (80/20 Inc., Columbia City, Indiana), as shown in Figure 2.2F, to minimize the effects of camera motion on the merging process. A pivot arm was constructed to bring the camera over the center of the bin of feed for scanning or used to move the camera out of the scan area. Attached to the side of the pivot arm was a swivel arm that allowed for 360 degrees of free rotation beneath the pivot arm about the point of attachment. The camera was manually positioned in the same location for the start of every scan in a test set. In the first experimental setup, the camera was at a distance of 99.1 cm from the floor and 61.0 cm from the top of the feed bin. The camera was intentionally placed at a distance from the feed surface below the 80 cm lower limit of the 3D depth sensor's optimal operating range in order to observe the effects on the accuracy of the image data.

For the merged image tests of the first and second experimental setups, the first image functioned as the anchor to which all of the successive images would be automatically merged and set the Cartesian coordinates to be assigned to all 3D scan data. The software then proceeded to collect 13 more images with a 2 s delay between each image capture as the user manually rotated the camera clockwise (looking down onto the bin) through one revolution with the swivel arm. As each image was captured, the KScan3D™ software automatically aligned and merged the new data with the previously merged data to produce an updated 3D surface.

A 0-kg scan, or empty bin scan, was the first scan collected with the system. The bin was then filled with 2.27 kg of feed, and the feed biased and scanned in seven different positions within the bin: feed with a flat top surface (**F**); feed biased in the back left (**BL**) corner; back right (**BR**) corner; front left (**FL**) corner; front right (**FR**) corner; biased in the center (**C**) of the bin; and feed with a hole (**H**) in the center or the feed pushed out towards the walls of the bin. Biasing with respect to this research meant that the majority of the feed volume in the bin was concentrated in that area of the bin. The biasing of feed was conducted in order to determine if it had any effects on the system, as a robust system for measuring the feed volume and weight would have to not be affected by the surface contour of the feed. After collecting data on the 2.27-kg bin of feed, the bin was then filled with another 2.27 kg of feed, and the same seven biasing scans collected by the system. This process was then repeated at 2.27 kg increments until the bin had 22.68 kg of feed at which point the plastic bin could not hold any additional feed without spilling over the edges or being heavily mounded in the center of the bin.

After all scans had been conducted, the KScan3D™ software was then used to reduce the 3D point cloud data to 10%, or roughly 80,000 data points, of the original data as this was all that was needed to accurately represent the original 3D scan. A larger percentage of the original data could have been utilized, but would not have significantly added to the accuracy of the representation of the feed in the bin. A larger data point set would require more processing time as well, which would reduce the operational speed of the system. The data were then processed to: (1) align the bins with the origin and the Z-equals-zero plane; (2) interpolate the scattered data of each scan; (3) calculate the difference of the current volume scan data file from the 0-kg scan (empty bin) data file; (4) create a new scan dataset to represent the feed volume by itself (without the bin); (5) determine the numerical cumulative depth average value corresponding to the averaged volume value of the feed surface; and (6) analyze the relationship of the 3D scanned volume values to the known scale-measured weight values by regression analysis.

The point clouds were saved to ASCII (.asc) text files of three columns of numerical values; each row representing the X, Y, and Z Cartesian coordinates of a single data point. This data was then imported to MATLAB® for further processing and analysis. An example of this file is shown in Figure 2.3. A MATLAB® script was created to align the bins with the origin and the Z equals zero plane, shown in Figure 2.4, interpolate the scattered data of each scan, take the difference of the current scan data file from the 0kg. scan (empty bin) data file, create a new scan dataset to represent the feed by itself (without the bin), then determine the numerical volume ovalue of the feed, and save this information to a Microsoft™ Excel™ file. The Excel™ file was then used to

analyze the correlation of the volume values determined in MATLAB® to the known weight values.
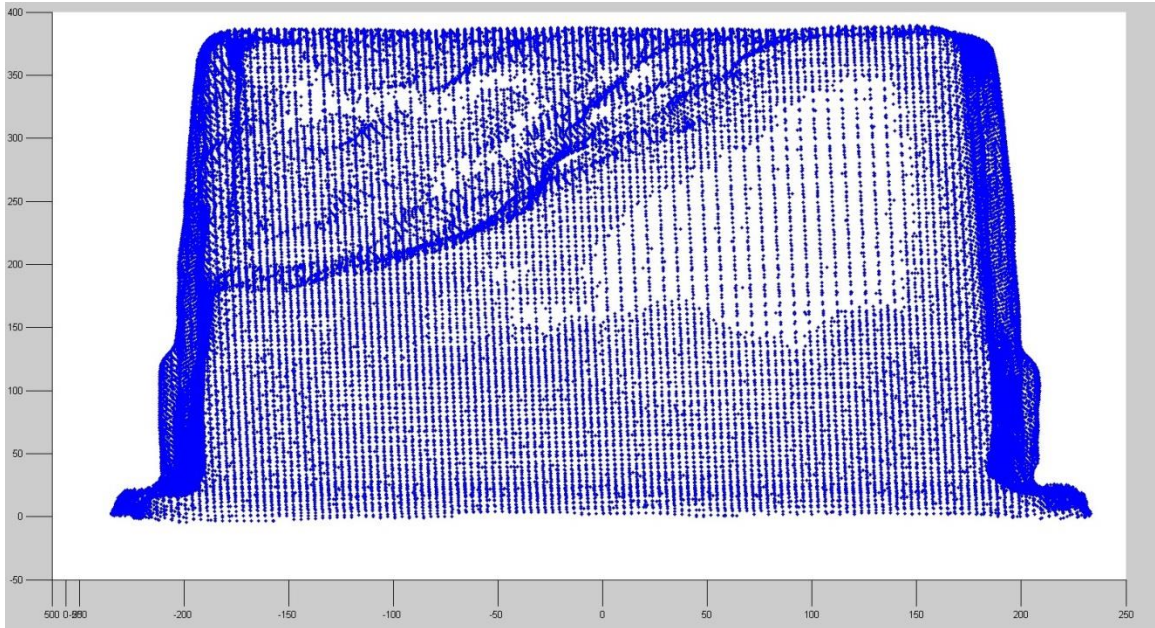
Figure 2.3 – ASCII point cloud of feed bin data points.
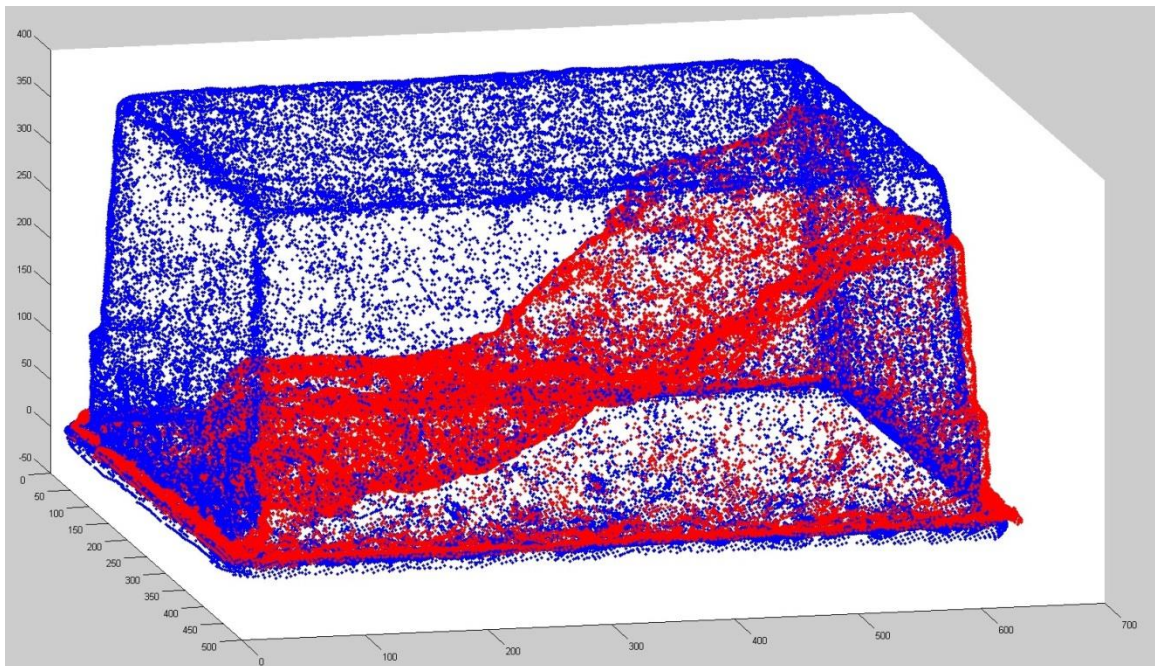
Figure 2.4 – Empty bin and bin of feed aligned together and with Z-axis.

Aligning the bins with the origin ensured that the corner with the lowest data value for both bins would lie as close to the origin as possible. Aligning the bins with

regards to the Z-equals-zero plane gave the data a view normal to the surface of the feed and the bin; as if the observer was looking directly down onto the bin and feed. The alignment of the bins allowed for the interpolation of each data set to remove duplicate data for the feed surfaces, ensuring an accurate representation of the actual surface. By taking the difference of the two data sets, the data that would have otherwise represented the plastic bin, and not the feed in the bin, could be removed from the final volume calculation. An example of this process is shown in Figure 2.5.
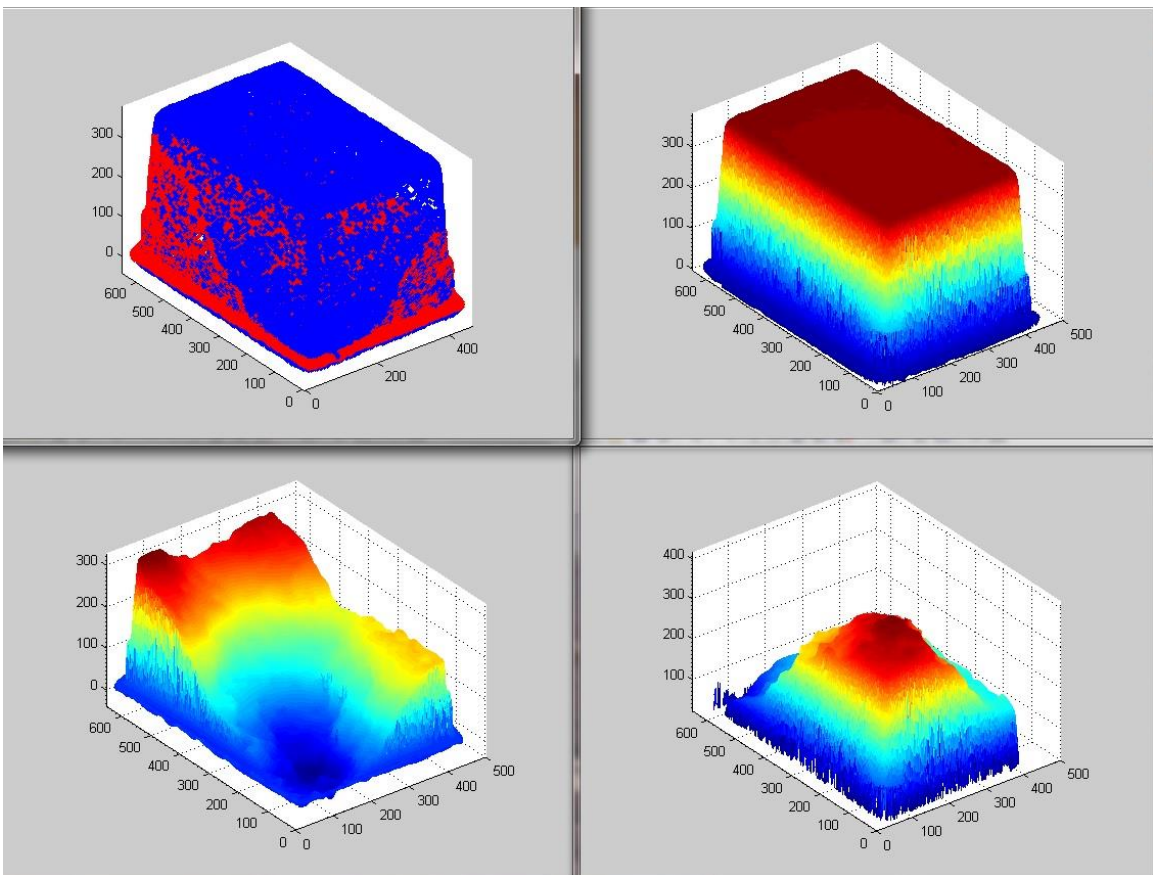
***Figure 2.5** – Aligned bins (top left), interpolated empty bin (top right), interpolated bin of feed (bottom left), and feed alone (bottom right).*

In the second experimental setup, the camera was moved to a distance of 138.1 cm from the floor and 100.0 cm from the top of the feed bin. The reason for this was to move the camera to a distance where the feed surface would be within the camera's

optimum operating range of 80.0 cm to 350.0 cm. Outside of this range, intrinsic errors from the camera itself are induced in the depth measurement data. The same experimental procedures conducted in the first experimental setup were repeated for this increased camera distance setup. No further camera distance changes were tested as any increased distance from sensor to scene would only reduce system accuracy.

In the third experimental setup, the camera was kept at 138.1 cm from the floor and 100.0 cm from the top of the feed bin, but instead of capturing and merging 14 successive images, the setup now allowed for a single image capture from directly above the center of the feed surface. This test was conducted to determine if a single image capture system could derive comparable image weight values as the first two setups tested without requiring multiple image captures, a rotation mechanism about the feed surface, or the need for computationally intensive image merging. The same data processing was conducted on the data collected in the third experimental setup as outlined for the first and second experimental setups. This data processing included the same ordered operation steps of data reduction, alignment, interpolation, differencing, cumulative feed surface depth average value derivation, and simple regression analysis as outlined in the data processing description of the first experimental setup.

Figure 2.6 shows the first and second-order least squares model fits for all three experimental setups. The results show a strong model fit ($R^2 > 0.99$) for both linear and quadratic modeling of the volumetric scan data with relation to scale-measured weight values. The initial hypothesis was that the relationship would be strictly linear. As can be seen in Figure 2.6, a strong relationship exists between the known scale weight values and the image volume values. As the scale weight value increased, so did the image

36

volume values. The more densely plotted the volume values for that weight class, the stronger and more distinguishable the relationship of image volume values to that known weight value.

(A) First Experimental Setup Regression Analysis

$\hat{y} = 3.95E\text{-}07x - 1.90$
$R^2 = 0.9868$
$\hat{y} = 2.23E\text{-}15x^2 + 2.41E\text{-}07x + 0.15$
$R^2 = 0.9934$

(B) Second Experimental Setup Regression Analysis

$\hat{y} = 4.16E\text{-}07x - 1.48$
$R^2 = 0.9929$
$\hat{y} = 1.68E\text{-}15x^2 + 3.08E\text{-}07x - 0.14$
$R^2 = 0.9960$

(C) Third Experimental Setup Regression Analysis

$\hat{y} = 4.51E\text{-}07x - 3.08$
$R^2 = 0.9927$
$\hat{y} = 2.77E\text{-}15x^2 + 2.68E\text{-}07x - 0.65$
$R^2 = 0.9991$
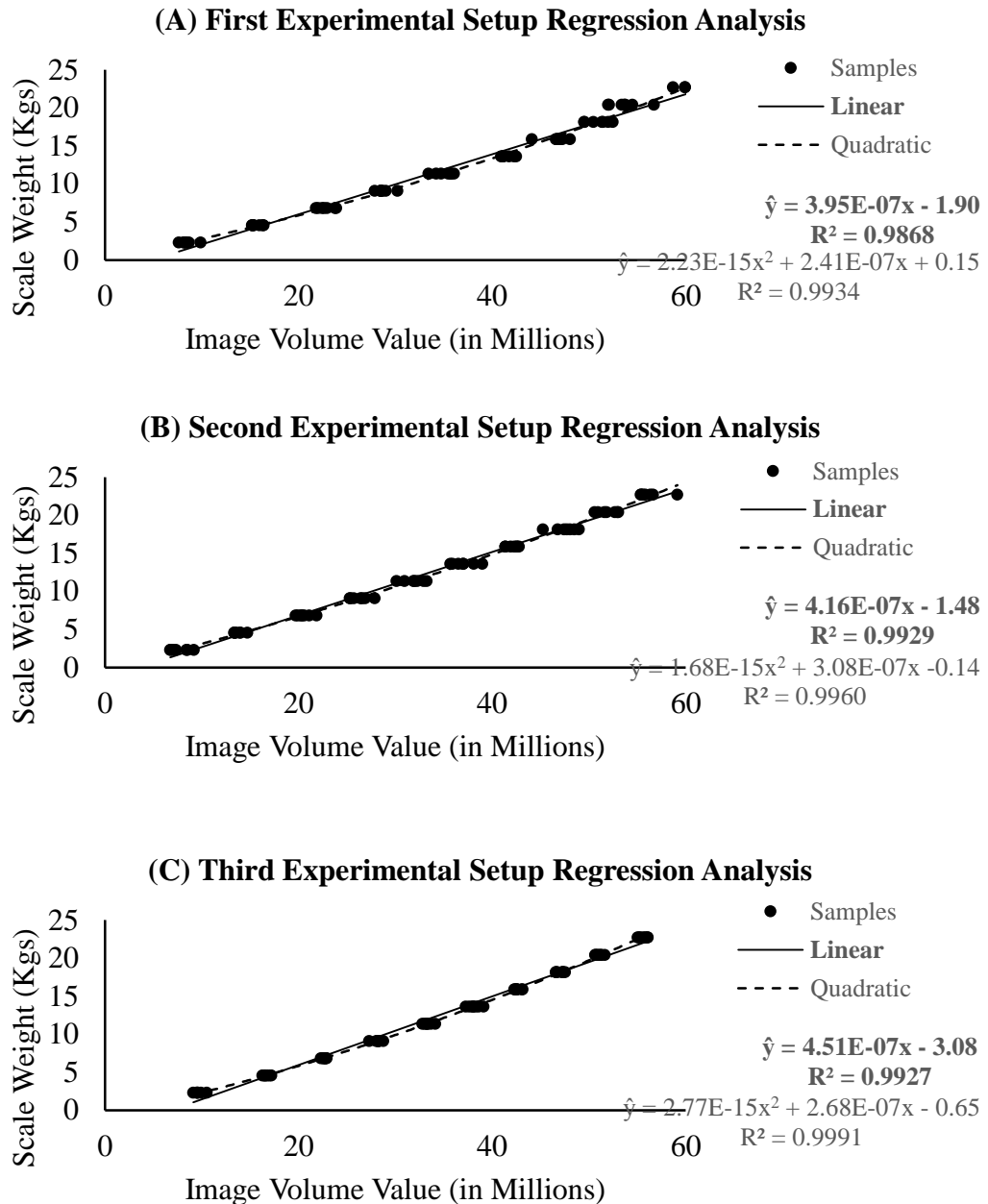
Figure 2.6 *- The collected data samples were plotted along with linear (solid line) and quadratic (dashed line) least squares regression models fit to the data comparing the image volume value to the scale weight for the first (A), second (B), and third (C) experimental setups tested. The equations of fit and R^2 values are shown at right for linear models (in bold) and quadratic models.*

The residual error seen in Figures 2.7A and 2.7B was determined to be mainly due to the inherent sensor noise error of the PrimeSense™ camera's depth sensor at short distances as expected. In the first experimental setup tested, where the sensor was intentionally placed below the manufacturer suggested lower operating range, the increasing variance directly due to the increasing sensor noise error is clearly visible. It was determined that a second-order fit instead would be optimal as it would include correction compensation for this residual sensor error at distances near this lower operating range. Figures 2.7C and 2.7E continue to exhibit a slight non-linear relationship between the scale weight and the image volume, which was still due to sensor noise but to a lesser degree as these experimental setups tested bin weights within the optimal operating range of the camera sensor. At the increased camera distance in the second and third experimental setups, the contribution of sensor noise is greatly reduced and the variance randomly distributed when a quadratic relationship between scale weight and image volume was considered, as can be seen in Figures 2.7D and 2.7F.

(A) First Experimental Setup Linear Residual Plot

(B) First Experimental Setup Quadratic Residual Plot

(C) Second Experimental Setup Linear Residual Plot

(D) Second Experimental Setup Quadratic Residual Plot

(E) Third Experimental Setup Linear Residual Plot

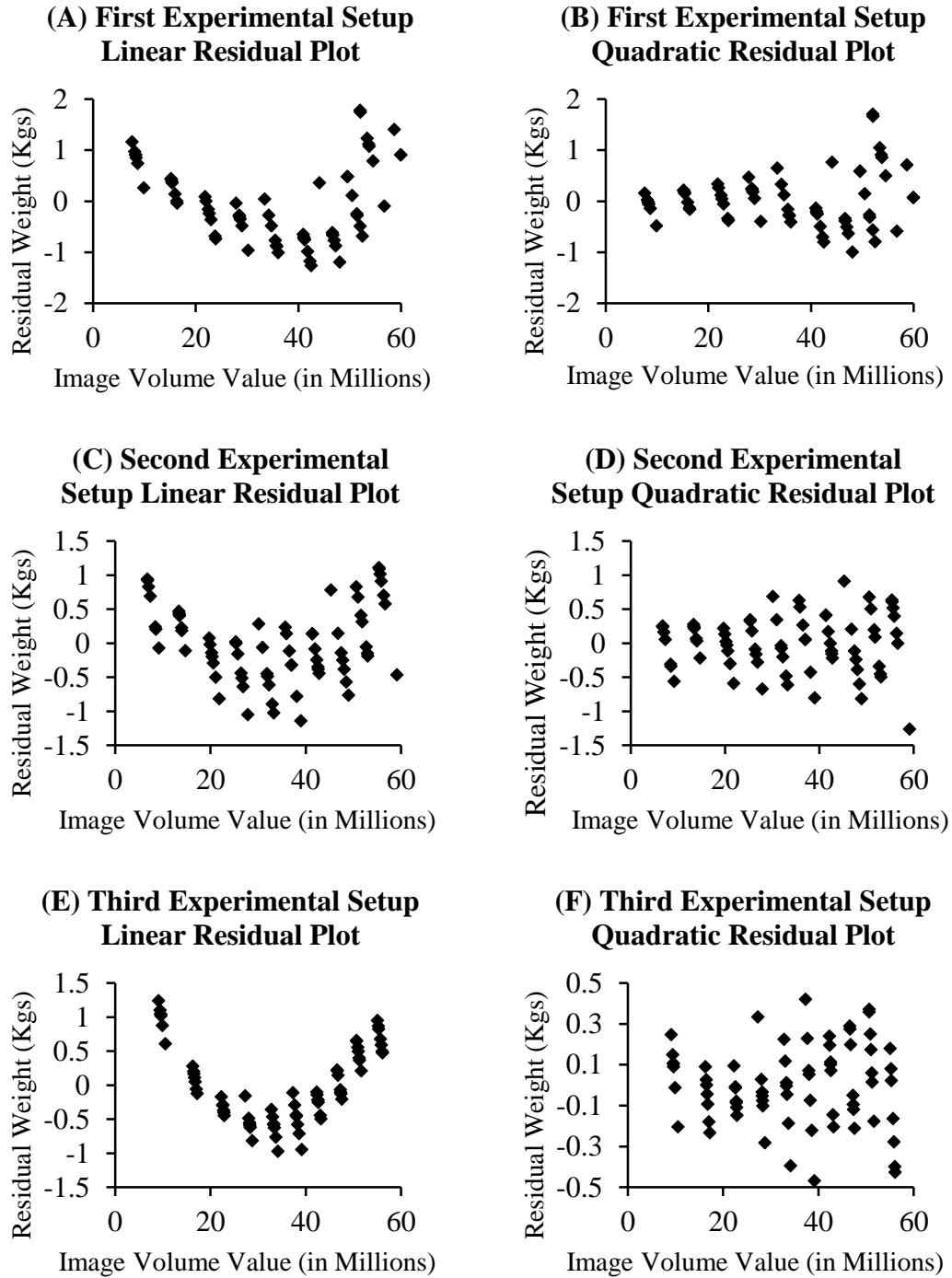**(F) Third Experimental Setup Quadratic Residual Plot**

Figure 2.7 – *The linear residual error plots for the first (A), second (C), and third (E) experimantal setups. The quadratic residual error plots for the first (B), second (D), and third (F) experimental setups.*

39

The linear standard error values achieved for the three experimental setups, in order, were 0.76 kg, 0.56 kg, and 0.57 kg. The single coefficients for the three linear models were observed to all be highly significant ($P < 0.01$). The quadratic standard error values achieved for the three experimental setups, in order, were 0.54 kg, 0.42 kg, and 0.20 kg. The P-values for the individual coefficients of the three quadratic models were all observed to be highly significant ($P < 0.01$). These results show that the second-order model with a single image capture system had the least statistical error and, therefore, had the best model fit to the data. Once the least squares regression analysis was able to accurately determine the best model fit representing the relationship between image volume and scale weight, the image volume values were input to the model-derived parametric equations with the resulting image weight conversion values output. In this manner, the known scale weight values can be directly compared to the calculated image weight values. Figures 2.8-2.10 show the 95% prediction and confidence interval plots of these converted image volume values into kilogram-based image weights. As can be seen in these figures, the prediction accuracy and confidence accuracy of the system is greatest with the third experimental setup.

First Experimental Setup 95% Prediction & 95% Confidence Intervals

95% Prediction Intervals, Linear

95% Prediction Intervals, Quadratic

95% Confidence Intervals, Linear

95% Confidence Intervals, Quadratic

Figure 2.8 – The plots above show the 95% prediction intervals (top row) and 95% confidence intervals (bottom row) for linear (left) and quadratic (right) regression analysis for the first experimental setup with image volume values converted to kilograms.

Second Experimental Setup 95% Prediction & 95% Confidence Intervals

95% Prediction Intervals, Linear

95% Prediction Intervals, Quadratic

95% Confidence Intervals, Linear

95% Confidence Intervals, Quadratic

Figure 2.9 – The plots above show the 95% prediction intervals (top row) and 95% confidence intervals (bottom row) for linear (left) and quadratic (right) regression analysis for the second experimental setup with image volume values converted to kilograms.

42

Third Experimental Setup 95% Prediction & 95% Confidence Intervals

95% Prediction Intervals, Linear

95% Prediction Intervals, Quadratic

95% Confidence Intervals, Linear
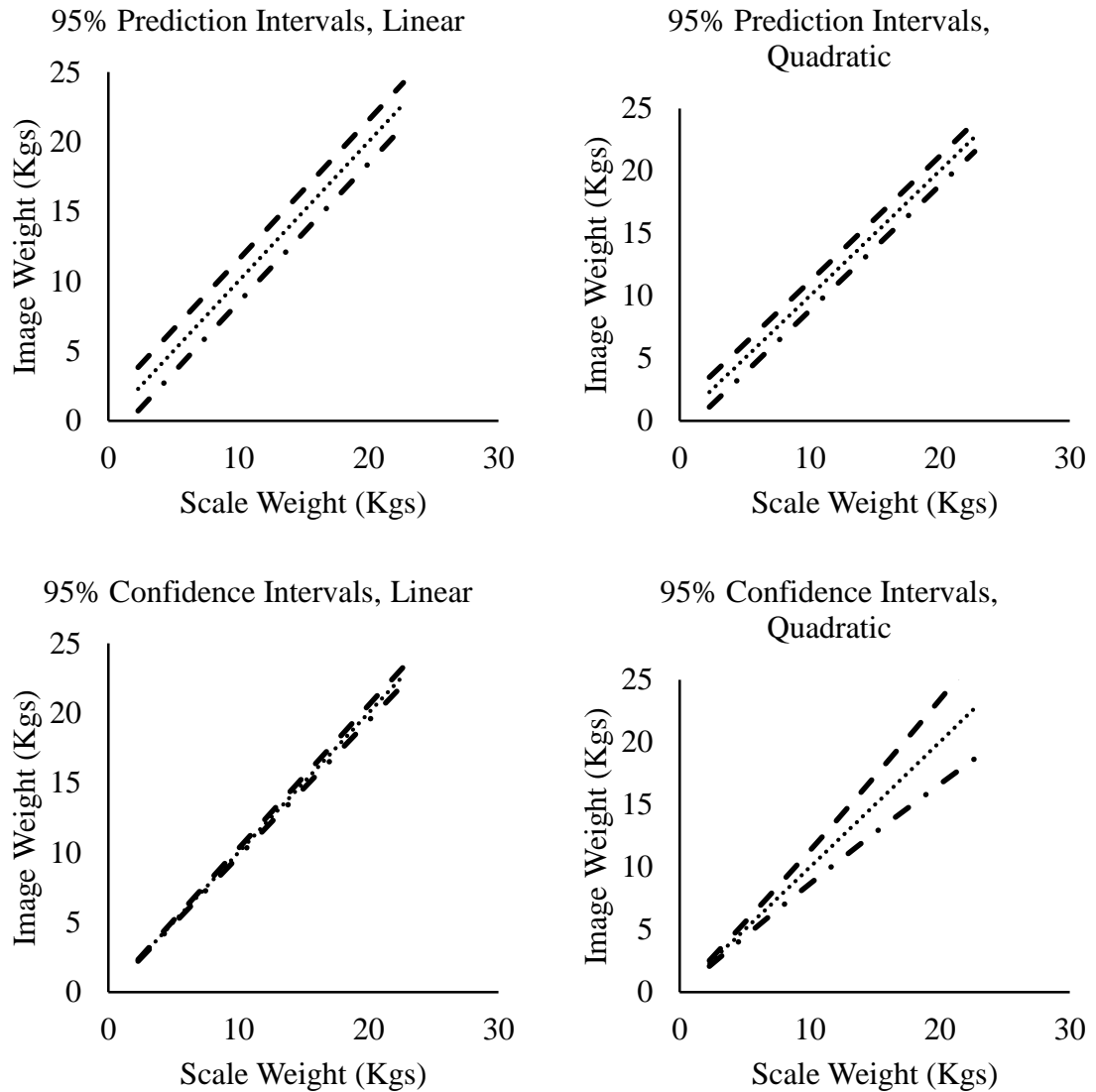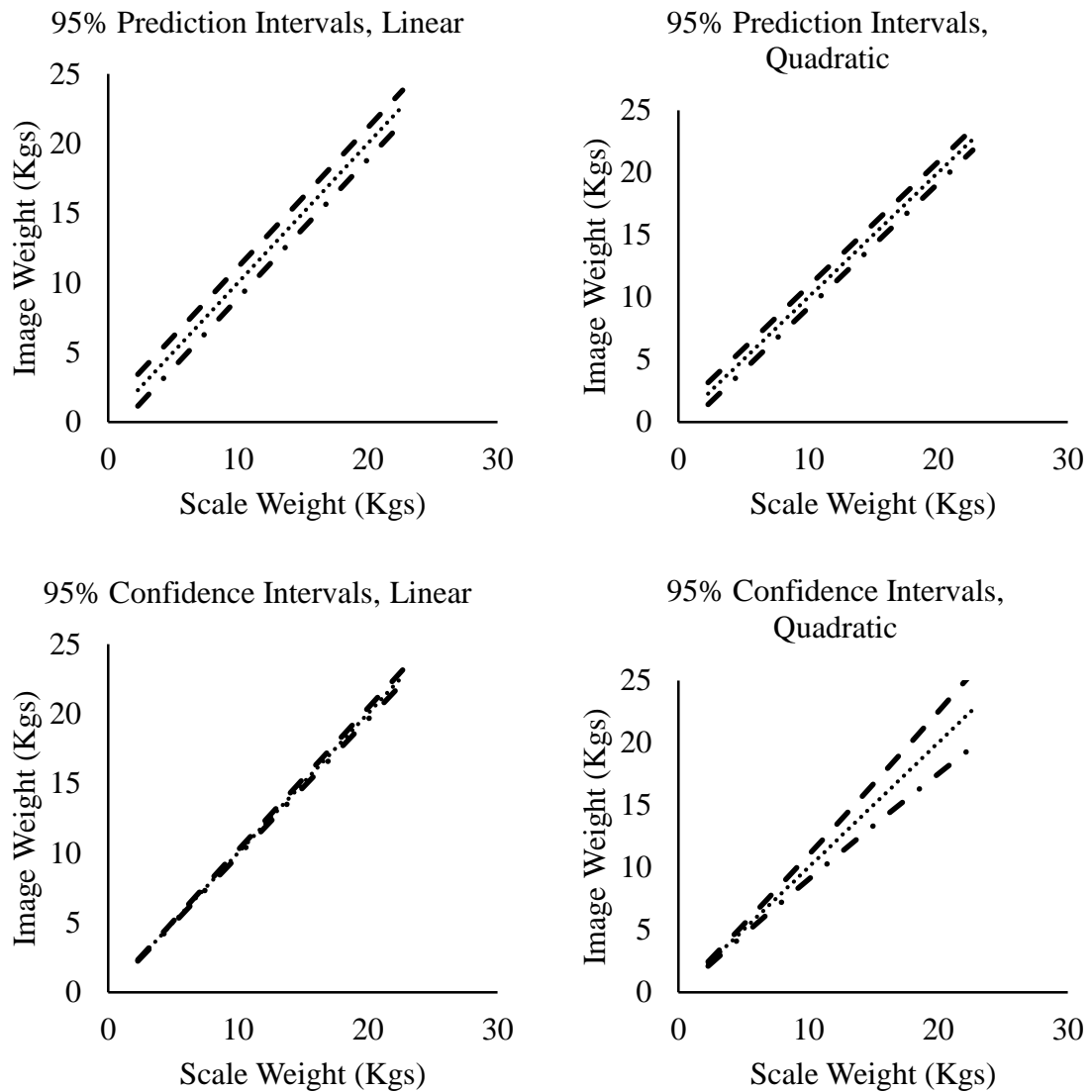

95% Confidence Intervals, Quadratic
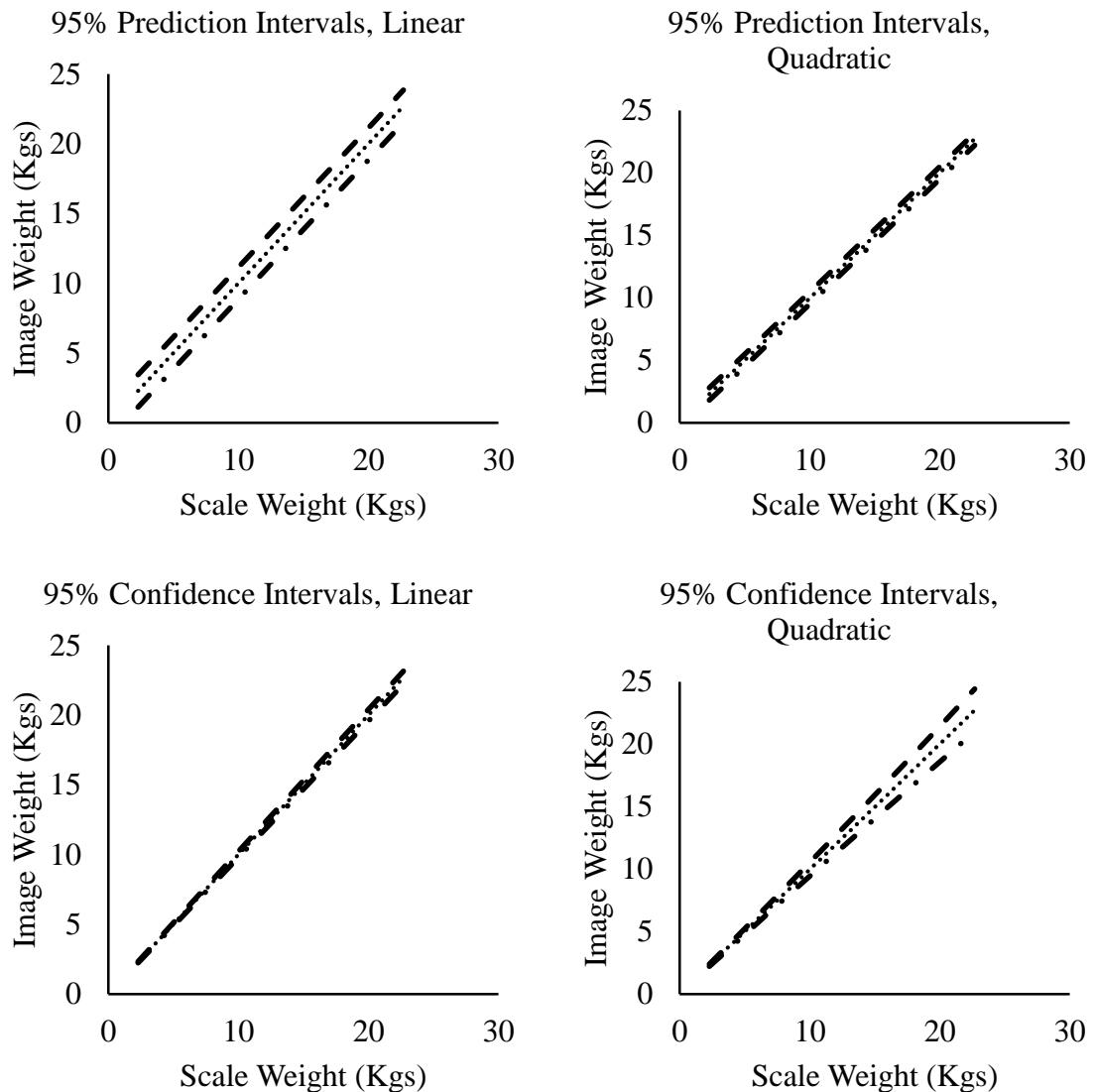
Figure 2.10 – The plots above show the 95% prediction intervals (top row) and 95% confidence intervals (bottom row) for linear (left) and quadratic (right) regression analysis for the third experimental setup with image volume values converted to kilograms.

The fact that the residual errors for all 7 biased image captures for each weight increment in the quadratic residuals did not vary by more than 2 kg in the second experimental setup and by no more than 1 kg in the third experimental setup, shows that the variations in the surface, where the feed creates peaks and valleys in the surface, does not inhibit the system from accurately producing image weight values. As long as the

system is calibrated before use at differing known scale weight values of the TMR, the system is able to produce image weight values to within a small percentage of error regardless of how the surface of the feed is arranged. Based upon the statistical results of the three experimental setups, the single image capture system at a distance of 100.0 cm from the highest point of feed surface which includes quadratic sensor error compensating conversion of volume to weight was deemed to be the best option in regards to both error minimization and practicality. A single image capture system can be run in real-time for continuous monitoring of the feeding area with no obstruction to the workflow or the cow's feeding behavior. The single image capture setup also has the benefit of no moving parts that can result in mechanical failure as well as having the smallest operating space requirement.

The main contribution of the total error discovered in the volume values determined by the software was the fact that the feed scan and the empty bin scan were not always aligned by the software perfectly. The process by which the software aligns the 2 input scans was rather simple and robust, but even slight misalignment in the X, Y, or Z direction along with any rotation of the data leads to an increased error the further misaligned the 3D scan data point clouds are for the 2 input scans. Future versions of the alignment software must include an even more robust alignment procedure that the one utilized here, such as iterative closest point. The main cause of misalignment was the manual nature by which the data was collected. Even though great care was taken to ensure that the camera was fixated in nearly the exact same location for the initial image of every scan for the first two experimental setups, manually aligning the camera would not be as exact as an automated system or stationary system such as in the third

44

experimental setup.   The fact that neither feed bin or camera moves in the third experimental setup is a direct indication of this reduced alignment error problem with a stationary system.

Testing was not conducted for bin weights greater than 22.68 kg as the feed in the bin at these values is either spilling out over the edges of the bin or is severely center biased as it must be piled in the center of the bin in order to accommodate this much feed. Another consideration that would need to be included in the analysis of the residual errors is the fact that the increase in weight will increase the deformation of the feed bin as the greater weight imparts a greater stress on the plasticity of the feed bin. This may also help explain part of the slight deviation of the data from a purely linear relationship at greater weights as the feed bin did indeed have some slight deformation as feed weight increased.

As a simple demonstration for the viability of expanding this research in future work with feed in a non-isolated and controlled manner, a sample test scan was conducted on a random sample of 4.99 kg laid out on the floor in such a manner as to mimic a pile of feed after having been visited by a cow. This sample can be seen in Figure 2.11. In Figure 2.11A, the final merged images and data point clouds can be seen in an overhead view. In Figure 2.11B, the depth information from the same view is shown with external factors such as framing material and empty floor space removed. In Figure 2.11C, the sample is shown from the side with the data point cloud converted to a mesh that accurately represents the feed surface. The sample was then run through the same software as the rest of the research conducted in this study with a final image

volume value derived and then converted to an image weight value. The scale-measured

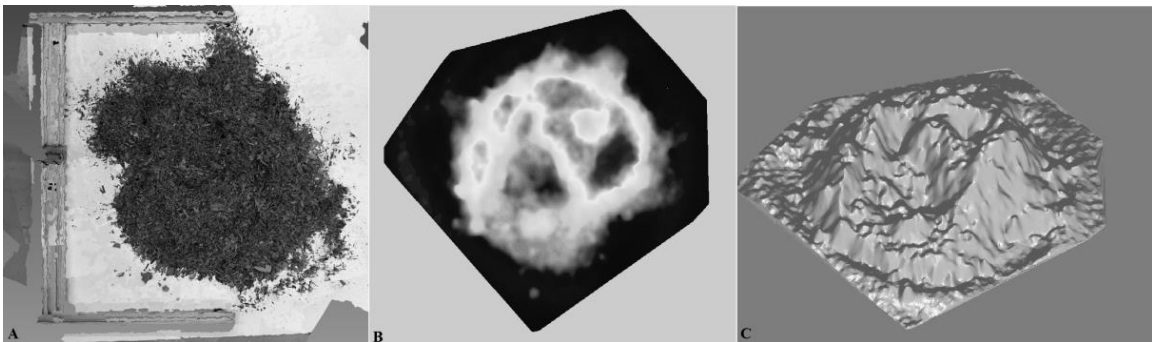weight value was 4.99 kg and the computer-generated weight value was 4.9928 kg.

*Figure 2.11 – A 4.99kg test scan shown in **A,** the depth map of the test scan data shown in **B**, and the data point cloud converted to a mesh model shown in **C**.*

This study demonstrates potential for the use of imaging to measure feed intake, feed volume, and feed weight. Future studies should address how the system functions in open feed bunks with multiple cows entering and exiting throughout the day as well as studying how feeding behaviors affect system accuracy. Facial recognition techniques or RFID may be used to identify when animals enter or exit the feed bunk and are actively eating. Separation panels extending from headlocks may be necessary if issues occur with cows entering their neighbors' defined areas to steal feed. Variations in TMR content and density would necessitate a change in calibration when making major ration changes or in evaluating rations across farms. This research was conducted in a laboratory setting. Future experiments should carefully monitor changes in TMR density that could result from sorting of the ration by cows thus changing the forage-to-concentrate ratio and possibly the moisture content in the feed bunk as well. Changes in ration density through time represent a potential technical challenge for this approach.

CHAPTER III: POTENTIAL FOR AUTOMATED MONITORING OF

GRADUAL CHANGES IN DAIRY COW BODY CONDITION SCORE

The body condition score of dairy cow provides a great deal of health information concerning the individual dairy cow. The human visual scoring scale utilized in body condition scoring (BCS) was not developed until 1982.[60] Since then, fervent research has been conducted to automate the process of BCS. Attempts in recent years have been directed at deriving a BCS from 2D image information. The results of previous studies confirm that 2D BCS is indeed viable utilizing image data, which has since progressed towards developing 3D BCS systems as cameras and computers available have increased in technology and capability while decreasing in upfront cost. Studies that have attempted automated 3D BCS have included a human element in the scoring process at some point, which does not make them fully automated. In order for a system to be fully automated, it must be able to collect, process, and analyze the data autonomously.

The system developed in this research does just that and produces a score comparable or superior to the human visual score. The main goal of this system is full autonomy, but equally as important is observing the ability of the system to detect and monitor the gradual change in BCS scores for an entire herd of dairy cow for an extended length of time. It is essential for an automated BCS system to be able to both accurately produce BCS scores and to monitor the gradual change in these scores for the individual cow, if such a system is to be reliably incorporated in dairy operation management decisions regarding individual cow health and performance. The end automated system was developed over several iterations of testing and studied over an observational period

of several months with the University of Kentucky Coldstream Dairy Research Farm dairy herd.

Concurrent with the autonomous data recordings, human visual BCS scoring from three independent scorers was also collected once a week per scorer for this same period in order to monitor the variability in BCS over an extended period of time for human scores. In this manner, it was possible to validate the computer-generated BCS values against those from the visual scoring in order to ensure that the processes and algorithms utilized in generating an automated score were indeed satisfactory. As well, the human scores were observed comparatively against the computer-generated scores so that the changes in BCS for each individual cow could be analyzed as to how the scoring changed over an extended period of time. The hope here was to be able to monitor the gradual change in BCS as the body condition and lactation cycle of the cow changed. In order to observe the correlation of the lactation cycle with BCS, the days in milk (**DIM**) was recorded for every individual cow in the herd for the observational period.

3.1 Body Condition Score (BCS)

The 5-point BCS scoring system, also known as the United States Body Condition Scoring (USBCS) system, used in this research was developed in 1982 by Wildman et al.[60]. The subjectively visual based BCS scale goes from 1.0 to 5.0 in increments of 0.25. One full point of body condition equals 100 to 140 pounds gain in body weight.[61] The BCS provides an estimation of the fat stores and energy status of the cow. This is important particularly in early lactation, as cows cannot eat enough to meet their energy needs during this time. The extra body fat is essential in helping to provide energy and milk production as the cow recovers post pregnancy. The BCS of a cow

48

should typically not change over an annual range from its highest point to lowest point by more than a full point on the scale, or, respectively, from just before calving to a few months post pregnancy when the fat stores of the cow will be at their highest and lowest. As long as the same scorer is used each time and the scoring system remains consistent, then the scores and information gained can be very useful in monitoring the health of a cow.

The BCS process directs the scorer to view certain anatomical sites in the cow's pelvic and loin areas for visual cues from which to ascertain a BCS value. Kellogg[61] provides descriptions of various BCS values that can be assigned to the cow as follows:

- 1.0 – Deep cavity around tailhead. Bones of pelvis and short ribs sharp and easily felt. No fatty tissue in pelvic or loin area. Deep depression in loin. Essentially just skin and bones; very emaciated.

- 1.5 – The cow, with a body condition score of 1.5, is ideal for demonstrating the key indicators, but little else. Each vertebra is sharp and distinct along the backbone. The short ribs are also visible as individual bones. The ligaments connecting the sharp and well defined hook and pin bones to the backbone are easily seen. Her thurl is extremely dished in and the area on either side of the tailhead is sunken and hollow. There are folds of skin in the depression between the tail bone and pin bone. This cow is too thin, will not milk well or reproduce, and is most likely unhealthy.

- 2.0 – shallow cavity around tailhead with some fatty tissue lining it and covering pin bones. Pelvis easily felt. Ends of short ribs feel rounded and

upper surfaces can be felt with slight pressure. Depression visible in loin area. The cow is too thin. She may be in good health, but her reproduction and milk production may suffer from a lack of body condition. Her backbones are easily seen, but they do not stand out as individual vertebra. The short ribs are also distinct and the scalloping at the edges is very apparent. The thurl is very hollow, with prominent hook and pin bones. The ligaments holding these bones to the back are very sharp and distinct. The spot where the thigh bone meets the pelvis is obvious, but unlike the BCS 1.5 cow, there is a little flesh here. The area on either side of the tailhead is hollow with folds of skin in the depression formed by the pelvis and tail. Still a thin cow which will suffer from low milk yields and poor reproduction capability, but may be healthy.

- 3.0 – No cavity around tailhead and fatty tissue easily felt over whole area. Pelvis can be felt with slight pressure. Thick layer of tissue covering top of short ribs which can still be felt with pressure. Slight depression in loin area. This cow is in ideal condition for most stages of lactation. The vertebra are rounded, but the backbone can still be seen. There is between a half inch and an inch of tissue covering the short ribs. The edges of the ribs are rounded and not as sharp as the BCS 2.0 and 2.5 cows. Hook and pin bones are easily seen, but are round instead of angular. The ligaments connecting them to the backbone form clear boundaries between the forward and rear pelvic areas, but the fat covering makes them appear smooth and round. The thurl is dished, but not to the

same extent as in the thinner cows. The area on either side of the tailhead is hollow, but the folds of skin are not as distinct. A cow in the range of 3.0 to 3.5 is considered to be healthy, with good milk yield and reproduction capability.

- 4.0 – Folds of fatty tissue are seen around tailhead with patches of fat covering pin bones. Pelvis can be felt with firm pressure. Short ribs can no longer be felt. No depression in loin area. Although many producers want their cows to be heavy at calving, research here [in the United States] and in England shows that fat cows lose more condition, eat less, and have more post-calving problems than cows that freshen at half a condition score lower. A BCS 4 cow looks fleshy. Her back appears almost solid, like a table top. The short ribs still form a shelf, but they cannot be seen as individual bones and only felt with deep palpation. The hook and pin bones are rounded and have obvious fat padding. The area on either side of the tailhead is not hollow and there are no skin folds.

- 5.0 – Tailhead is buried in thick layer of fatty tissue. Pelvic bones cannot be felt even with firm pressure. Short ribs covered with thick layer of fatty tissue. An obese cow is at high risk for metabolic problems, lameness, and will most likely remain open for months at a time. Her backbone and short ribs cannot be seen and only felt with difficulty. The shelf formed by the short ribs is well-rounded. Her thurl is filled in. The hook bone looks like a ball and the pin bone is buried in flesh. Fat deposits at the tailhead give her a dimpled appearance.

Generally, the visually based BCS scoring method indicates that a score of around 3.0 is optimally what is being sought after. Anything less than this is too thin and anything higher is too fat.

On the lower end of the scale, there are cows that are malnourished and whose reproduction may suffer from a lack of body fat stores. She may milk fine currently, but this may suffer if not corrected. This can lead to health concerns both for her and for any calf she may be with. On the higher end of the scale, there are cows that are obese. These cows may be at risk for metabolic issues along with decreased fertility. Being obese will depress their appetite and can even lead them to go off feed while calving. Keeping the BCS around 3.0 allows the cow to have moderate body fat stores while keeping a healthy appetite. The health conditions associated with a cow having this BCS score include items such as the cow is not stressed, should have no metabolic or other health issues, and should be able to go through pregnancy and lactate fine while continuing to maintain a good feed diet.

3.2 Machine Vision Based Automated BCS

Several attempts have been made at developing an automated BCS system which utilizes a machine vision camera to score the cow.[62,63,64,65] In order for such a machine vision based system to be deemed viable, there are several criteria that optimally should be met in an ideal system. First, the system must be relatively affordable and easy to install and operate for it to be adopted. Second, it must provide accurate BCS scores well within the range of human error of 0.25 between independent scorers. Third, the system must be able to integrate with other precision dairy farming technologies to provide a broader system for better and more informed management decisions. Finally, it

must be able to collect, process, and store individual records for each cow to assist in future monitoring and aid in cow history referrals which influence individual cow decision making.

The methods tested can be broken down into the two categories of behind view or top view approaches. The method of behind view is akin to the human visual scoring of cow as it relies upon anatomical information obtained from the hips, hooks, pins, and tailhead regions of the cow body, but at a perspective normal to the rear of the cow and in line with the spine of the cow. The research conducted by Krukowski[62] is an example of this behind view approach where a time-of-flight camera was employed in order to obtain data samples of cow body for BCS scoring. Such systems have been tested to within an accuracy of half of a point on the 5-point BCS scoring scale. These results prove that the majority of information necessary for determining an accurate body condition of the cow are located in the region between the tail and the hips.

The behind view approach does incorporate the majority of anatomical points employed in visually based scoring, but it does not take into consideration cow anatomy beyond the hips nor does it take into consideration greater emphasis on the region between the tail and hips where the fat reserves are typically stored. The behind view approach is very similar to the current human visual calculation of BCS, but has limitations in the ability to see all the necessary anatomical structures necessary to provide the most accurate score possible. When considering just the rear section, the tailhead and pinbone are mostly used for scoring along with some information from the hook bones but the vertebrae and the line between the hook bone and pinbone cannot be seen with this system setup and, therefore, are not used in accurately determining a BCS.

The method of top view captures the entire contour of the cow in an image frame from some point above the cow's body, mainly ensuring that the rear portion of the cow is collected as this is where the majority of anatomical structures necessary for a proper score are located. The added benefit of a top view over a behind view is that the sides of the cow can be added into the estimated BCS. This is even more like the human visual scoring as the human scorer has the ability to view all sides of the cow in order to provide a more accurate score. The top view imaging approach still incorporates the anatomical information necessary for proper scoring, but only in a 2D format when utilizing traditional camera technologies for data capture, which can make it difficult to get a good visual of the tailhead, pinbone, and the cavity between the two for scoring. The research conducted by Bewley[10] is an example of this top view approach where 23 anatomical data points were manually identified in 2D grayscale color image data samples collected and then a BCS score derived from the angles between the points.

The research by Halachmi et al.[63] is an example of a more automated top view system employing the use of polynomial curve fitting to the cow contour information of 2D thermal images for BCS scoring. The cow contour boundary in these thermal images can be separated from the background information and then used for scoring. The ability to score this contour boundary, either manually or with automated processes, has been proven to be as accurate as visual scoring to within half of a point on the 5-point BCS scale. The ability to reduce this scoring error range is of importance if automated scoring systems are to ever be fully deployed in dairy operations for scoring on a regular basis. A major drawback of both the work by Bewley and Halachmi et al. is that the cow had to be

stopped under the camera for data collection. This inhibited the natural movement of the cow and the workflow of the dairy.

A more competent system would allow both the cow and workflow to proceed as they normally would within the imaging scene. The work by Halachmi et al.[63] also indicates that it is not just the boney anatomical points of the cow's body that are necessary in deriving an accurate BCS, but that the entire body contour between these points are also a critical element in proper scoring. Therefore, it has been determined from previous research that the best approach moving forward is to utilize an imaging method that can collect information about the 3D shape of the cow's body, such as with a 3D machine vision camera, for automated BCS scoring.

The approach considered in this research study was geared towards a 3D map of the body contour of the cow. This will take the previous work from 2D and add a depth component that will incorporate the best of both behind and top views. This added dimension will give the most realistic body contour possible and therefore the most accurate as it includes anatomical reference points, such as the spinal ridge, the hook bones, and the tailhead, which are essential in scoring. Even the human visual inspection cannot compete with the ideal, fully automated computational 3D BCS system. The systems developed and tested for this study included several modifications that would ultimately derive a solution that met our research needs. Though several small modifications were made during this process, only two preliminary systems developed and tested are discussed in this chapter along with the developing, testing, and analysis of the results for the final system utilized. The preliminary systems discussed are provided

here as a reference to show what did and did not work, including what elements of these systems helped to shape the final system design.

The end desire of this research was to have a system that the individual dairy producer could install and operate with minimal learning of the system or involvement. During milking, all the energies of the individual worker are needed to keep the process flow timely and with minimal problems as most production facilities are very hands-on during the milking. Therefore, the end system goal was to have a system designed to work on its own with minimal user input. Having a system that does not require the user to constantly leave their other obligations to check on or use the system allows them to focus on maintaining as productive and efficient an operation as possible. Stopping every cow to conduct BCS scoring only adds costly time to the process and stress for the animal. Therefore, the walkway was left unaltered to allow cow to move freely beneath the system as they normally would.

A fully automated BCS system is essential to precision dairy farming as it can potentially be used as frequently as on a daily or per milking basis to monitor the gradual changes in BCS score of every individual cow. The end system developed in this study was developed to operate at every milking, twice per day, to ensure reliable BCS scorings and in order to collect data that could be used to monitor these gradual changes in BCS for every individual in the herd over any time frame review of the cow's data history selected by the system user for both short and long term analysis. Recording data twice per day also allowed for any possible unanticipated downtime of the system, such as the system being offline due to a power outage or component failure. In these instances, the maximum amount of time that the system would be offline was expected to be one week.

3.3 Initial System Architecture Designs

The first step in this process was to select the site for system setup and data collection. The site chosen needed to not impede the normal movement of the cow, could record data samples for every individual animal without system movement, and had to have external variables, such as lighting and weather elements, easily controlled to minimize their possible influence on the results. The Holstein milking herd located at the University of Kentucky Coldstream Dairy Research Farm was selected as the basis for data collection. The cow herd was milked twice a day, once in the morning approximately from 4:30am to 6:30am and once in the evening approximately from 3:30pm to 5:30pm. After leaving the milking parlor, all cow exited via a roofed walkway walled on both sides and which included a concrete slab floor. This walkway was selected for system placement due to the restrictions to movement that it placed on the cow, the possibility to maintain consistent lighting conditions in the walkway if needed, and the protection provided to the system from the natural elements.

The focus of the system architecture was to have the system remain fixed above the walkway while the cow passed beneath. Since we needed the cows to continuously move through the scene, it was decided to place the system at approximately the mid-way point of the walkway length. At this position, cow tended not to stop, but instead consistently and at a moderate pace walk through the scene. Since the system was placed in a stationary position mid-way of the walkway length, having only one direction of motion for moving objects into and out of the scene reduced the error possibility of not being able to collect the entire cow body in image data as it passed beneath the system. The stationary nature of the camera system did impose a field of view limitation on the

camera's image frame. Thus, the cameras were positioned at a distance high enough from the floor of the walkway that the entire width of the walkway could be captured at the same height that the sides of the cow could rub against the wall on either side. This ensured that the entire top view of the cow in the scene would be captured even if the cow veered to the extreme left or right side of the walkway.

Our initial approach was to incorporate a two camera stereovision based approach which operated on the basis of optical flow. Optical flow is the apparent change of velocities of movement for objects in a field of view, which arise from the relative motion of objects, such as the cow in the scene, and the viewer, such as the cameras. This relative motion can provide important information about the spatial arrangement of the objects viewed and the rate of change of this arrangement. Discontinuities in the optical flow can help in segmenting images into regions that correspond to different objects.

The cameras used for the stereovision system were two Prosilica™ GC640 cameras connected via Category 5 Ethernet to a computer which stored the grayscale intensity images sent from the camera system. The two camera stereovision based approach was abandoned after testing revealed lighting and imaging issues associated with calibrating two independent cameras to operate in a dynamically lit scene. The background image pixel intensities could not remain static between the two cameras or individually for each camera, which made the background subtraction of image data not associated with the cow, such as the walls and floor, difficult. Instead, the stereovision system was altered to operate with a single Prosilica™ GC640 camera so that a single set of camera adjustments and parameters needed to be considered. This reduced the

58

problems associated with having to perfectly align the setup conditions of two cameras, which had become repetitive manual adjustments to both cameras and to the camera operating parameters.

System automation was realized by allowing the optical flow processing to have complete control over data collection. The software would monitor the central horizontal row of pixels from one frame to the next in order to determine if a moving object was present in the scene. Data recording would start when significant change in pixel values occurred in this monitored region and data recording would stop when pixel values remained consistent in this monitored region from one frame to the next. The optical flow processing method used worked adequately, but there were alignment and data collection errors in the image merging process that could lead to miscalculating BCS. The most important area of the cow's body for scoring lay around the tailhead region. In some images, the switching of a tail or erratic twist of the cow's body caused the tailhead region of the resulting image to not accurately portray the true body contour. The prominent issue with the optical flow process was the fact that data recording would occur when no object was present in the scene. The highly sensitive nature of the pixel value monitoring scheme meant that the slightest change in pixel values for the monitoring region would cause the system to record multiple false samples where no cow was present. Simple water and other fluid movement across the alleyway floor gave rise to the floor being too much of a reflective surface for the automation process chosen. This reflective surface caused pixel values in the intensity image to change as the fluid moved, which would cause the system to record unnecessary data samples.

The alternative approach was to instead use a light source of a constant value for which to monitor for optical flow. A laser light source along with a textured, plastic diffraction medium that changed the point-source laser beam into a stripe, was incorporated in order to cast a stripe of the laser beam onto the floor perpendicular to the direction of cow motion through the walkway. In this manner, when the field of view beneath the laser stripe is empty, only a straight line is seen. Once a cow enters the field of view and the straight line of laser light is obstructed by the cow body to create a curved line of laser light, the data collection begins. When the laser light returns to a straight line in the monitoring region, the data collection stops. By incorporating the monitoring of the change of the laser light line for system automation and data collection, the system had now become a structured light system. The goal by doing this was to have the capability of creating a 3D contour map of the cow's body still using optical flow to automate the process, but now monitoring the shift in the constant intensity value laser line in order to automate data recording. In order to achieve this, three 7mW, 750nm lasers were added to the system. This system can be seen in Figures 3.1-3.2.

The use of this laser light source did significantly reduce the number of false data collections, but it did not eliminate them. It did not, however, reduce the optical flow image merging errors as had been expected. The cow contours still did not adequately reflect the true outline of the cow body. The recording of multiple cow also occurred on occasion as well as missed recording if a cow went too fast across the image scene. Due to these continued errors with using an optical flow based approach, eventually it was decided to abandon this approach and to instead search for a different camera and machine vision process.
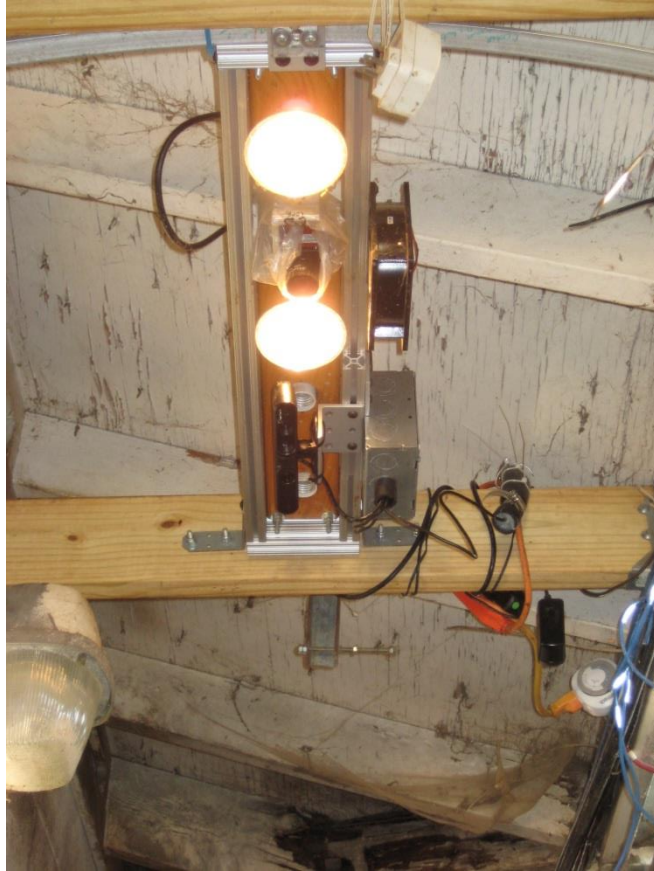
Figure 3.1 – BCS systems shown (side view).
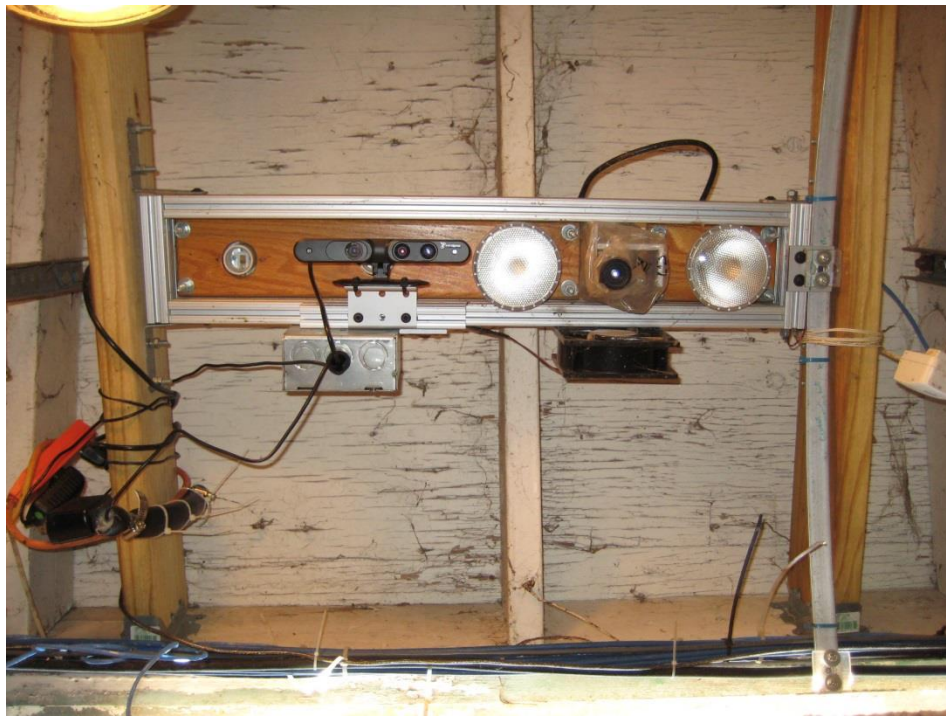
Figure 3.2 – BCS systems shown (view up from image scene).

3.4 Final System Architecture Design

The final system architecture design utilized for the automated BCS system research incorporated the use of a PrimeSense™ Carmine 1.08 RGB+depth sensor. The use of a structured light camera system that employed the use of a calibrated light pattern that illuminated the entire scene greatly enhanced the quality of samples collected. Instead of relying on pixel intensity values to change, this system could use its depth channel to monitor for foreground movement. Therefore, if an object moved across the scene that had a closer distance to the camera than the concrete floor, then it would trigger data collection. This camera also greatly reduced the problem of creating a depth map of the cow body. With the Prosilica™ camera, the software would have to create an accurate merged image model of the cow contour first and then involve computationally time expensive algorithms in order to resolve the depth map of the cow contour. With the PrimeSense™ camera, the incorporation of an NIR laser structured light constellation of predefined points meant that the problem of depth mapping had already been defined in the design of the camera. Based upon the change in position of the constellation of infrared light points from the manufacturer's predefined known constellation mapping, the distance to objects in the scene from the camera sensor could be determined in real-time, with the camera sensor being rated at up to 60 fps operational speed.

The BCS system is shown in Figures 3.1-3.2. The PrimeSense™ camera was positioned in the walkway in the same location as the previous imaging device, but in such a manner that the horizontal direction of the camera was the axis of motion for cow to cross the scene and the vertical direction of the camera was the axis that was bound by the walls of the walkway. Therefore, the horizontal direction was 640 pixels in length

and the vertical direction was 480 pixels in width since these are the dimensions for the sensors of the PrimeSense™ RGB and depth cameras. The camera was mounted at a distance of 3.05m from the lens to the floor of the alley way. The camera was positioned at a distance high enough from the floor of the alley way that the entire width of the 1.03m wide alley way could be captured at the same height that the sides of the cow would rub against the wall on either side. This height averaged to approximately 1.5m from the camera lens to the back of the cow.

This camera system was setup to automatically start the data recording software at 4am and 3pm and to automatically stop the data recording software at 6:30am and 5:30pm. The lighting in the walkway was also controlled via the camera framing by a single lighting element that was designed to turn on and off at the same times as the software was via an electrical outlet timer. The data collected by the camera was sent to a computer in a separate building which houses the administrative office of the farm. The camera was connected to the computer via two 20m sections of Tripp Lite™ USB 2.0 Active Extension Cable (Tripp Lite, Chicago, IL). The USB 2.0 extension cables were needed as the distance from the camera to the computer was further than the 5m operating distance limitation of USB 2.0 cabling. The extension cable was connected to the camera via a USB 2.0 hub. The camera, lighting element, and USB hub were housed on an 80/20® aluminum frame which was fastened just beneath the roofing covering the walkway, and anchored into the walls on both sides of the walkway via truss joist anchor plates. The 80/20® aluminum frame also allowed for minute adjustments to the position of the PrimeSense™ camera in the three Cartesian axial directions of rotation ensuring

proper alignment of the camera with the walls and floor of the walkway and nominal positioning in height above the walkway to capture the full width of every cow.

Due to the physical restrictions of the walkway's dimensions and the PrimeSense™ sensor's capabilities and limitations, the entire length of cow could not be captured in a single image frame. Instead, software was developed to record data samples as the cow passed beneath the system. The software developed for this research recorded the initial background image data as the first image file of the sample. Then, it successively recorded alternating depth and texture, or RGB color, frames. The signals to start and stop recording were automated via the use of four truth lines in the image scene. A screenshot of the software with the four truth lines is shown in Figure 3.3.
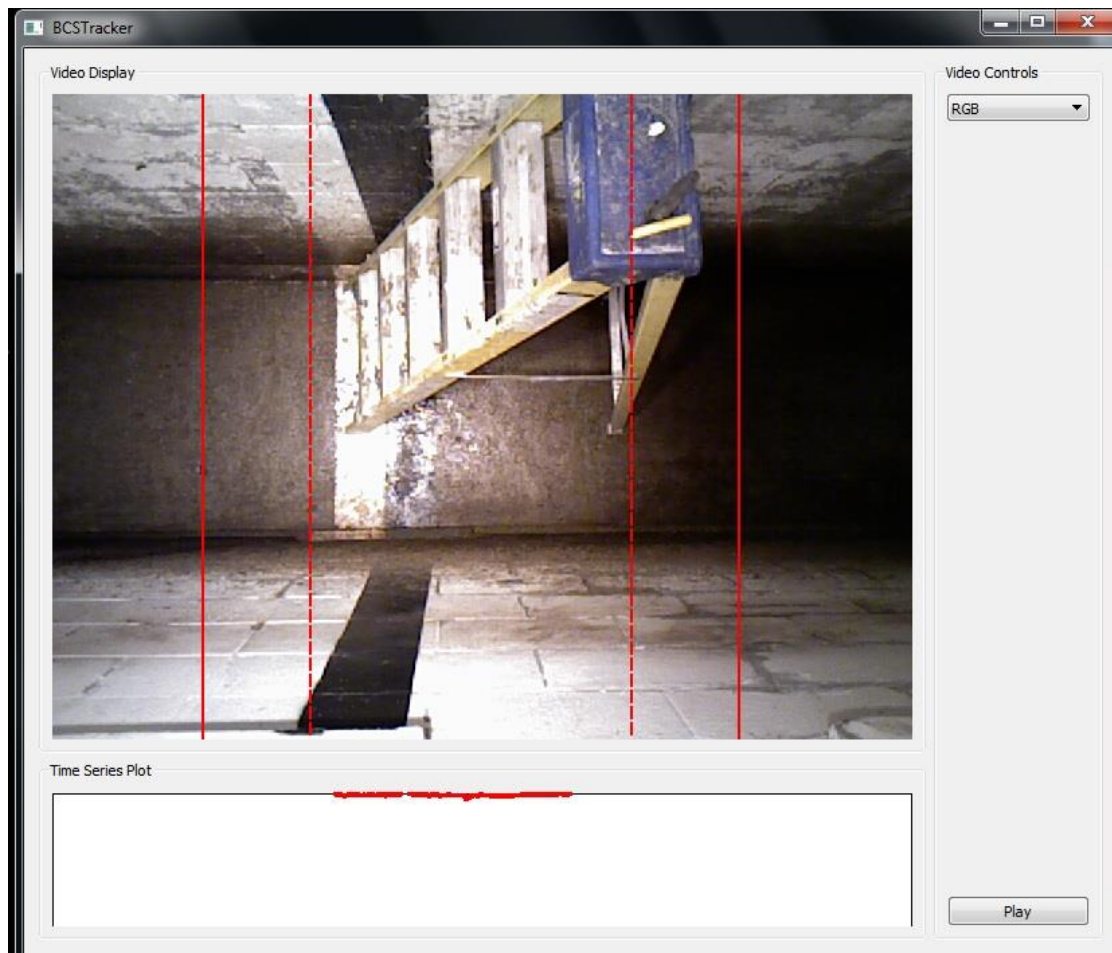
Figure 3.3 *– BCS software showing truth lines that start/stop recording.*

The cow always walks from the left side of the scene to the right side. The truth lines represent the number of pixels in that particular column with a depth less than the background or equal to it. If the depth value of an individual pixel in that column changes to a value less than the background depth value, then it is said to be "on" or equal to "1." If the depth value of the individual pixel does not decrease from the background depth value, then it is said to be "off" or equal to "0." When the pixel depth value is equal to the background depth value, it remains "off" and the answer to the question of, "Is the percentage of 'on' pixels greater than the threshold?," remains "false." Once the percentage of "on" pixels exceeds the minimum threshold, percentage required for that column, 5% in the software used for this study, then the question becomes "true" and its value is set to "true." When the number of pixels on in the first three truth lines reaches the minimum threshold, a data sample starts recording.

For this system setup, the minimum threshold for each truth line was 100 "on" pixels. The truth lines must be activated from left to right in order to properly record a data sample. As the cow moves across the scene, the fourth truth line becomes populated with "on" pixels as well. Eventually, the tail end of the cow passes the first truth line, which causes the number of "on" pixels to decrease below the minimum threshold needed and simultaneously causes the software to stop recording data for that sample. The cow continues to walk across the scene from left to right until all four truth lines return to values below the minimum threshold.

Once this occurs, the software is ready to record again once the initial recording condition is met. If the cow does not leave the scene before 300 depth and 300 texture frames have been recorded, the software is programmed to automatically stop collecting

data for that sample so that its file size does not become significantly large, as each image frame collected was 225KB in size. This limited the file size of a collected sample to 135 MB. With the software developed for this system and the data transfer speed limitation from the use of such a long section of USB 2.0 extension cables, the camera's operational speed was reduced to operate at 30 fps, which gave the cow 10 seconds to move across the scene. The average time for a cow to pass through the scene was greater than 1 second and less than 5 seconds with most cow passing through in approximately 2 seconds.

The use of 4 truth lines to initialize and cease data capture were a direct result of attempting to reduce the number of false data captures. The previous systems tested utilized only a single line of observation for the automation of the recording commands. Because objects of variously smaller sizes than the length of a cow could pass beneath the system, several recordings of objects not containing a cow were collected with these previously tested systems. The use of 4 truth lines ensures that only an object of sufficient size to represent a possible cow body in the scene can trigger the collection of data samples. As well, the use of a single line of observation was not able to determine if the animal in the scene was going in the correct direction for data capture in the walkway. With the setup of this system, all samples collected must have the cow walk in the same direction for data recording. Any animal going the reverse direction would lead to a sample that cannot be properly scored. The use of these 4 truth lines and having the software monitor the order in which they are turned "on" ensures proper data collection and a reduction in the size of data collected for any false samples obtained by a cow going the wrong direction in the walkway.

Incorporated in the depth images captured was a pre-determined background subtraction method. The automated background subtraction begins by building a background image over several video frames in real-time. The use of non-overlapping blocks of 1,200 camera depth frames was chosen for which to build the background image. The background image was then continuously updated to avoid the possible error of one particular background image affecting the data collection results for an entire milking data set. The background image acquisition began by filling a circular cue with the 1,200 most recent depth frames and then searching these 1,200 depth frames, on a per pixel basis, to find each pixel's supremum. Thus, if the depth frame sequence used to develop the background image included a cow walking across the field of view and at least one depth frame included the floor and walls of the scene, then there existed at least one depth measurement of the walls and floor in the background image stack. Pixels with a distance greater in length than any point on the animal were preserved by the supremum operation as background pixels. Any pixels less than that distance were identified as pixels associated with the cow body. Figure 3.4 shows an example depth frame and texture frame from the data collection. As can be seen in the depth image, the cow body is already segmented out from the background.
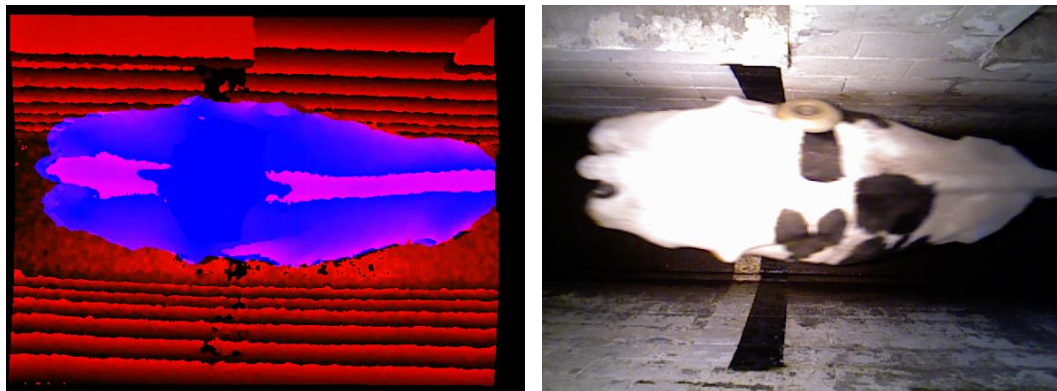
Figure 3.4 *– Example segmented depth frame and texture frame captured with the PrimeSense™ Carmine 1.08.*

67

In some situations, there existed some pixels that did not have at least one depth estimate over the depth frame sequence used for creating the background image. For those pixels, hole filling was performed in the composite depth image using a process of inpainting where pixel depth values surrounding the hole are copied into the hole locations. The next step of developing the background image involved the use of the image erosion process, which expands lighter shades of gray outward to mask neighboring pixels judged to be further away. In the PrimeSense™ depth camera sensor, pixels along edges in the scene tend to fluctuate between the frontside and backside of the edge, for which the supremum operation preserved the backside. The frontside edge was not accounted for in the composite image, thus applying the erosion operation preserved the frontside of the edge. The final step of building the background subtraction involved adding a threshold buffer to the background which subtracts values beyond a fixed distance from the sensor out of the depth image captured. Therefore, any pixels closer than this threshold were identified as cow pixels.

3.5 Automated BCS Software

The processing steps needed to convert the raw data samples into information that could be assigned a BCS value did not take place immediately after data sample collection. Instead, the samples were saved to disk by date and sample number and then later processed using MATLAB® where the data was loaded by date and sample number. The software could be ran for a single day and sample or for as many consecutive days and samples as desired. This flexibility was needed as the processing time needed to process the image data and generate a BCS for a single sample was approximately 3 minutes. With total daily recordings averaging 170 samples, it took several hours to

process a single day's worth of data. This allowed the computer's full processing potential to be focused on data collection during milking times and then shifted the emphasis to BCS generation afterwards when data analysis was more power and time efficient. As well, the samples as collected were not associated with cow identity. As the main goal of this study was to monitor the gradual change in BCS on a per animal basis, the samples needed to be reorganized by cow identification first. Therefore, immediately processing the samples after data acquisition would not have proved useful since this study was not as interested in real-time BCS scoring, as this has already been proven feasible, but instead was interested in the long-term view of BCS on a per cow basis.

In order to generate a BCS, the sample must undergo several processing steps. The first step was to utilize the last depth image of the sample to create a depth point cloud. In order to derive a value from which to determine a BCS score, the approach used in this system would need to next determine the difference between a smoothed cow body surface and the actual cow body surface represented in the depth point cloud. By finding the difference between the two surfaces, it can be estimated how much of the fat reserves are missing from the body condition. The process of determining the difference between a smoothed sample surface and the original sample surface is known in the study of aggregates as the angularity of the sample. With an aggregate, the surface of the material can be categorized based upon the smoothness of its surface. Smoothness is determined by fitting a smoothed curve against the angular surface of the aggregate sample. The differences between points along the smoothed surface and the actual surface are then taken with respect to the center of the aggregate sample. The total difference represents the amount of the actual aggregate surface that did not fit along this

idealized smooth surface. It can be determined from this missing aggregate material difference value just how angular the surface is of the sample.

If we refer back to the work of Halachmi et al.[63], it can be seen that aggregate angularity is practically the same manner undertaken in that study. Instead of using an aggregate, the 2D contour of the cow body is used as the sample. A fitted curve can then reveal how angular the cow contour is with respect to a smoothed version of the cow contour. In our study, the research expands upon this fitted polynomial approach into the realm of 3D. Instead of fitting a polynomial curve to just one position along the cow body, the process in this research fits a polynomial curve to every transverse cross-section of the cow body between the hips and tail.

If selected to undergo further processing, the data point cloud was then reorganized to align the individual data points with their nearest integer column value. This realignment of individual points allowed the data cloud representing the body to be dissected into unique transverse columns consisting of sufficient data to represent the cow's dorsal body curvature at that location, much like a computed tomography (**CT**) scan is capable of neatly dissecting the view of internal organs for better viewing at different distances through the body.

In order for an integer column value to be considered as containing a sufficient number of data points to properly construct a fitted polynomial curve, a lower minimum limit of 20 data points for each column was set in the software. The minimum limit ensured that columns containing only a few data points would not be able to insert erroneous fitted polynomial curve errors into the sample. As well, to ensure that the column being observed actually covered the entire width of the cow in the sample, a

lower minimum limit of 150 was set for the distance between the minimum and maximum row values of the data points observed for each candidate column considered. Now that each distinct column had a sufficient number of data points to accurately represent the curvature of the body, a curve could be fitted to the data points which represented the estimated curvature of a smoothly surfaced cow body. Examples can be seen in Figures 3.5-3.8 of these shifted data points shown as distinct cross-sections of the cow body with the collected 3D data points shown in red and the fitted polynomial data points shown in blue.
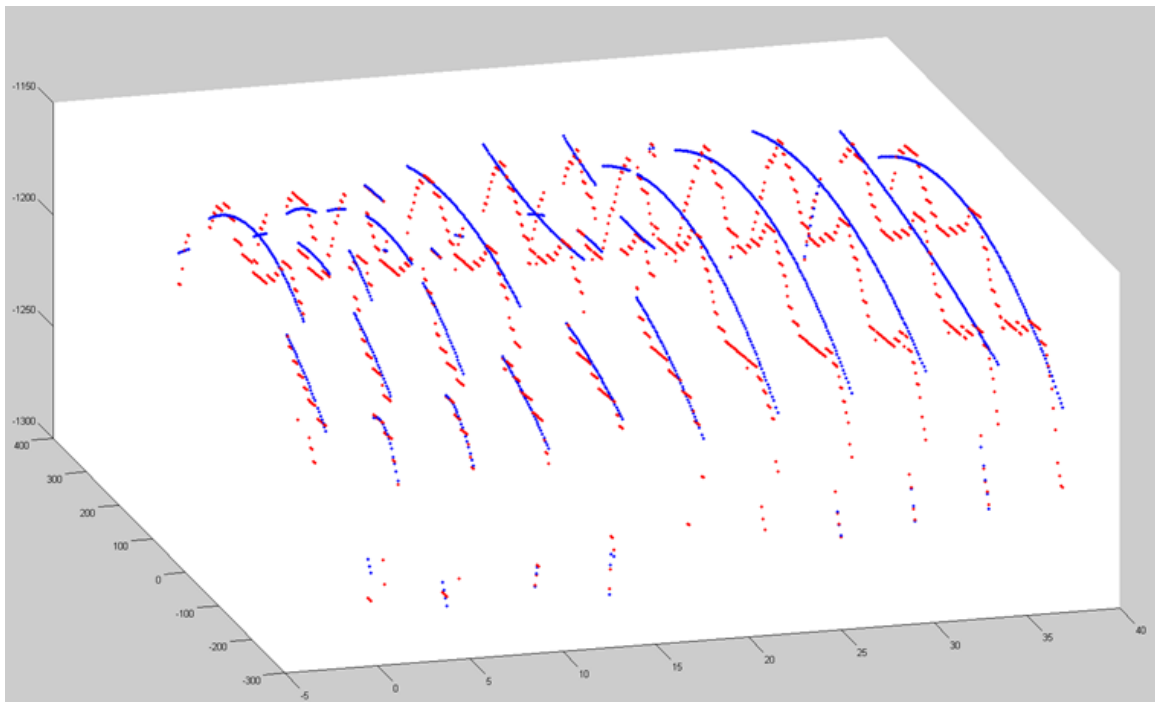
Figure 3.5 *– Transverse cross section example showing 11 distinct cross sections across the body of the cow for data points in the area around the hips of the cow body (red) and the respectively fitted parabolic curves (blue) for each of the 11 distinct cross sections.*

71
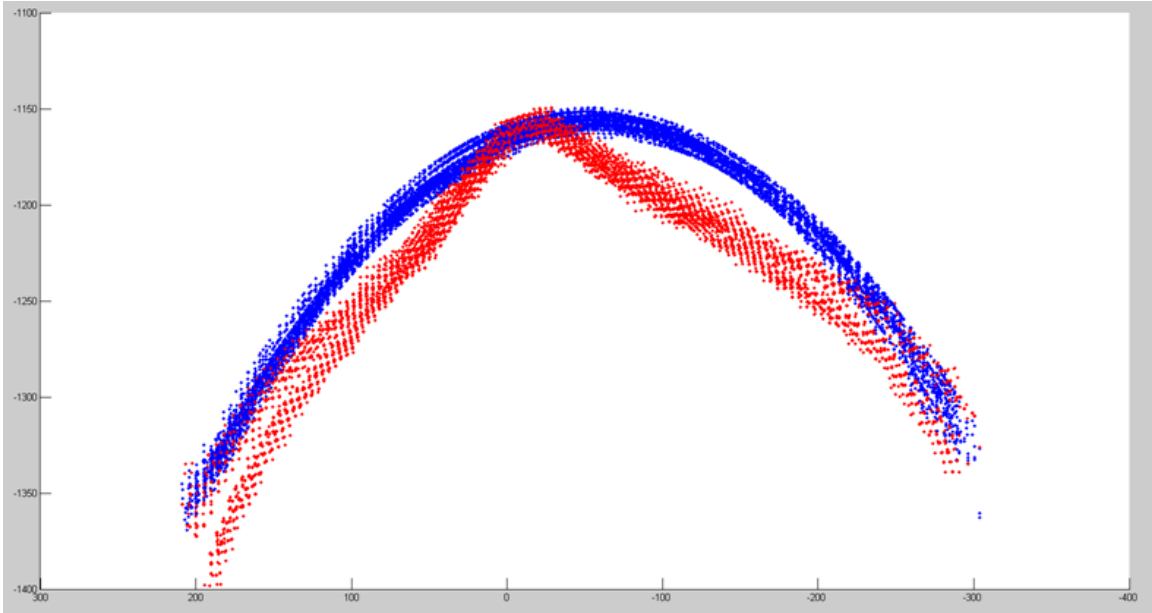
Figure 3.6 – *Cross section showing data points for the area around the shoulders region of the cow body (red) and fitted parabolic curves (blue) to these data points.*
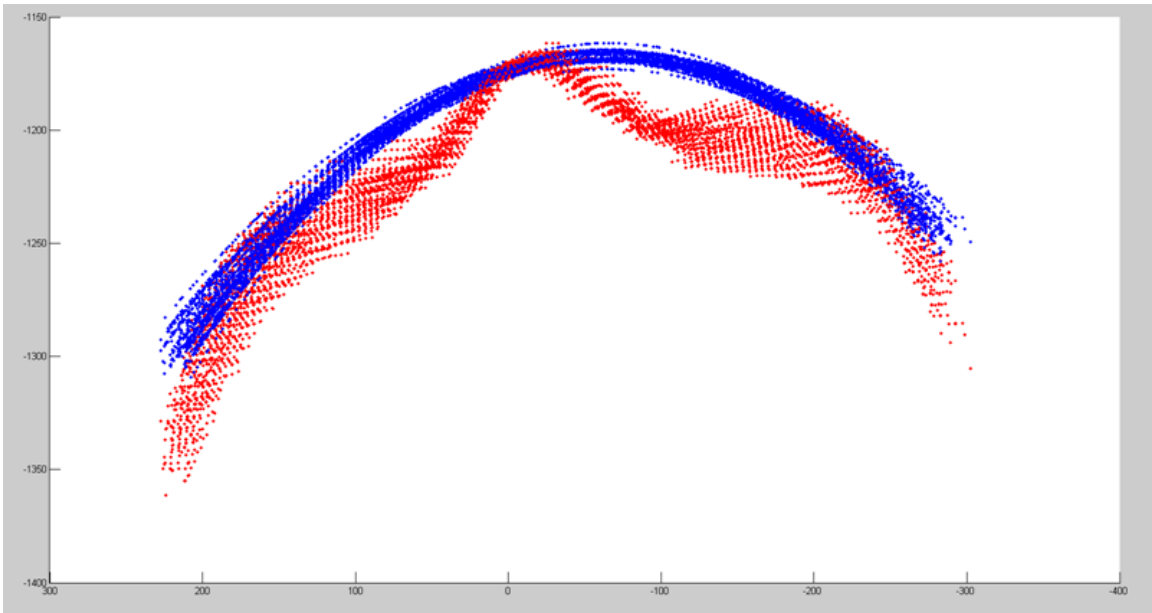
Figure 3.7 – *Cross section showing data points for the area around the hips region of the cow body (red) and fitted parabolic curves (blue) to these data points.*
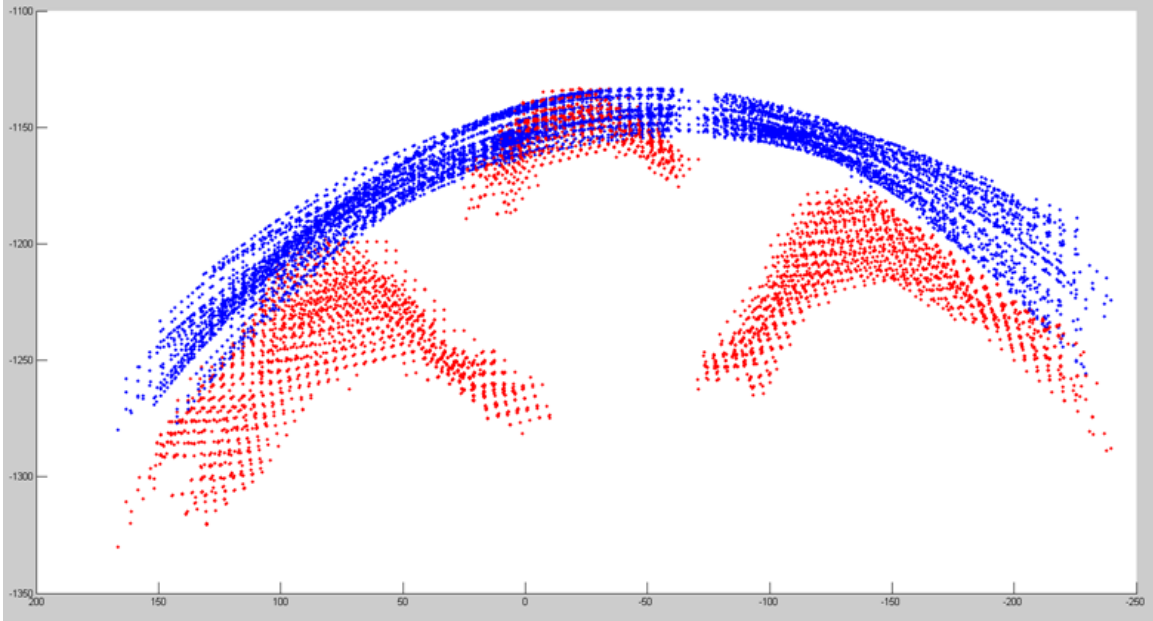
Figure 3.8 *– Cross section showing data points for the area around the tailhead region of the cow body (red) and fitted parabolic curves (blue) to these data points.*

The use of third-order polynomials was selected for the curve-fitting process. A higher order polynomial was too unstable to accurately represent the cow body curvature along the various transverse cross-sections of the cow body and a lower order polynomial was not able to accurately follow the unsymmetrical curvature across the cow body. The difference between the fitted polynomial body curve data points and actual body curve data points was then determined, which represented the lack of possible fat reserves that could have been fitted into that region. The absolute value of the deviation for each data point, i, along the cow contour, c, from the fitted parabola, p, along a single column, d, is expressed in Equation 3.1.

$$d = \frac{1}{N} \sum_{i=1}^{N} |c_i - p_i| \tag{3.1}$$

The value of N is only dependent upon how many data points exist for the current column under inspection. Equation 3.1 is also known as the mean absolute error (**MAE**) for that column.

73

Example output point clouds with the original data points shown in red and the fitted polynomial data points shown in blue can be seen in Figures 3.9-3.13 where the full set of data points are shown on the left side of the image and the reduced set of data points used for BCS scoring are shown on the right side of the image. Several possible bad candidate samples for BCS scoring are shown as well as samples of ideal point clouds which the software moves forward for scoring.

Figure 3.9 and Figure 3.10 show example point clouds where some excess tail data points are shown. The extra points of the tail are removed by setting a minimum difference of 150 on the minimum and maximum row values, along the y-axis, at each transverse cross section column value, along the x-axis, less than 0. Since the data points of the tail do not meet the criteria for minimum difference for column values less than 0, they are removed. The reduced data point clouds shown on the right side in Figure 3.9 and Figure 3.10 provide examples of ideal samples that move forward for further processing.

Figures 3.11-3.13 show example data point clouds where the data does not include the appropriate cow body region necessary for BCS scoring. The software recognizes the point cloud of Figure 3.11 as a bad sample because several of the first data points encountered have y-values that are at or 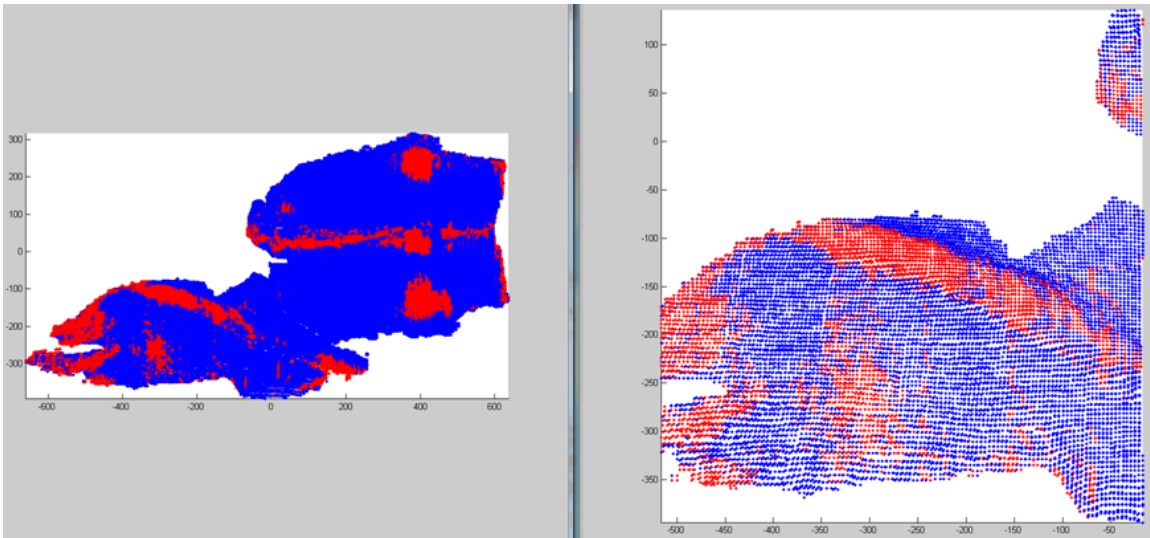exceed 200 pixels left of the 0 pixel y-axis $(y \geq 200)$. The software recognizes the point cloud of Figure 3.12 as a bad sample because several of the first data points encountered have y-values that are at or ex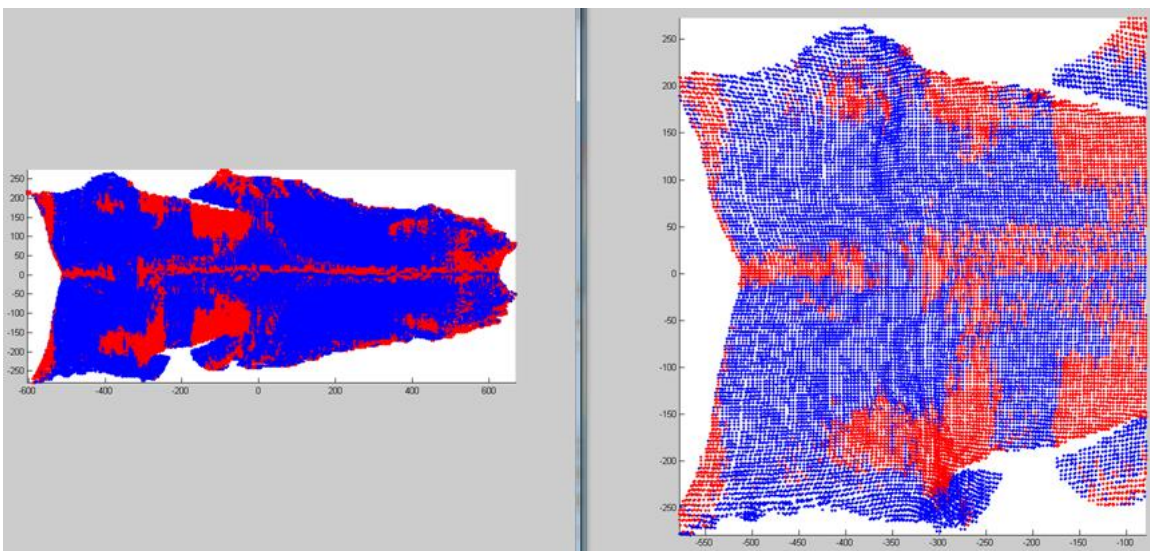ceed 200 pixels right of the 0 pixel y-axis $(y \leq -200)$. As well, there are multiple cows in the sample. Since the alleyway is only wide enough for one cow at a time to proceed through, the rear cow must nudge the front cow to move forward, which is typically done

by the rear cow pushing on the left or right side of the front cow. This requires the rear cow to move its body to the far left or right of the image scene, thereby exceeding either the left or right y-value limits of the software ($-200 \leq y \leq 200$). The software recognizes Figure 3.13 as a bad sample because several of the first data points encountered have y-values that are at or exceed 200 pixels either left of the 0 pixel y-axis ($y \geq 200$) or right of the 0 pixel y-axis ($y \leq -200$). Just as is shown in Figure 3.13, this is an excellent indication that the sample has stopped data collection mid-cow and has not collected the appropriate data points around the rear region of the cow. By allowing the software to be able to determine good and bad samples for further processing on its own, this allowed the system to be even more autonomous and to save processing time.
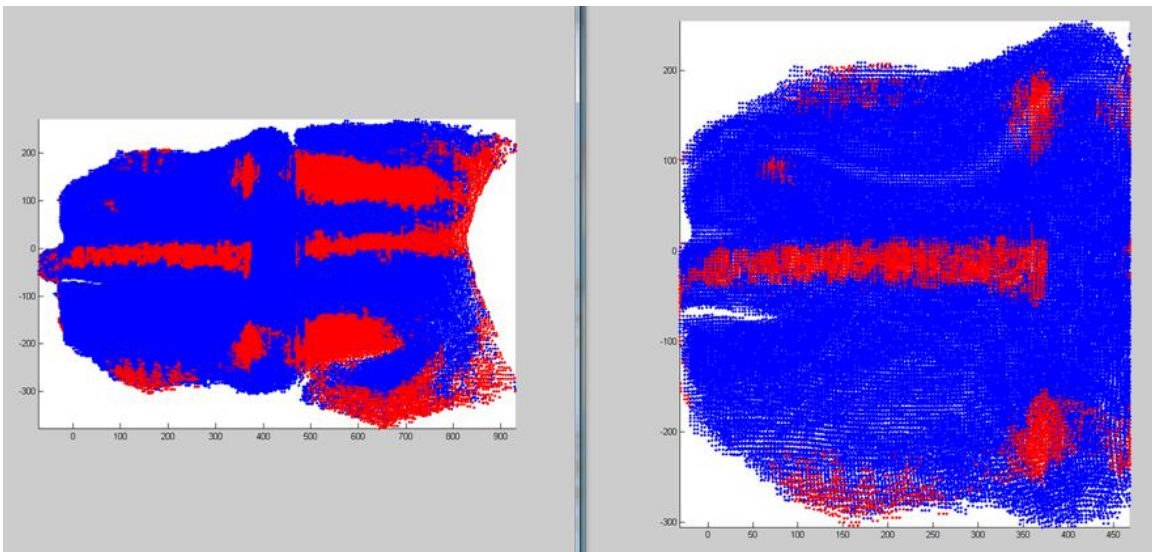
Figure 3.9 *– A full data point cloud is shown (left) and the reduced data point cloud with tail data points removed shown (right) for which a BCS value is to be determined.*
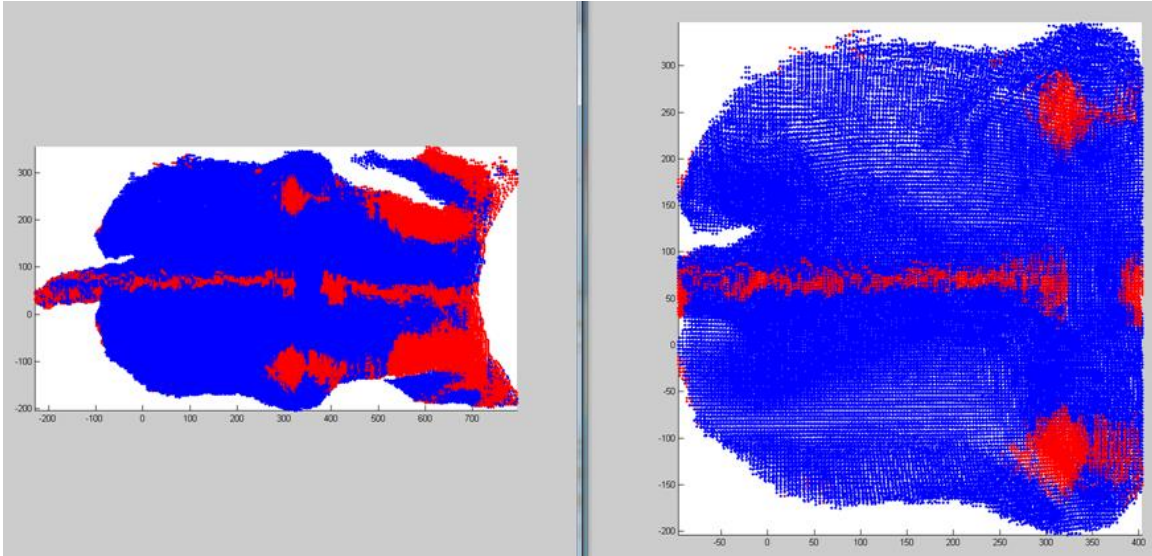
Figure 3.10 – *A full data point cloud is shown (left) and the reduced data point cloud with extended tail data points removed shown (right) for which a BCS value is to be determined.*
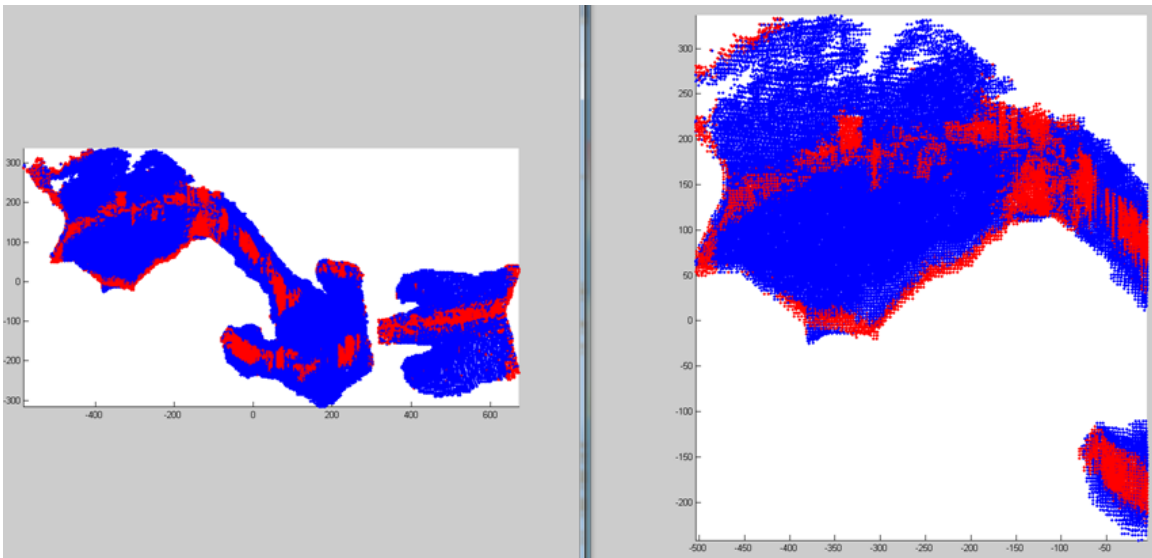
Figure 3.11 – *A full data point cloud is shown (left) and the reduced data point cloud (right) for a bad sample in which several of the first data points encountered have y-values that are at or exceed 200 pixels left of the 0 pixel y-axis (y ≥ 200).*

76

Figure 3.12 *– A full data point cloud is shown (left) and the reduced data point cloud (right) for a bad sample in which several of the first data points encountered have y-values that are at or exceed 200 pixels right of the 0 pixel y-axis (y ≤ -200).*

Figure 3.13 *– A full data point cloud is shown (left) and the reduced data point cloud (right) for a bad sample in which several of the first data points encountered have y-values that are at or exceed 200 pixels either left of the 0 pixel y-axis (y ≥ 200) or right of the 0 pixel y-axis (y ≤ -200).*

The last step of the automated BCS software was to derive a computer generated BCS value using the MAE values derived for a sample. In order to do so, the range of columns to be included in the scoring had to be specified. Since data points beyond the hips region of the cow are not necessary for derivation of BCS, we simply specified a

77

column range limit which generally falls within this region. Therefore, the first column containing 20 data points or more was assigned to be the minimum column value, minimum x-value column. From this column, the software then moves forward, in the positive direction along the x-axis, 499 more columns, for a total of 500 columns of data points included in BCS derivation. The right side of Figures 3.9-3.13 include this cutoff 500 column range in the plots shown.

The specification of 500 columns was chosen rather than integrating software to search for the hips because developing such software was deemed too computationally time expensive for this system. Identifying the data points associated with the hips in the point cloud can also be rather subjective when determining where the cutoff is to be located. By specifying a predetermined large column cutoff value, the software is capable of including all of the columns across the length of cow from tailhead to hips in order to arrive at a final value that represents the total error difference between the smoothed cow body contour and the actual body contour within this region.

Following the same logic as outlined in the work by Halachmi et al. [63], if a cow is fatter, her body shape is more likely to be round and therefore the parabola might fit the cow's shape better and the MAE would be smaller. Conversely, if a cow is thin, her body shape is less round and the MAE is larger. The deviation from a parabola for each integer column value along the length of cow from tailhead to hips is calculated and stored in a vector. Once all MAE integer column values have been determined, then the software calculates the sum of all of the individual MAE values, d, to arrive at a total MAE, represented by A in Equation 3.2. N, which represents the number of columns summated, is generally anticipated to conclude at some value less than or equal to 500,

with the vast majority of samples able to be scored attaining the 500 column cutoff length.

$$A = \sum_{i=1}^{N} d_i \qquad (3.2)$$

A is then used by the software to derive a computer generated BCS value by means of Equation 3.3, where S represents the computer generated BCS determined.

$$S = 7.9434 * (A^{-0.467}) \qquad (3.3)$$

Equation 3.3 was derived by the empirical analysis of human BCS values as observed against the total MAE, A, values derived. The determination of S came about after comparison of several models of fit for the data of A versus human BCS. The research conducted by Bewley[10] also determined that a non-linear relationship may be a better model fit than the linear model derived in that study. The analysis of our research concluded the same results, arriving at a non-linear power model representation of the data as the best fit.

The BCS was generated in the same manner for every sample collected from April 1, 2014 to November 7, 2014. The samples were further analyzed on a per cow basis, viewing the variability of the BCS over time for both human visual scores and the computer generated scores. Over this observational time period from April 1, 2014 to November 7, 2014, three independent human scorers manually scored every cow in the herd once a week on the same day when possible or at most within a few days of one another. One of the manual scorers was able to consistently score the herd on the same day and at the same time throughout the study. There were occasions where only this scorer or only 2 of the 3 scorers were available to score within a week timeframe, but the fact that this scorer remained consistent throughout the study ensured that the human

visual scores did not have any gaps or inconsistencies in the data. These once weekly, manually derived BCS values were collected in order to have a known set of reference values for which to compare the computer generated BCS values against on a per sample basis.

Variations existed between the independent human scores due to the inherent subjective nature of BCS. It was therefore decided to average the human scores for each week together in order to mitigate some of the subjective nature of the scoring. Therefore, if one of the scores differentiated from the others by a value of 0.5 or greater, then this value was rejected from averaging as human scoring error was present in this independent score and instead only two values were averaged together. If all three values were spread from one another by 0.5 or greater, then the scores from the previous weeks were reviewed to see which of the scores most closely matched a logical BCS value determination for that week. The manual BCS scores of the three independent scorers were saved in a matrix arranged by date and cow ID. These manual BCS values were initially collected outside of the software, so the manual scores matrix in the software had to be updated by user input.

The software had been written to account for this user input, and therefore automated to be able to autonomously select the associated date of manual BCS values from the manual scores matrix to compare to the computer generated BCS values. The manual BCS values were then plotted against the computer derived BCS values over the entire observation time period of testing and analyzed. Shorter time frames could have been comparatively analyzed, but again, the main goal of this study was to determine if it

was possible to observe the gradual change in body condition of every individual cow in the herd over an extended amount of time.

3.6 Automated BCS System Results and Discussion

Over the seven month data collection period, a total of 116 unique cow were examined at various stages of lactation and body condition. The plots of the manually derived BCS scores versus the computer derived BCS scores over time can be seen in Appendix A. The results show similar trends of change for both manual and computer derived BCS values for each cow over the entire testing period. The most notable major difference was that for the majority of animals tested the computer derived BCS values changed gradually and relatively smoothly over time whereas the averaged human BCS values tended to exhibit erratic changes over time. These results indicate that the computer-generated BCS values may be more reliable than human BCS values, but further investigation was necessary in order to reach any conclusion with certainty.

Figure 3.14 plots the computer-generated BCS values derived with the autonomous system compared with the averaged human BCS values. An ideal mapping would achieve a parity, $\hat{y} = y$ or $y = x$, between the two scoring methods. The system developed in this research achieved a linear model fit shown in Equation 3.4.

$$y = 0.519x + 1.344 \tag{3.4}$$

Although parity was not achieved, the linear model fit does justify a strong model fit between the human BCS values and the computer-generated BCS values.
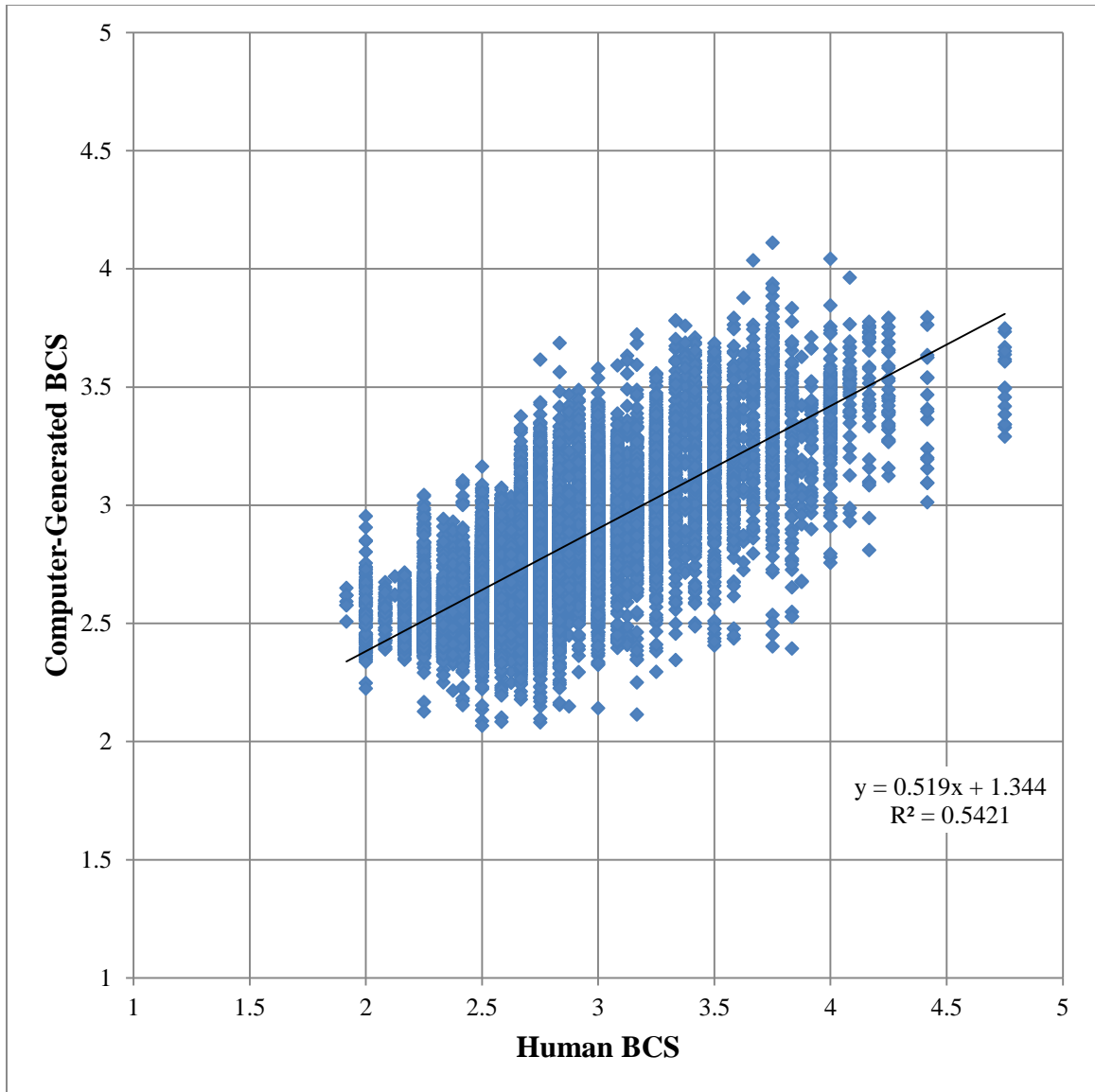
Figure 3.14 – Human BCS versus computer-generated BCS results.

Figure 3.15 plots the computer-generated BCS residual values against the human BCS values. Table 3.1 shows the residuals for the computer-generated BCS when compared to the human BCS.
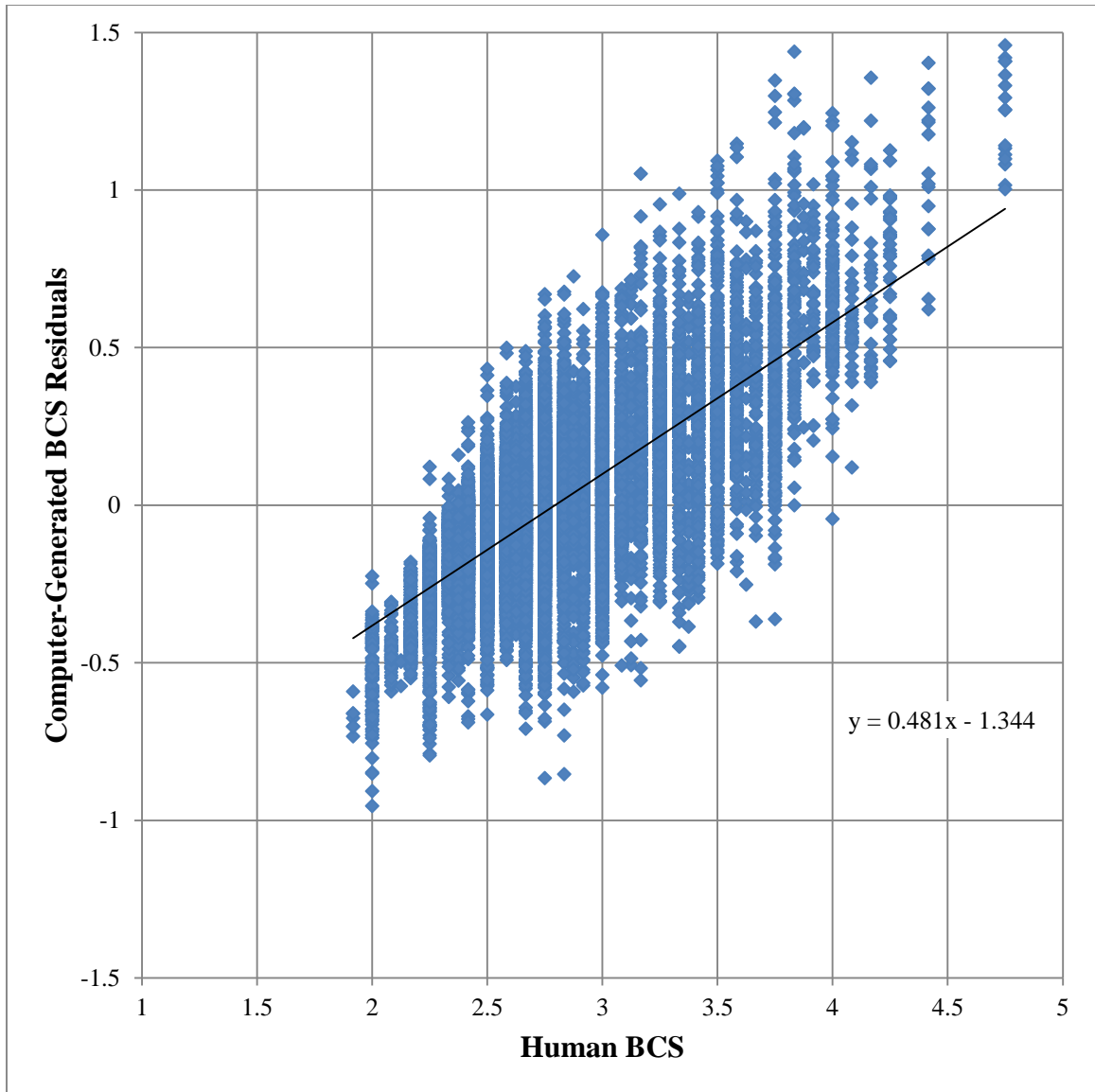
Figure 3.15 *– Human BCS versus residuals of computer-generated BCS values in comparison (y-ŷ).*

Table 3.1 – Residuals analysis for the automated BCS system samples dataset[1]

BCS Residual	Total	Per Division	Total (%)	Per Division (%)
≤ 0.1	6258	6258	33.80	33.80
≤ 0.15	9029	2771	48.76	14.96
≤ 0.2	11386	2357	61.49	12.73
≤ 0.25	13212	1826	71.35	9.86
≤ 0.3	14598	1386	78.84	7.49
≤ 0.35	15696	1098	84.77	5.93
≤ 0.4	16438	742	88.77	4.01
≤ 0.45	16985	547	91.73	2.95
≤ 0.5	17389	404	93.91	2.18
≤ 0.55	17677	288	95.46	1.56
≤ 0.6	17889	212	96.61	1.14
≤ 0.65	18029	140	97.36	0.76
≤ 0.7	18154	125	98.04	0.68
≤ 0.75	18238	84	98.49	0.45
≤ 0.8	18312	74	98.89	0.40
≤ 0.85	18352	40	99.11	0.22
≤ 0.9	18395	43	99.34	0.23
≤ 0.95	18420	25	99.48	0.14
≤ 1	18440	20	99.58	0.11
> 1	18517	77	100.00	0.42

[1]*Residual values for computer-generated BCS compared to human BCS. Second column is the total number of samples at or below the respective BCS residual value. Third column is the total number of samples greater than the previous BCS residual value listed and the respective BCS residual value. Fourth column is the total percentage of samples at or below the respective BCS residual value. Fifth column is the total percentage of samples greater than the previous BCS residual value listed and the respective BCS residual value.*

It can be seen from the above residuals plot and table that the automated scoring system

developed in this research has a slightly positive trend with increasing BCS value and

that the error range is within the range of previously developed systems whose residual BCS error was within 0.5 on the 5-point BCS scale. The fully automated system tested achieved scores within 0.5 on the 5-point BCS scale for 93.91% and within 0.25 on the 5-point BCS scale for 71.35% of the 18,517 samples that were able to be scored. The research by Bewley[10] achieved scores within 0.5 on the 5-point BCS scale for 100% and within 0.25 on the 5-point BCS scale for 89.95%.

The results of our study indicate that the automation process of our system could use some refinement. While the results are promising in terms of the plausibility of a fully automated BCS system, further research into data sample preparation for scoring must be conducted. It is our determination that although the accuracy of our automated system is reliable, a higher precision is compulsory. In order to achieve this higher precision, a trade-off between the amount of data collection and software processing speed may be necessary. Viewing a moving average of the BCS on a weekly or twice weekly basis instead of a daily or twice daily basis should remove the majority of variation in scores seen as well as provide a more reliable analysis of the gradual change in individual cow BCS over time. Additionally, the use of more seasoned and consistently reliable human visual BCS scorers as opposed to novice scorers could greatly benefit the comparison index between human and computer generated BCS values.

During the observational period, the DIM for each individual cow was also recorded. By comparing the DIM to the BCS, the change in BCS over the lactation cycle could be monitored. Instead of viewing these changes on an individual cow basis, the entire sample data set was utilized. In this manner, we could observe a statistical average

BCS value as it correlates to DIM and vice versa. A histogram of the total number of

individual cow samples at a particular DIM is shown in Figure 3.16. The resulting plot of

BCS with respect to DIM can be seen in Figure 3.17 for the computer-generated BCS and

in Figure 3.18 for the human BCS, respectively.
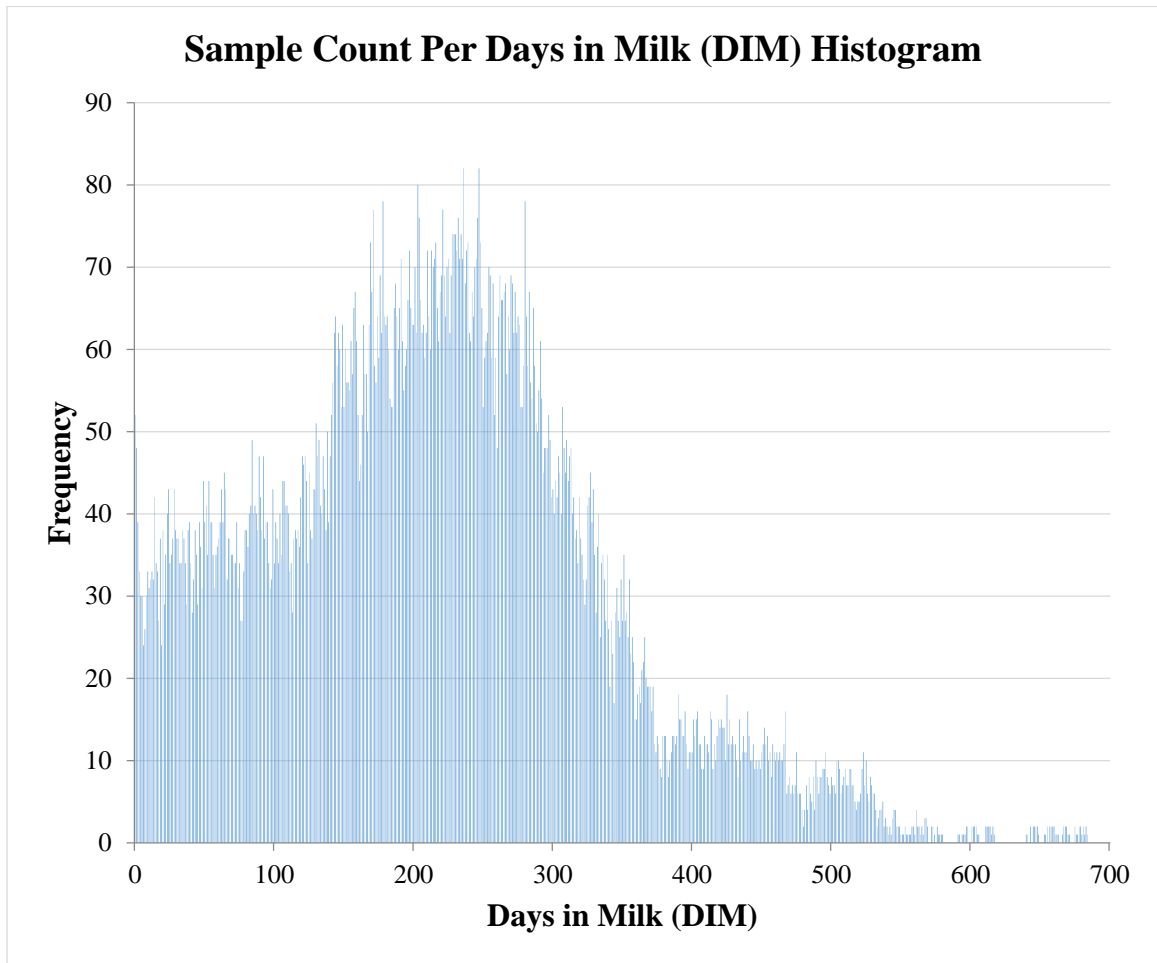
Figure 3.16 – *Histogram counting the number of samples in the data set per DIM.*
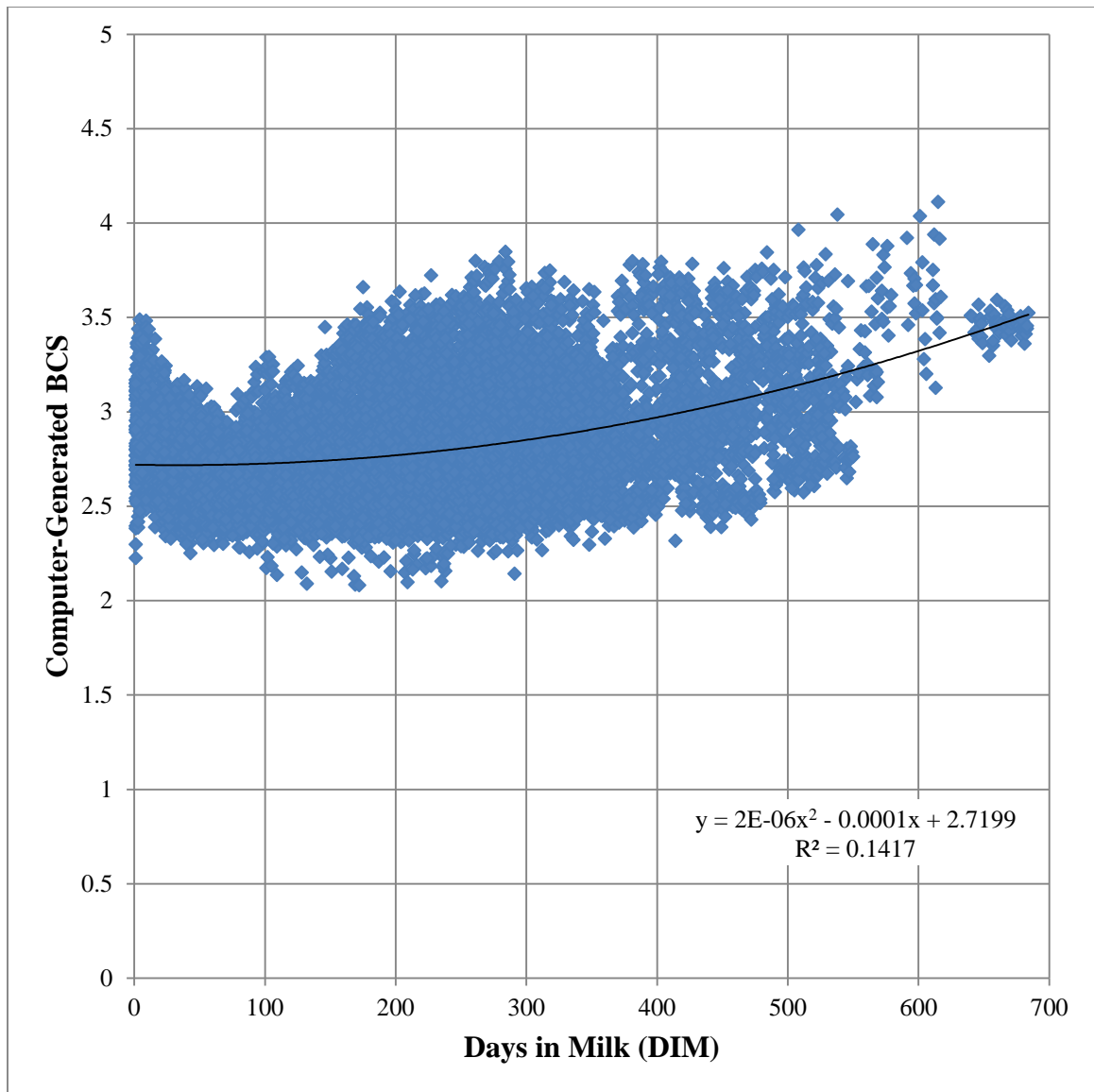
Figure 3.17 – DIM versus computer-generated BCS.

The plotted equation reads: $y = 2\text{E-}06x^2 - 0.0001x + 2.7199$ with $R^2 = 0.1417$.
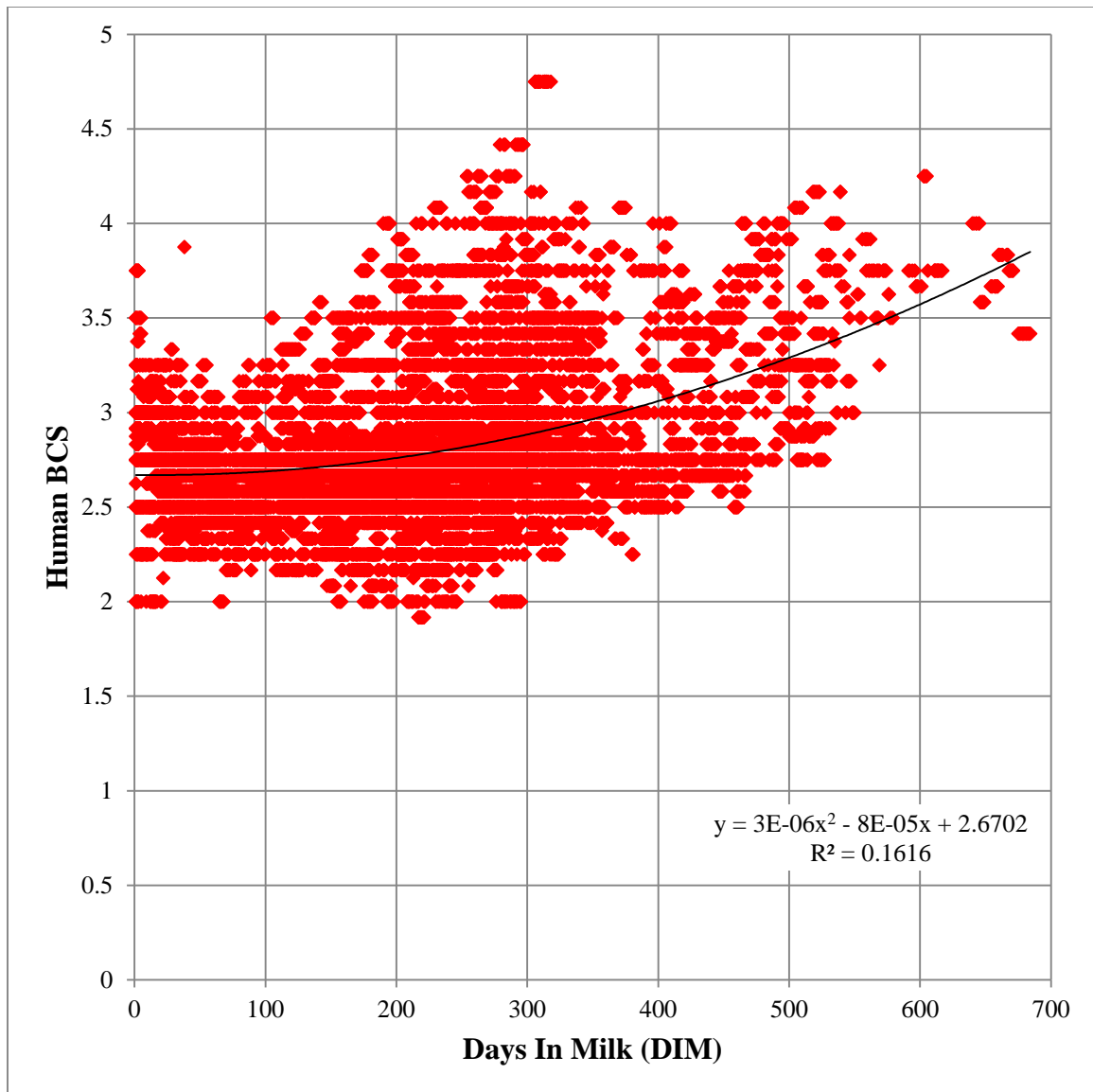
Figure 3.18 – *DIM versus human BCS.*

As can be readily seen in Figure 3.17 and Figure 3.18, the two plots show a similar trend in the data. These observed trends are as expected based upon previous research into the correlations of BCS, body weight, and DIM. During the first few months of the lactation cycle, known as early lactation, the body fat reserves are utilized by the cow to produce milk. This causes the body weight of the cow to decrease, and therefore the BCS value decreases as well. During the next stage of lactation, the mid-

lactation stage, the amount of milk produced by the cow begins to steady and so does the amount of body condition on the cow. During this stage, the BCS of the cow will reach its minimum expected value as the amount of available body fat reserves that can be converted into milk production are at their lowest. Towards the end of this stage, the cow will begin to rebuild body fat reserves as her milk production begins decreasing. The late lactation stage which is exhibited next by the cow is indicative of further decreasing milk production which leads to increasing body fat reserves and BCS scores. The last stage of the lactation cycle is the dry period when the cow does not produce milk. During this stage, the cow continues to accumulate body condition in expectation of the next upcoming lactation cycle. The highest BCS values expected for an individual cow can be seen in the latter days of the dry period.

In Figured 3.17-3.18, these stages are exhibited by the shape of the data. The initial days of the data show a decrease in average BCS with an increase in the number of DIM, followed by a steadying off of BCS at its lowest values, and then followed by a steady increase in BCS for the remainder of the DIM. Therefore, this plot shows that the BCS values generated by the automated system can be monitored over the lactation cycle of the individual cow in order to monitor whether or not the cow is exhibiting the expected body condition. If not, then corrective measures can be taken early to avoid possible losses in future milk production.

Additionally, these DIM plots show that the computer-generated BCS was far better than the human BCS. Whereas the DIM versus human BCS shows quite erratic correlation, the DIM versus computer-generated BCS shows a clearly distinct trend. These results further reinforce our assumptions that the human scoring during this data

collection period was not consistently reliable; an assumption already anticipated as the human BCS system is much more subjective than quantitative, where animal pose and scene lighting can greatly influence visually based scoring. Future testing and validation of such an automated BCS system must be done so along with expert human BCS scoring in a controlled environment or other consistently reliable scoring means incorporated.

3.7 Conclusions

The research conducted in this study was able to develop a fully automated BCS scoring system with no user input. With this research, the system is left to operate on its own with automated system turn on and turn off. As the cow walks past the camera, it begins to record the data for the sample. Once out of the field of view, the recording automatically stops. Then, the processing of the sample to create a depth data point cloud for scoring is automatically conducted. Once this point cloud has been created, the system then automatically scores the body contour of the cow represented in this point cloud in order to assign a proper BCS and stores this score in the software for further review. Every aspect from data collection to BCS scoring was automated with the only user input being the cow number and timeframe selected for viewing. In this study, the entire timeframe of observational data collection was reviewed, but shorter timeframes could also have been reviewed by a user of this system. In situations where a significant change in BCS has occurred, such as an illness or change in eating habits, the short-term history of that cow can be observed in order to identify when the change began and how it changed.

The results display the ability of the computer automated system to accurately and smoothly detect subtle changes in BCS over time much better than human visual scoring

by three independent scorers. Whether these changes occur in a short-term or long-term frame of reference, it is extremely beneficial to be able to monitor sub-0.5 point changes in BCS. Because scoring variability still exists in the BCS values produced by the software, it is advisable to use the average change of BCS values over time instead of independent samples as a guide. The inherent freedom of movement for the cow and the workflow in the system allows the cow to move through the imaging scene as it wishes. This freedom of movement can impart variably small error into the results as the kinetic nature of the cow body in the region of the thurl, between the pin and hook bones, slightly alters the shape of the cow body from one frame to the next and from one sample to the next.

Future studies should look at the possible inclusion of gait analysis of cow in consideration of data collection for freely moving animals. Observing the motion of the rear region of the cow could provide insight into how to address the influence motion of the cow across the scene may have on data collection and results. Not only could gait analysis benefit the accuracy of a BCS system, but it is also another precision dairy farming topic that can help to give a better understanding into the health of individual cow. Future versions of this system would benefit from the inclusion of a method of fully automated cow identification, whether it be based upon RFID technology, machine vision techniques, or a combination of the two. Fully automated cow identification was not used in this research as the researchers desired to manually inspect every image of the entire data set in order to ensure that correct cow identification was made in every sample.

CHAPTER IV: POTENTIAL FOR IMAGING BASED AUTOMATED

DETECTION AND RECOGNITION OF INDIVIDUAL DAIRY COW

Various precision dairy farming systems incorporate the use of cameras in their data collection needs which operate on the basis of image processing.[10,62,63] These metric monitoring systems can further be classified into those that use 2D cameras and those that use 3D cameras. The realm of 2D camera systems include color, grayscale, or other such gradient color imaging scales. The realm of 3D camera systems includes cameras which solely operate with depth mapping information and those which can also collect 2D colorized data.[66,67,68,69,70,71] Most of these camera technologies require some human input or they rely on rudimentary techniques as to when to start and stop data collection. Because of this, such camera systems are not fully automated or they fail to properly collect data.

Along with automated animal presence detection for data collection, a machine vision based system should also incorporate automated individual dairy cow identification, which is essential in the adoption of precision dairy farming technologies. The currently prominent method of identification is via RFID. Automated machine vision individual cow identification is based solely upon the 2D image data acquired by the camera. An example machine vision system already in use that could benefit from this imaging based identification would be the DeLaval™ (DeLaval, Inc., Tumba, Sweden) BCS scoring system.

The RFID of each single head of cattle is already mandatory in many countries for some species.[72] The United States does not yet require this mandatory identification, but is under competitive pressure to develop identification programs to serve its livestock

industries as several countries continue to work towards an international harmonization of identification processes.[73]   The reliability of an RFID traceability system for livestock applications depends on 2 main factors: the persistence of the tag on the animal and the readability in different conditions in the stable.[74] The majority of these technologies are stand-alone monitoring systems that require little to no input from humans.   Those monitoring systems that are isolated from the cow, at some distance away from the cow, often utilize RFID sensors and readers in order to keep track of individual cow in the data samples collected.

The identification accuracy rate of stand-alone RFID has been consistently tested to be well over 95%, with some estimations as high as only 1 read error for every 1,000 animals.[33,75]   Although RFID is fairly robust, it is not without error and operational limitations.[76,77,78]   RFID read errors may result from tag-to-tag collision, short reading distance, low reading rate, dense tag environment, and electrical noise.[79,80,81] Example RFID based systems include GrowSafe™ and Calan™ gates. RFID technology works best when sensors and readers are expected to cross paths only where arranged to do so and within a short range of one another. Because of this, misidentifications as well as missed identifications are possible, which can lead to incorrect storage of metrics data for the individual animal and invalid entries within the data collection system.[76,77,78] Though errors are few, they can inject erroneous results in data collection that may go unnoticed by humans utilizing the data. As well, there is no secondary system to verify the single output identification assignment.

Some countries also do not allow transmission in the frequency bands that some RFID tags operate and still other RFID tags operate in frequency bands shared by other

technologies which can potentially lead to interference.[76,77,78] Because RFID tags

operate on the basis of wireless communication coverage with little to no data protection,

the data transmitted is also open to data breaches, including but not limited to falsified

data, blocked signals, and unauthorized third party data collection. An area of increasing

interest in individual animal identification includes insurance, mostly dealing with

insurance fraud.[82]   Having an RFID tag and data record provides an electronic

verification of the animal's existence, but this does not necessarily prove that the animal

supposedly wearing the tag is indeed the animal for which there are records. Including a

visual data reference record could potentially provide strong clout on the side of either

the insurer or the insuree in matters relating to insurance claims, such as recuperating the

value of deceased animals lost to natural disasters or disease.

Schwartzkopf-Genswein et al.[83] monitored the feeding patterns of feedlot cow

by means of an RFID system. The study determined that the RFID nature of the system

had some inherent factors that produced errors, such as non-grounded (looped) metal

panels used to construct feedlot pens acting as unintended antennae and the transponder

tags in the ear themselves causing missed identifications simply due to the orientation of

the tag with respect to the reader. Another factor of error potential is simply the limited

read range of the system, meaning that actual feeding data had the potential to go

unrecorded when the RFID tag was out of range.[83]

A similar study by T. J. DeVries[50] noted similar errors from physical structures

substituting as unintended antennae with RFID technology. In the study by T. J. DeVries

et al.[50], 12.6% of the observations that animals were confirmed present at the feed alley

using video, the GrowSafe™ RFID-based feeding system failed to record animal

presence. Another 3.5% of observations when the GrowSafe™ systems indicated that a cow was present at the feed alley, the video showed that the cow was not present.[50]

In light of the detection and identification errors present with RFID systems and consistent with our theme of employing machine vision in precision dairy farming, we propose the use of 2D and 3D cameras for the detection and recognition of dairy cows. In particular, we propose an animal detection scheme based on a Haar classifier pioneered for facial detection in 2D video to detect and track an animal in 3D video. For animal identification, we propose a texture analysis scheme of calculating the mean gray level of the animal in a 2D grayscale image along the animal's spine. While these proposed techniques fail to achieve the same level of accuracy as RFID, they present a substantial improvement in accuracy when used as a supplement to RFID.

There exists the potential for an automated data collection process solely based upon whether or not the desired cow anatomy is within the camera image frame. Subsequently, the potential for identification of the animal present in this image frame is also possible using the intensity values of this image. Our research approached this topic in terms of object detection and object recognition. Object detection was realized in our research by use of the same PrimeSense™ Carmine 1.08 camera already utilized in both the feed intake and BCS research studies previously outlined. Because the 3D shape of dairy cow remains fairly consistent across different animals, including different dairy cow breeds, the camera system was directed at determining the feasibility of feature detection by exploiting visible dairy cow anatomy. Object recognition was realized in our research by use of a Prosilica™ GC640 grayscale camera. The change in camera was necessitated by the limitation in frame rate of the PrimeSense™ Carmine 1.08 due to its

operation at a distance of over 60m away from the host computer. The required use of USB 2.0 extension cable reduced the frame rate of this camera from 60fps to 30fps, which induced motion blur as cows walked beneath the system. With the Prosilica™ GC640, we were able to operate over 60m of Category 5 Ethernet cable at 50fps. This higher frame rate capability practically eliminated the motion blur seen in image captures of cows moving in the scene.

Because of the unique coloration of the Holstein dairy cow breed, the object recognition camera system was directed at determining the identity of the cow in the camera scene based upon the hide coloration of the individual animal. An added benefit of machine vision based identification over RFID is that it can be designed to accurately identify more than 1 object at a time. Several cow can potentially be accurately distinguished from one another in the same camera scene. The method of identification using the 2D image data that was to be chosen had to address the issues of speed and accuracy for quickly moving objects as well as chosen based upon the proximity of the camera system to the scene under surveillance.

Several 1D and 2D pictorial image code technologies, called symbologies, exists for automatic identification, such as barcodes, QR codes, and Maxi codes.[84] Automatic identification has been thoroughly tested with human faces and other objects utilizing similar approaches that reduce a 2D or 3D image into a less complex problem that deduces identification based upon features such as shape, intensity, or color pattern.[85,86,87] Research has also been conducted for object recognition with invariance to pose, lighting, scale, and surrounding clutter.[88,89]

The computational processing power needed for object recognition invariance to all of these factors is far more than what is needed for our study. In our study, the scene does not vary, so including factors for background clutter are unnecessary as we were able to operate on the basis of background subtraction due to our static scene and system setup. The problems of pose and scale are also negated since the distance from camera to objects studied does not change nor does the pose. As well, because the lighting of our scene could easily be controlled, this was not an issue either. The reduction in external factors that requires a highly complex object recognition scheme works to our benefit in this research as we were able to create an automated identification process that was quite simple yet robust.

4.1 Automated Dairy Cow Detection

Precision dairy farming has increased its use of 3D cameras and their depth mapping information in order to monitor individual animal welfare with systems that are not obstructive to workflow or cow comfort.[55,90,91] Systems which monitor the physiological changes of dairy cow with range imaging cameras require that individual animals be imaged as they pass through the camera scene. For the majority of these camera based metric monitoring systems, there is only a rudimentary process involved in the software for determining when to start and stop data collection or, even worse, there is only a manual human involvement in this decision making process.[92] Such systems are defined as automated, but human error and ill-defined software failures to properly collect data make such systems less than ideal for precision dairy farming applications. In order for a monitoring system to be truly automated, there must be a highly accurate data collection process included in the system which requires no human input.

Automated feature or object detection imaging systems have been thoroughly tested and verified with human subjects as well as static objects in both 2D and 3D images.[93,94,95] Such detection systems rely heavily upon initial proper classification of the feature or object of interest as these classifications are the user dependent training stage of the system for which future independent identification will be based upon. Several such detection schemes exists and each has its own specialty for automated detection.[96,97,98,99,100,101,102,103,104,105,106,107,108,109,110]

Because our interests were in identifying physiological regions of a cow body, it was decided that a 3D camera which includes depth information was best suited for this task rather than a 2D camera. Data collection was conducted using a PrimeSense™ Carmine 1.08 RGB+depth sensor for this research with only the depth image data utilized. The use of this camera provided depth range information which was accurate to within a few millimeters of actual cow body shape. The ability of this camera to return such highly resolved cow body depth information made it possible to resolve several anatomical regions of interests across multiple cow.

The method selected for object detection in this research was the Haar cascade classifier first developed by Viola and Jones[111]. Haar functions have been used since 1910 when they were first introduced by the Hungarian mathematician Alfred Haar.[112,113] the Haar transform is one of the earliest examples of what is known as a compact, dyadic, orthonormal wavelet transform.[113] The Haar function, being an odd rectangular pulse pair, is the simplest and oldest orthonormal wavelet with compact support.[113] The space frequency localization and multi-resolution analysis capability of a wavelet makes it an efficient tool in analyzing images. The Haar scaling function

$\varphi(x)$ and the Haar wavelet function $\psi(x)$ are as shown, respectively, in Equations 4.1 and 4.2 and an example of each of these 1D basis functions are shown in Figure 4.1.

$$\varphi(x) = \begin{Bmatrix} 1 & 0 \le x < 1 \\ 0 & otherwise \end{Bmatrix} \tag{4.1}$$

$$\psi(x) = \begin{Bmatrix} 1 & 0 \le x < 1/2 \\ -1 & 1/2 \le x < 1 \\ 0 & otherwise \end{Bmatrix} \tag{4.2}$$

$\varphi(x)$ $\psi(x)$

Figure 4.1 – Haar low pass scaling function $\varphi(x)$ and Haar high pass wavelet function $\psi(x)$.

The Haar wavelet transform can be obtained using the analysis filters for decomposition and the synthesis filters for reconstruction. As we are interested in obtaining the features for classifications purposes and image compression, we are dealing with only the analysis filter. The scaling function $\varphi(x)$ and the wavelet function $\psi(x)$ associated with the scaling filter h_φ and the wavelet filter h_ψ are:

$$\varphi(x) = \sum_n h_\varphi(n)\sqrt{2}\varphi(2x - n) \tag{4.3}$$

$$\psi(x) = \sum_n h_\psi(n)\sqrt{2}\varphi(2x - n) \tag{4.4}$$

In two-dimensional wavelet decomposition, the analysis scaling function can be written as the product of two one-dimensional scaling functions $\varphi(x)$ and $\varphi(y)$.

$$\varphi(x, y) = \varphi\varphi(x, y) = \varphi(x)\varphi(y) \tag{4.5}$$

If $\psi(x)$ is the one-dimensional wavelet associated with the scaling function, then the three two-dimensional analysis wavelets are defined as:

$$\psi^H(x, y) = \varphi\psi(x, y) = \varphi(x)\psi(y) \qquad (4.6)$$

$$\psi^V(x, y) = \psi\varphi(x, y) = \psi(x)\varphi(y) \qquad (4.7)$$

$$\psi^D(x, y) = \psi\psi(x, y) = \psi(x)\psi(y) \qquad (4.8)$$

Where $\psi^H(x, y)$, $\psi^V(x, y)$, and $\psi^D(x, y)$ correspond to horizontal, vertical, and diagonal wavelets, respectively.

The Haar transform can be used for image compression, where each image pixel is represented by a corresponding element in an image matrix. Multi-resolution analysis can be implemented using sub-band decomposition in which the image is decomposed into wavelet coefficients. The rows and columns of the original image are convolved with the low pass filter h_φ and the high pass filter h_ψ followed by decimation by a factor of 2 in each direction to generate lower scale components namely low-low(**LL**), low-high(**LH**), high-low(**HL**), and high-high(**HH**) sub-images. LH, HL, and HH correspond to the high resolution wavelet coefficients in the horizontal, vertical, and diagonal directions, respectively. The LL sub-image is the approximation of the original image and all four sub-images contain one-fourth of the original number of samples. Figure 4.2 explains the decomposition, in which *j+1* stands for the starting scale and *m* and *n* are, respectively, row and column directions.
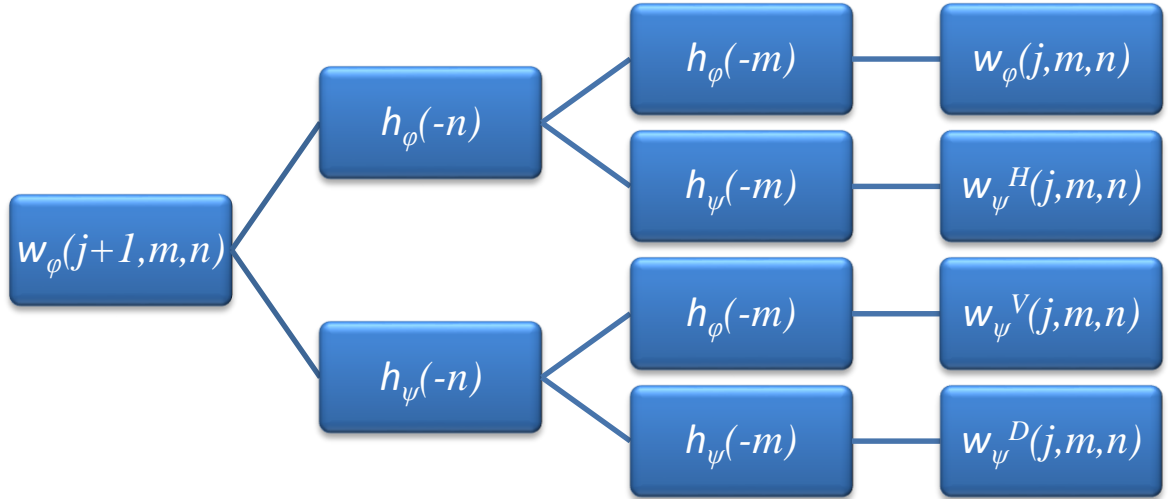
Figure 4.2 – *Haar wavelet transform decomposition using analysis filter banks.*

Alternatively, if we let *A* represent an input image with dimensions of *M* x *N* and let *W* represent the Haar wavelet transform, then *B* represents the resulting matrix product output image:

$$B = W_M A W_N^T \qquad (4.9)$$

Where W_M is applied to process each column of image matrix *A*, so the output should be an *M* x *N* matrix where each column is *M/2* weighted averages followed by *M/2* weighted differences. In order to process each row of image matrix *A* we proceed by multiplying the rows of $W_M A$ by the columns of W_N^T. Transposing the matrix puts the filter coefficients in the columns. If we next allow *H* to represent the low pass filter and *G* to represent the high pass filter of the Haar wavelet transform, then Equation 4.9 can be rewritten as:

$$B = WAW^T = \begin{bmatrix} H \\ G \end{bmatrix} A \begin{bmatrix} H \\ G \end{bmatrix}^T = \begin{bmatrix} H \\ G \end{bmatrix} A \begin{bmatrix} H^T \\ G^T \end{bmatrix} = \begin{bmatrix} HA \\ GA \end{bmatrix} \begin{bmatrix} H^T \\ G^T \end{bmatrix} = \begin{bmatrix} HAH^T & HAG^T \\ GAH^T & GAG^T \end{bmatrix} \qquad (4.10)$$

Using this resulting matrix, we can rewrite Equations 4.5-4.8 as:

$$\varphi(x, y) = HAH^T \tag{4.11}$$

$$\psi^H(x, y) = HAG^T \tag{4.12}$$

$$\psi^V(x, y) = GAH^T \tag{4.13}$$

$$\psi^D(x, y) = GAG^T \tag{4.14}$$

Figure 4.3 demonstrates the results of a Haar wavelet transform processed image. The upper left image of Figure 4.3 represents the result of Equation 4.11. *HA* averages columns of *A* and the rows of this product are averaged by multiplication with H^T. Therefore, the upper left sub-image is the low pass approximation of the entire image which results in a blur of the original image. The upper right image of Figure 4.3 represents the result of Equation 4.12. *HA* averages columns of *A* and the rows of this product are differenced by multiplication with G^T. This sub-image holds the high frequency information about the intensity variations along the image columns as we move down the image, where higher values indicate a larger horizontal change resulting in defining the horizontal edges of high contrast boundaries. The bottom left image of Figure 4.3 represents the result of Equation 4.13. *GA* differences columns of *A* and the rows of this product are averaged by multiplication with H^T. This sub-image holds the high frequency information about the intensity variations along the image rows as we move across the image, where higher values indicate a larger vertical change resulting in defining the vertical edges of high contrast boundaries. The bottom right image of Figure 4.3 represents the result of Equation 4.14. This equation differences across both the columns and rows of the image matrix which results in a sub-image that derives the high frequency information for the image matrix along lines of ±45 degrees.

Figure 4.3 *– Low frequency resultant blur output image (LL), high frequency horizontal edges sub-image (LH), high frequency vertical edges sub-image (HL), and high frequency diagonal edges sub-image (HH) derived from using a Haar wavelet transform on an input image.*

Figure 4.4 shows examples of 2D Haar features derived from the product of two 1D Haar wave transform basis functions. The boundary features used by Viola and Jones [111] included those shown in Figure 4.4 as two-rectangle features and four-rectangle features as well as additional three-rectangle features. These features can be utilized for object recognition alone or in a cascade of features.
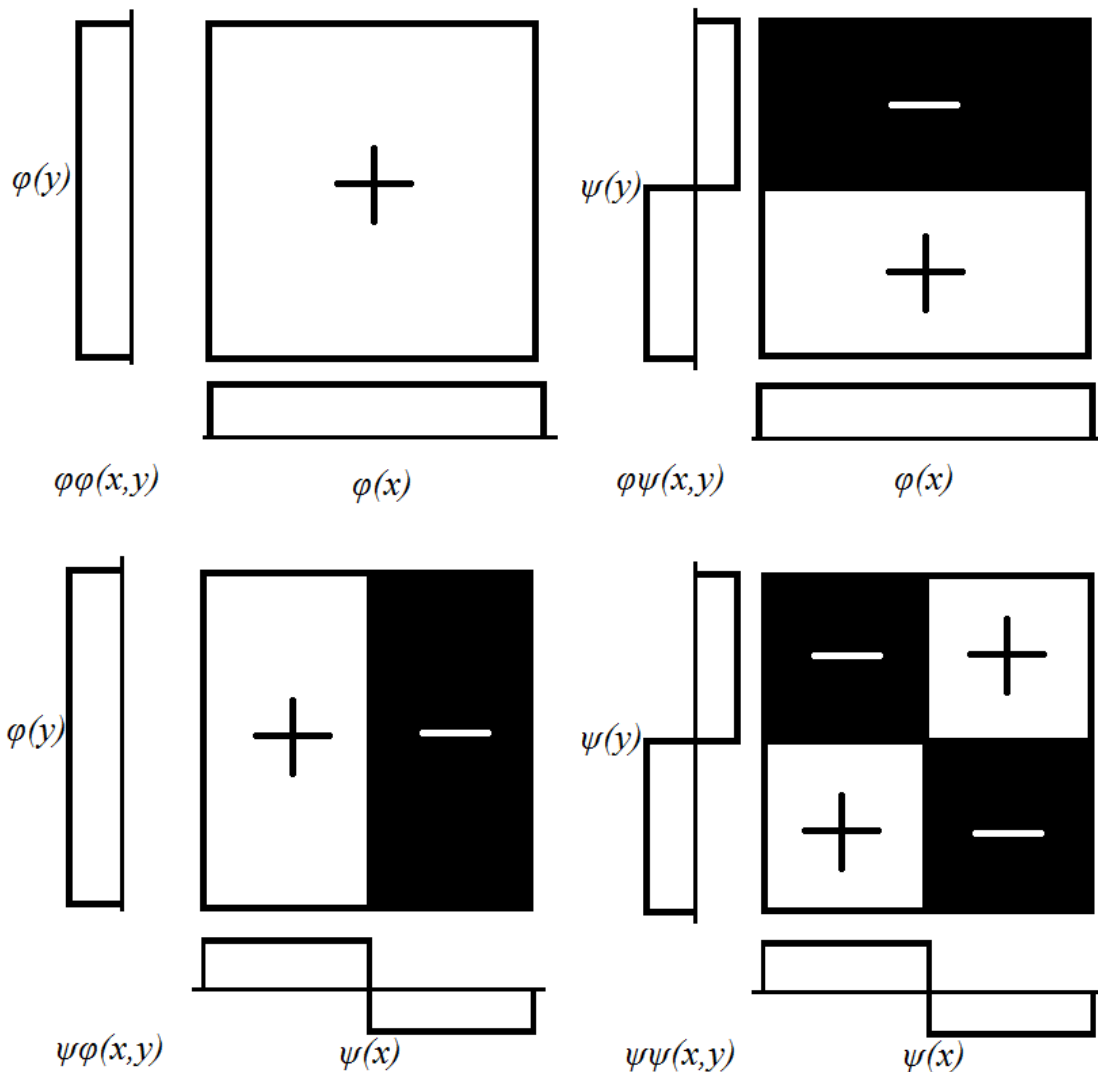
Figure 4.4 – *2D Haar features derived from 1D Haar wavelet transform basis equations.*

The features available to the Haar cascade classifier were expanded upon in the work by Lienhart and Maydt[114]. A properly configured Haar cascade classifier consists of multiple classification stages for which each must be met in order for positive identification of an object.[115] Failure to pass any stage of the cascaded classifier results in the software concluding that the object is not present. At each stage, there may be a single feature or multiple features that must be met. The Haar classifiers are designed to work with grayscale images, whether native grayscale or a color image being converted to grayscale. The depth information of 3D cameras is often represented in or can be converted to grayscale intensity values. Because grayscale intensity images can be best thought of as dark and light regions, or black and white, Haar features are often described simplistically as a combination of black and white regions. A feature may consists of just a single black and a single white region, or they can be a more complex combination, but there must be at least 2 regions being comparatively tested. This is because a Haar feature works on the basis of calculating the mathematical difference between adjacent regions in order to determine if the feature is present.

An example grayscale intensity image and Haar features are shown in Figure 4.5. In a 2D grayscale image of a human face, such as in the left image of Figure 4.5, the eyes are typically a darker region than the cheeks region just beneath the eyes. Therefore, the eyes can be represented as a black region and the cheeks region as a white region, such as seen in the middle image of Figure 4.5.

Figure 4.5 *– The left image is the input grayscale intensity image. The middle image shows a Haar cascade classifier feature used for distinguishing between the eyes and cheeks of the frontal face. The right image shows a second Haar cascade classifier feature used for further distinguishing the presence of eyes on the frontal face image.*

The pixel values are totaled for each region in order to derive a representation of the image contrast between the comparative regions and the difference taken between the 2 adjacent regions. This difference should result in a value that accurately reflects that the pixel intensity of the cheeks region is higher than that of the eyes. A further sub-classification to determine if eyes are present in the image would include the nose region, such as seen in the right image of Figure 4.5. Each eye would be represented by a black region and the nose represented by a white region. The total pixel intensities of the eyes should be lower than that of the nose region in between. Further sub-classification features can be utilized in distinguishing if eyes are present in the current image if desired or necessary. This method works quite well for relatively static objects whose shape and coloration do not change much and the classifier can be setup to be rotation invariant as well as scale invariant.

All of these specifications for a proper Haar cascade classifier make it an ideal choice as a feature detection scheme for surface based cow anatomy. Because our

research focuses on the use of 3D structured light grayscale depth images for dairy cow detection, the data coming directly from the camera source is already in the ideal color format and eliminates any concerns of consistent scene lighting. Additionally, the cow body contour image data provides a contrast gradient which is necessary for the use of Haar features for object detection. The shape, height and width most notably, of each individual cow varies, but is addressed by the fact that the Haar cascade classifier scheme already incorporates a scaling factor that compresses the image in order to detect the feature of interest regardless of size or distance from the camera. Since the Haar cascade classifier is not computationally intensive, which allows for faster processing times than comparable other feature detectors, we also do not have to concern ourselves with the fact that the cow can potentially move across the scene in a matter of seconds.

The focus of this research is interested in identifying those anatomical structures most useful in BCS scoring of dairy cow, which includes the entire region of the cow from tail to hips, recognized as encompassing the entire rear region of the cow body. As so, this was the first feature region to be tested. Since the hips signify the starting point and the tail signifies the stopping point of the cow anatomy used for BCS, these 2 feature regions, hips and tailhead, were also tested independently. The objective was to develop a Haar cascade classifier that would accurately detect the region specified for detection. It was predicted that the more rigid regions such as the rear and tailhead would be easier for object detection whereas the section that was centered about the hips was far too dynamic in its shape to be a highly accurate region for object detection. While a feature detector for the entire rear region would be best suited for an automated BCS system, being able to automatically identify the starting and stopping points of data collection,

respectively the hips and tailhead regions, are just as beneficial for minimizing data storage needs, increasing system speed and performance, and returning orientation information.

The implementation code for the feature detector relies upon the OpenCV (Itseez, Nizhny Novgorod, Russia)[116] CascadeClassifier base class for object detection. Of the many function calls within this class, the detectMultiScale function is the function call responsible for detecting the object in the image frame. The detectMultiScale function includes many modifiable parameters. The first parameter of the function is the input image to be tested for object detection. The second parameter creates a vector of objects which will hold and indicate the location of object detections within the input image. The next parameter is the scaleFactor parameter which specifies how much the image size is reduced at each image scale. The default value for scaleFactor is 1.1 and this value was utilized in this research as well. The minNeighbors parameter specifies how many neighbors each candidate rectangle should have in order to retain it. If the candidate rectangle falls below this minimum number of neighbors, then it is eliminated from the list of possible object detection candidates. The flags parameter is not used as it is a legacy parameter only, and therefore its value is set to zero. The last two paramters of the detectMultiScale function are minSize which indicates the minimum possible object size and maxSize which indicates the maximum possible object size. Objects smaller than or larger than these object size limits are ignored. Specifying minimum and maximum object size limits eliminates many potential false detections as well as speeds up the operational speed of the feature detector.

Of these parameters, the minimum number of neighbors (**minNeighbors**) parameter was the only parameter that was changed for performance evaluation while all others were kept constant at user defined values. Similar Haar classifier performance analysis was conducted by Lienhart et al.[117] on a frontal face dataset. The classifier scans the image pixel by pixel in a sliding window approach for all possible detections of the desired feature. The result is that there will often be several overlapping candidate detections for the desired feature in the same region of the image where the feature is present.

The minNeighbors parameter can help reduce the number of candidate detections by requiring a certain minimum integer value of detections to overlap. If this threshold is not met, then those candidate feature identifications are discarded. Adjusting this parameter was done so in order to attempt to reduce the number of feature identifications returned to only 1 per depth image since the feature could only possibly occur once per image. Adjusting the parameter was also done to attempt to increase the identification sensitivity of the detector in order to reduce the number of images falsely determined as not containing the feature when the feature would indeed be present. This study was aimed at possibly finding a value for this parameter that could maximize upon both of these desired results for each classifier. Figure 4.6 provides examples showing the different Haar classifiers of this study correctly identifying the different regions of interest on the same sample depth image. In this figure, the left image shows the rear classifier region, the middle image shows the tailhead classifier region, and the right image shows the hips classifier region. Just as in the research conducted by Lienhart et al.

(2003), a receiver operating characteristic (**ROC**) curve analysis was conducted on the performance of the Haar classifiers developed in this study.
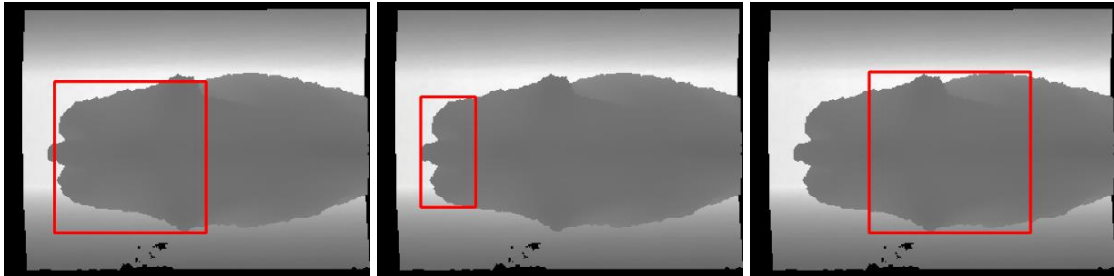
Figure 4.6 – *Example showing the classifier correctly identifying the different regions of interest on the same sample depth image with a red box. Left image shows the rear classifier region, middle image shows the tailhead classifier region, and the right image shows the hips classifier region.*

As previously stated in Chapter 1, the cow at the University of Kentucky Coldstream Dairy Farm used in this study exit the milking parlor via a roofed alley way that is walled on both sides floor to roof and has a concrete slab floor. Since the range of motion for these cow is limited for the length of the alley way, and the fact that lighting conditions can be controlled and made static, it was determined that optimal placement of the camera was mid-way of the alley way length. This walled alley way inhibited the cow's movement to be able to only go directly beneath the camera, entering the frame from the left and exiting on the right. The camera was mounted at a distance of 3.05m from the lens to the floor of the alley way. The camera was positioned at a distance high enough from the floor of the alley way that the entire width of the 1.03m wide alley way could be captured at the same height that the sides of the cow would rub against the wall on either side. This height averaged to approximately 1.5m from the camera lens to the back of the cow.

This camera system was fully automated to turn on just prior to the start of milking and to turn off just after the end of milking. This was made possible because of

the fairly consistent schedule of the morning milking lasting from 4:30am to 6:30am and the evening milking from 3:30pm to 5:30pm. The lights, camera, computer, and software would all turn on at 4am and 3pm and turn off at 7am and 6pm. In the majority of cases, this gave ample time allowance in case milking began earlier than or ended later than usual. In order to minimize the data storage space required, the camera data collection was automated to start recording a sample when the cow's nose passed the center of the frame and to stop recording for that sample when the cow's tail passed the center of the frame.

The data collected by the camera was sent to a computer in a separate building which houses the administrative office of the farm. The camera was connected to the computer via two 20m sections of Tripp Lite™ USB 2.0 Active Extension Cable (Tripp Lite, Chicago, IL). The USB 2.0 extension cables were needed as the distance from the camera to the computer was further than the 5m operating distance limitation for full speed USB 2.0 device cabling. The extension cable was connected to the camera via a USB 2.0 hub (Belkin International, Inc., Playa Vista, California). The camera, lighting element, and USB hub were housed on an 80/20® aluminum frame which was fastened just beneath the roofing covering the walkway, and anchored into the walls on both sides of the walkway via truss joist anchor plates. The 80/20® aluminum frame also allowed for minute adjustments to the position of the PrimeSense™ camera in the 3 Cartesian axial directions of rotation ensuring proper alignment of the camera with the walls and floor of the walkway and nominal positioning in height above the walkway to capture the full width of every cow.

Data was collected for 8 days. The first 2 days were used as training data for the feature detector and the remaining 6 days were used as testing and evaluation data for the software. For the training data, a total of 149 samples were collected from various cows with an average of 30 frames per sample, or 4,400 frames of depth data. For the testing data, a total of 1,110 samples were collected from various cows with an average of approximately 43 frames per sample, or 48,194 frames of depth data. After the raw data was collected, the study then moved its focus to developing the object detection software.

The Haar cascade classifiers of this research were developed utilizing OpenCV. In order to create a Haar cascade classifier, the user must first create a folder of negative images, which do not contain the feature to be detected, and a folder of positive images, which do contain the feature to be detected. The region of interest containing the feature to be detected in each positive image is then manually cropped, and these cropped pixel coordinates stored in a text file. Using the command prompt of the computer, the prepackaged OpenCV executable for creating a Haar cascade classifier was then ran which automatically uses the negative and cropped positive images in order to create a cascade of Haar classifiers to a degree predetermined by the user. Two Haar cascade classifiers were created for the rear region of the cow; the first classifier had 2 stages and the second classifier had 5 stages. These 2 classifiers were developed with the same 751 positive images and 2,095 negative images. A single Haar cascade classifier with 7 stages was created for the tailhead region. This classifier was developed with 800 positive images and 2,295 negative images. A single Haar cascade classifier with 6 stages was created for the hips region. This classifier was developed with 751 positive images and 2,095 negative images.

Because we were searching for simplistic, mostly rigid features with few attributes and the scene and scene objects almost never change, a higher order cascade classifier would not have been entirely necessary as any gains in feature detection would have been negated in equal or higher value in operational performance by slowing down the speed of the feature detector. As well, a cascade classifier with a lower order would have potentially increased the speed of the feature detector at the cost of a much higher number of false positives and false negatives returned by the feature detector. Another consideration is that as the number of stages increases, so does the required number of negatives and positives for the training of the classifier. Again, since our features to be detected were not complex, it was decided that the first 2 days of our depth image data collection were sufficient enough to provide ample variation in the features to be detected for Haar cascade classifier training.

Nine tests were ran which independently tested each Haar cascade classifier created. The Haar cascade classifiers created were tested utilizing ImageJ (National Institutes of Health, Bethesda, Maryland) and Microsoft® Visual Studio® Community 2013 (Microsoft Corporation, Redmond, Washington) with OpenCV. ImageJ was used to combine the individual raw depth frames captured during data collection into a 30fps movie clip in AVI format. This movie clip was then passed through a C++ script written with Visual Studio® and OpenCV along with the XML classifiers created with the help of the prepackaged OpenCV classifier training executable. This software took each frame and analyzed it against the current Haar cascade classifier being tested in order to determine if the feature was present and, if so, drew a red rectangle around it.

In this study, the 3 values tested for the minNeighbors parameter were 10, 5, and 1. In the first test of each of the 4 classifiers, this required there to be a minimum of 10 overlapping detections onto the candidate feature region, or a group size of 11 feature detections. In the second test of each of the 4 classifiers, this required there to be a minimum of 5 overlapping detections onto the candidate feature region, or a group size of 6 feature detections. The results of the previous 2 tests returned favorable results for all of the classifiers except the second rear classifier. Therefore, a ninth test of minNeighbors set to 1 overlapping feature, which equates to 2 detections that overlap in the feature region, was only tested on the second rear classifier developed.

In order to verify the identification accuracy of the automated software, these Haar cascade classifier identifications were compared against human visual identifications of features in every depth frame of the test data set. All 48,194 depth frames for the 6 test days were separated 3 times into either a positive or negative folder for each day for the rear, tailhead, and hips region based upon human visual identification of whether or not the feature was present in the depth image. The automated identification frames were then compared and sorted (i) as true negatives, if also present in the visually identified negatives folder; (ii) as true positives, if also present in the visually identified positives folder; (iii) as false negatives, if an automated identification occurred in a visually identified negative image; and (iv) as false positives, if an automated identification occurred in a visually identified positive image. As well, if multiple automated identifications occurred in an image, only 1 identification was counted as true positive if also present in the visually identified positives folder, and the rest were marked as false positives. If the feature was not present in the image and

114

multiple identifications occurred, then all identifications were treated as false positives. Though the software developed by OpenCV is capable of multiple detections of a feature in an image, the desire of this research was to have only a single detection as the feature only occurred once per positive image. Once the automated identifications were separated into 1 of these 4 folders, then an ROC analysis could be conducted on a per day basis and an overall performance basis for each of the 9 Haar cascade classifier tests performed.

The true positive rate (**TPR**), true negative rate (**TNR**), false positive rate (**FPR**), false negative rate (**FNR**), positive predictive value (**PPV**), and negative predictive value (**NPV**) can be seen for each of the 9 tests performed in Table 4.1. This table comprises the average of all 6 test days of 48,194 depth frames. From this table, we are able to derive the sensitivity and specificity values necessary for creating ROC plots for the evaluation of the tests conducted on the Haar classifiers for the anatomical regions of interests.

Table 4.1 – Statistical results for the Haar cascade classifiers tested for feature detection

Classifier[2]	Statistic (%)[1]					
	TPR	TNR	FPR	FNR	PPV	NPV
H	78	98	2	22	95	90
H5	89	94	6	11	88	94
R3	64	98	2	36	82	95
R4	2	100	0	98	100	87
R53	84	95	5	16	70	98
R54	15	100	0	85	99	89
R541	79	99	1	21	94	97
T	82	100	0	18	100	97
T5	91	100	0	9	99	98

[1]*Statistic: true positive rate (TPR), true negative rate (TNR), false positive rate (FPR), false negative rate (FNR), positive predictive value (PPV), and negative predictive value (NPR) shown as percentages.*
[2]*Classifiers: 7-stage Haar cascade classifier for anatomical hips region with 11 overlapping hips regions detected (H) and 6 overlapping hips regions detected (H5); 3-stage Haar cascade classifier for anatomical rear region with 11 overlapping rear regions detected (R3) and 6 overlapping rear regions detected (R53); 4-stage Haar cascade classifier for anatomical rear region with 11 overlapping rear regions detected (R4), 6 overlapping rear regions detected (R54), or 2 overlapping rear regions detected (R541); 7-stage Haar cascade classifier for anatomical tailhead region with 11 overlapping tailhead regions detected (T) and 6 overlapping tailhead regions detected (T5).*

The results of the first rear region classifier tested at a minNeighbors value of 10 (**R3**) and at a minNeighbors value of 5 (**R53**) can be seen plotted in Figure 4.7. The second rear region classifier tested is also plotted in this figure for minNeighbors values of 10 (**R4**), 5 (**R54**), and 1 (**R541**). The classifiers are plotted on a per day basis and averaged (respectively, **AR3**, **AR53**, **AR4**, **AR54**, and **AR541**). The first 2 classifiers tested contained the region of the cow body from the hooks to the tail, or the rump or rear section of the cow. Since this research desired to create a classifier that would be optimal for an automated BCS camera system, this large region was selected as it included all of the physiological identifiers necessary in deducing a human visual BCS score.
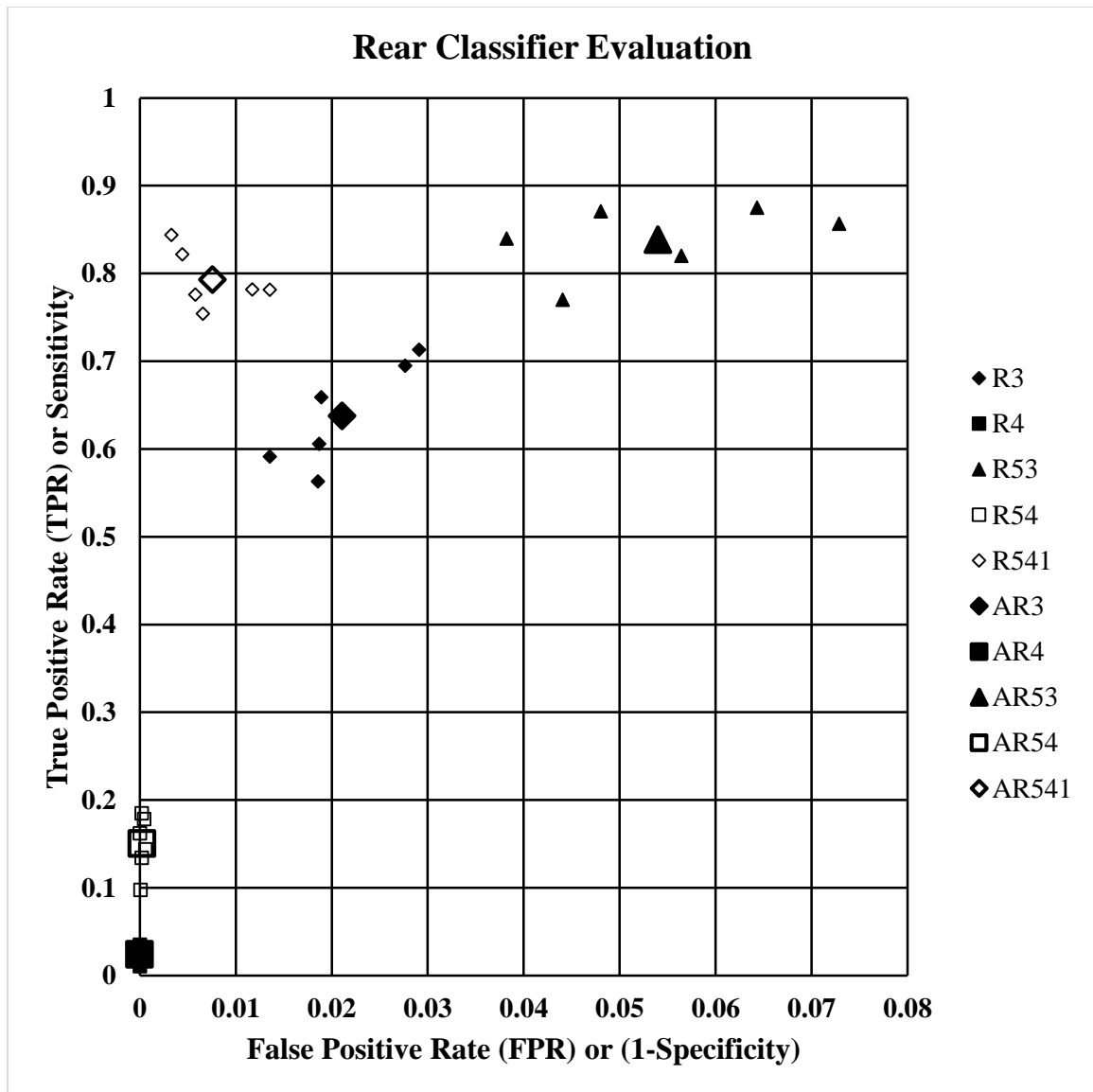
Figure 4.7 *– The ROC plot for the 2 rear classifiers tested with minimum rear detection group sizes of 10 (R3 and R4), 5 (R53 and R54), and 1 (R541) for 6 independent days along with the group size 10 average result (AR3 and AR4), the group size 5 average result (AR53 and AR54), and the group size 1 average result (AR541).*

The accuracy of this classifier was possibly affected mainly by the kinetic use and shifting shape of the body fat and muscles in the region between the pins and the hooks, or the thurl region. With every gait stride or shifting of weight that a cow undertakes, the contour of this region changes and can be highly different from one depth frame to the next, especially when erratic tail movement occurs. Figure 4.7 shows that reducing the

117

minNeighbors value for the first rear region classifier increases the TPR, but reduces its overall performance. Alternatively, reducing the minNeighbors value for the second rear region classifier increases both the TPR and the performance of the classifier. Therefore, R541 is the optimal choice for rear region feature detection.

The results of the tailhead region classifier tested at a minNeighbors value of 10 (**T**) and at a minNeighbors value of 5 (**T5**) can be seen plotted in Figure 4.8 on a per day basis and averaged (respectively, **AT** and **AT5**). The third classifier tested contained only the tailhead region of the cow body starting at the pins and ending at the tail. The motivation for selecting this region was to be able to create a feature detector that could automatically stop the recording of depth data when the tail, or end, of the cow had entered the frame. It is also a highly useful region on its own in the determination of BCS and the orientation of the cow in the frame. The tailhead region being present in a depth frame also works well for other precision dairy farming technologies that require the entire rear section of the cow to be present.
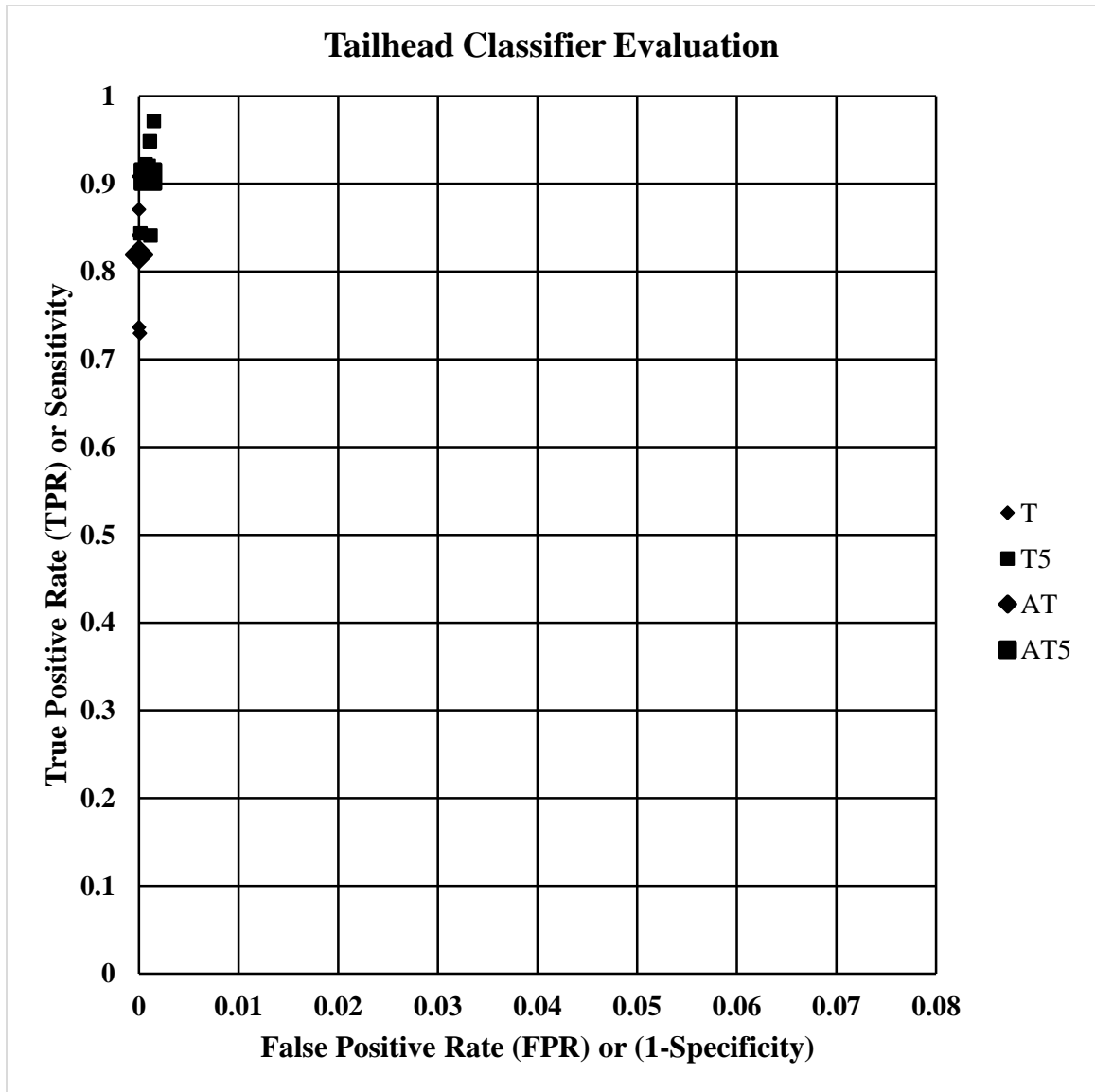
Figure 4.8 *– The ROC plot for the tailhead classifier tested with minimum tailhead detection group sizes of 10 (T) and 5 (T5) for 6 independent days along with the group size 10 average result (AT) and the group size 5 average result (AT5).*

The accuracy of the performance of this tailhead classifier was possibly affected by the highly erratic nature of tail motion. Part of the accuracy of this classifier is due to the fact that the overall shape of this region changes only marginally even with tail motion. Figure 4.8 shows that T5 performed better than T, which indicates that T5 is the optimal choice for the tailhead region feature detection.

The results of the hips region classifier tested at a minNeighbors value of 10 (**H**) and at a minNeighbors value of 5 (**H5**) can be seen plotted in Figure 4.9 on a per day basis and averaged (respectively, **AH** and **AH5**). Figure 4.9 shows that H performed better than H5, which indicates that H is the optimal choice for the tailhead region feature detection. The fourth classifier tested was centered about the hips, or hooks, region of the cow body starting approximately at the posterior half of the loins region and ending at the anterior half of the rump region, covering the majority of the lumbar and sacral regions of the spine. The motivation for selecting this region was to be able to create a feature detector that could automatically start the recording of depth data when the hooks had entered the frame. In image or visual based BCS scoring systems, the hooks are the furthest anatomical point forward on the cow body considered. In that regard, this region can be used to compliment the opposing tailhead region when defining the section of the cow body to be used for BCS scoring. Additionally, the hooks are a rigid anatomical feature that can be readily used for identifying when a cow's body is centrally present in a depth frame as well as determining the orientation of the cow's body for a variety of precision dairy farming technology uses.
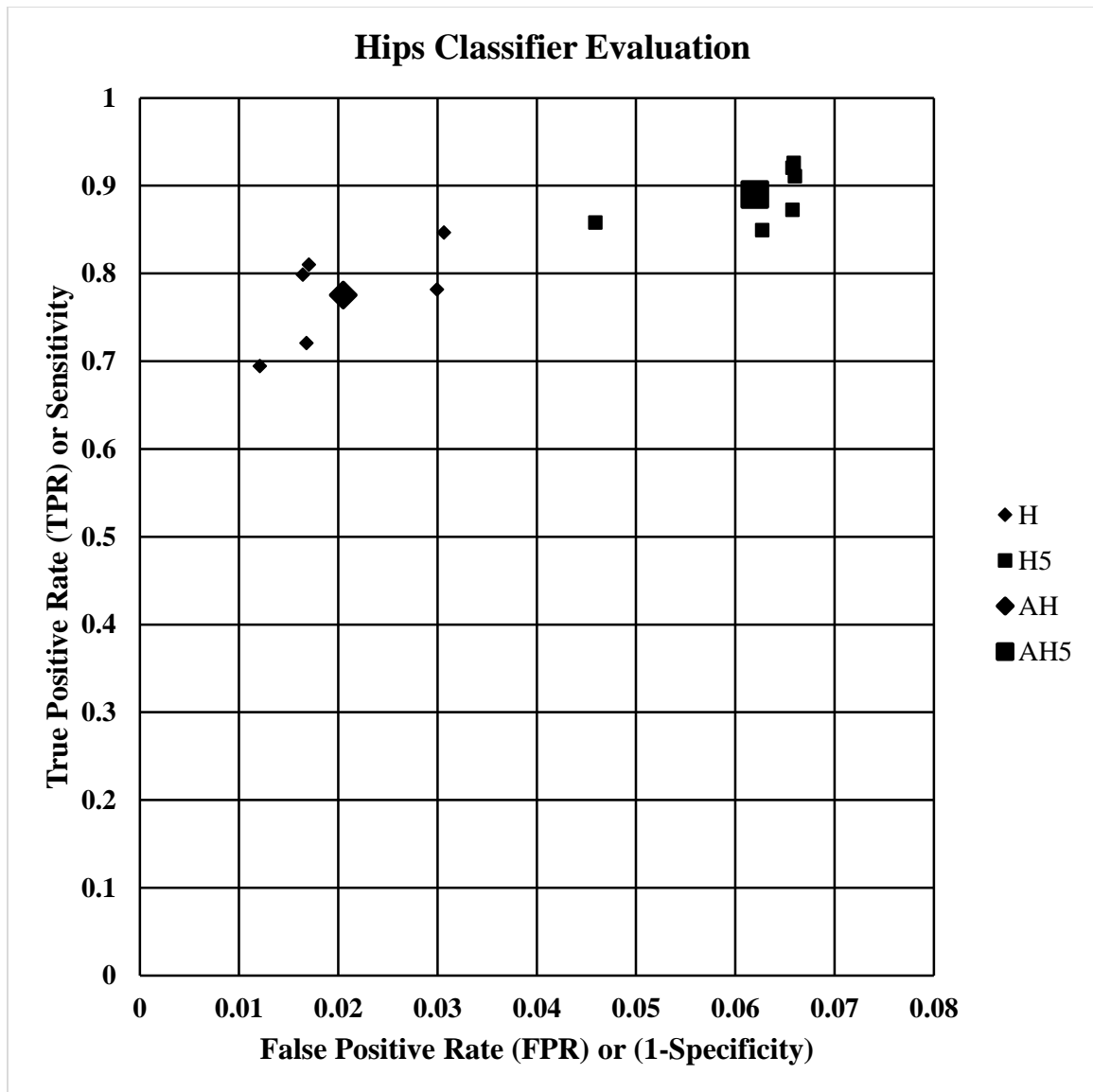
Figure 4.9 *– The ROC plot for the hips classifier tested with minimum hips detection group sizes of 10 (H) and 5 (H5) for 6 independent days along with the group size 10 average result (AH) and the group size 5 average result (AH5).*

The accuracy of the performance of this hips classifier was possibly affected by the highly kinetic nature of this region of the cow's body. This is a large region that encompasses several muscular and fatty structures, which are not ideal for a feature detector. The left edge of the region includes the anterior half of the thurl region. Again, this is an area that can appear differently from one depth frame to the next as the positions of the legs stretch and compress the muscle and fatty tissues of the region. The

right edge of the region includes the posterior half of the lungs. This is a mostly boney region as seen from above since the rib cage dominates the field of view in this section of the classifier region. The trailing rib bones themselves can be confused by the classifier as hips. In Figure 4.10, 2 depth image frames are shown for which the classifier has identified a hips region. The left depth image is a false positive and the right depth image is a true positive. There were 3 depth frames recorded in between the 2 depth frames shown in Figure 4.10. The visual selection process of true negatives and true positives for this anatomical region also incurred this decision problem, but the human benefit was that we could look ahead in the frame sequence to verify if the hips were present whereas the computer did not have this advantage and must decide based solely upon the depth frame presented. Looking at the 2 depth frames of Figure 4.10, it is easy to see the confusion of the hips classifier between hips and trailing rib bones. Since this is a highly occurring classification error, the hips classifier of this research was deemed ineffective as tested.
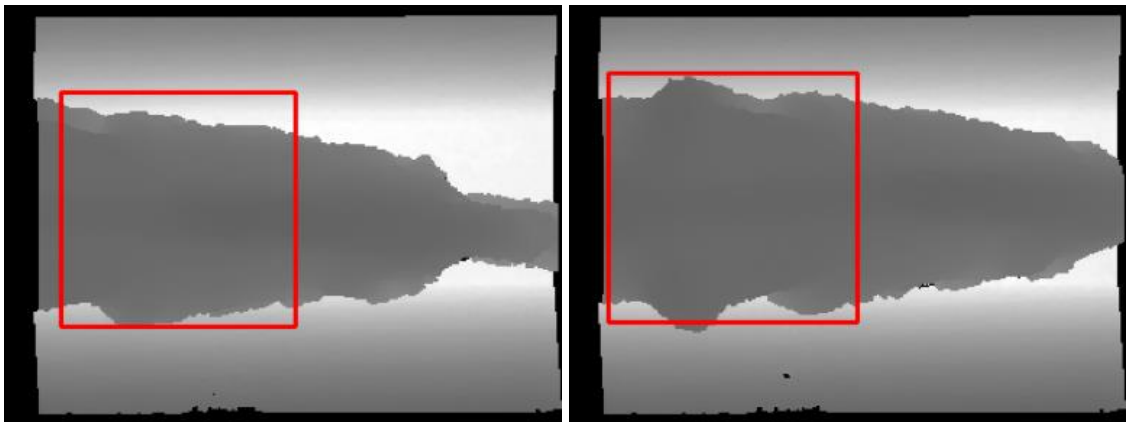
Figure 4.10 – The left image is a false positive for hips detection whereas the right image is a true positive for hips detection collected 4 frames later.

Figure 4.11 shows all 9 test cases plotted together for comparative ROC analysis. This plot reinforces our choices of R541, T5, and H as the best performing classifiers for

122

their specific anatomical region of interest. Of these 3, R541 and T5 performed the best and could be potentially utilized in a computer vision precision dairy farming system which automatically monitors BCS. The classifier that performed the best overall was T5, as expected. In a real time system where the cow walks across the scene below the camera, T5 would be preferred over R541 because R541 would have less depth image frames in a sample from which to make a true feature detection than T5, mostly due to the size difference of each feature in an image. Consequently, T5 can afford a higher false negative rate per frame or per sample than R541.
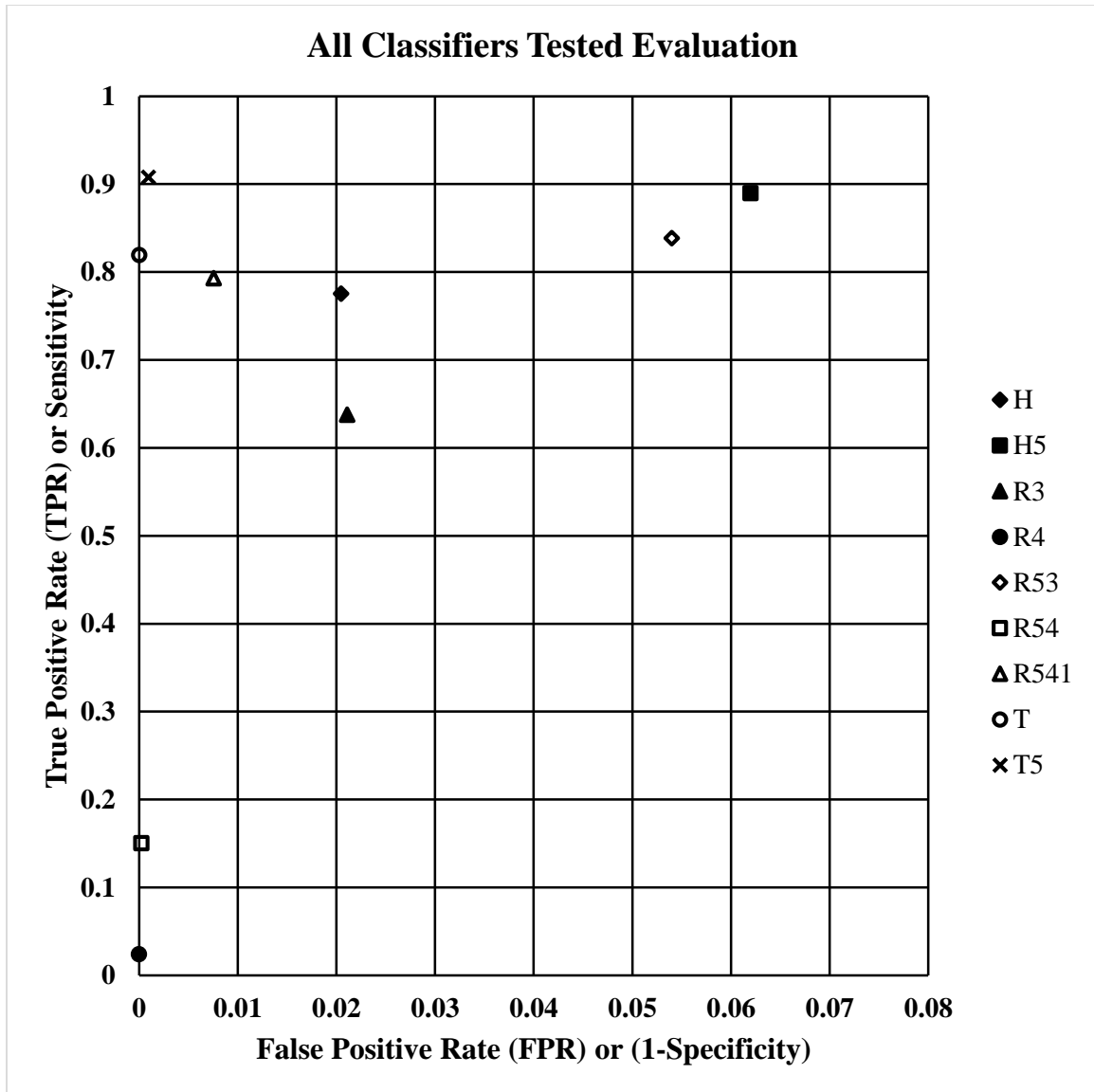
***Figure 4.11** – The ROC plot for all 4 classifiers (1 tailhead region classifier, 2 rear region classifiers, and 1 hips region classifier) developed and tested with minimum detection group sizes of 10 (T, R3, R4, and H), 5 (T5, R53, R54, and H5), and 1 (R541) for a total variation of 9 classifiers tested and evaluated.*

Adjusting the minNeighbor parameter allowed the software to reduce the number of candidate feature identifications returned per depth image to 1 for all but 14 images tested. Since the 48,194 depth images were independently tested 9 times, this means that only 14 images out of 433,746 images had multiple feature identifications. Future research should investigate the tradeoffs of false negatives, false positives, and possible

124

multiple identifications for minNeighbors values of less than 5 for each of the 4 Haar classifiers developed. Since this study was aimed at discovering the potential for use in systems monitoring the BCS of dairy cow that were milked at least twice per day, the total number of false negatives incurred were not viewed as important or detrimental as the total number of false positives since multiple milking times provides multiple opportunities to collect BCS data on a per cow basis.

Feature detectors for other regions of the cow body could have been tested, but were beyond the scope of this study. Based upon the findings of this research, ideal features would include those with a limited ability to deform in natural cow movement. Future research should test feature detectors for additional regions of interests. It would be pertinent to test feature detectors at different pose positions other than a strictly top view to gain access to other regions of interests not seen in the camera pose of this study. The top view approach was selected here because the number of moving body parts seen by the camera, which can decrease the accuracy of the feature detector greatly, is much less than from any other pose position.

This research shows that automated feature based imaging systems have the potential to be utilized in precision dairy farming. Such practical implications to be tested would possibly include automated BCS and automated respiration rate monitoring, both of which would rely solely upon depth image data centered about specific cow anatomy. One limitation of this type of system is when the feature of interest is occluded from view of the camera, such as when another object comes between the camera and the object of interest. This limitation is common amongst imaging based systems and is unavoidable unless the cow is kept isolated at all times, which is impractical unless there

is a specific immediate health risk being monitored. The benefit that this non-tactile system has is that it has a much lower risk of being broken or otherwise damaged by the cow as it is placed out of reach and in a sturdy, secure location.

4.2 Automated Dairy Cow Recognition

The objective of the machine vision based identification study was to investigate the potential for a 2D grayscale imaging camera to accurately determine the identity of a Holstein cow in a camera scene based solely upon its hide coloration. The identification process reduces the 2D grayscale image to a 1D vector of cumulative pixel intensities for vector matching along the length of the cow. An initial test dataset of Holstein cow images were collected to test for the feasibility of continuing on to include a full herd of Holstein cow. After verification from the smaller test set of Holstein cow as to the abilities of the camera based identification process, the study then proceeded to test the accuracy of the same system for a much larger test set of Holstein cow. Because image noise increases and cow hide variations decrease as the number of Holstein cow subjects tested increases, it was predicted that the overall accuracy of the system would decrease but remain suitable as a redundancy identification process.

As previously stated, the cow at the University of Kentucky Coldstream Dairy Farm exit the milking parlor via a roofed alleyway that is walled on both sides floor to roof and has a concrete slab floor. Since the range of motion for these cow is limited for the length of the alley way, and the fact that lighting conditions can be controlled and made static, it was determined that optimal placement of the camera was mid-way of the alley way length. The data samples in this research were collected using a Prosilica™ GC640 (Allied Vision Technologies, GmbH, Stadtroda, Germany) camera mounted at a

distance of 3.05m from the lens to the floor of the alley way. The camera was positioned at a distance high enough from the floor of the alley way that the entire width of the 1.03m wide alley way could be captured at the same height that the sides of the cow would rub against the wall on either side. This height averaged to approximately 1.5m from the camera lens to the back of the cow. This ensured that the entire top view of the cow in the scene would be captured. The size of each frame captured from the camera is 640 pixels horizontal by 480 pixels vertical. The entire length of the cow could not be captured in this limited field of view as even the shortest cow was at least 1,200 pixels in length from nose to tail at this fixed distance.

The camera was made static and the fact that the cow moved across the scene, in the vertical direction of the camera, allowed for the use of optical flow to piece together a complete image of the cow from nose to tail. In the layout of this study, optical flow is the pattern of apparent motion of an object or objects, the cow, in a visual camera scene, the hallway, as caused by the relative motion between the camera and the scene or objects within the scene, the cow walking down the alleyway. In order to generate images of the animal from nose to tail, the subject imaging system behaves similar to panoramic imaging in smart phones [118], except that the motion of the animal walking under the camera replaces the sweeping of the camera across a scene. In each frame of video, the process of MPEG motion compensation [119,120,121,122] is applied where one frame of video, the reference frame, is divided into non-overlapping sub-blocks of 16x16 pixels. Each of these sub-blocks is then compared to equal sized blocks in the subsequent frame of video, the target frame, looking for the particular 16x16 block that minimizes the sum of absolute differences between pixels of the reference block. The horizontal and vertical

shift of the 16x16 block from the reference to target video frame defines a motion vector for that block.

Having 640x480 pixels per frame, each frame is composed of 40 by 30 sub-blocks, and hence, each frame of video will produce 1,200 motion vectors. Many of these sub-blocks contain background pixels and not cow pixels. As such, out of the 1,200 motion vectors, only those blocks that correspond to motion vectors of at least 4 pixels, horizontal or vertical, are considered to derive from cow motion. And out of all motion vectors considered to be from cow motion, the single median vector is selected and defined as the motion of the animal between frames. The image is then clipped to its center horizontal row pixels with the number of center row pixels preserved equal to twice the vertical motion of the animal, and this center row image is then divided into the left center row image and the right center row image so that you get two separate images, both as wide as the vertical motion of the animal. The two center row images are then separately appended to the left and right center row images from the previous frames until the animal leaves the field of view, at which point the images are complete. This allowed the camera to collect sample images of independent cow from nose to tail, regardless of the length of the cow. The process then starts anew as the next animal enters the field of view.

Before data collection took place, a single white stripe and a single black stripe were painted on both walls and across the floor, horizontal to the camera view, in order to aid in predefining the walls and floor as background pixels in the resultant image captures. These stripes can be seen in Figure 4.12. When the camera would collect data, it would alternate between capturing pixels in the white stripe region for the right center

row image and capturing pixels in the black stripe region for the left center row image. The resulting final image capture can be seen in Figure 4.13, where the left image contains a cow sample with a black background, as if the cow were standing over a black floor, and the center image contains a cow sample with a white background, as if the cow were standing over a white floor.

***Figure 4.12** – This image shows the camera scene with the black and white stripes painted across the floor and up the walls.*
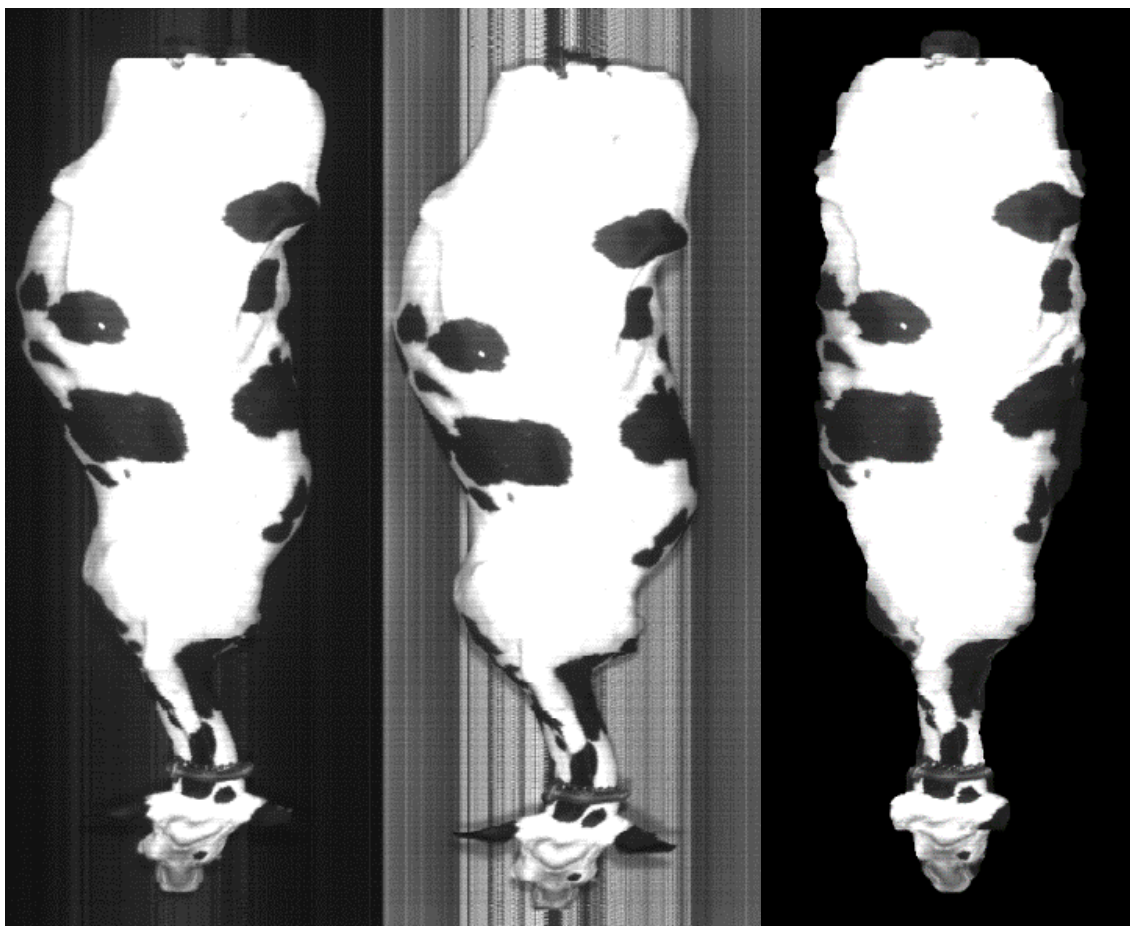
Figure 4.13 – An example sample image collected by the optical flow based automated software, with the black background (left) and the white background (center). An example test image after background subtraction and alignment processing (right).

This camera system was fully automated to turn on just prior to the start of milking and to turn off just after the end of milking. This was made possible because of the fairly consistent schedule of the morning milking lasting from 4:30am to 6:30am and the evening milking from 3:30pm to 5:30pm. The lights, camera, computer, and software would all turn on at 4am and 3pm and turn off at 7am and 6pm. In the majority of cases, this gave ample time allowance in case milking began earlier than or ended later than usual. Networking capabilities were also utilized which allowed for the camera to be connected remotely to a computer via an Ethernet cable of approximately 40m in length and the data transmitted from this computer over the internet in real-time to a computer

located back at the University of Kentucky campus where the images from the optical flow data collection process were stored.

The data set of sample images collected did include some bad data samples, such as when cows would turn their head back onto their body or false captures of objects moving below the camera that were not cow, such as a cat or a human. These bad data collections were easily eliminated by placing a simple row length threshold on the image. If the object in the image fell below the threshold, it was not further processed. As well, there were images captured with 2 cow in the same field of view. These samples were eliminated from the data set by inducing a maximum row length threshold as well. If the object did meet the length requirement, meaning it fell between the minimum and maximum row length thresholds, then it moved on to preparing the image for the background subtraction stage.

The next step in image processing was to perform image registration in order to align the right center row image with the left center row image for the purpose of background subtraction. The differences seen in cow position between the capture of left and right images is due to the time difference between image captures. During image capture, the gait can quickly change pace and so can the shifting of body weight, causing the left and right images to not have a consistent alignment method across independent samples. In order to account for this randomness, subpixel image registration by cross-correlation was conducted by means of discrete Fourier transform processing on each sample to find the best fit shift difference for both the horizontal and vertical dimensions between the left and right images. A variation of the MATLAB® algorithm developed by Guizar-Sicairos et al.[123] was employed in this task. As well, the raw data capture

did not eliminate the contortion of the cow body as it walked across the scene and down the alley way. In order to correct the resultant image to show a cow contour in line with the spine of the cow, the pixels of each row of data were shifted left or right to straighten the cow contour centrally in the image, which was conducted solely for making human visual identification of the cow contained in the image easier and had no influence on the computer software's identification process.

Removing the background is then performed by comparing the left and right center row images of the optical flow image samples collected looking for substantial differences in pixel intensity. As previously stated, when the camera would collect data, it would alternate between capturing pixels in the white stripe region for the right center row image and capturing pixels in the black stripe region for the left center row image. Therefore, wall and floor pixels of the left and right images would sharply contrast from one another in image intensity. Pixels with substantial differences in intensity between the two images corresponded to wall and floor pixels, which equated to being identified as the background pixels, while pixels close in intensity belonged to the animal. Masking these difference pixels then isolates the animal from the background, therefore eliminating the background pixels by setting their values equal to zero. It is this final isolated animal image that is used to identify the animal. An example final test image with the background removed and the cow body straightened can be seen in Figure 4.1c.

The last step of image processing required each pixel of row data in the background subtracted final test image to be summated across all columns, or per row cumulative summation along the length of the cow. This reduction of 2D grayscale images to a 1D vector of values is what was known in this research as the sample's

signature for that particular cow image. The 1D vector created was the same row length as the original input image with only a single pixel value comprised of the cumulative sum of all the columnar pixel values in that row. The 1D vector created for the sample signature is comprised of the image row data rather than the column data because of the greater length in the image row size than column size. This length difference allowed for a 1D signature that could contain a larger permutation of unique cumulative intensity values in the rows direction rather than the columns direction.

Another reason that the 1D vector created for the sample signature was comprised of the image row data rather than the column data was because there were less motion changes in the direction of the rows than that of the columns. For instance, a swinging tail would generally move in a horizontal frame motion of the cow's body. As well, the head and neck of the cow would also be more likely to change in a horizontal frame motion of the cow's body along with any changes in the vertical frame direction. Just the general stride of the cow would shift the body of the cow horizontally while in motion beneath the camera. These changes as seen by the rows impart less of a cumulative change than if viewed along the columns. The only body parts that would impart a large variable change in the direction of the rows are the legs and feet of the cow, which generally cannot be seen by the camera, and the ears of the cow, which are orders of magnitude smaller in total pixels than the rest of the cow body. Although more rare, typically only seen if a cow is standing still below the camera and not in forward motion, is a cow reaching its head back towards its shoulder which would result in a large change in row data. Rarely does a cow stop directly beneath the camera, so most of the changes that could affect row data do not occur.

Since the data collection was 8-bit unsigned (uint8) grayscale with integer values ranging from 0 to 255, the image pixel values were subsequently changed to 64-bit (double) floating-point values which ranged from 0 to 1. In this manner, no single row of pixel values could be greater than the columnar pixel width of the image, which was 640. Because the image width was directly related to alley way width, image captures remained consistent for all cow along this dimension. The only dimension that changed was the length of the cow, for which longer cow would have longer sample signatures and shorter cow shorter sample signatures.

The identification of individual cow in samples was first conducted manually to ensure that the correct cow identified in the image was present, which made this the baseline known identifications for which to compare the automated identification matches against. Then, once every independent sample had been manually identified, the research moved the focus to creating an identification signature for each sample cow included in the study.

Individual ground truth identification signatures for each cow were created using sample signatures selected from the data as the training set. In this research, a ground truth identification signature was developed to represent the average sample signature produced by individual cow across a subset of sample images. All of the data for each cow of the training set is aligned in order to produce an average identification signature of that individual cow. The reason that an averaged identification signature was used is because of the various variables that exist that can slightly alter the identification signature derived between independent images of the same cow. Some of these variables include, but are not limited to, lighting of the scene may change slightly, border pixels

around the cow body that are included in the sample signature, debris on the cow's body, alterations in body pattern seen by the camera from cow motion, and erratic motion of the cow, such as a swinging tail or neck and head, that can misrepresent that section of the body where the erratic motion occurs.

An example of several sample images for the same cow plotted together after being aligned with one another can be seen in the left image of Figure 4.14. By taking the average of a training set of sample images for a particular cow that may vary only slightly from one another, we obtained an averaged unique identification signature for each cow that eliminates these small differences between independent sample signatures. An example identification signature derived from a subset of sample signatures can be seen in the right image of Figure 4.14. Figure 4.15 shows a dairy cow with a darker hide coloration compared to a dairy cow with a lighter hide coloration. The two signatures are readily distinguishable just by the human eye. The pink line shows the unique cow signature being updated with each sample signature added.
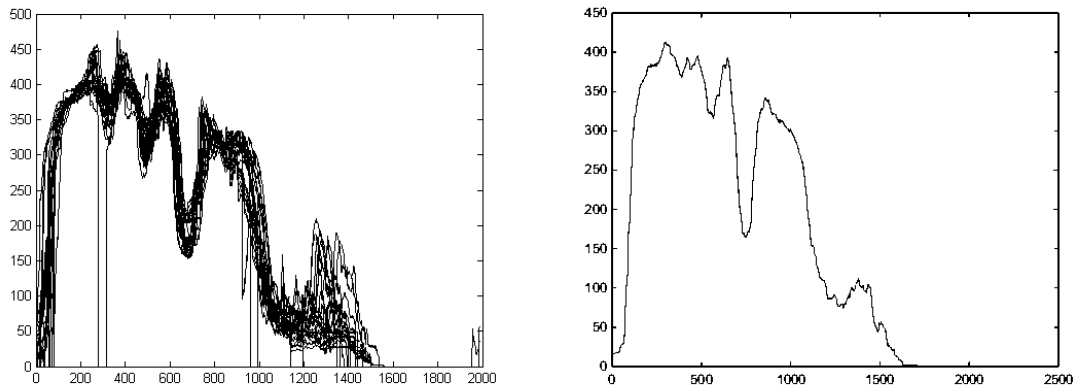
Figure 4.14 *– Plot on left showing the 1D vectorization of the grayscale image intensity of several 2D test images for the same cow after the vector is rotated 90° counterclockwise. Plot on right is showing the averaged 1D signature derived for this cow which can be tested against future sample images in order to determine the cow present in the sample.*

135
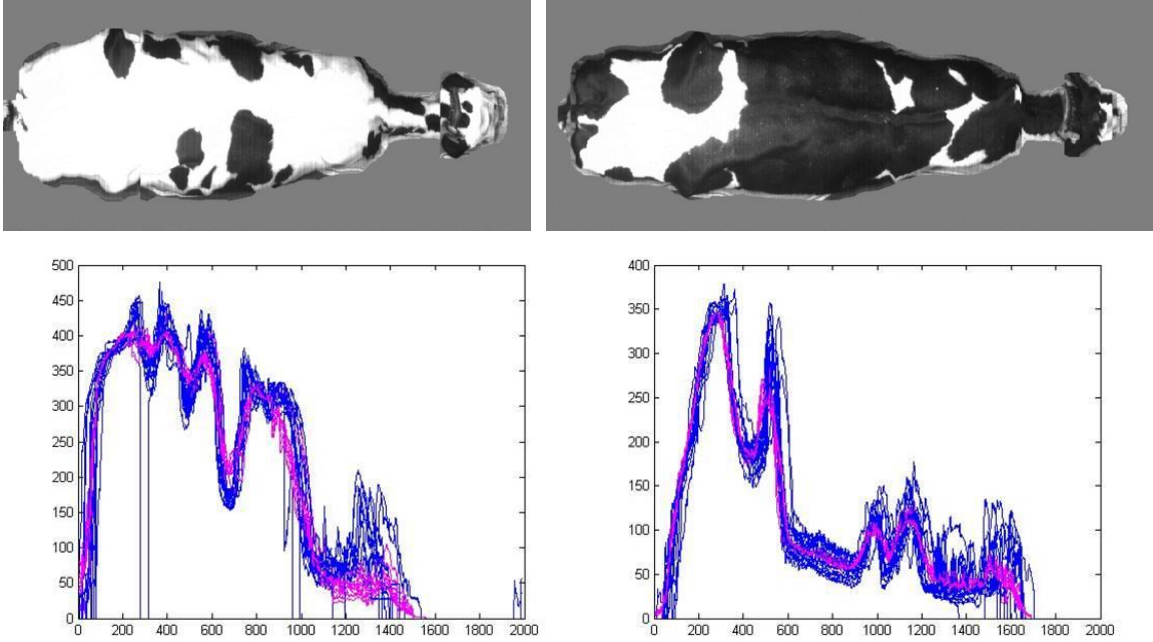
Figure 4.15 *– Two dairy cow shown (top row) with their respective signatures shown below them (bottom row). The background is shown in gray for easier viewing, but is black in the original sample image.*

Because the alignment was different for each sample signature due to gait and contour differences during capture, the 1D sample signatures had to be shifted in order to find the alignment of least error between the known identification signature and each additional independent sample signature included in the averaging of the identification signature, if more than a single sample was used to derive the identification signature. The error shifting and decision-making of least error alignment was automated in MATLAB®. Each 1D sample signature was shifted by the length of either the initial or previous 1D identification signature one row pixel at a time in order to find the alignment of least cumulative sum of difference between the 2 signatures. The closer the current sample signature was to the identification signature it was being tested against, the smaller the error difference value would be. Once the error for each alignment had been determined, the software then averaged the 2 signatures in order to create a new averaged

unique identification signature to be used for individual identification matching. This process was repeated for each individual sample signature being used to create the final set of averaged unique identification signatures, if the number of samples being used to create the unique identification signature ranged from 2 to 5 samples. If only a single sample was being used to create the unique identification signature, then that sample signature was determined to be the unique identification signature.

Once the ground truth identification signatures for individual cow were created, they were tested against the complete set of data samples. Each 1D sample signature was shifted by the length of the independent ground truth 1D identification signatures one row pixel at a time in order to find the alignment of least cumulative sum of difference. The closer the input sample signature was to the ground truth identification signature it was being tested against, the smaller the error difference value would be. This alignment of each input sample was conducted against all of the ground truth identification signatures with the error values of all comparisons stored in the software. Once the error for each alignment had been determined, the software then chose the alignment with the smallest error value as the identification match.

The first test conducted contained a total of 351 samples collected from 25 independent Holstein cow. The results of the signature alignment identification software was that it was able to accurately identify the cow in 344 out of 351 samples, or an identification accuracy of 98%. Of the 7 incorrect identifications, 4 were because the cow was solid black and the automated subpixel image registration alignment of the left and right images resulted in misalignment, which distorted the signature of those samples. Based on these results, the identification method of this research is only

feasible if there is enough variation in the coloring of cow in the herd for accurate subpixel image registration during background subtraction.

If the background cannot be properly subtracted from the image or the left and right images cannot be properly aligned, then the current dimensional reduction method cannot operate properly for accurate identification. Therefore, solely Holstein herds make for great candidates for this type of identification process whereas solely Jersey herds possibly would not. The brown texture of the Jersey cow under bright lighting appears as white or near white pixel values in grayscale images. Therefore, the individual signatures of Jersey cow would rely less on coloration and more on cow differences in body shape, length, width, and height such as can be determined with the use of a 3D camera for image alignment and background subtraction. As well, Holsteins that are solid black or have little to no white coloration on their backs are hard to distinguish amongst, unless the cow length and width differences are enough to help distinguish individuals. The same is also true of Holsteins that are solid white or have little to no black coloration on their backs, which makes distinguishing between very similar colored Holsteins difficult, but not impossible. In most general dairy operations, the entire herd is typically of a uniform breed, such as the Holstein herd of this study, and therefore the patterning of the cow hide will be as unique as the herd of this study. Future testing should be conducted which specifically addresses these concerns.

The preliminary testing validated a need to investigate a larger dataset with a full herd being monitored. In the secondary test, a total of 80 cow were observed with 6,484 image samples collected. The same software was utilized and the same data analysis was conducted as in the first test. The second test was able to accurately identify the cow in

the image on the first attempt with an accuracy of 78.10% and was able to accurately

identify the cow in the sample within the first 5 attempts with an accuracy of 95.60%.

The results of the second test are shown in Table 4.2.

Table 4.2 – Identification accuracy of the herd size 1D signature testing

Identification Attempt	Accuracy[1] (%)
1	78.1
2	89.22
3	92.12
4	94.21
5	95.6

[1]*Accuracy here refers to the cumulative total number of correct identifications for the entire test dataset as the identification software is allowed additional identification attempts.*

The identification accuracy of the system proposed in this research was expected

to decrease with an increase in subjects. Therefore, the identification process was

designed to incorporate the top 5 identification possibilities provided by the software

instead of just looking at the initial identification. By reducing the possible identity from

80 subjects down to just 5, the software is able to reduce the choice of identity to only

6.25% of the total herd. When used in conjunction with other identification technologies,

such as RFID, the process studied here has the potential to greatly reduce, if not

eliminate, identification errors. The results of this second test show that further testing

should be conducted along with the incorporation of RFID technology. While RFID is

the industry standard, it could potentially benefit from the identification redundancy

provided by the work of this study with cameras. If the RFID identification returned

matches 1 of the 5 identification possibilities returned by the software of this research,

then it will be able to provide a higher certainty of proper identification than the

utilization of RFID alone which only provides a single identification, whether it is correct or not.

This research tested the capability of identifying individual cow from image data acquired with a 2D grayscale camera. The results of this research showed that fully automated individual cow identification by means of machine vision utilizing only the coloration variations amongst cow in a herd was possible. The degree to which this identification method is accurate depends upon several factors, most of which can be minimized by the incorporation of other technologies or physiological cow data. Future research should include the use of 3D cameras that would provide cow body shape information for differentiation. Future work should also research the use of signature developing software that can accommodate for animals entering and leaving the herd automatically, such as using the codebook method, which will search for the signature of the cow in the software identification database and develop a new signature to add to the identification database if it does not already exist. Developing a system that utilizes both RFID and camera data should also be tested so that both technologies can be developed to work together to verify and complement one another in automated cow identification.

CHAPTER V: CONCLUSIONS AND FUTURE WORK

The feed intake system proposed in this dissertation was able to produce accurate feed weight values when compared to scale weight values of the same bins of feed. Future work should include studying this system in an open feed bunk design as well as being used with individual dairy cow over a long term observational period of time. In order for such a system to be readily adopted, it must be able to provide accurate feed intake monitoring results for an extended period of time and be able to keep track of the individual animal records. Because our study was only interested in determining the feasibility of such a system to determine the weight of feed in a bin, these issues were not addressed. As well, feed of different mixtures and moisture content ought to be thoroughly analyzed with this system in order to determine how these different TMR affect the results of the system.

Part of the reason for creating an automated BCS system is to eliminate the subjective error of human scoring. The score can change by as much as 0.25 on the 1.0-5.0 scale, even when using the same scorer on the same cow and the same day. The automated system is completely objective and therefore reduces the error greatly because the algorithms and software are going to be the same every time with no bias injected into the data. The insight gained from this research is a great leap forward in being able to ultimately provide an end user commercial system that can be readily installed and used at almost any dairy production facility. When it comes to health and management in a dairy facility, being able to have historical data on individual cattle is essential. The new system proposed by this research was less susceptible to noise and image interferences and was able to have near 100% useable data collection every time.

Future research should focus primarily on making the BCS system to also be able to accurately make individual identification along with the collected data samples. This can include modifying software such as that used in this research to visually do so or to integrate other technologies such as RFID tags and readers. The imaging approaches tested in this dissertation for dairy cow detection and recognition provide a starting point for utilizing machine vision based applications in order to determine the presence and identification of cow in an image frame. Future work ought to analyze further machine vision based identification based approaches for detection and recognition, but they also ought to include the RFID identification as well since these identifications are already in use in many dairy operations and even mandated across several countries.

In order for precision dairy farming to reach its full potential of benefit to dairy operations, it must be able to provide the most accurate and detailed reports and records possible. These reports and records will greatly help in operations management decision making, herd health choices, and future planning for the facility. Being able to plan ahead is important in any business or industry, and the agricultural and dairy sectors are no different. Simple mistakes and wrong choices can lead to the failure of a dairy operation and the better informed the operator is, the chance of making such errors is minimized. Therefore, the future of machine vision based precision dairy farming systems must foresee the integration of many technologies into a cohesive network of data collection. The dairy producer does not want to spend valuable time on a daily basis learning how to use a plethora of software programs possibly across several different computers in order to obtain the results desired. Instead, having several precision dairy farming systems, machine vision based and otherwise, integrated into a single software

program that can provide quick and easy access of data results is the ideal approach going forward.

Based upon the success of the precision dairy farming machine vision systems already developed, tested, and verified in this dissertation, we have already begun looking into other venues for the use of machine vision systems for resolving precision dairy farming topics of concern. Initial data collection and analysis has already been conducted for a system that is aimed at monitoring the respiration rate and stance of dairy cow. The ideal system would be able to monitor multiple freely housed dairy cows, but the initial testing was conducted on individual dairy cow with restricted movement so that system performance could be observed in an isolated manner for an extended period of time. In order for such a system to be readily adopted, it must be able to accurately monitor the respiration rate and stance of the cow over an indefinite period of time.

Respiration rate monitoring of individual dairy cow involves counting the number of breath inhalations or exhalations the cow makes on a per minute basis. A visual monitoring approach is impractical as it requires personnel to devote their time and efforts solely to this task when their abilities could be best utilized elsewhere. Tactile technology based approaches exists which afford the user the benefits of freeing up personnel and automating data collection. Such technologies include spirometers, waist bands, and leg bands. A spirometer is an instrument for measuring the air capacity of the lungs based upon inhalations and exhalations. As such, it can monitor respiration rate based upon the movement of air flow into or out of the lungs. Such a system can either be setup for direct mouth attachment or adjacent placement. The direct mouth approach is impractical as it would require the cow to continuously wear the device in its mouth or

it could only be used for discrete data collection events. Using a system which places the monitor adjacent to the nose or mouth is slightly more practical, but is still quite infeasible as it comes as an annoyance to the cow to continuously wear such a device against its nose or mouth. Inevitably, the cow will work to move the device away from its nose or mouth. The use of waistbands measure respiration rate via an elastic band which stretches during inhalation and contracts during exhalation. This is an effective technology for individual cow respiration rate monitoring, so long as the band has free movement. If the band's movement is inhibited, such as by being pinched between the cow and the ground, another cow, a wall, etc., then the devices ability to accurately monitor respiration rate is greatly reduced. A leg band is a device worn on one of the legs of the individual cow which monitors respiration rate based upon the oxidation of the blood in the cow's body. The major pitfall of this device is that it can be broken, damaged, or otherwise lose contact with the cow's body. It requires indefinite wearing for data collection. For monitoring a respiratory condition that directly affects the cow's immediate health, such as heat stress, time is a valuable asset in possibly saving the life of the animal. The sooner that heat stress can be detected, the faster that corrective action can be taken to eliminate it. If the leg band or other tactile technology used is lost from the cow's body or data collection ceases during this crucial timing, then it becomes more of a liability than an asset.

Stance monitoring of dairy cow simply involves monitoring the amount of time that a cow is standing up or lying down. Monitoring the stance of a cow in standing and lying bouts is a major indicator of an individual dairy cow's comfort. Visual monitoring is again impractical for the same reasons as in respiration rate monitoring. Tactile

technologies for stance monitoring exist, such as leg bands. A leg band is worn on one of a dairy cow's legs and monitors stance typically based upon an accelerometer. The accelerometer provides axial data collection which infers whether the leg is bent horizontally or vertically straight. The vertically straight nature of the leg infers a standing position while a horizontally bent leg infers that the cow is lying down. Again, the major pitfall of this device is that it can be broken, damaged, or otherwise lose contact with the cow's body. Such events cause data collection cessation, which can only be corrected when the device is fixed or replaced. Being able to continuously and accurately monitor cow comfort is essential in obtaining the best production results possible from each cow and can aid in early detection of lameness or other ailments.

This research aims to show that an automated depth camera machine vision based system has the potential to be utilized in respiration rate and stance monitoring of individual dairy cow. Because our interest was in monitoring the physiological changes of the lungs region of the cow body and in monitoring the stance of the cow, it was decided that a 3D camera with depth information would be best utilized for this study. The camera chosen was a Microsoft™ Kinect™ V2 which is capable of recording depth data, RGB color information, infrared imaging data, and audio data. The data streams utilized by this study were the infrared and depth streams. The only use for the infrared stream collection was during the testing and development stage of the system as it allowed for playback of visual recordings for verification of the respiration rate and stance of the cow. The infrared data stream was chosen over the RGB color data stream because infrared video was able to record in low light and even night time conditions

when no naturally occurring external light sources were available. This provides the user the ability to visually monitor the cow 24 hours a day.

The Kinect™ V2 manufacturer's camera connection was a 2m USB 3.0 cable connection, which does not allow for many options for safe placement of the host computer in an operating dairy farm environment. The 50m distance between the ideal host computer location and the research data collection location called for the camera to be connected remotely to the computer. USB 3.0 does not have a specified operating limit, but data transfer performance is greatly reduced after 3m of cabling. Therefore, the camera cabling of the Kinect™ V2 was replaced with a 61m LC-LC fiber optic cable connection which incorporated the use of a set of Newnex FireNEX-5000H™ optical repeaters (Newnex Technology Corporation, Santa Clara, California) which maintained the necessary USB 3.0 data transmission rates.

The cows at the University of Kentucky Coldstream Dairy Research Farm used in this study were individually isolated from physical contact with one another so as to not interfere with the data collection process. Because we were able to isolate individual cow into a specific stall, and also because the depth information we were interested in could be monitored best from a position above the cow, a camera frame was engineered with 80/20® aluminum which placed the camera in a fixed position above the cow and stall. This camera frame and setup can be seen in Figures 5.1-5.3. The camera frame was designed to be quickly and easily adjustable in order to position the camera at an ideal height above the individual cow's back and to position the camera centrally over the individual stall area. Steps were taken in the designing and setup of the camera frame to isolate as much camera motion as possible. This setup allowed for the maximum limited

freedom of movement and comfort for the cow in the camera scene while providing

continuous, long-term monitoring over several consecutive hours for this study.

Figure 5.1 – Respiration rate monitoring system viewed at an angle from the cow with the system operating above the cow. The current system is capable of expanding to include a second monitoring camera above the middle cow in the image.

Figure 5.2 *– Respiration rate monitoring system viewed from beside the cow with the system operating above the cow.*

Figure 5.3 *– Respiration rate monitoring system viewed from behind the cow with the system operating above the cow.*

During the software development stage, over 20 hours of data was collected and stored with the Kinect™ V2 camera for playback in order to refine the algorithms necessary for automated monitoring of respiration rate and stance. The recording and playback of files was made possible by employing the use of Microsoft™ Kinect Studio (Microsoft Corporation, Redmond, Washington). With the Kinect Studio software, any recorded file could be played back to simulate a connected Kinect™ V2 camera, which allowed for rapid development and testing. The Kinect Studio software also allowed for recording only select data streams, which minimized the amount of data storage needed per frame of video. Recording only the depth and infrared streams exhibited possible recording times of up to just over 2 hours and approximately 220GB of data storage space required. The Kinect Studio software also allowed for looping of recorded data as well, allowing for shorter recordings and subsections of longer recordings to suffice for robust algorithm development. Figures 5.4 – 5.9 show example frames of data captured with the Kinect™ V2 using the Kinect Studio software. As can readily be seen, the resolution of the color image with the Kinect™ V2 is much higher than that of the PrimeSense™ Carmine 1.08 and the edge detail as well as the general depth information in the depth images of the Kinect™ V2 are much more detailed than those collected with the PrimeSense™ Carmine 1.08. The inclusion of an infrared data stream with the Kinect™ V2 that the user can access is beneficial for evening, night, and other low light monitoring.
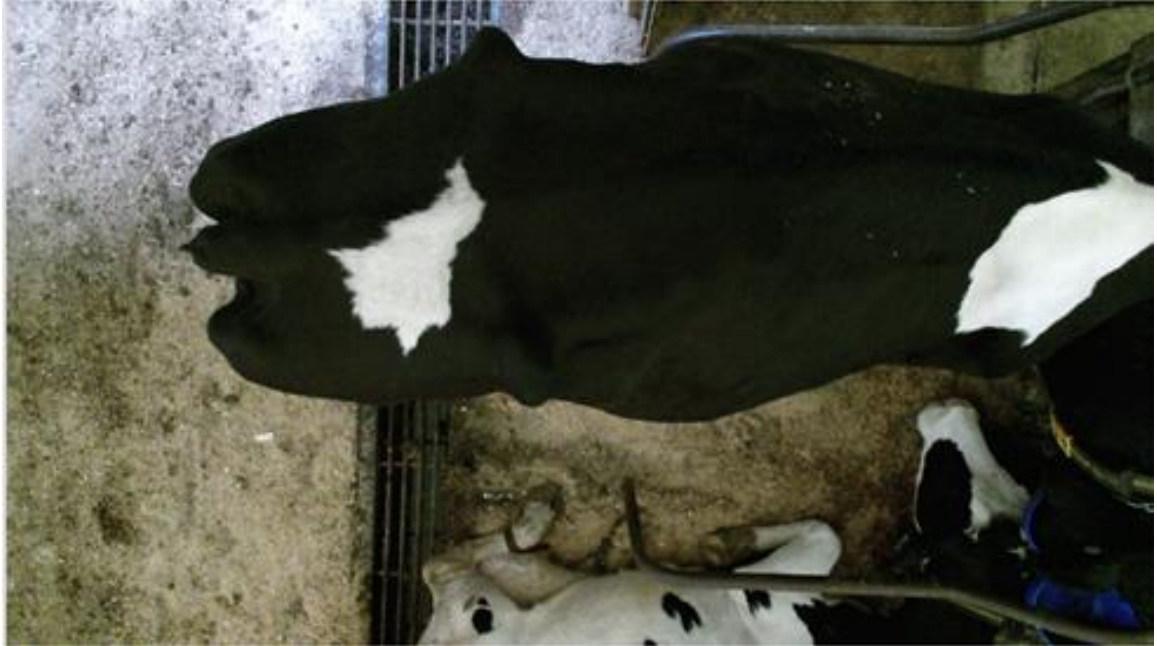
Figure 5.4 *– Kinect Studio in "Color" image mode showing the RGB color data stream.*

Figure 5.5 *– Kinect Studio in "Grey Point Cloud" image mode for the depth frame.*

Figure 5.6 – Kinect Studio in "Surface with Normal" image mode for the depth frame.

Figure 5.7 – Kinect Studio in "Infrared" image mode.

151

Figure 5.8 – Kinect Studio in "Grey Point Cloud" image mode for the depth frame.

Figure 5.9 – Kinect Studio in "Surface with Normal" image mode for the depth frame.

The software for this system was developed using Visual Studio® Community 2013 and the OpenCV library. There were two positions to be monitored for stance: standing up and lying down. As well, respiration rate monitoring by means of observing the depth information of the lungs required different algorithms for these two positions. Therefore, the software was developed to incorporate one set of instructions for when the cow was standing up and a second set for when the cow was lying down. The algorithm

for stance monitoring was simple and straightforward. The software placed a set of lower and upper threshold limits on the depth frame data as well as a cropping of the frame to remove parts of the camera scene in which the individual cow did not have free access to move, which allowed for background and noise reduction. The image also had a threshold applied which removed the floor and any other items in the background, primarily leaving only the pixels associated with the cow. The software would then find all of the contours within the cropped frame, identifying the largest contour as the outline of the cow's body. The depth data of the pixels inside of this contour were then averaged to arrive at a value which represented the average depth of all of the cow body data points. If this value was at or above a predetermined threshold, then the frame was assigned to having a cow standing up. If this value was below the predetermined threshold value, then the frame was said to have a cow lying down. This was the extent of the stance monitoring software, but played a vital role in the structure of the respiration rate monitoring algorithms.

For the respiration rate monitoring, once the frame was assigned as either a standing up or lying down cow from the previous step, it would then proceed to isolate a predefined region of interest from the cow body for depth data monitoring. When the cow transitions from one stance to the other, the software is incapable of accurately monitoring the breathing because of how the algorithms are setup to monitor respiration rate based upon the stance. Therefore, during times of stance transition, the software will stop the current respiration rate monitoring algorithm, provide for a pause in data analysis until the cow has settled into its new stance, and then resume respiration rate monitoring with the appropriate algorithm based upon the current stance.

If the cow was standing up in the frame, this provided the software the ability to observe the left lung, the right lung, or both at the same time. From the contour information of the cow body, a centroid pixel could be determined which represented the center point on the back of the cow's body. Two 50 pixel by 50 pixel squares could then be offset from this center, one for the left lung and one for the right lung. Each square would then search for the nearest cow body contour pixel point to this area. The algorithm was setup for this to automatically take place for every depth frame. By monitoring the change in pixel distance for this minimum value over time, the breathing of the cow standing up could be determined. Although both lungs were monitored separately at the same time, only a single lung could be monitored if desired or necessary. Such reasons for only wanting to monitor a single lung would include if the opposing lung's depth information became occluded from view or if only a single lung were visible in the camera scene. The setup of this research accounted for these factors as much as possible beforehand so that both lungs could be continuously monitored simultaneously. This also allowed for the verification of the breathing by comparing the two values to each other. If both values were relatively close, then both areas were returning essentially the same lung capacity displacement value.

If the cow was lying down, a similar approach was derived but for a single lung since only one side of the cow was visible in this position. Again, the cow body contour data and centroid pixel information were used to determine the region of the cow body to monitor breathing. For the lying down position, a single 50 pixel by 50 pixel square was positioned at an offset from the centroid which placed this square optimally over the lung in the camera scene. The average value for the depth data of the pixels contained within

154

this area was then derived. The algorithm was setup for this to automatically take place for every depth frame. By monitoring the change in average depth value for the pixels in this region over time, the breathing of the cow lying down could be determined. Because the cow did not move much once in the lying down position, this region could be continuously and consistently monitored from one frame to the next.

This research tested the capability of monitoring both the respiration rate and stance of individual dairy cow by non-tactile means utilizing a 3D camera. The results of this research show that such a system can accurately and effectively monitor both. The system of this study was programed to monitor only a single cow at a time, isolated from other physical contact with other cow or any other external objects. This was done in order to preserve data integrity by diminishing as many possible outside effects that could impart erroneous results as possible. Future systems should develop software that can aptly handle multiple cow in a camera scene, possibly including different pose positions than just the top view approach of this study. Preliminary testing results also indicate that it may be better to offset the camera towards one side of the cow so that the standing position of the cow does not occlude the flank of the cow. By offsetting the camera to either the left or right side, it may be possible to better observe the respiration of the cow. This system has been tested with only a few cow so far, so the study must also be expanded to include several more test subjects before any results can be deemed conclusive. The preliminary results seen in Figures 5.10 and 5.11, though, for example observational periods of respiration rate monitoring data provide insight into the ability of this system to perform accurately. The respiration rate determined for the examples in Figures 5.10 and 5.11, as well as for various other samples tested, have so far fallen

within a range of 36 ± 3 breathes per minute (**bpm**). The human visual observation of this same sample was 36 bpm. Therefore, further testing is deemed necessary as this system proves plausible and accurate at determining the respiration rate of individual dairy cow as well as monitoring their stance.
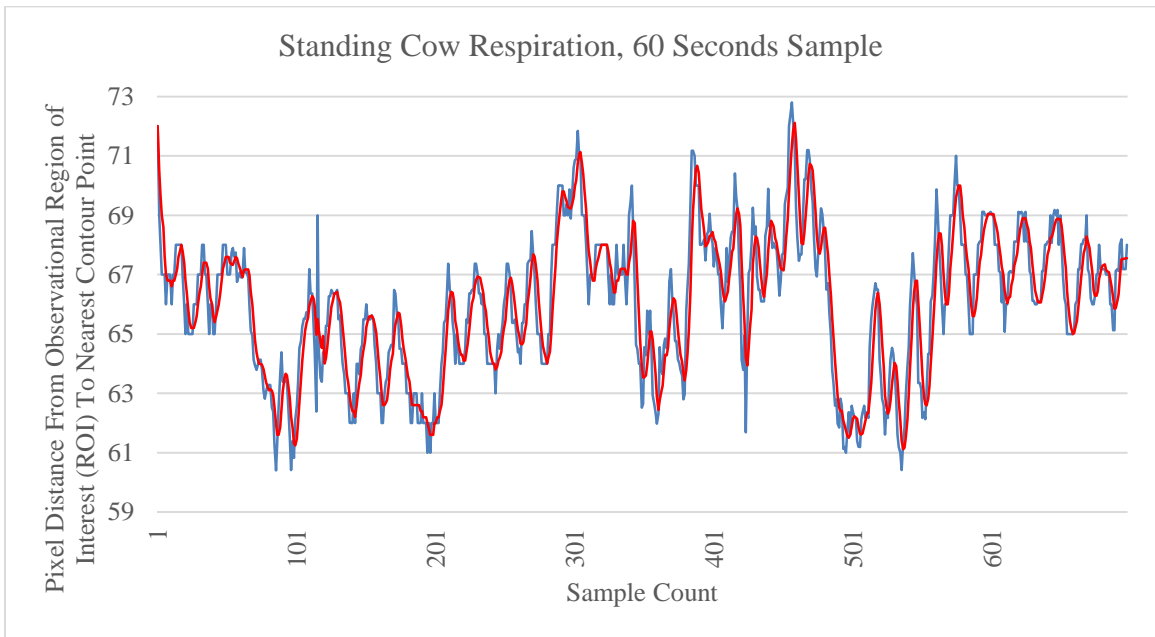
Figure 5.10 *– The above plot shows a standing respiration rate sample. The blue line is the raw data and the red line is the averaged data.*
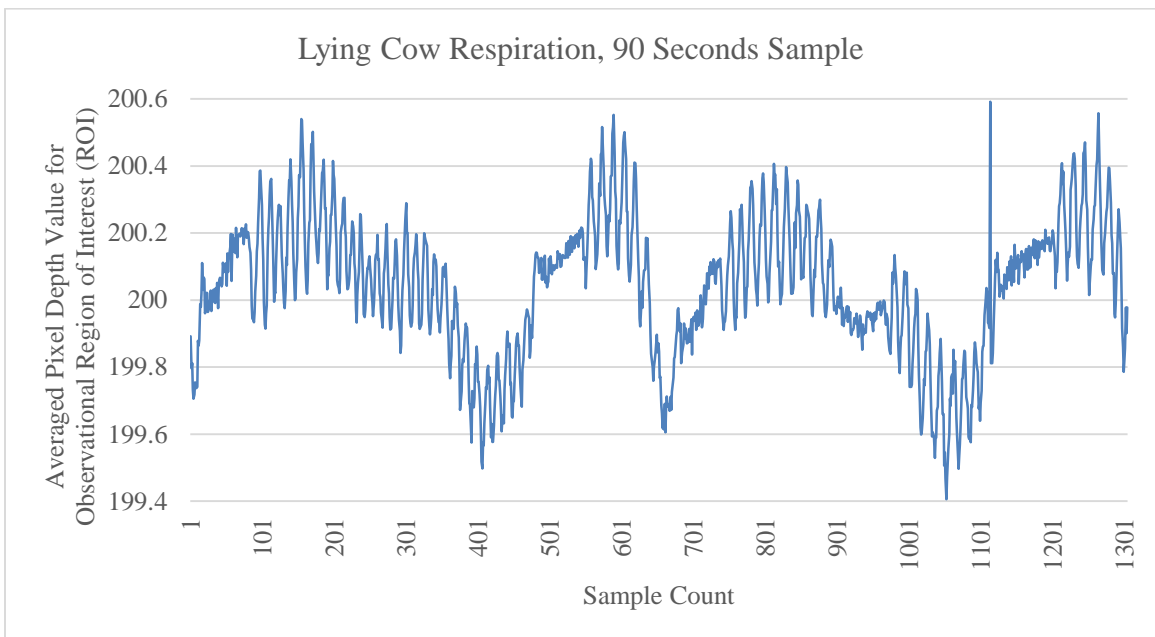
Figure 5.11 *– The above plot shows a lying respiration rate sample.*

Although many precision dairy farming machine vision systems have been studied in the research of this dissertation, it is not an exhaustive use of this approach. There exist several other topics of concern in regards to animal welfare that have yet to be addressed. Using the principles, methods, and results of this dissertation, it is hoped that future work will continue to build upon the work presented here to disseminate these systems across several modes of use. It is easy to envision the use of these systems in other livestock operations, conducting the same data collection and analysis. Although harder to visualize, the use of results of this dissertation research can be directed to observe several other biological lifeforms for biometric data analysis. Such systems would potentially be capable of providing a better understanding into the life processes and individual health of many different organisms. Systems similar to the ones outlined in this research have already been developed, tested, and verified with human subjects. As imaging technology advances and the appreciation of individual welfare continues to increase, it is expected that such beneficial health monitoring systems will become quite commonplace.

APPENDIX A

The following plots contain the comparisons of human visual BCS scoring, shown with red data points, versus computer-generated BCS scoring, shown with blue data points. There were 116 dairy cow included in this observational study over a period of 221 days from April 1, 2014 to November 7, 2014. The data were recorded at most twice per day, so some data points are BCS scores for samples recorded from the morning milkings and the others are from evening milkings. This study aimed at observing the gradual changes in BCS for each individual animal of the dairy cow herd over the entire monitoring period. Dairy cows in various stages of lactation were included. Therefore, some cows only have a small dataset of BCS monitoring values because they either left the herd early on due to going dry or they came into the herd towards the end of the study due to beginning their lactation cycle. The plots of this appendix are listed by cow identification number.

1103

1332

1366

1370

1429

1430

1497

1498

1510

1517

1530

1533

1543

1544

1551

1552

1553

1554

1555

1556

1571

1573

3010

4918

4924

4927

4948

4950

Copyright © Anthony Neal Shelley 2016

216
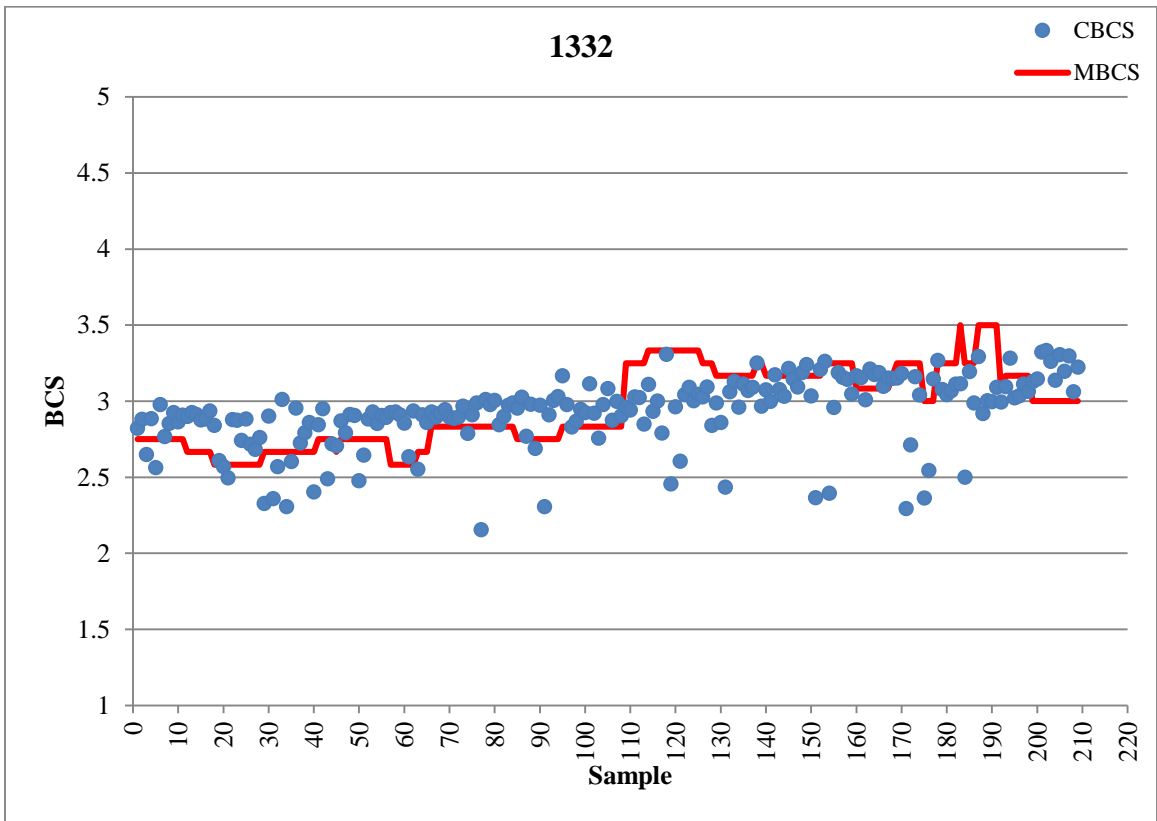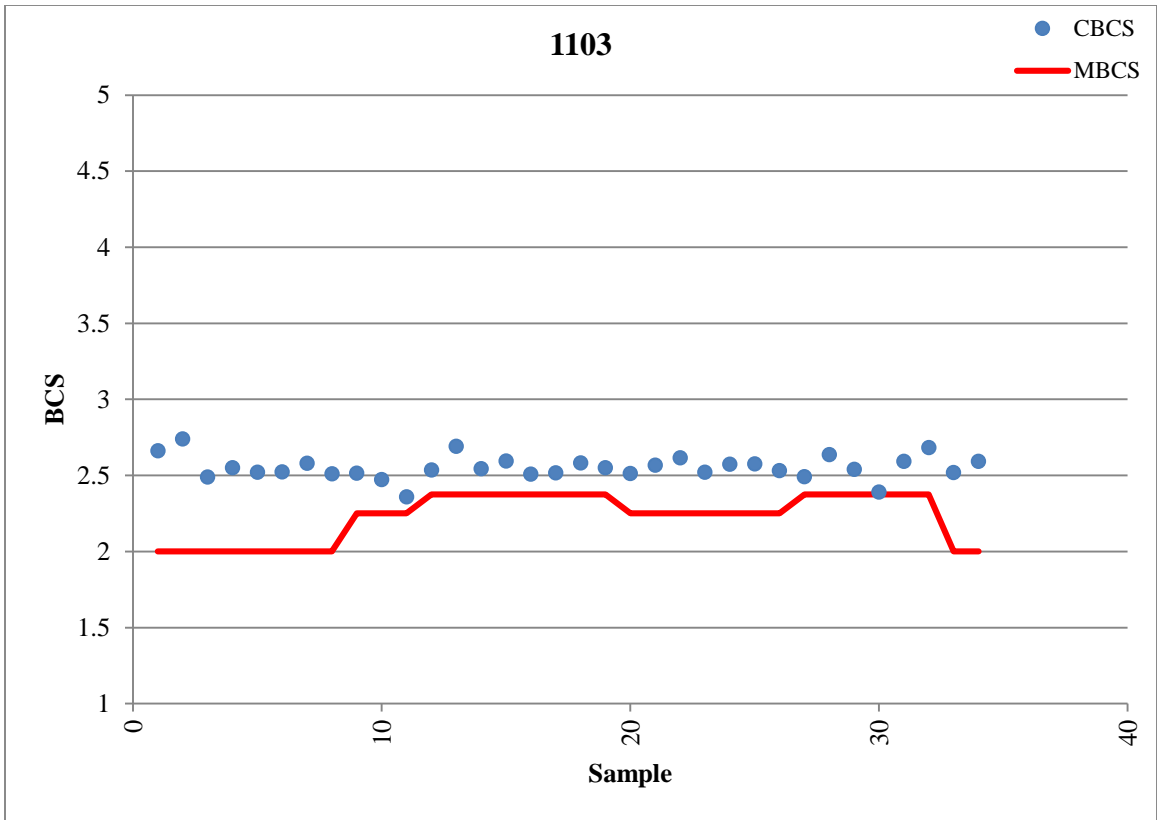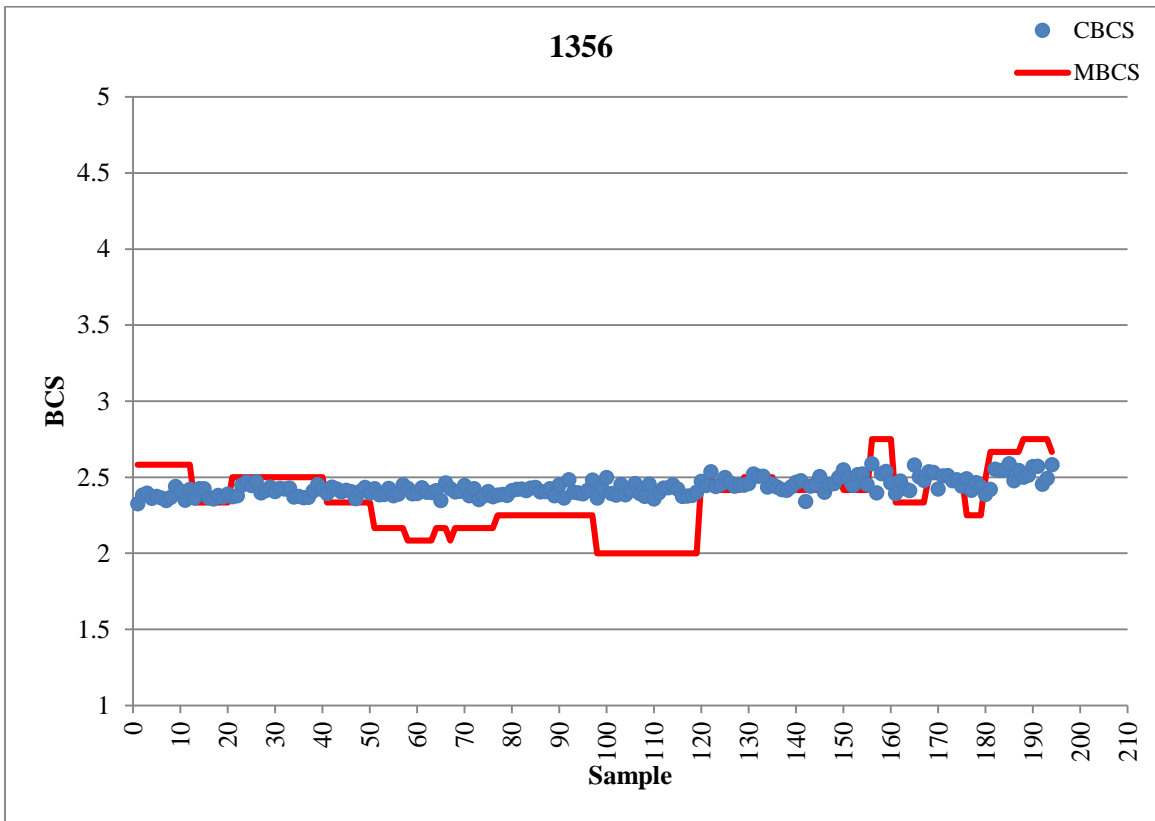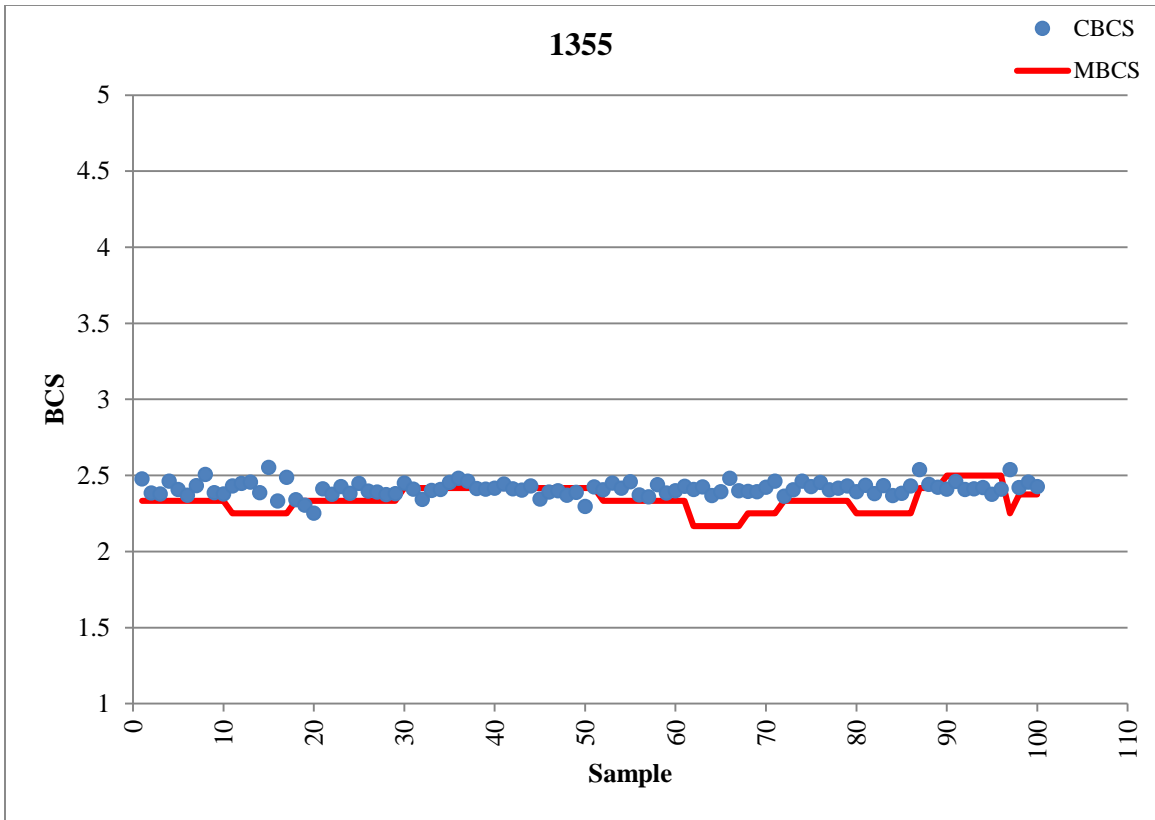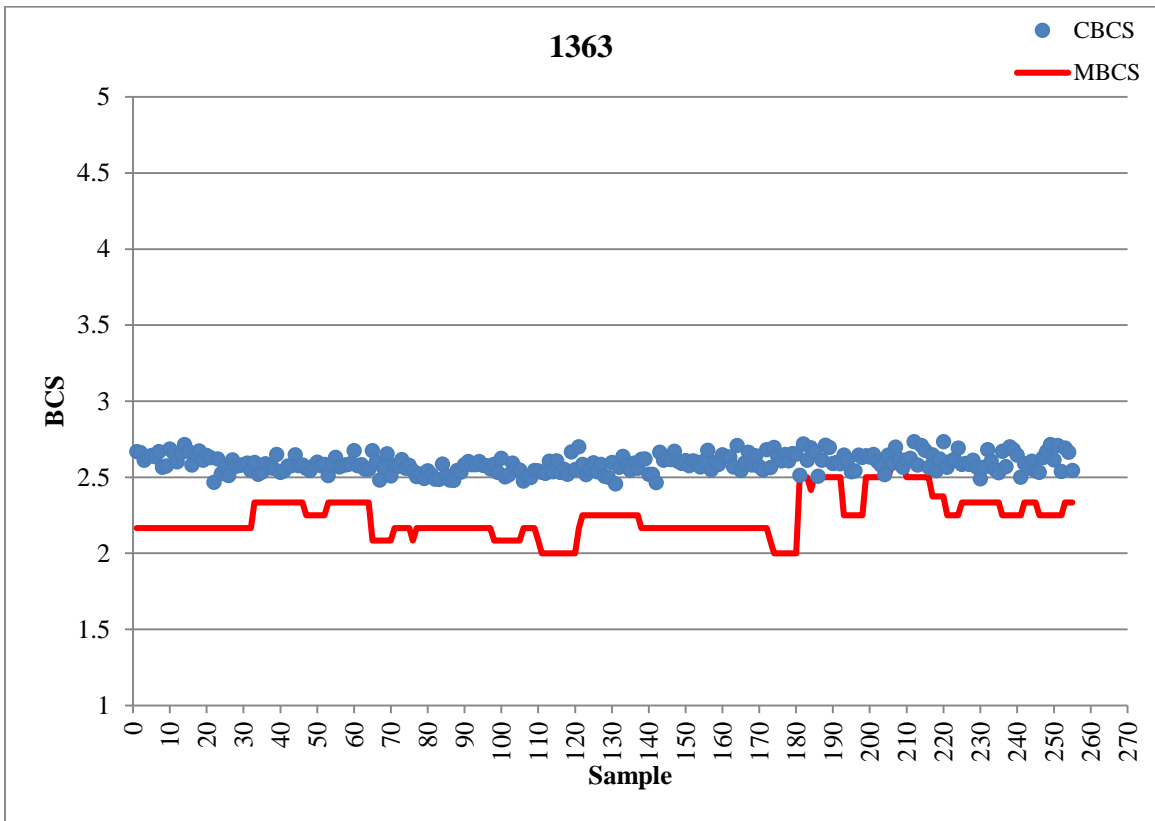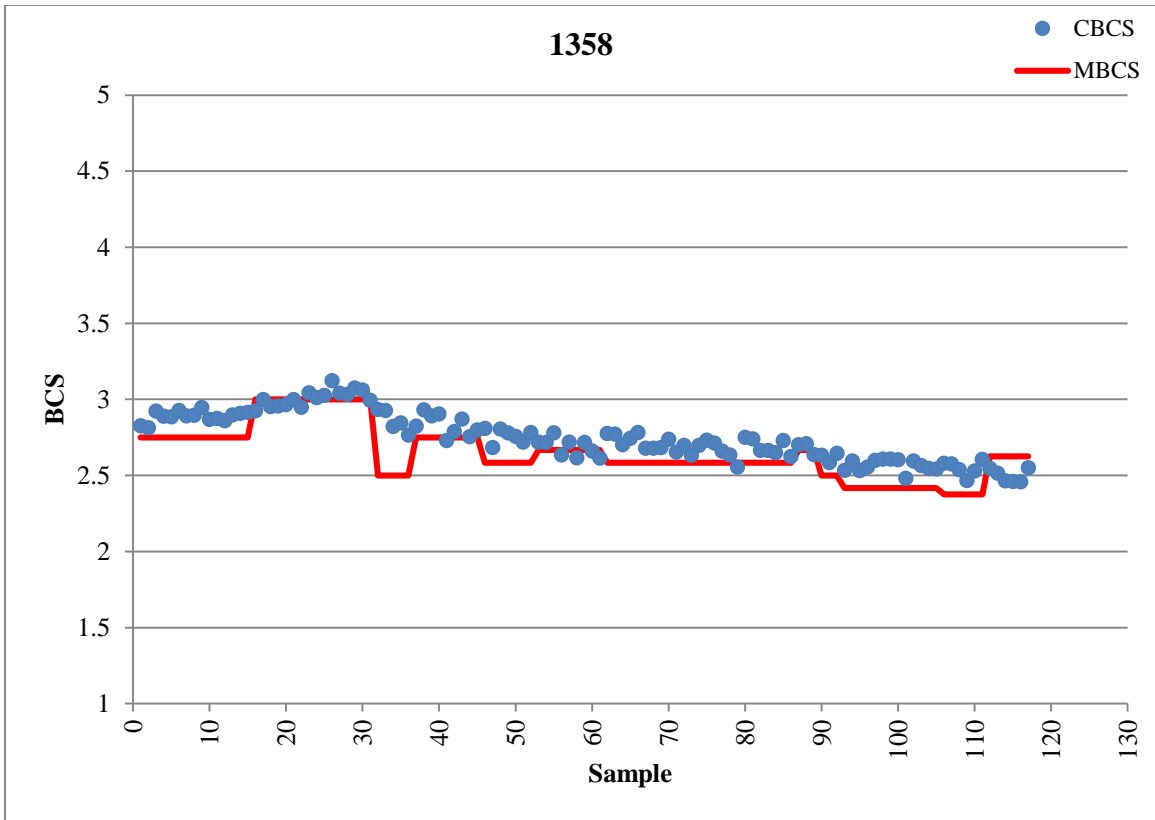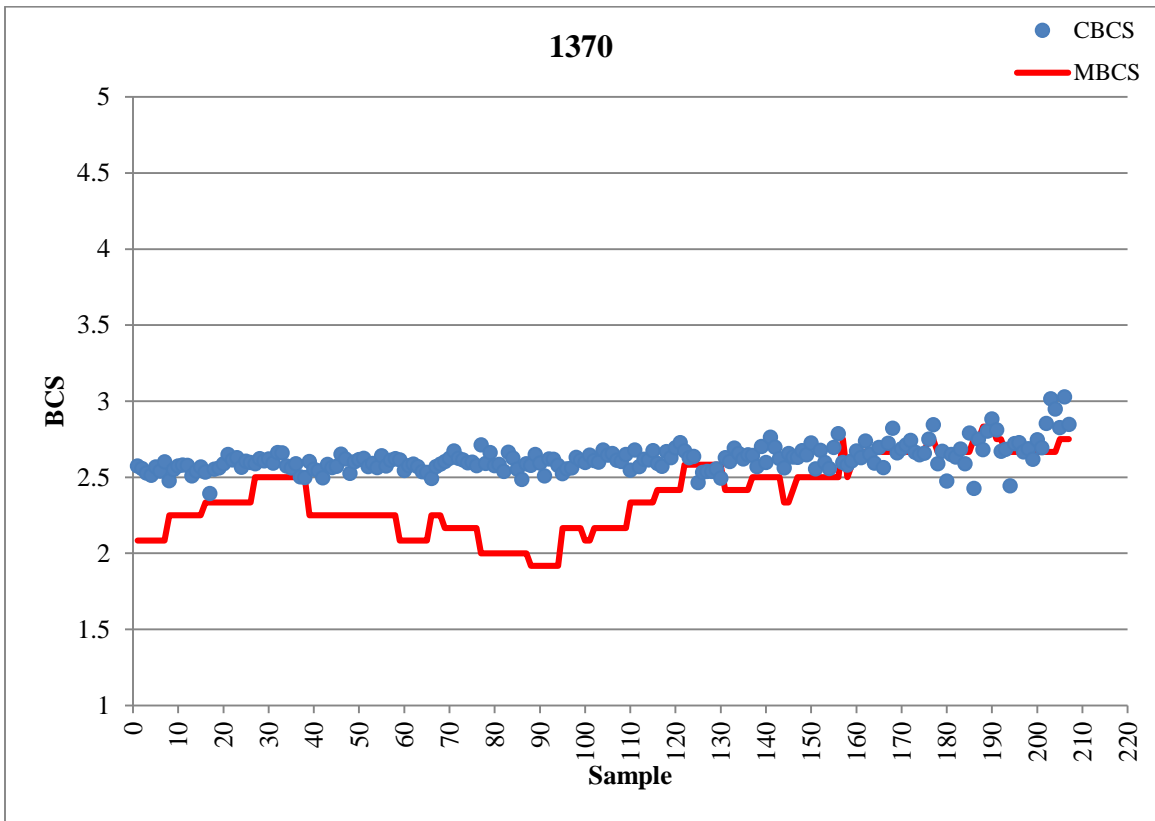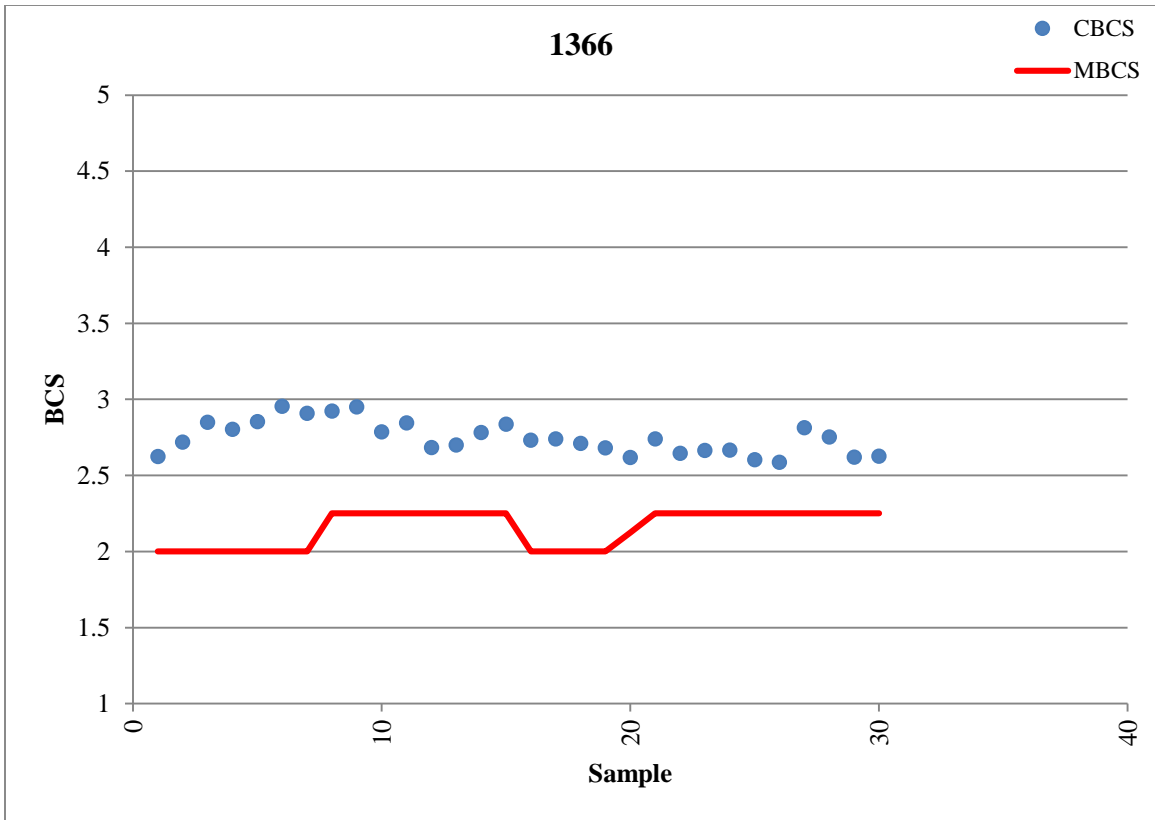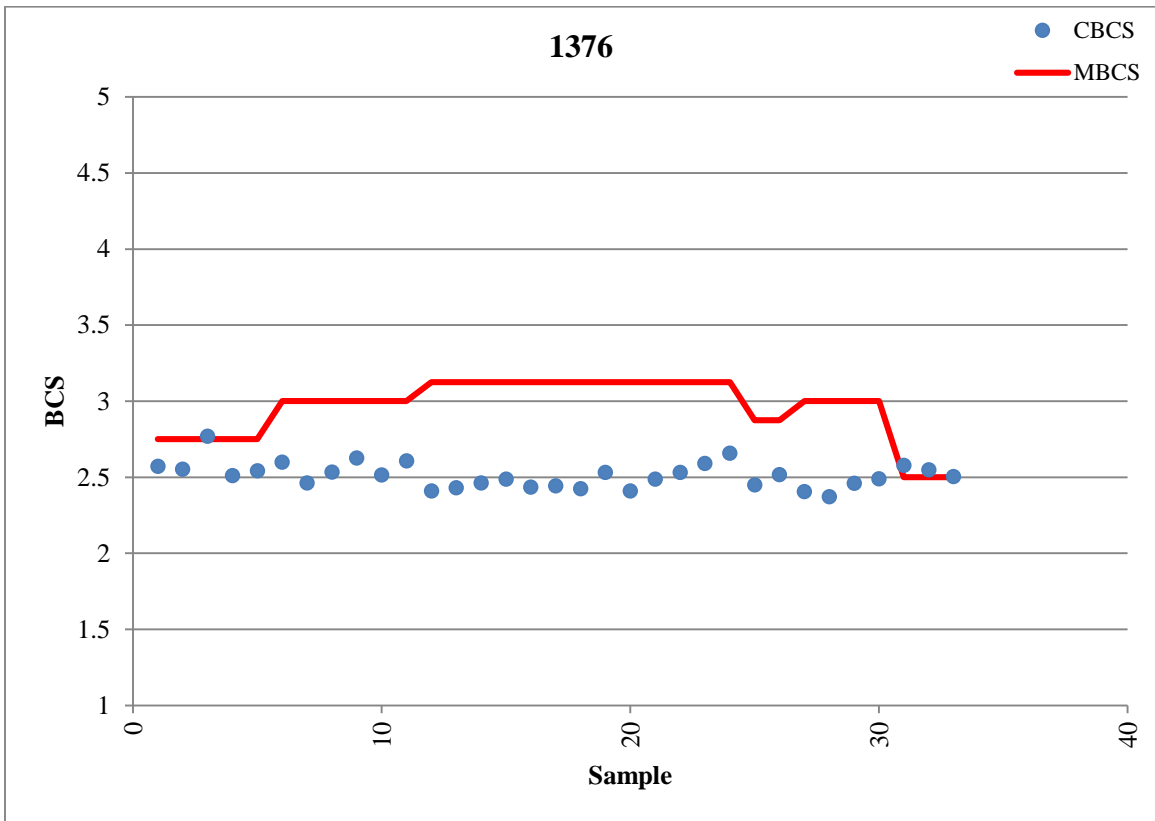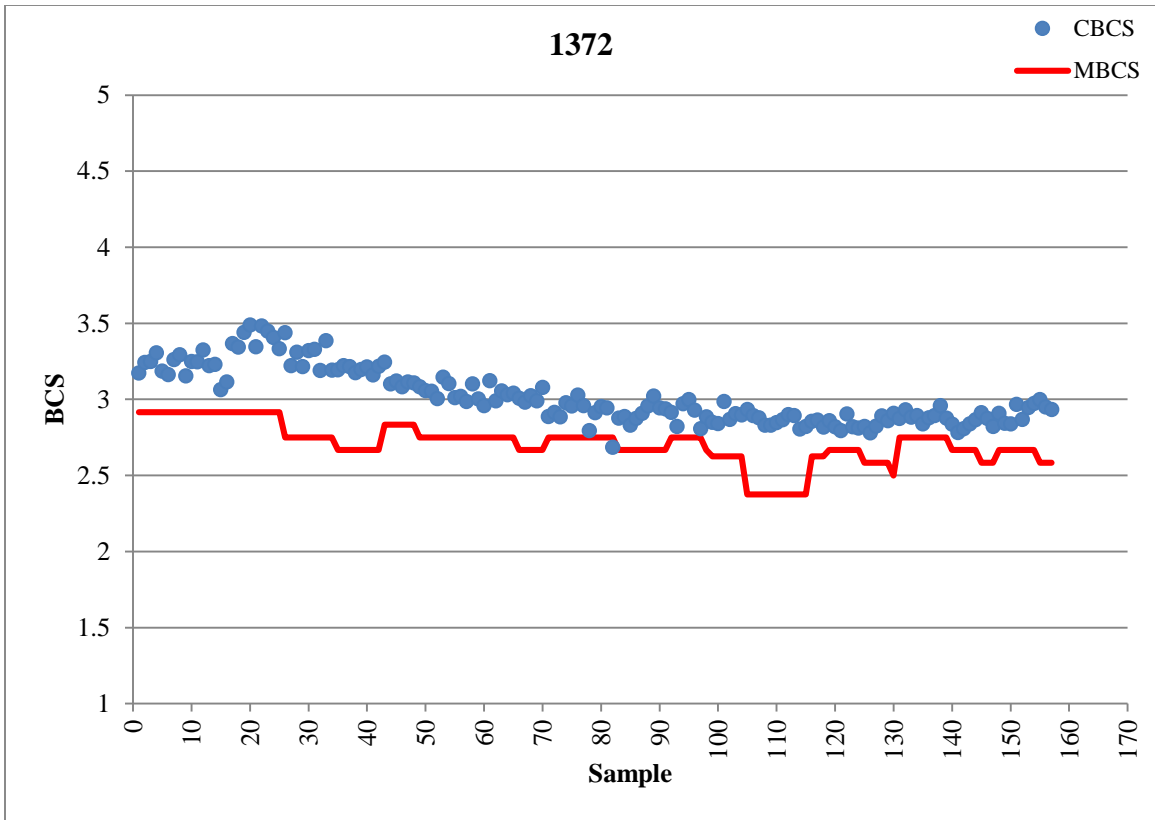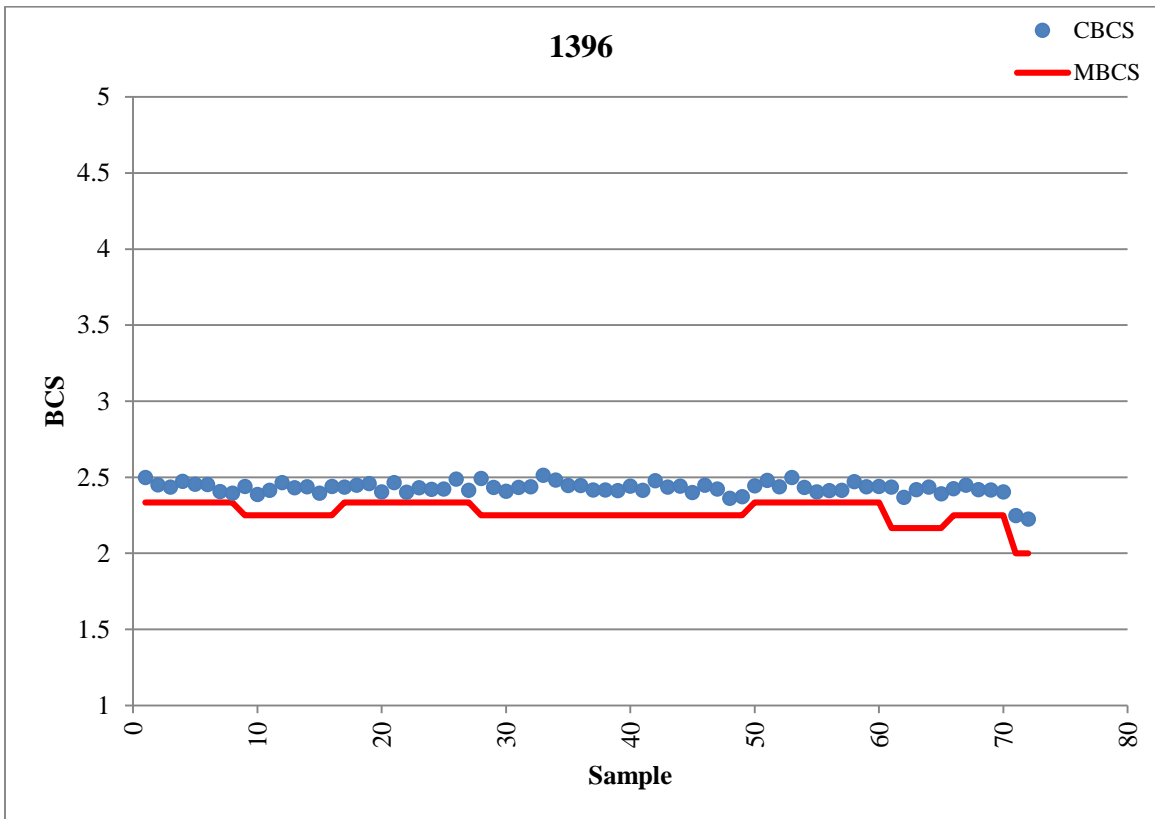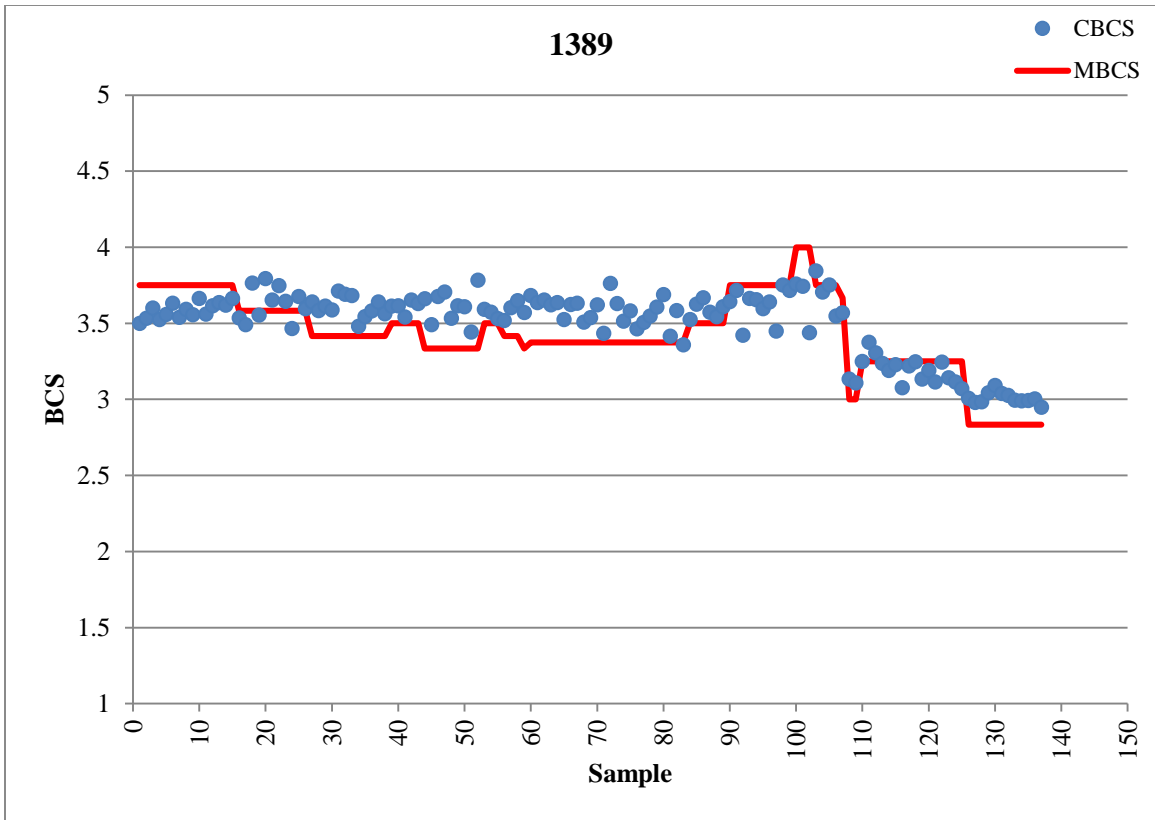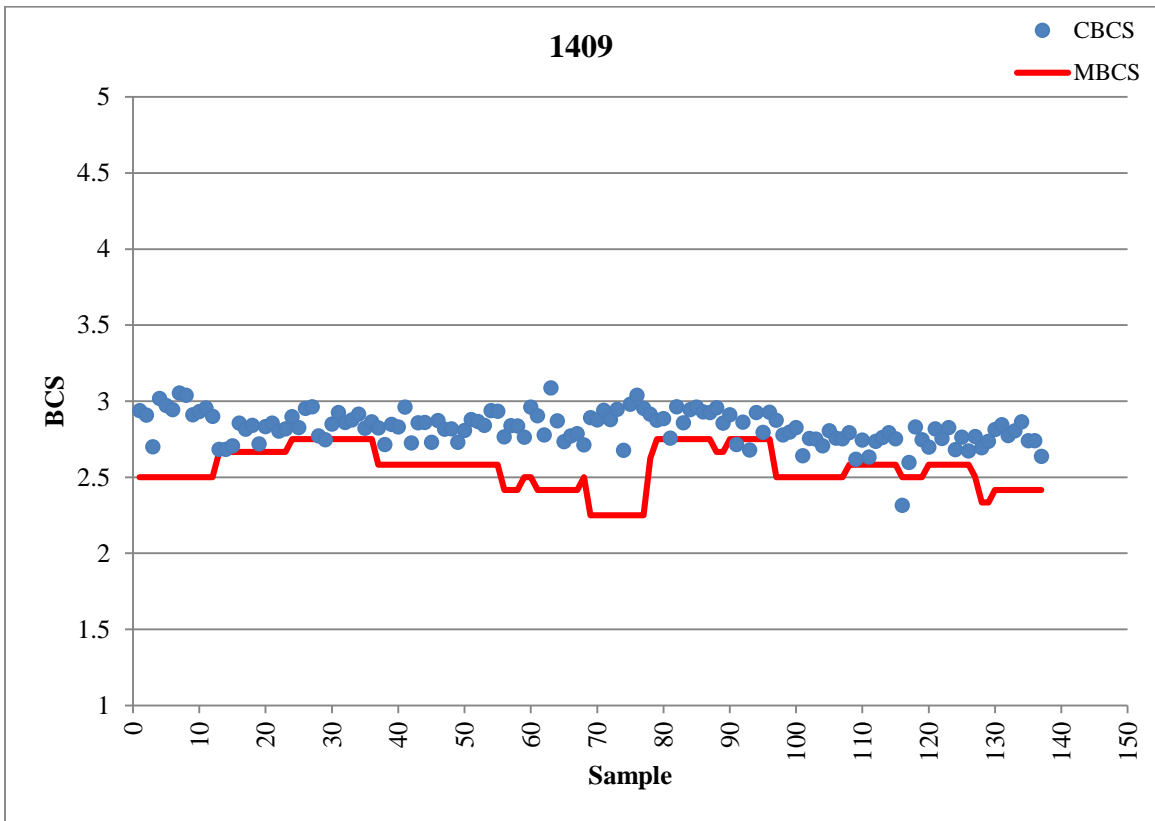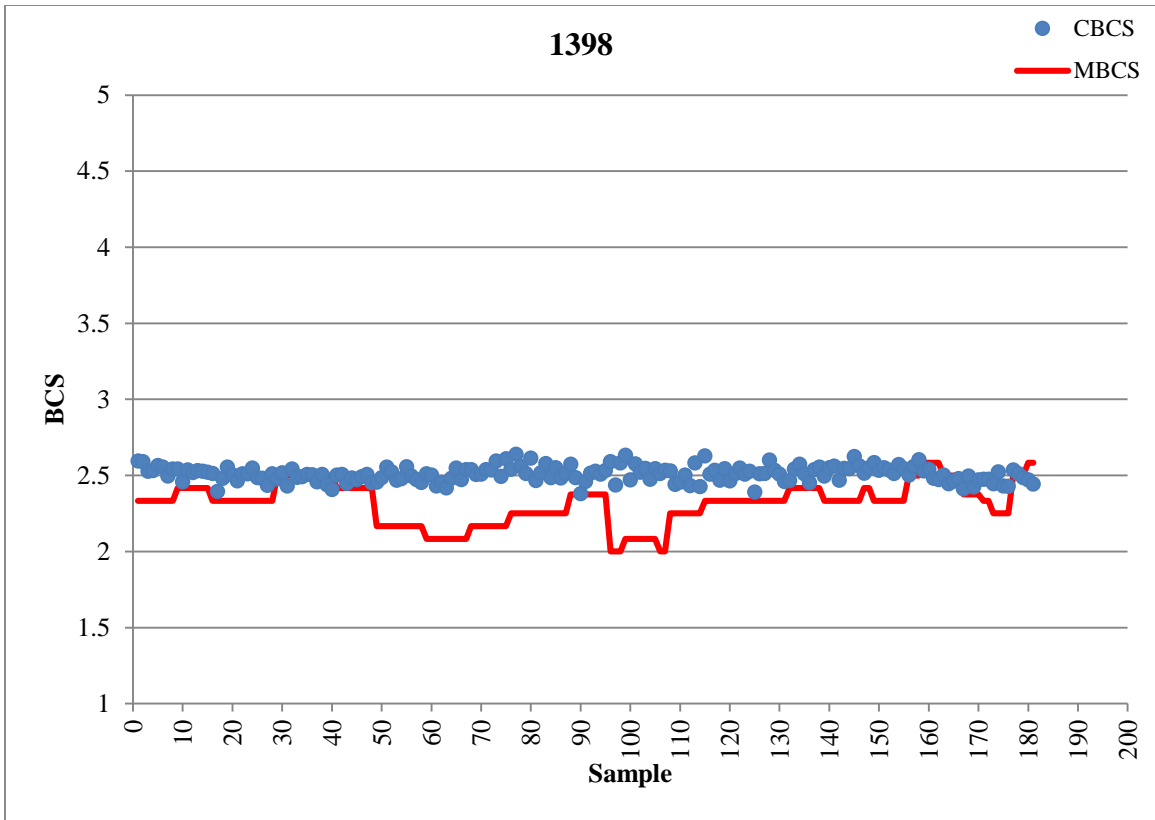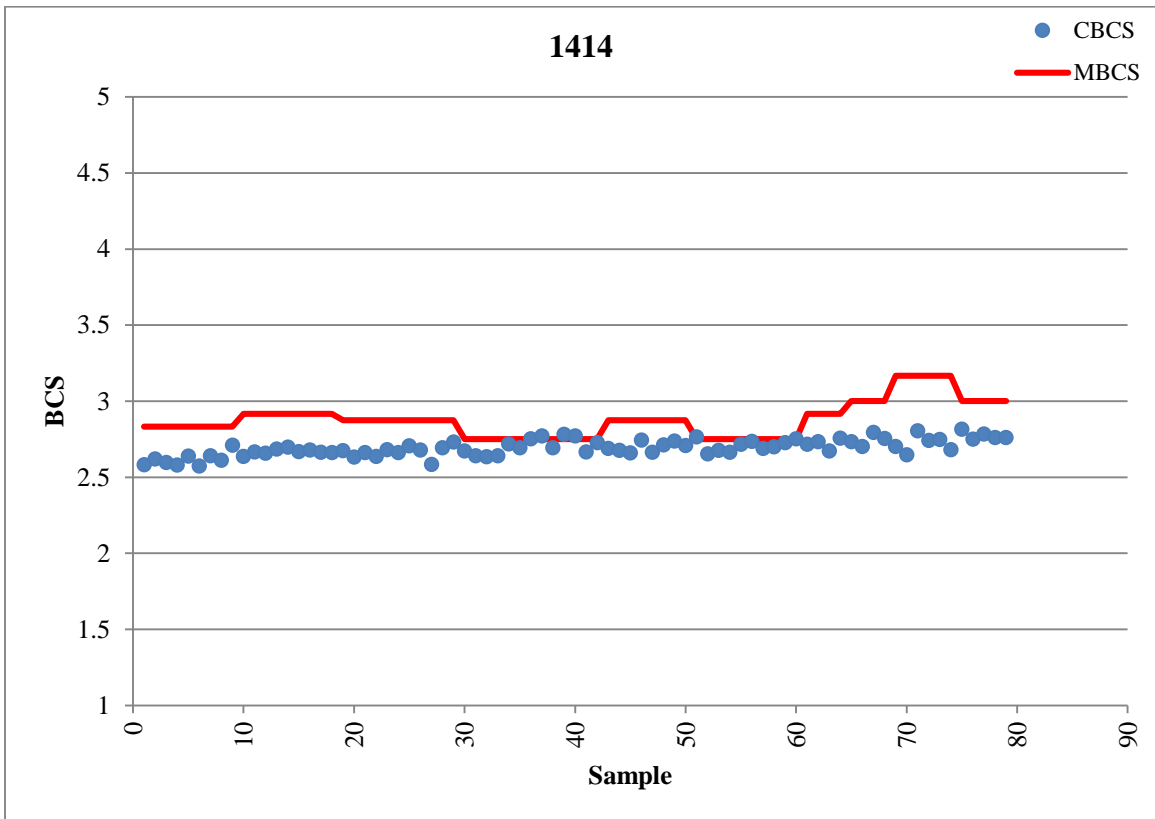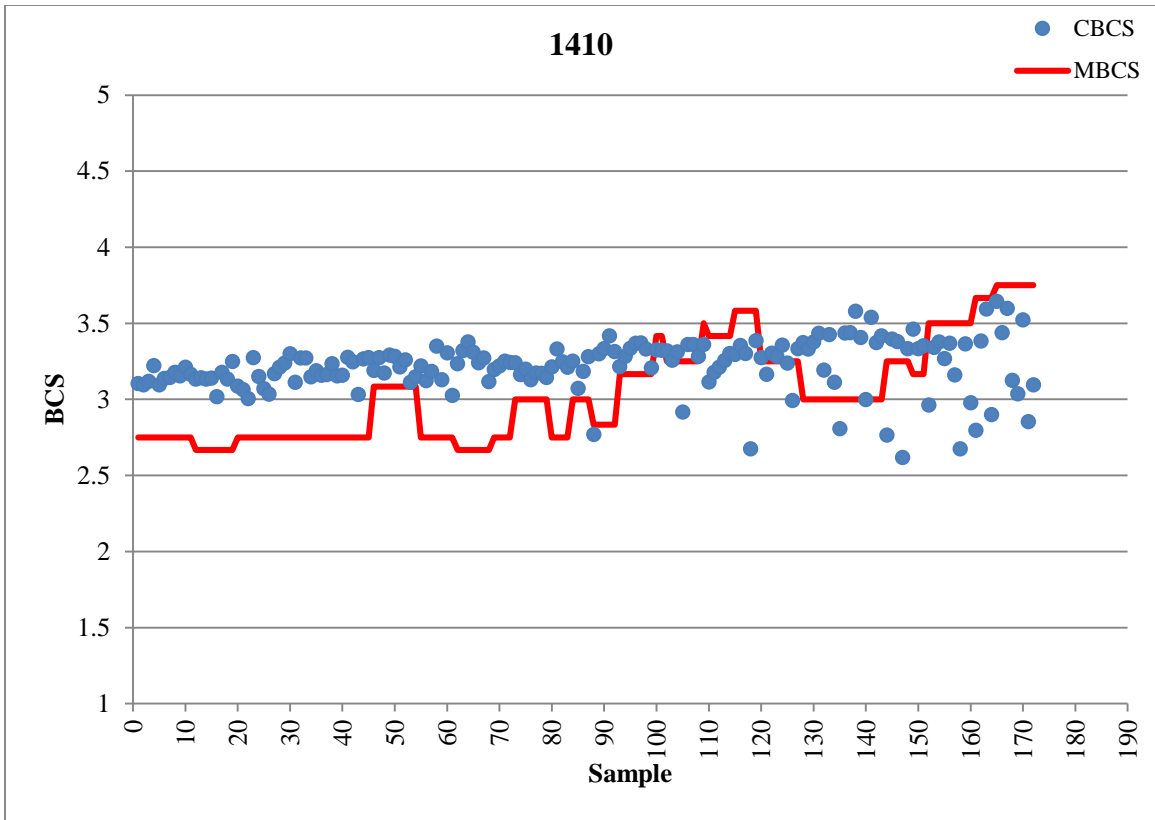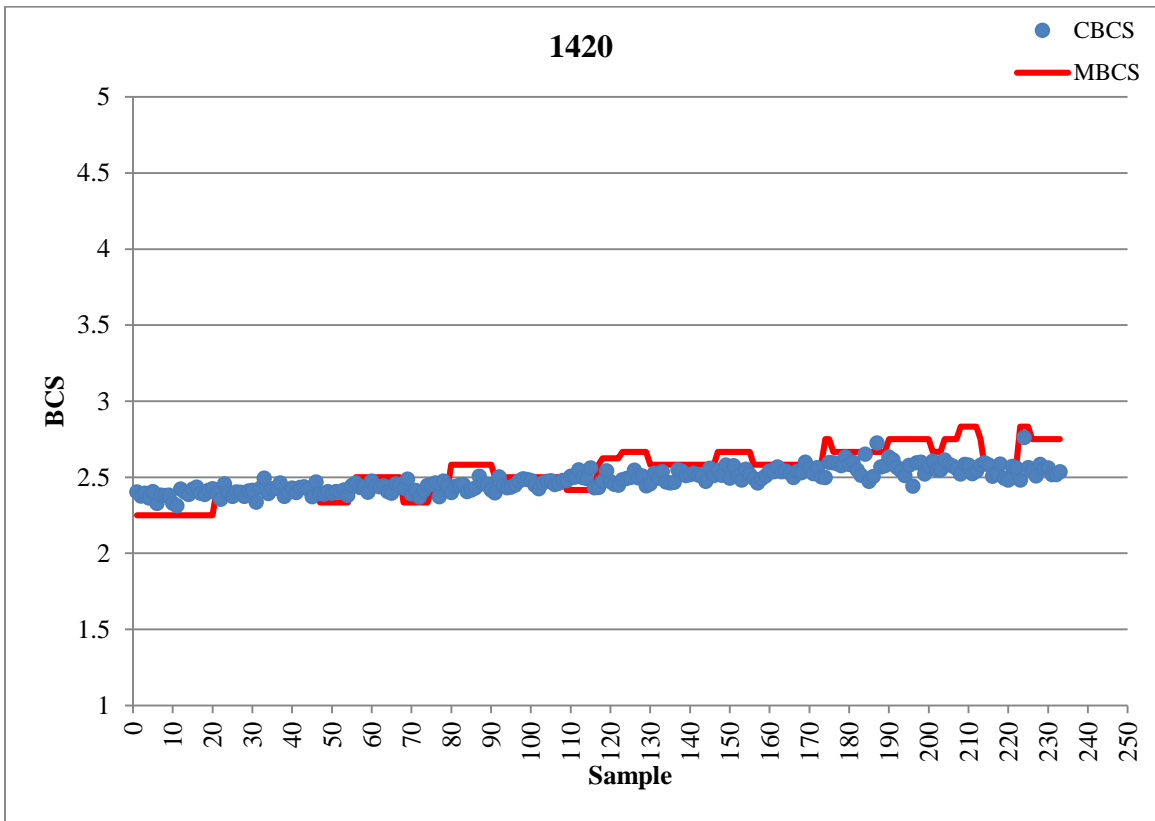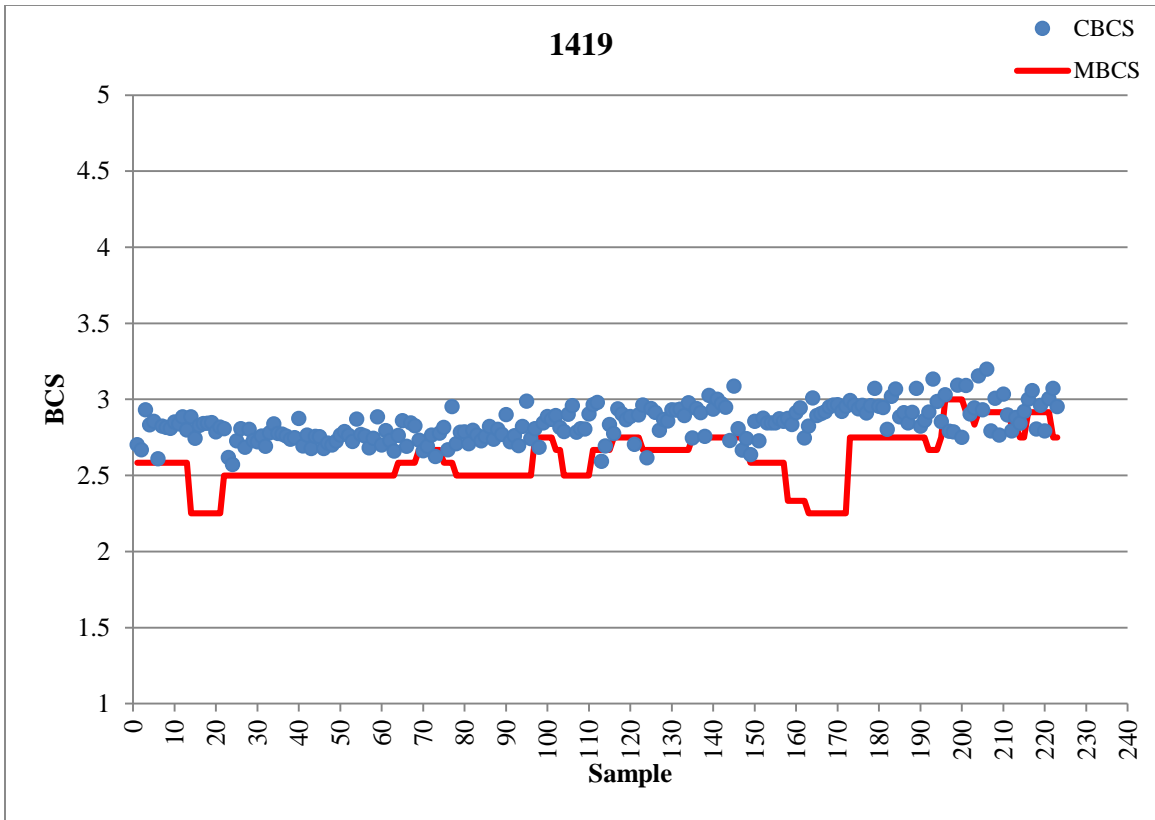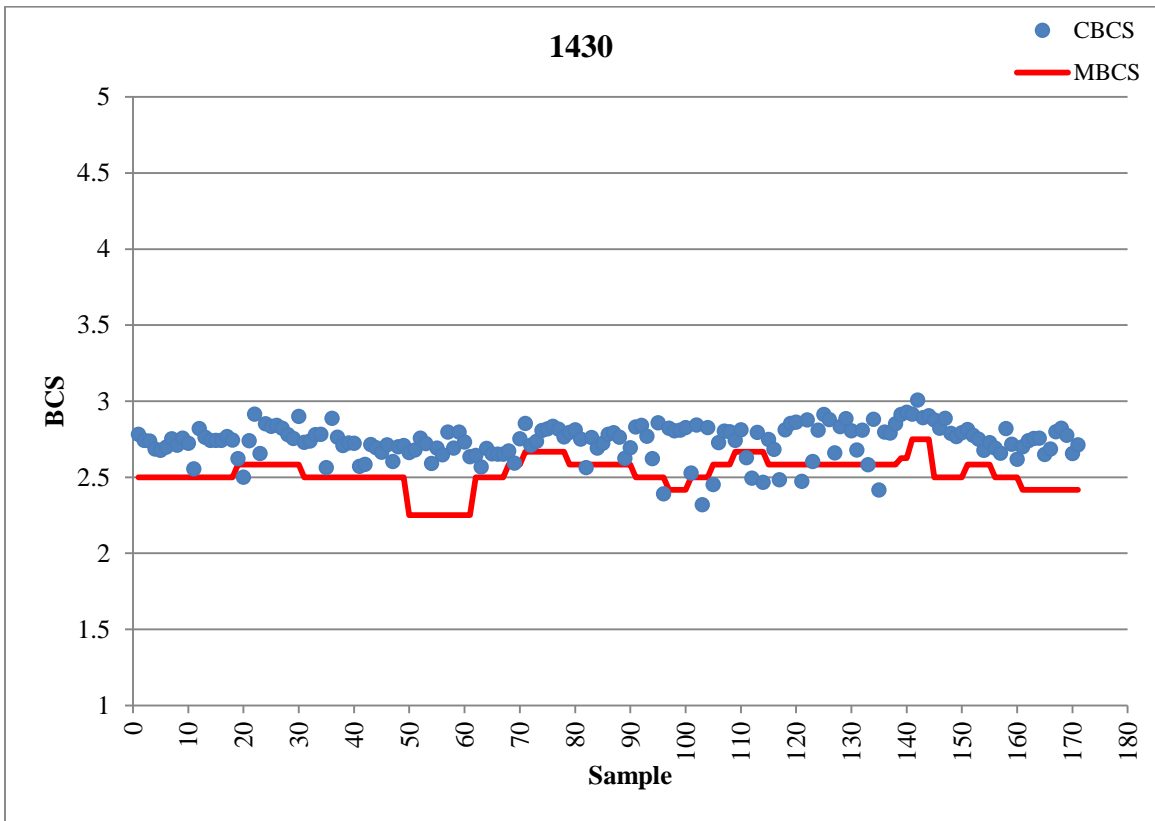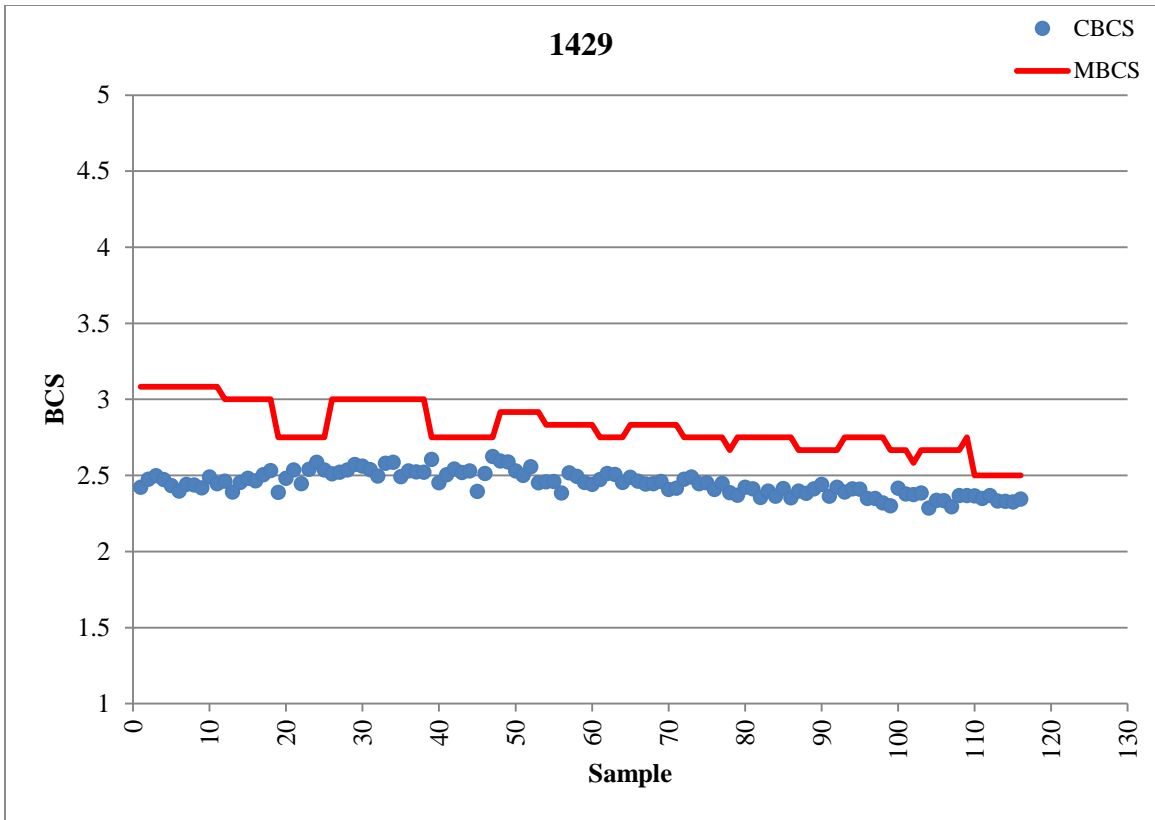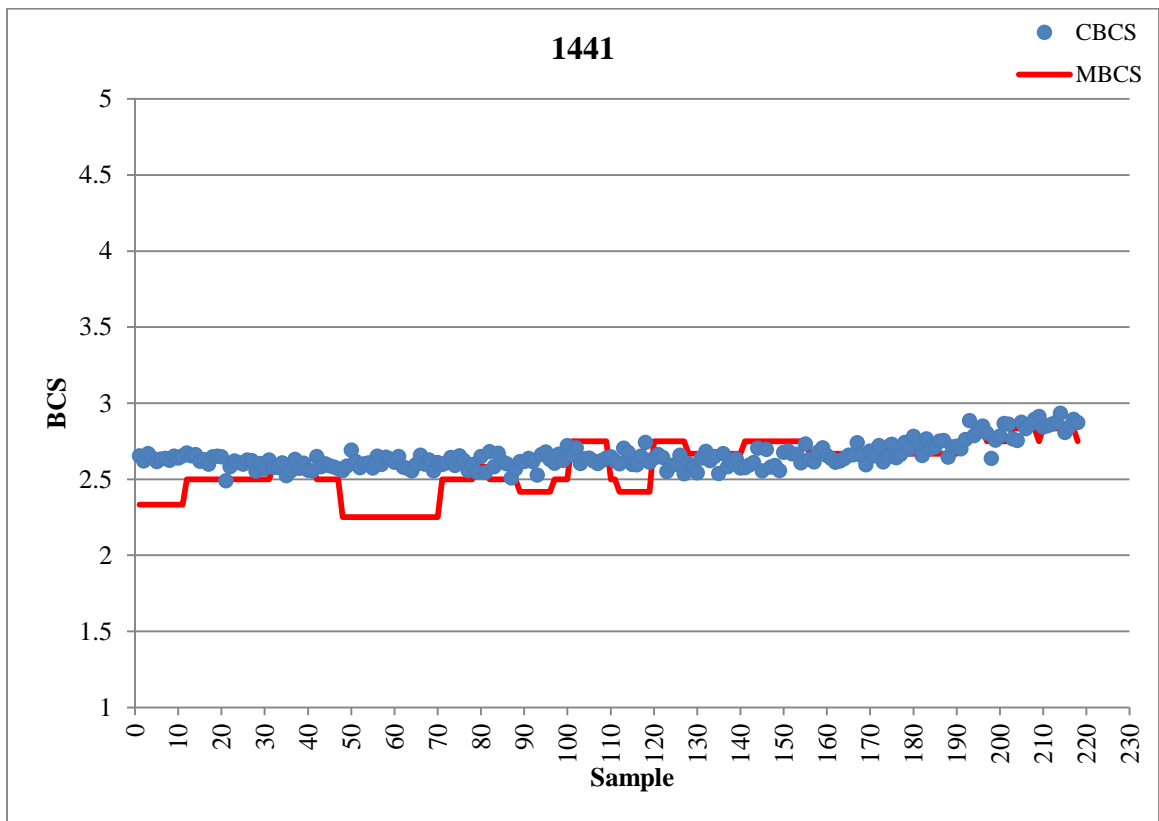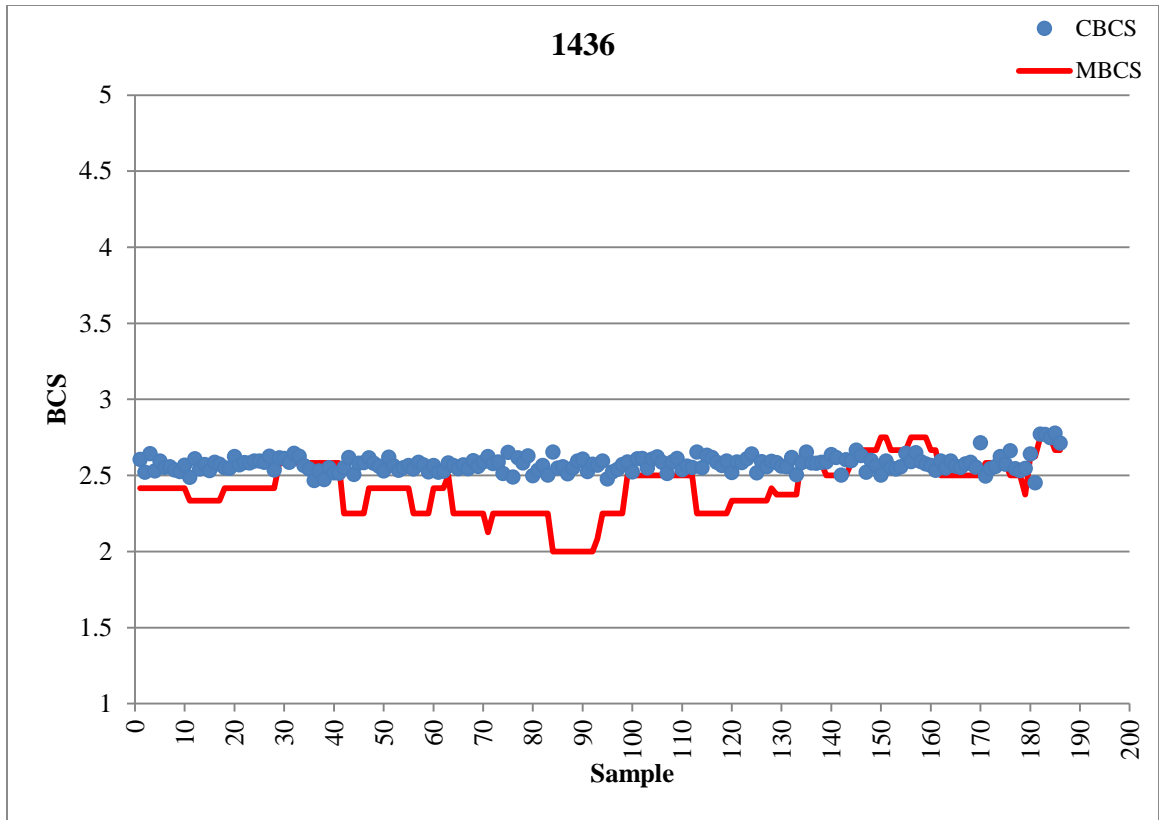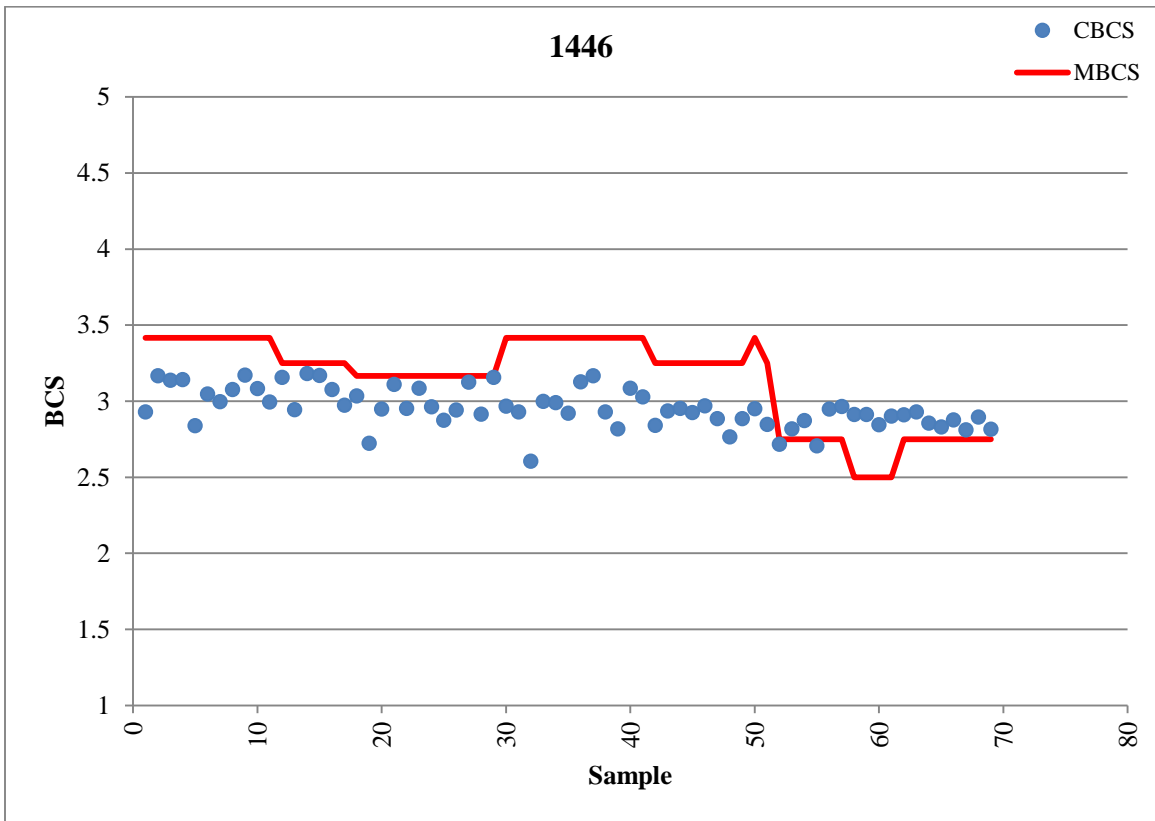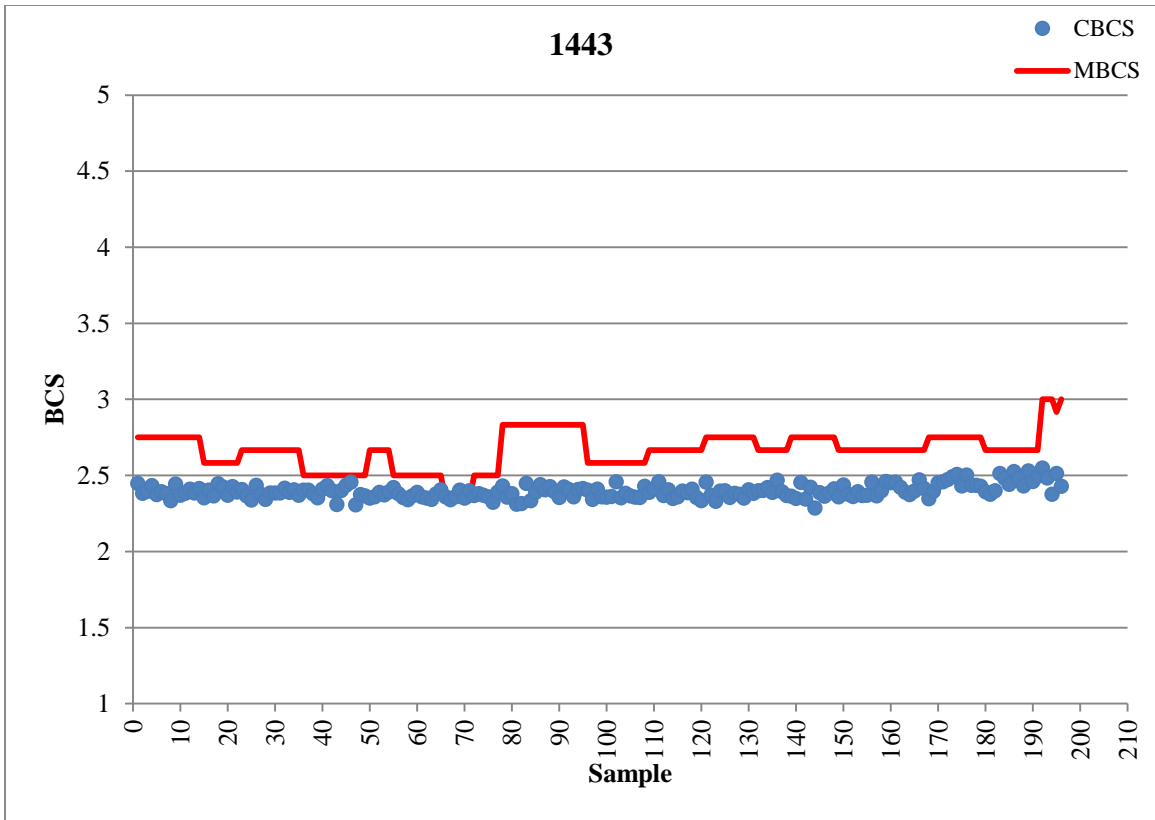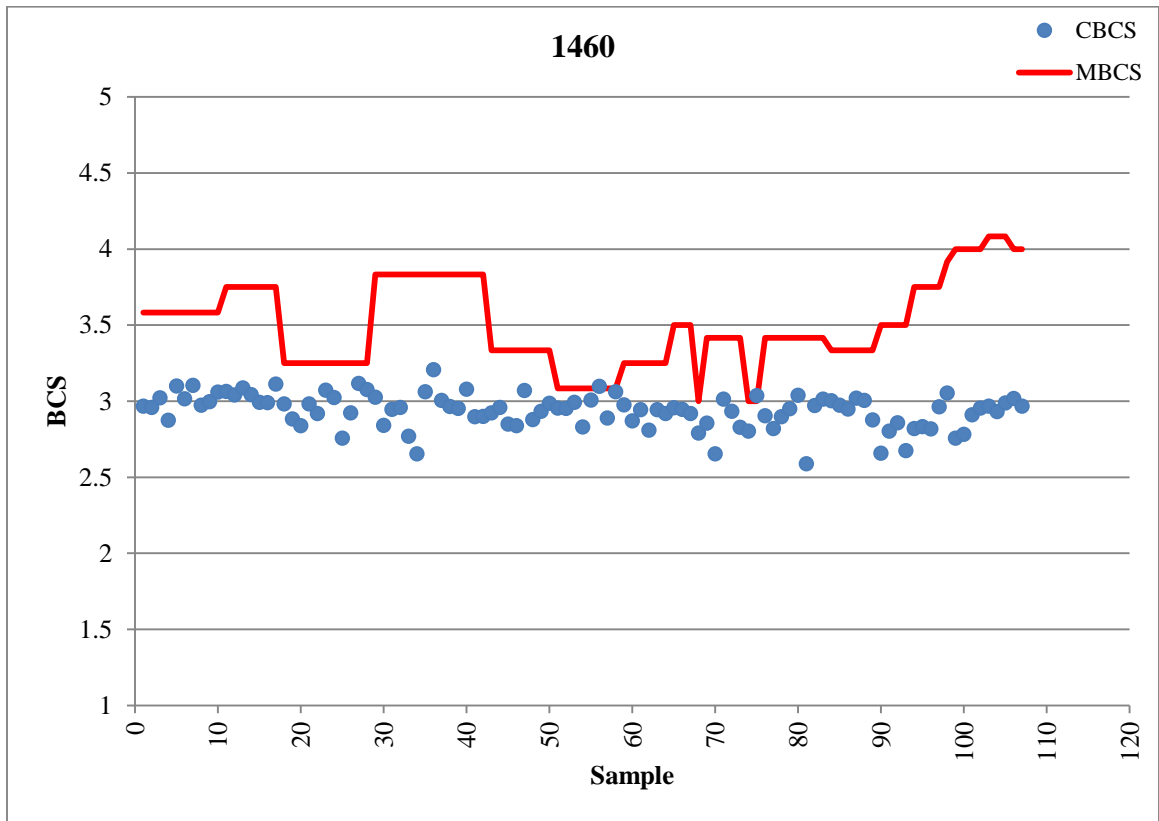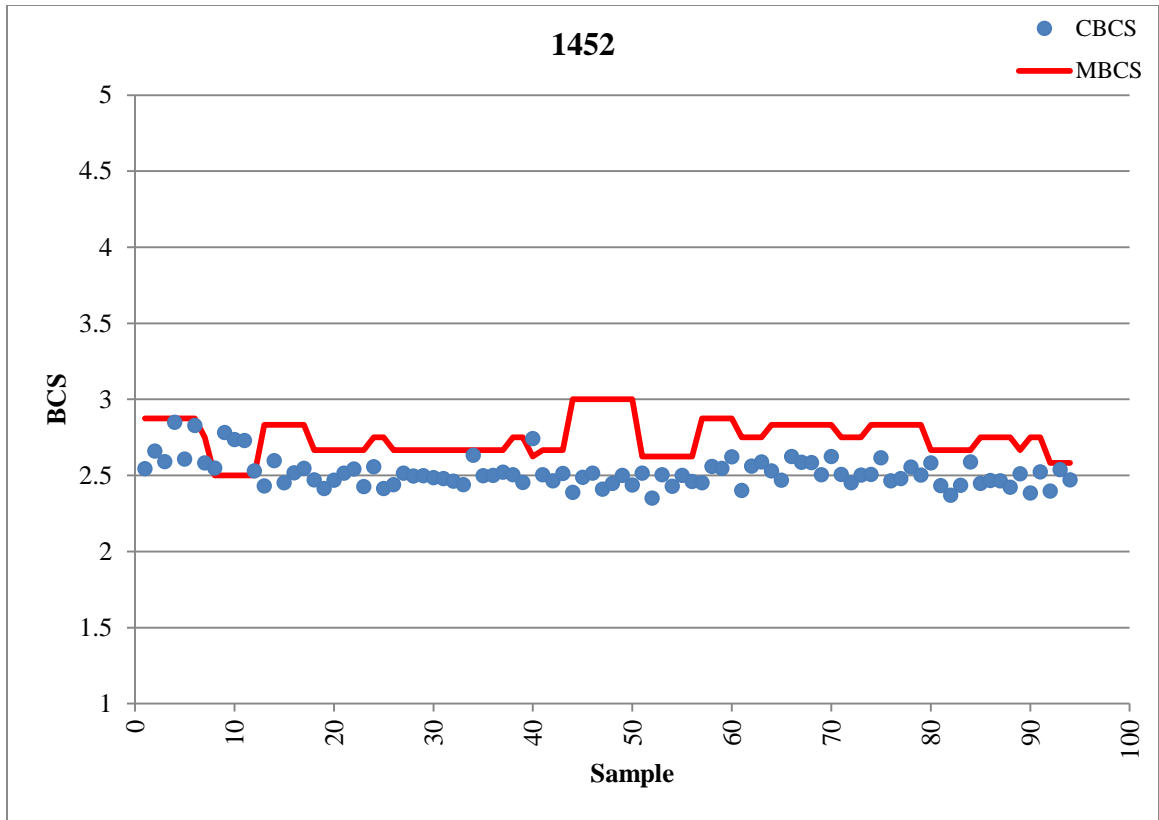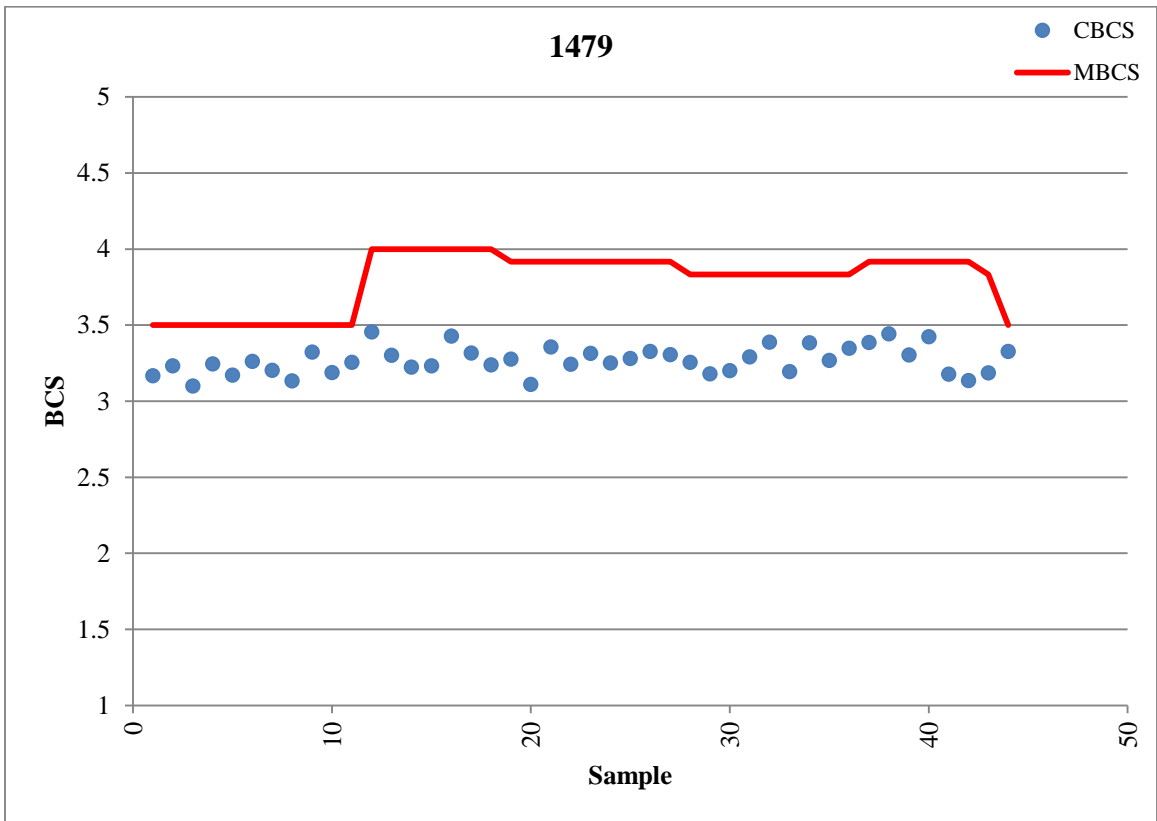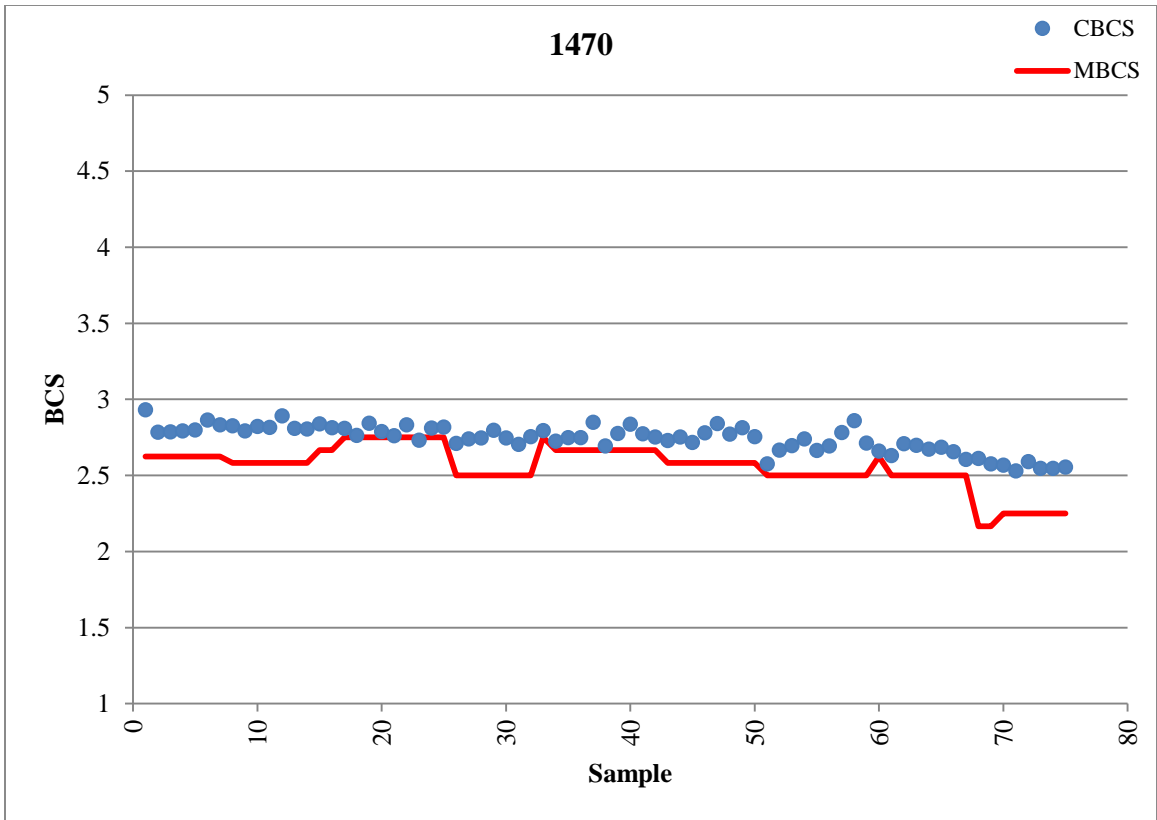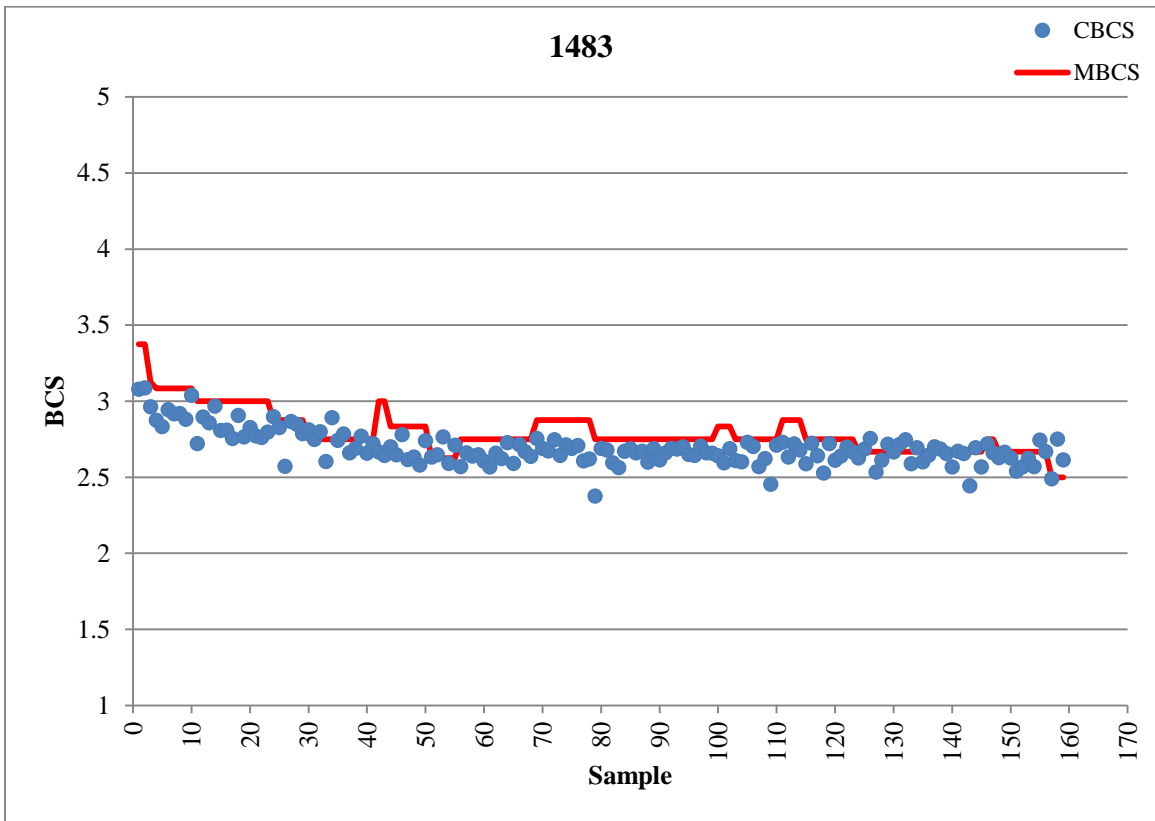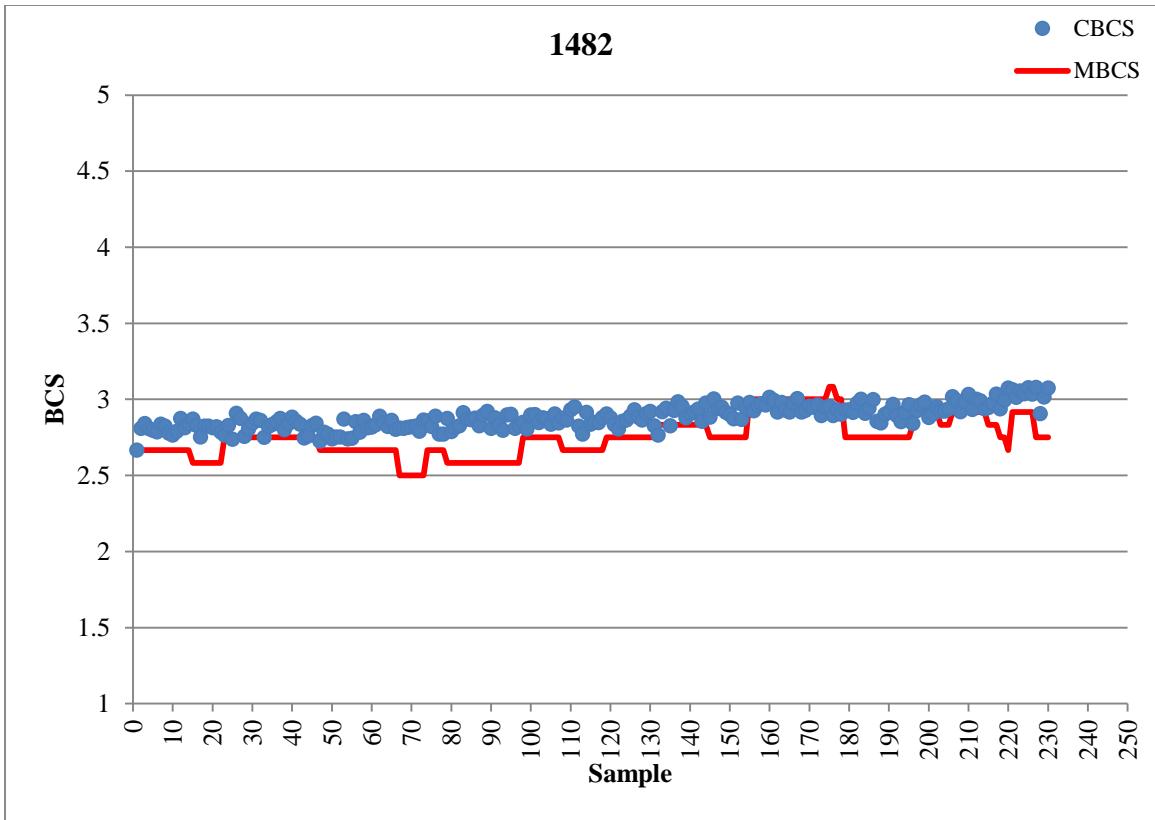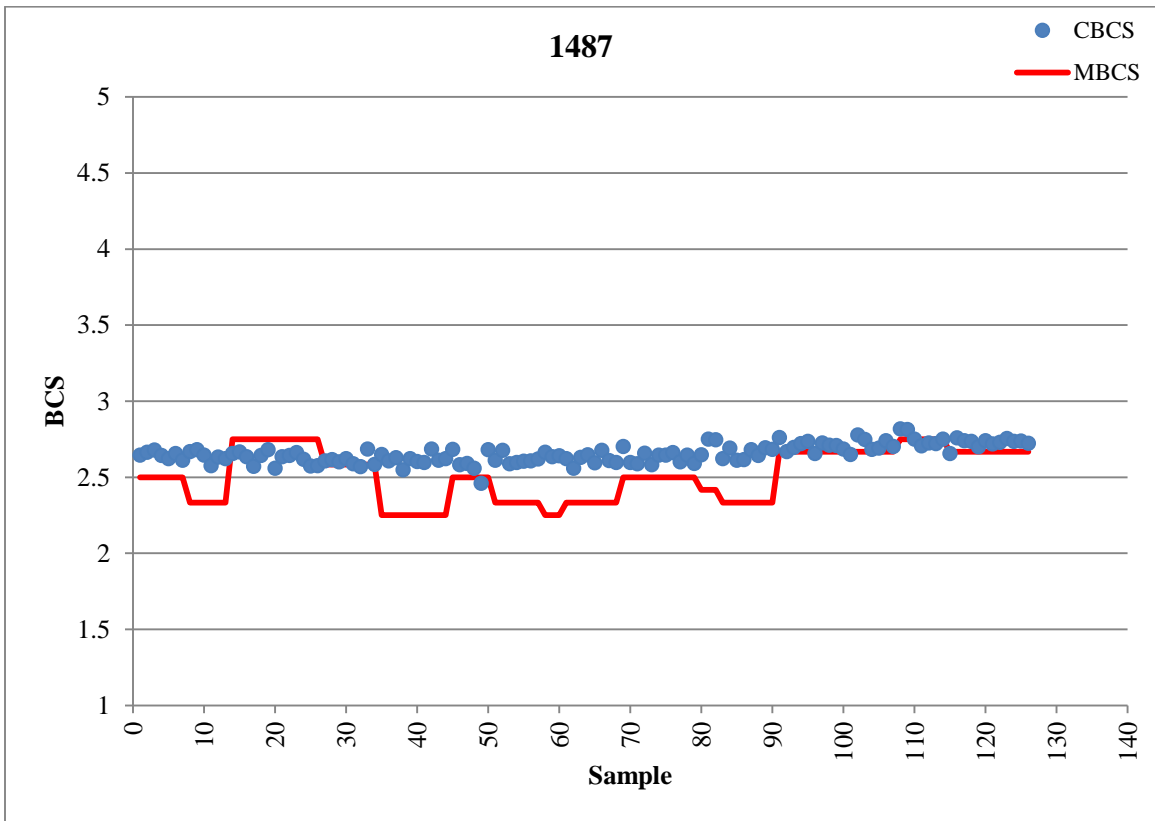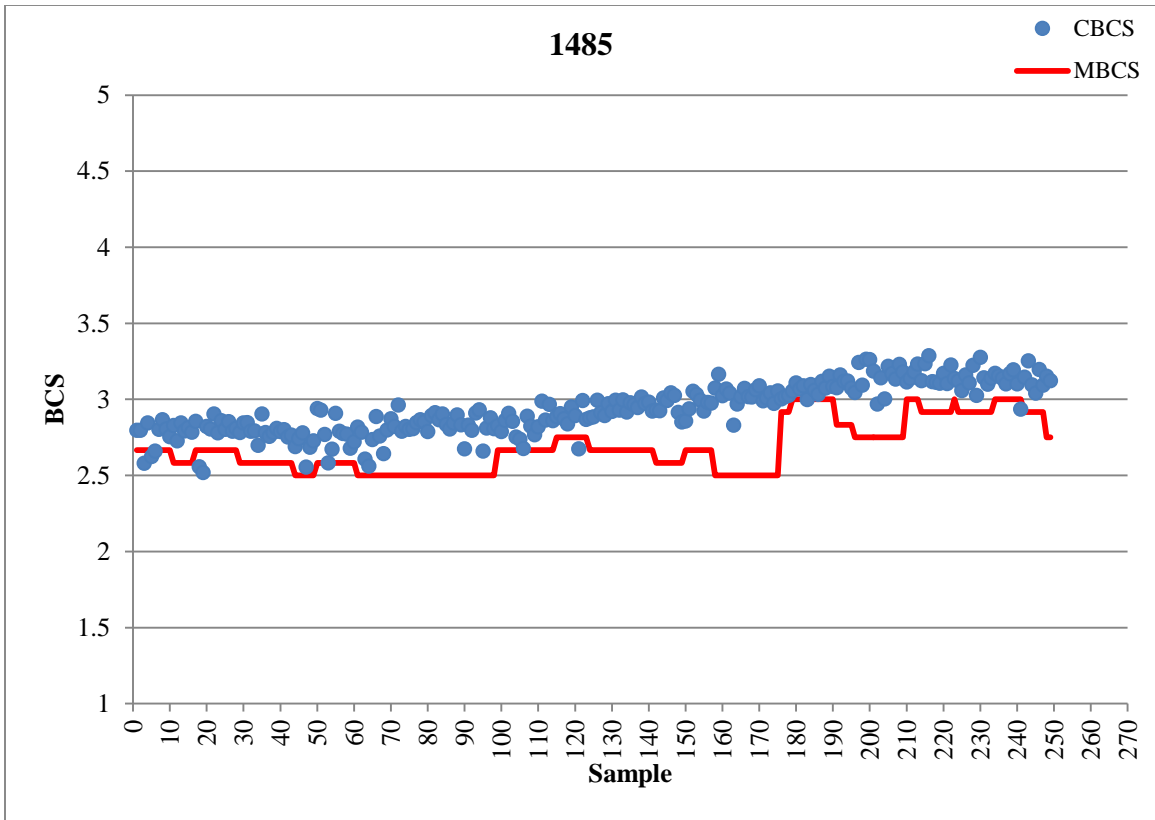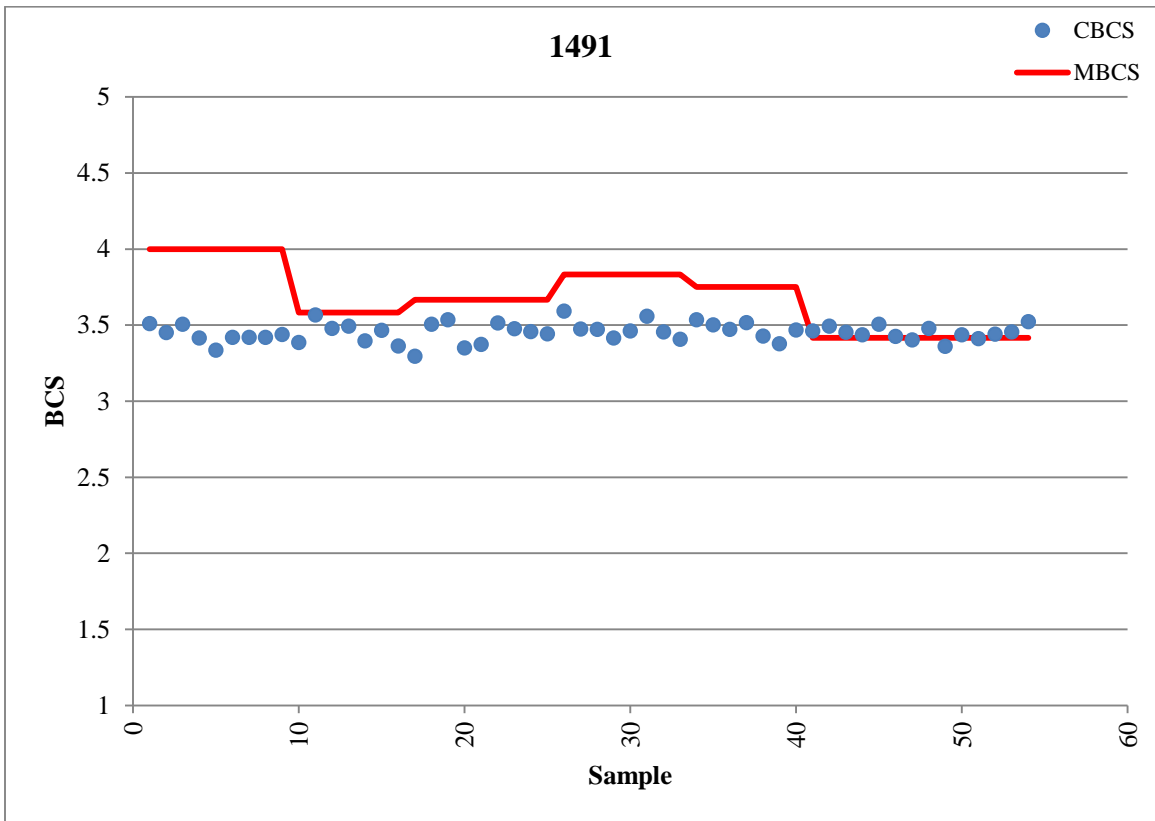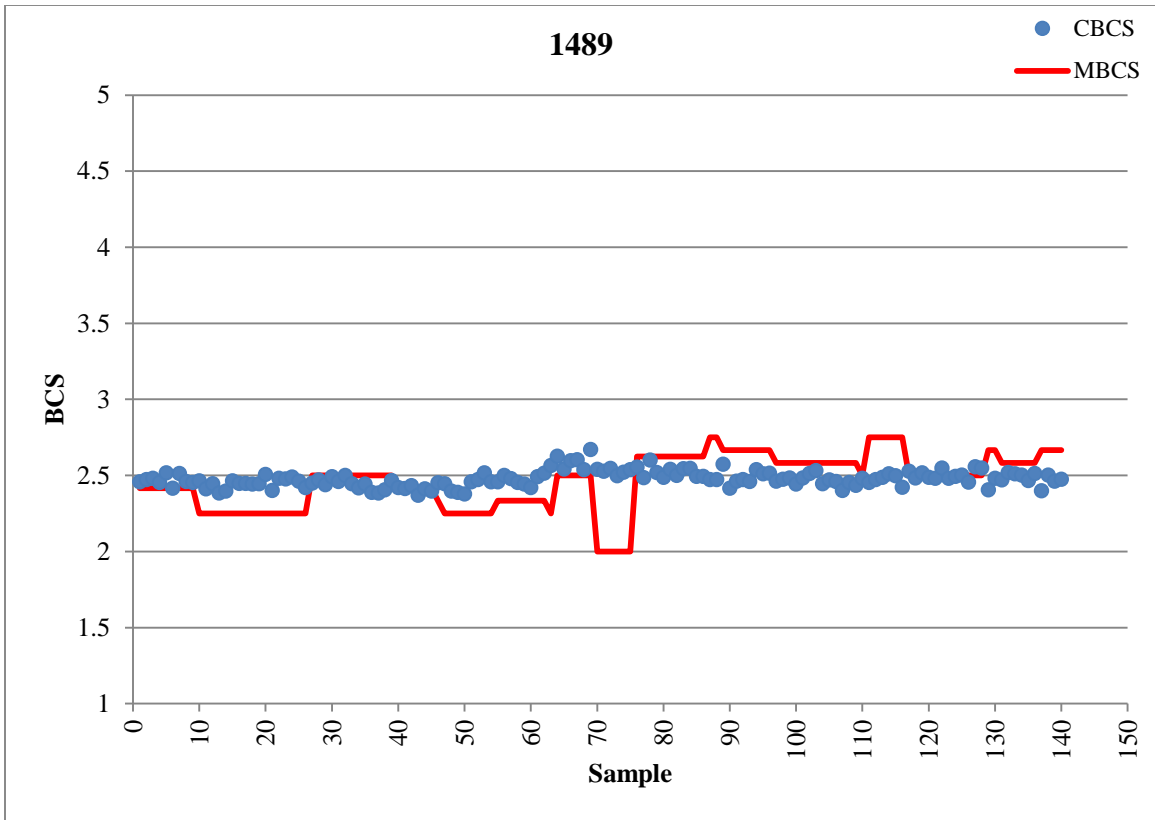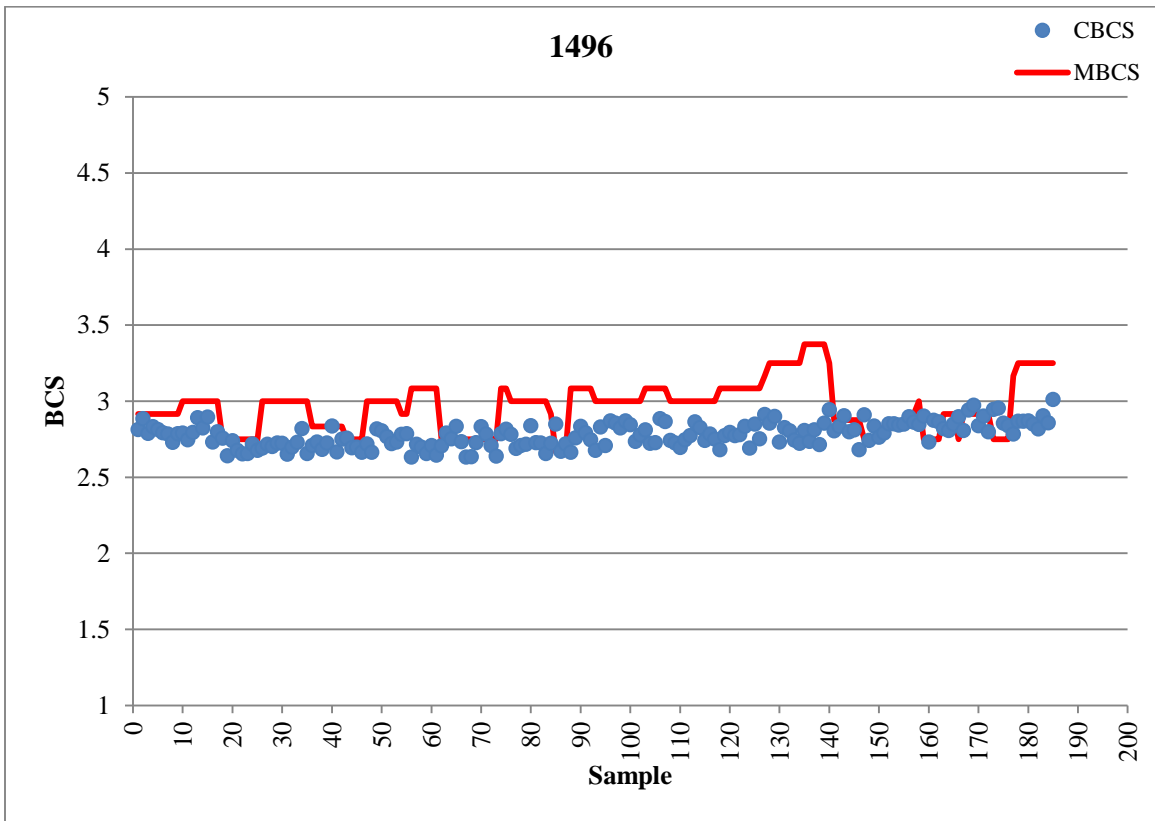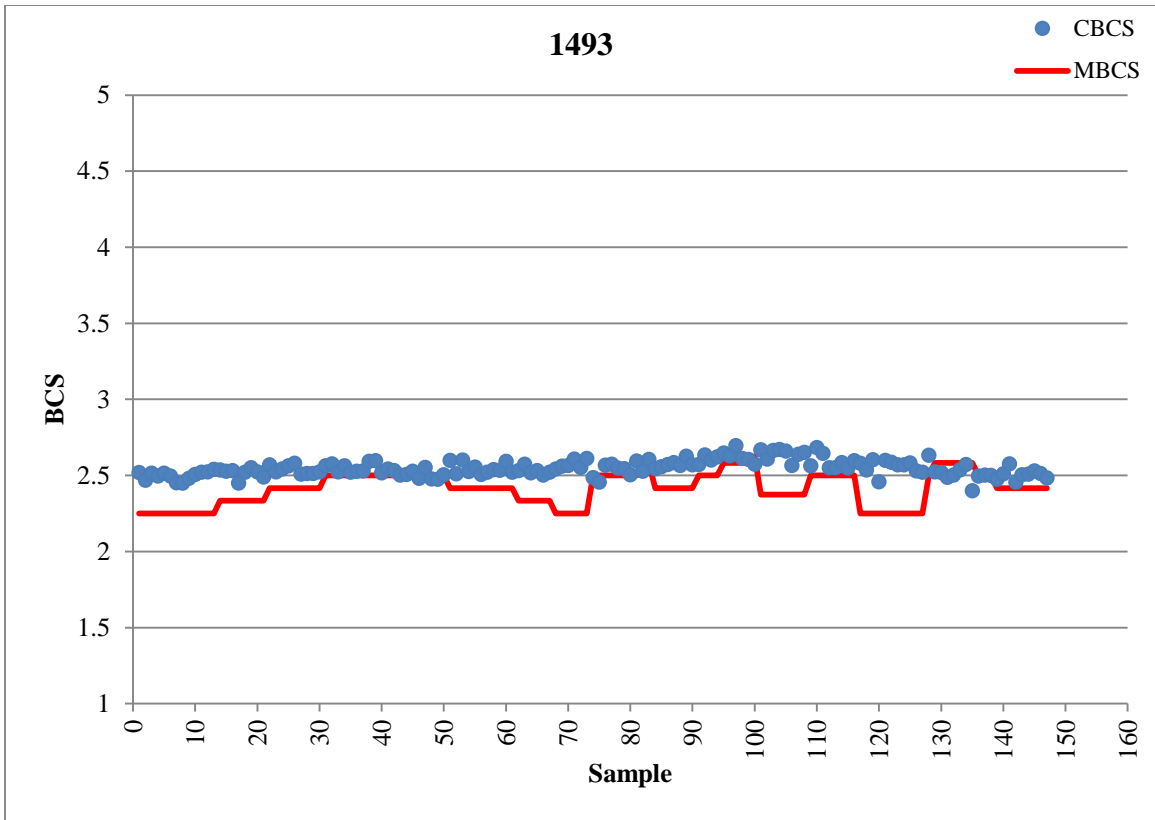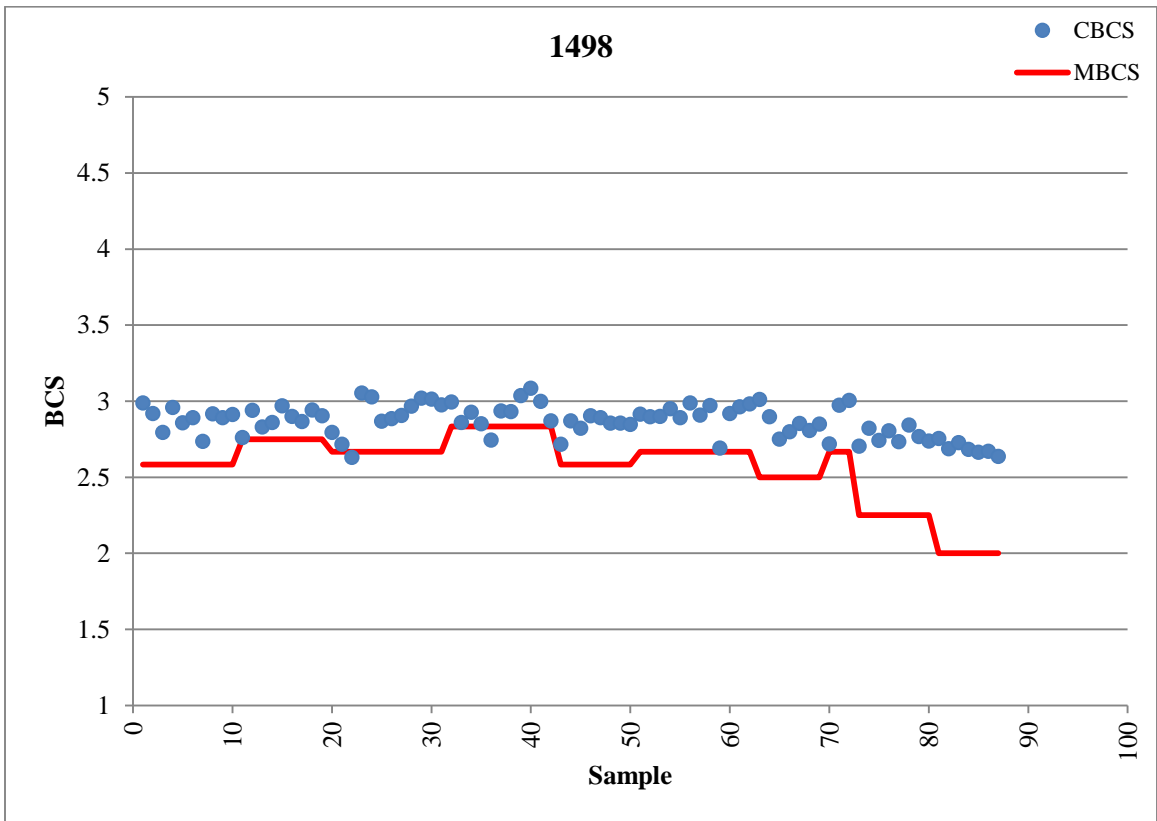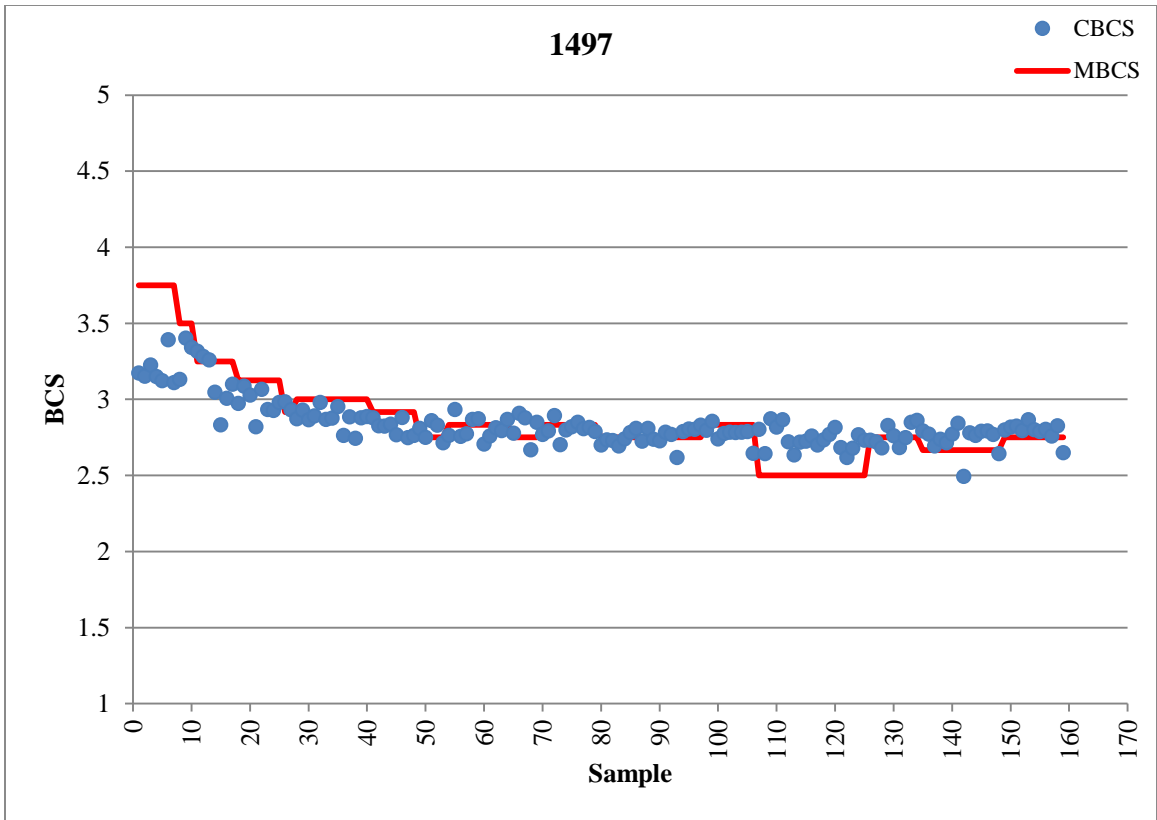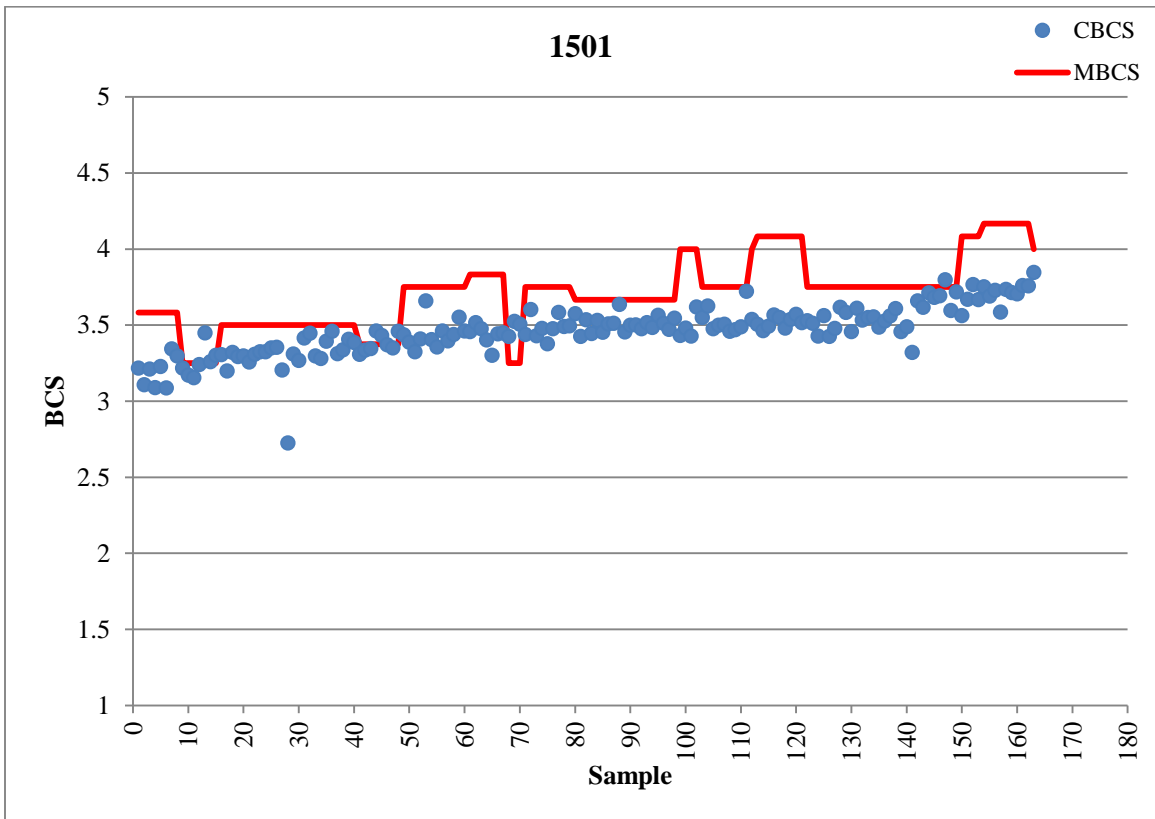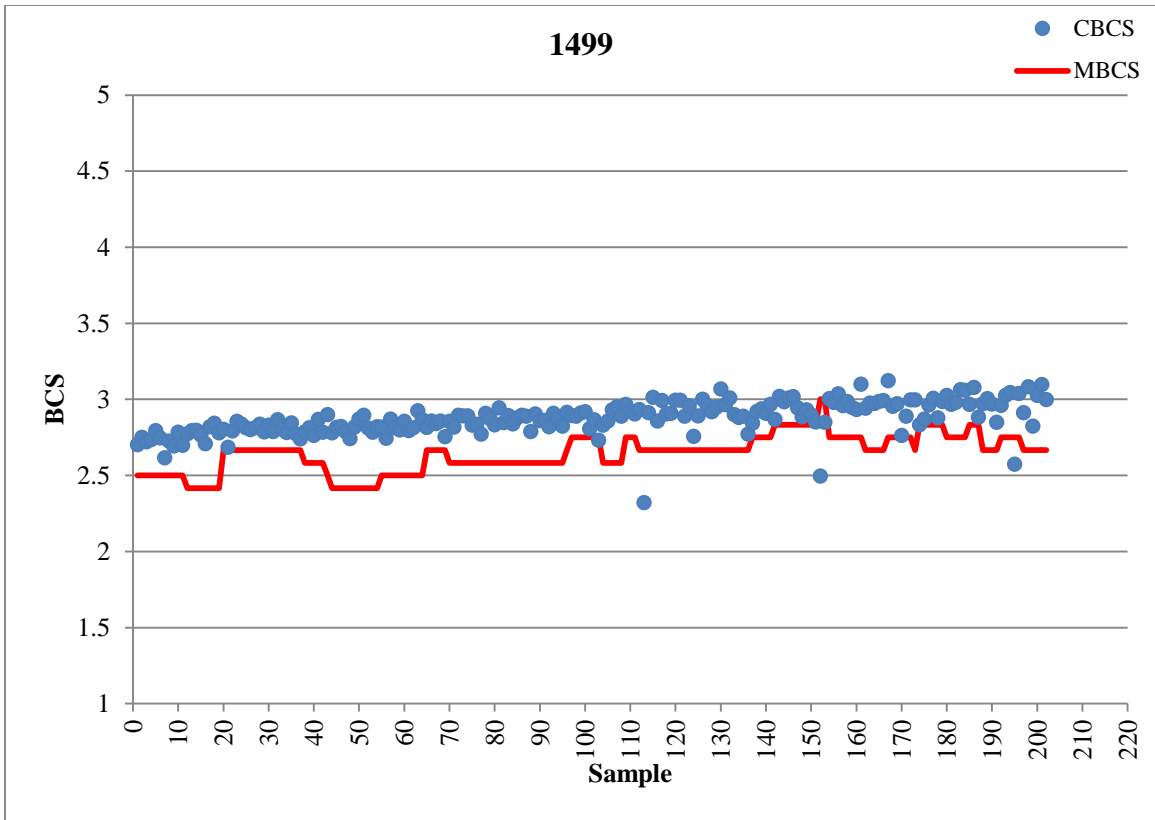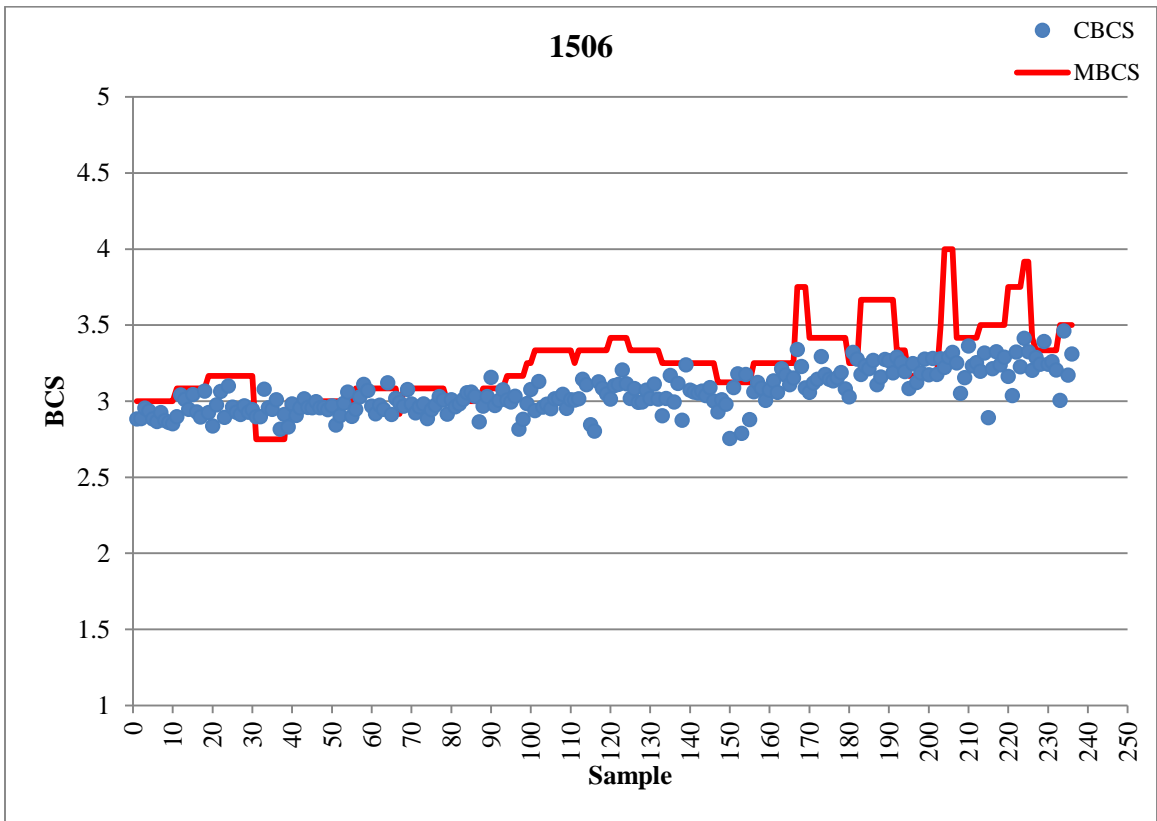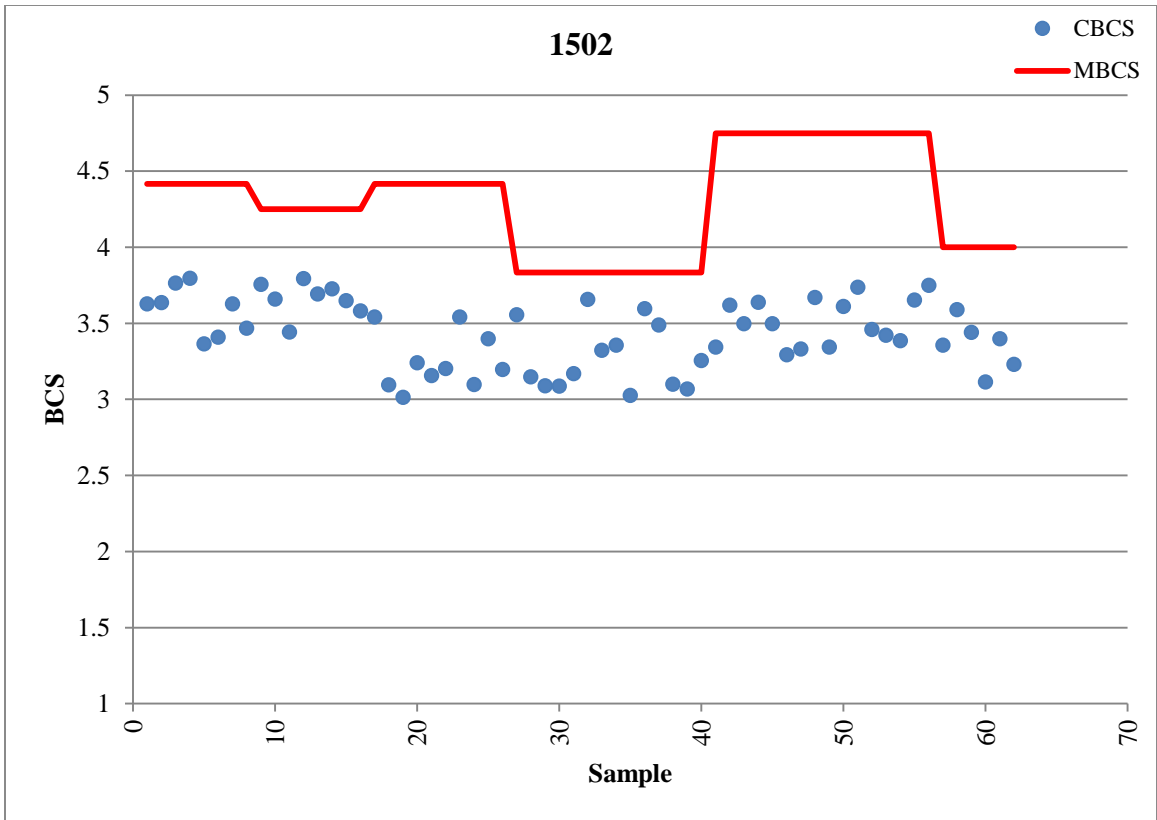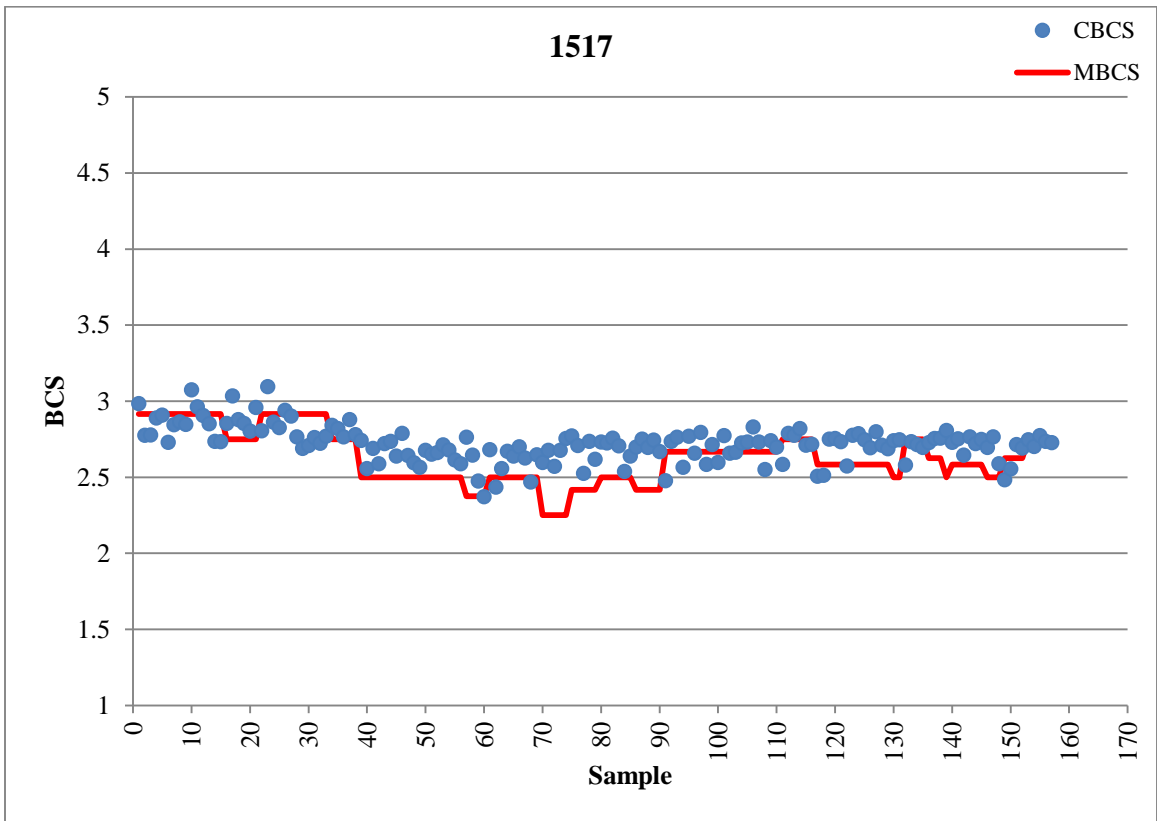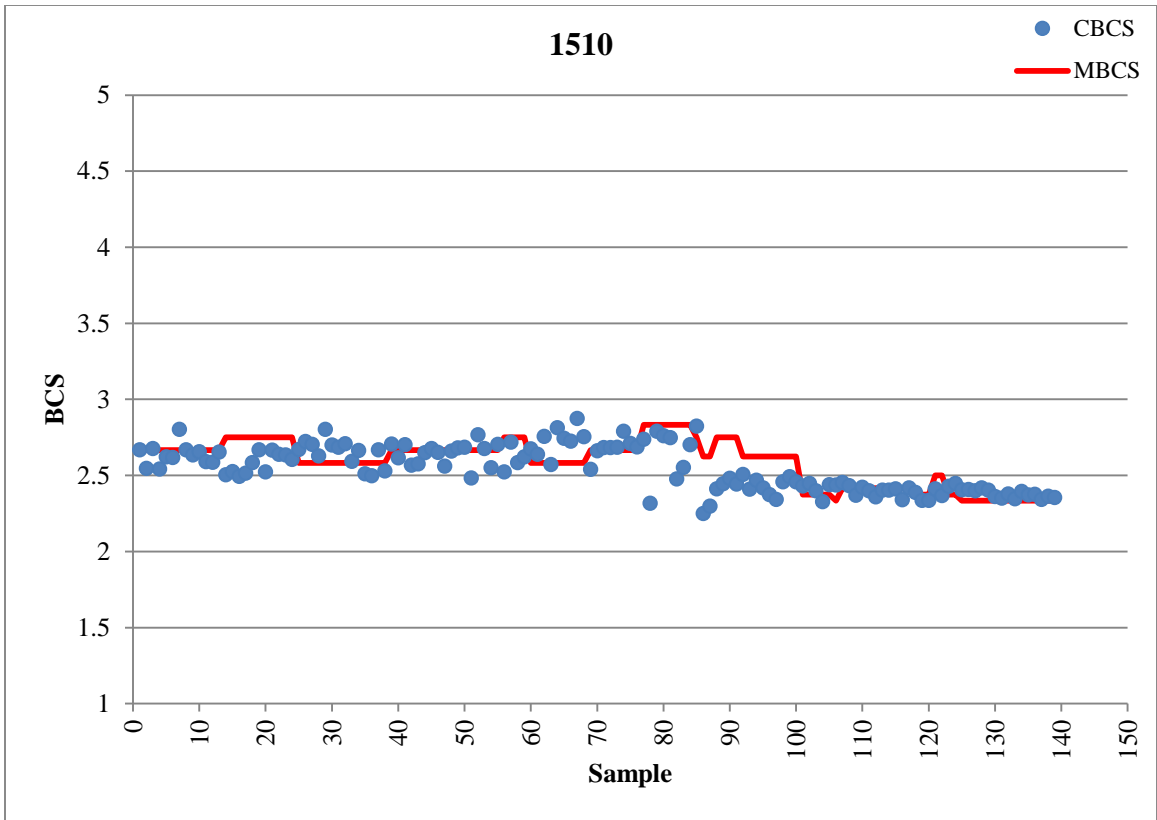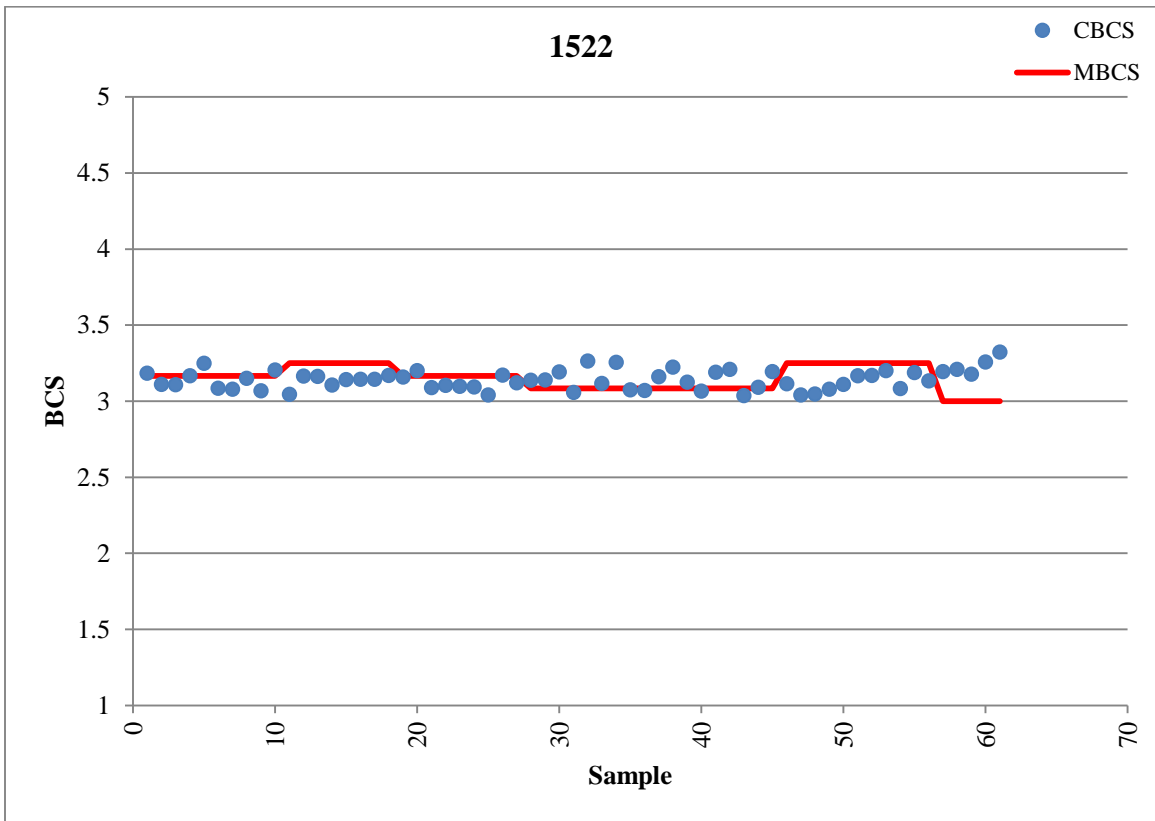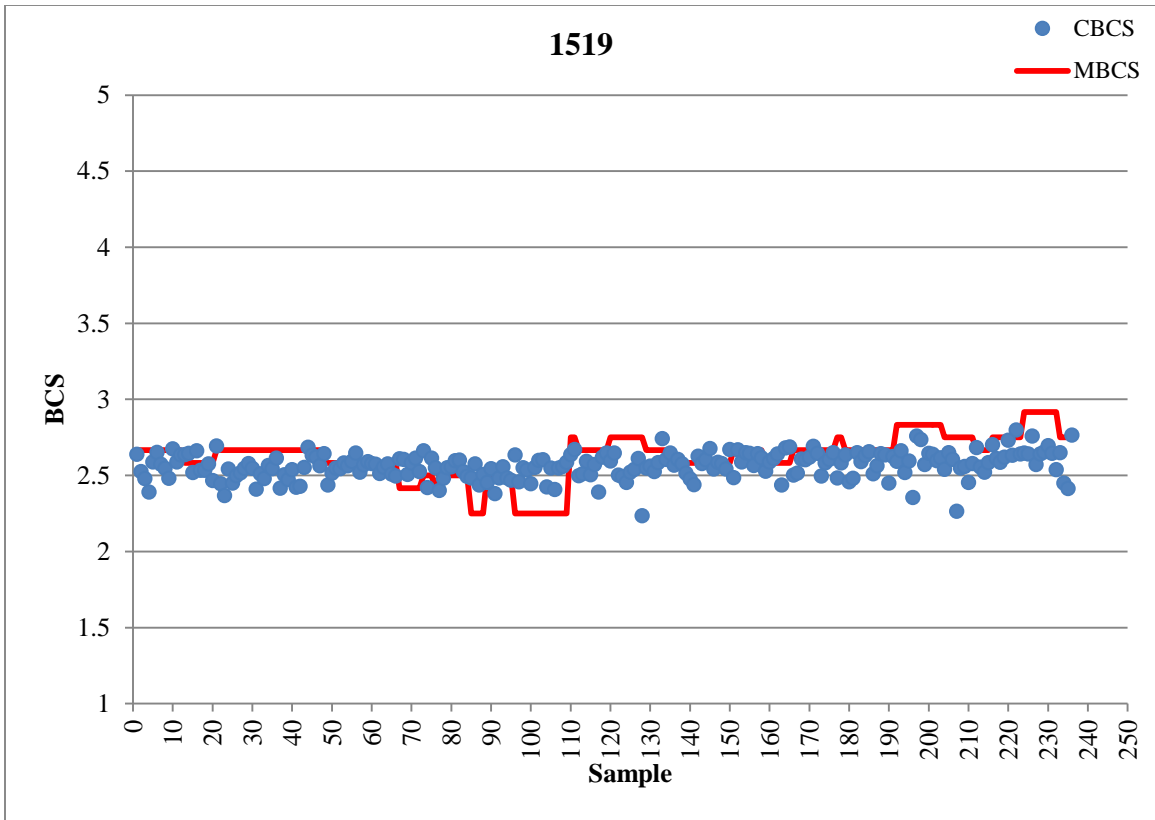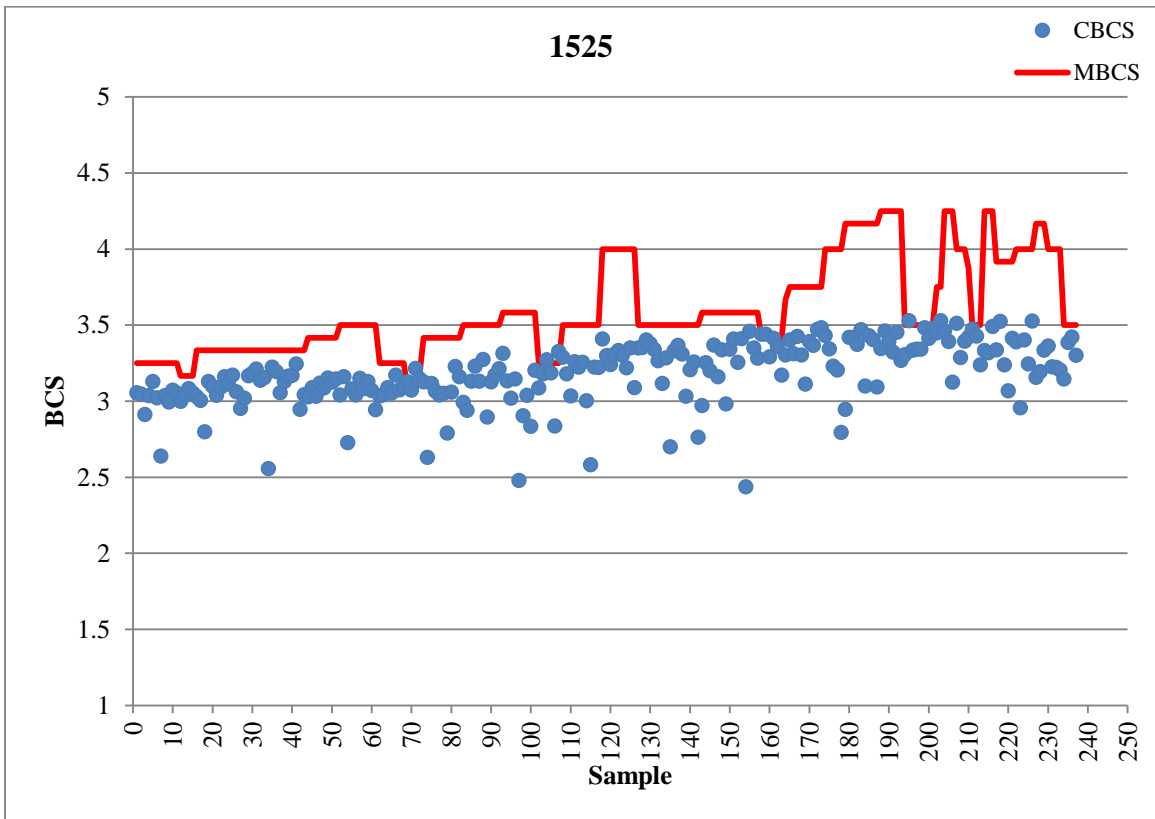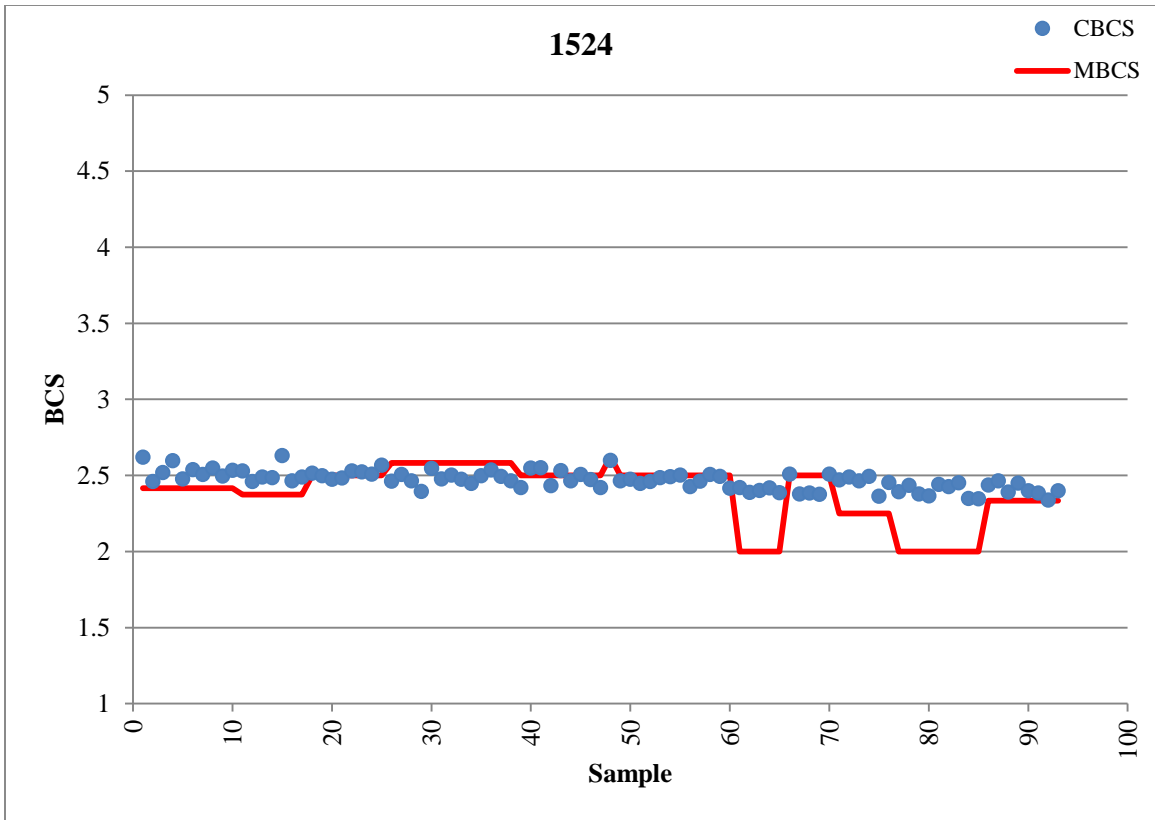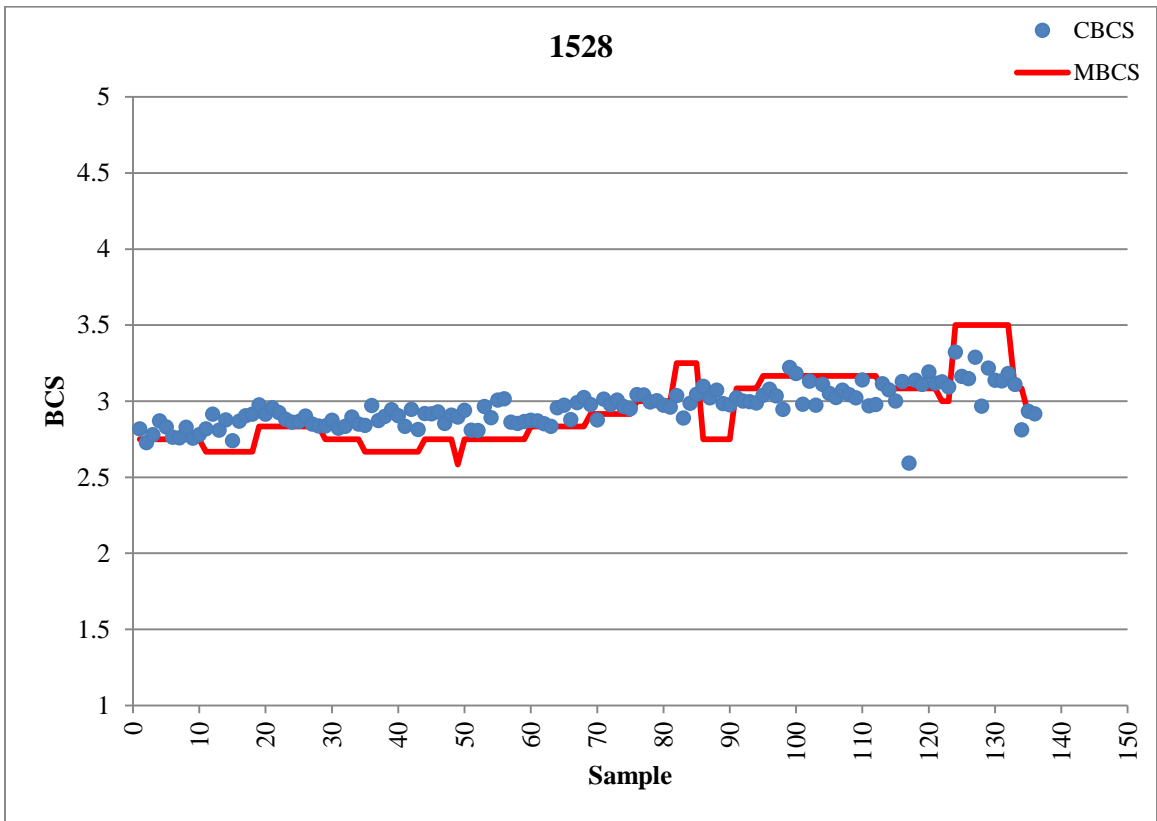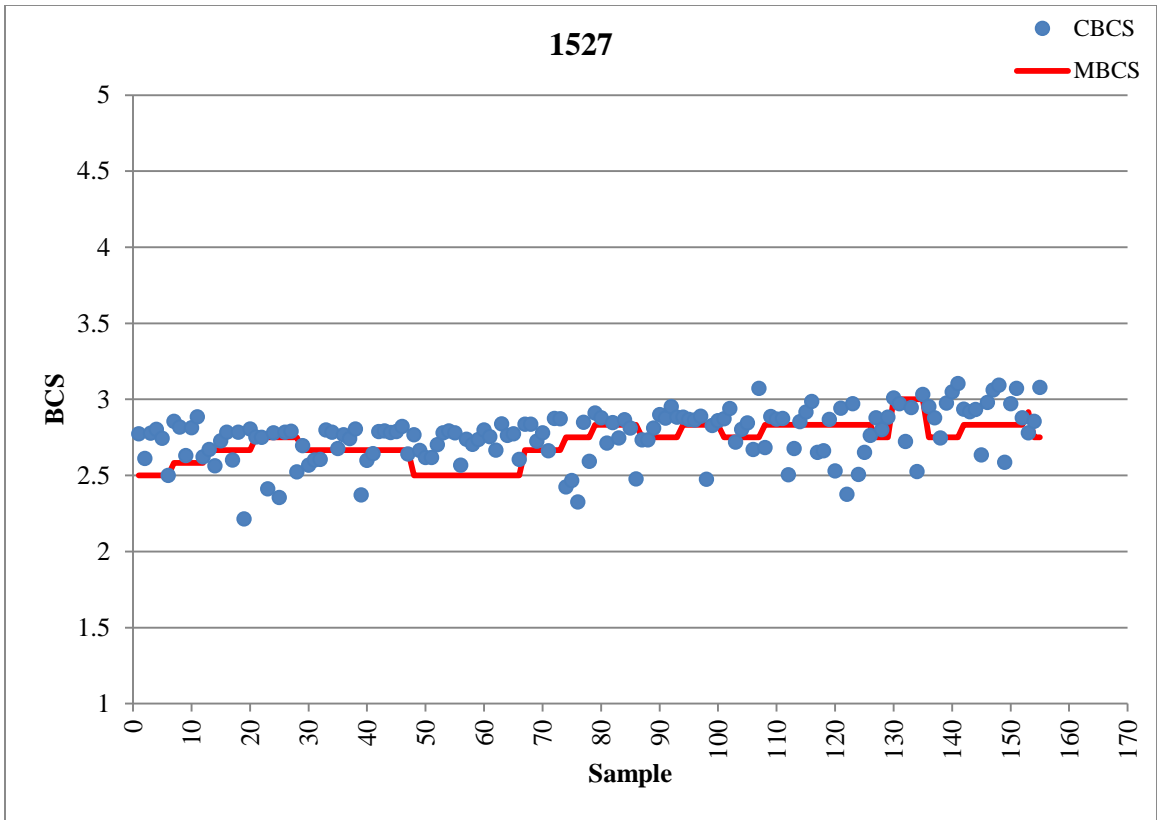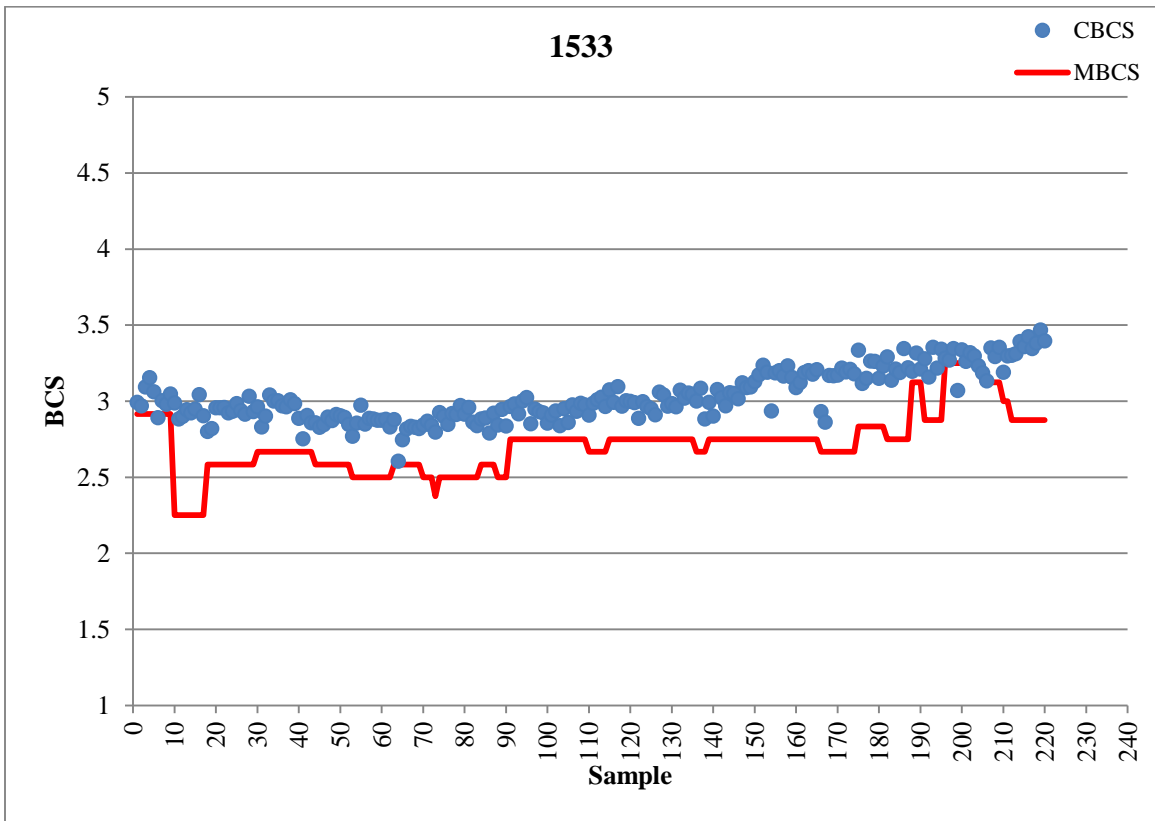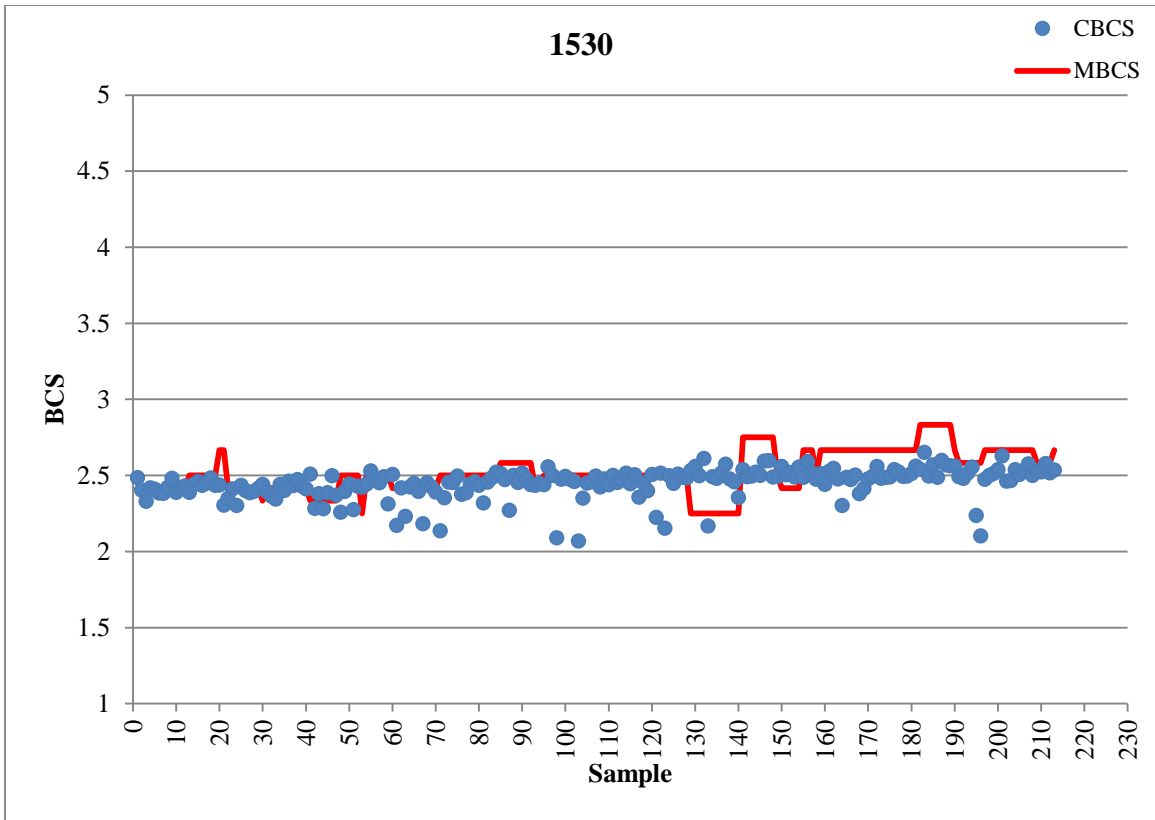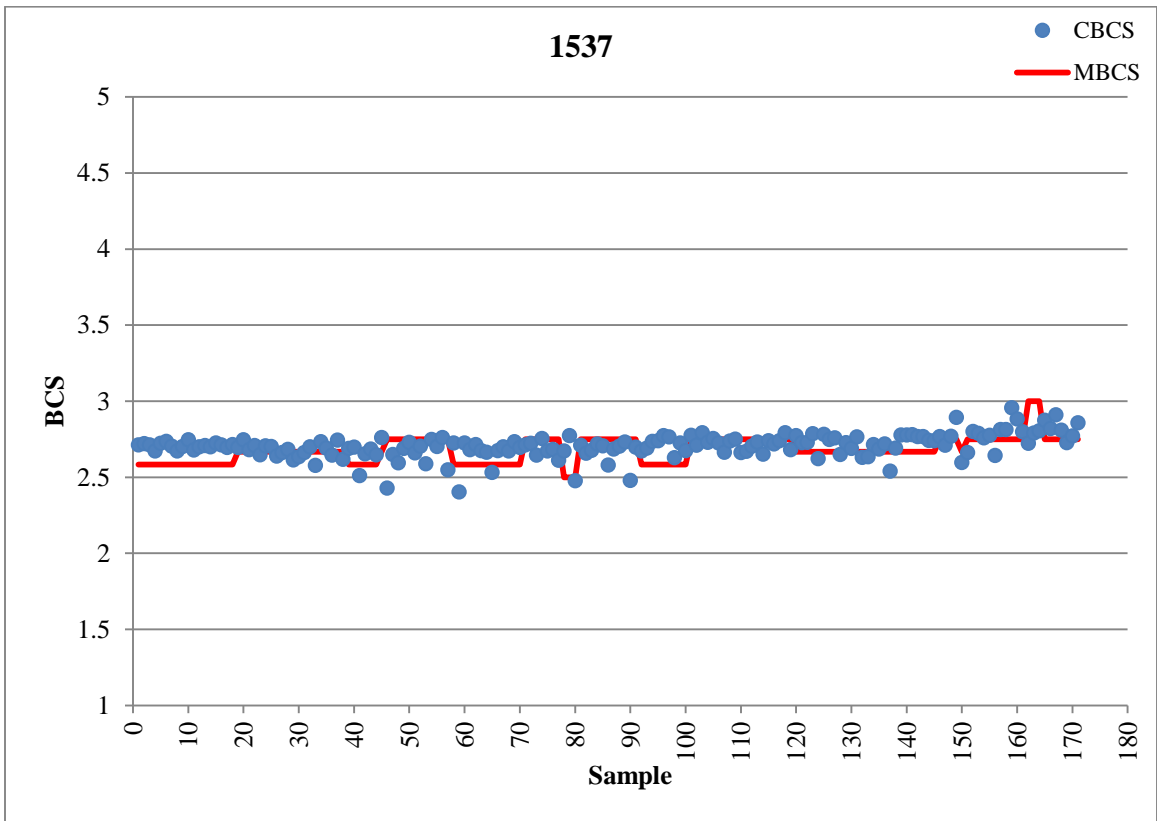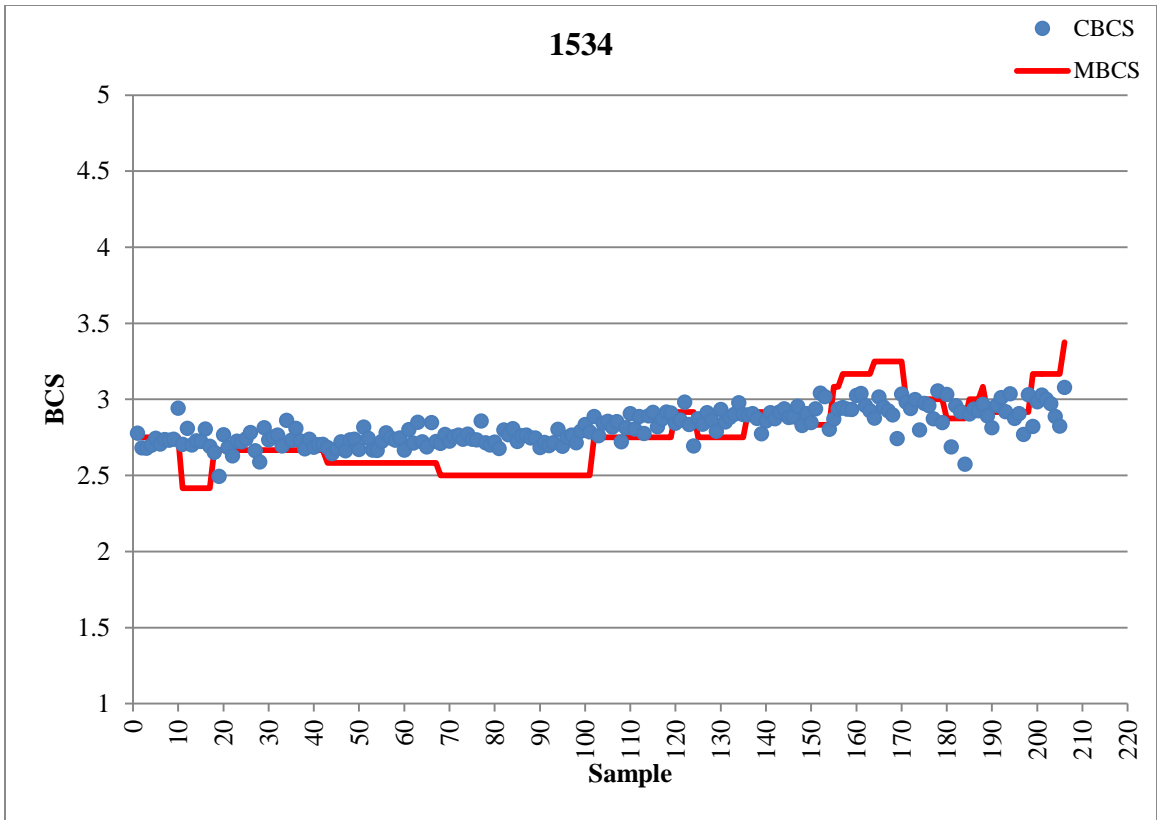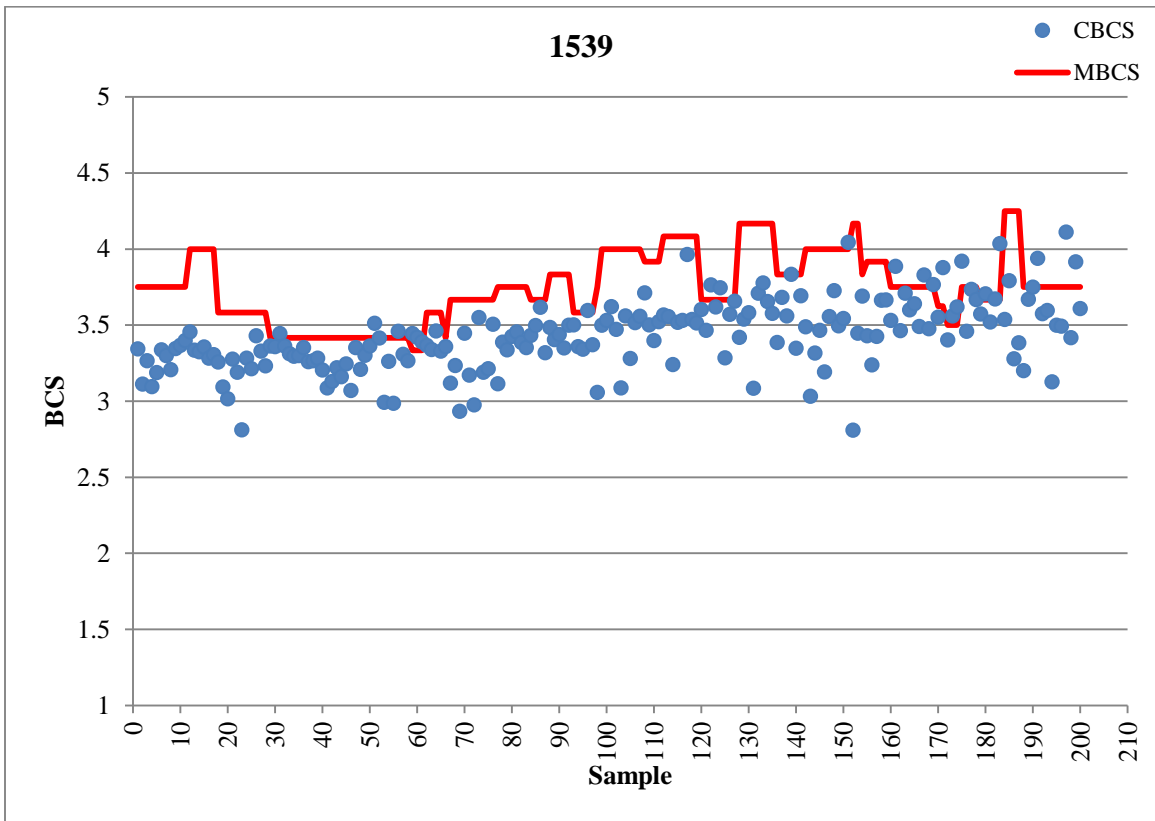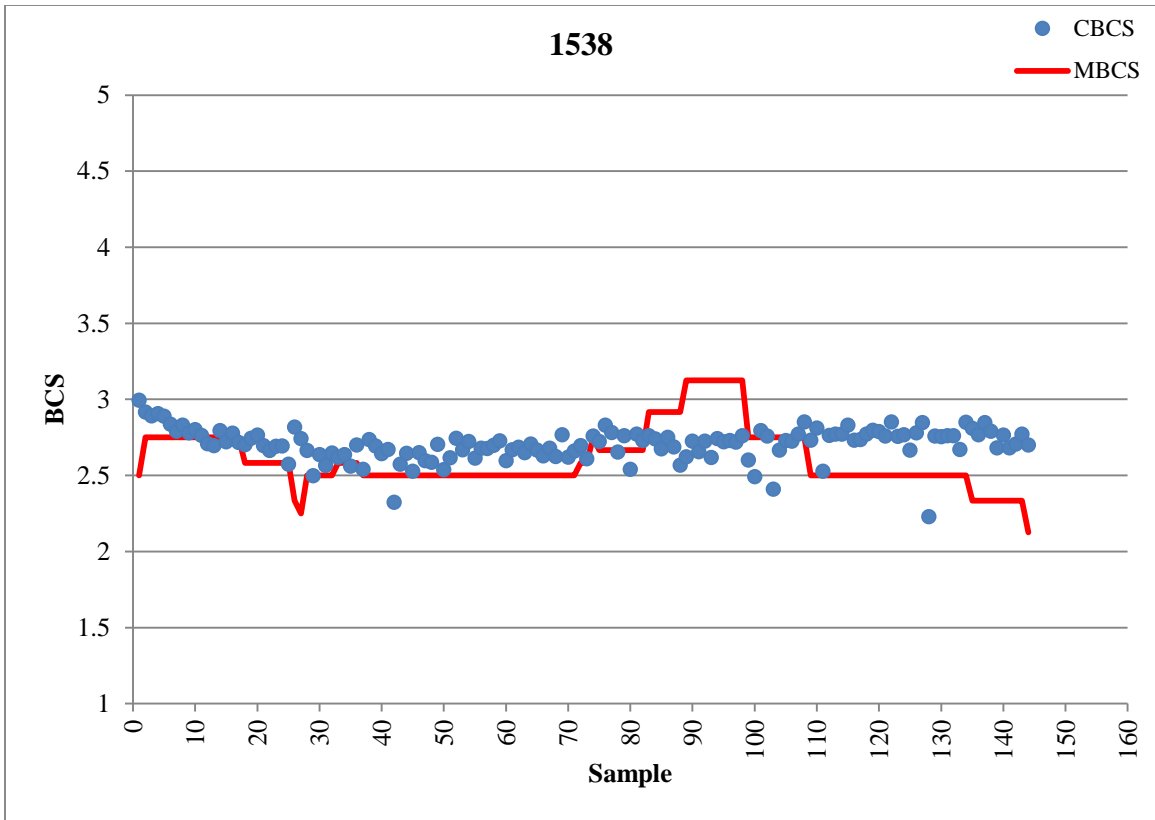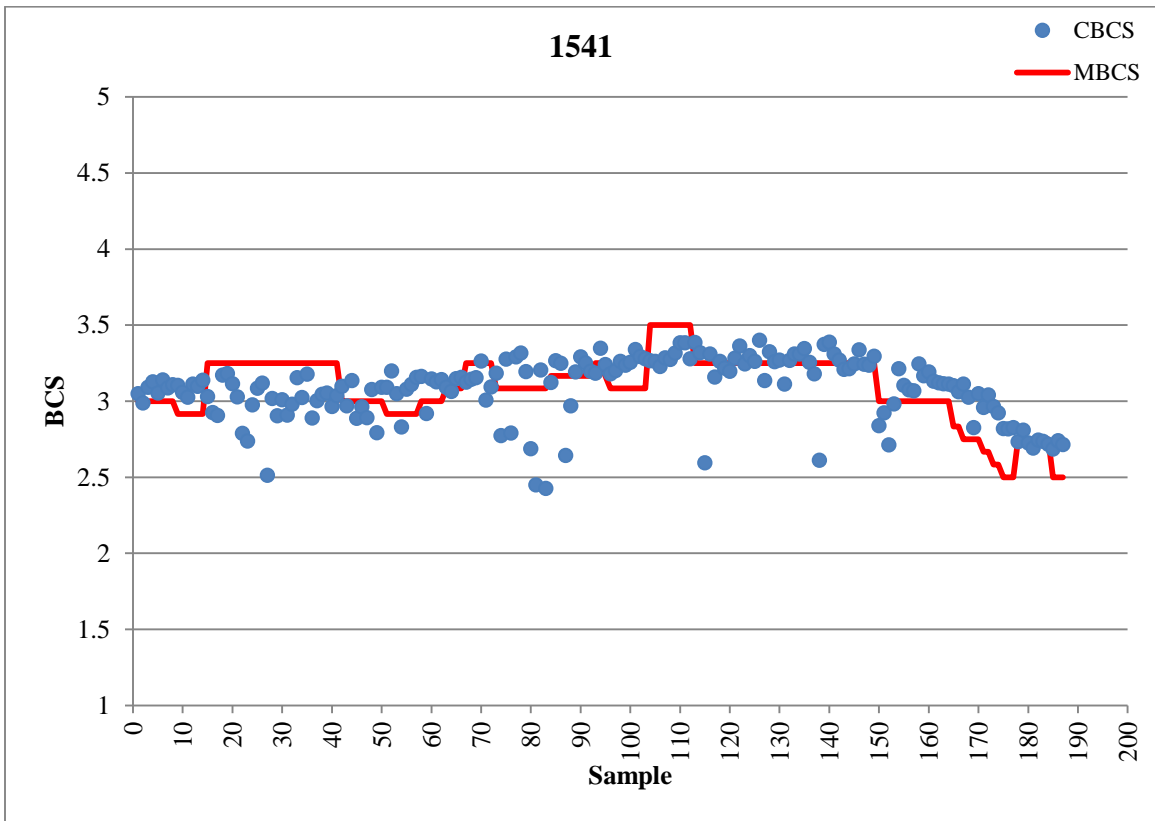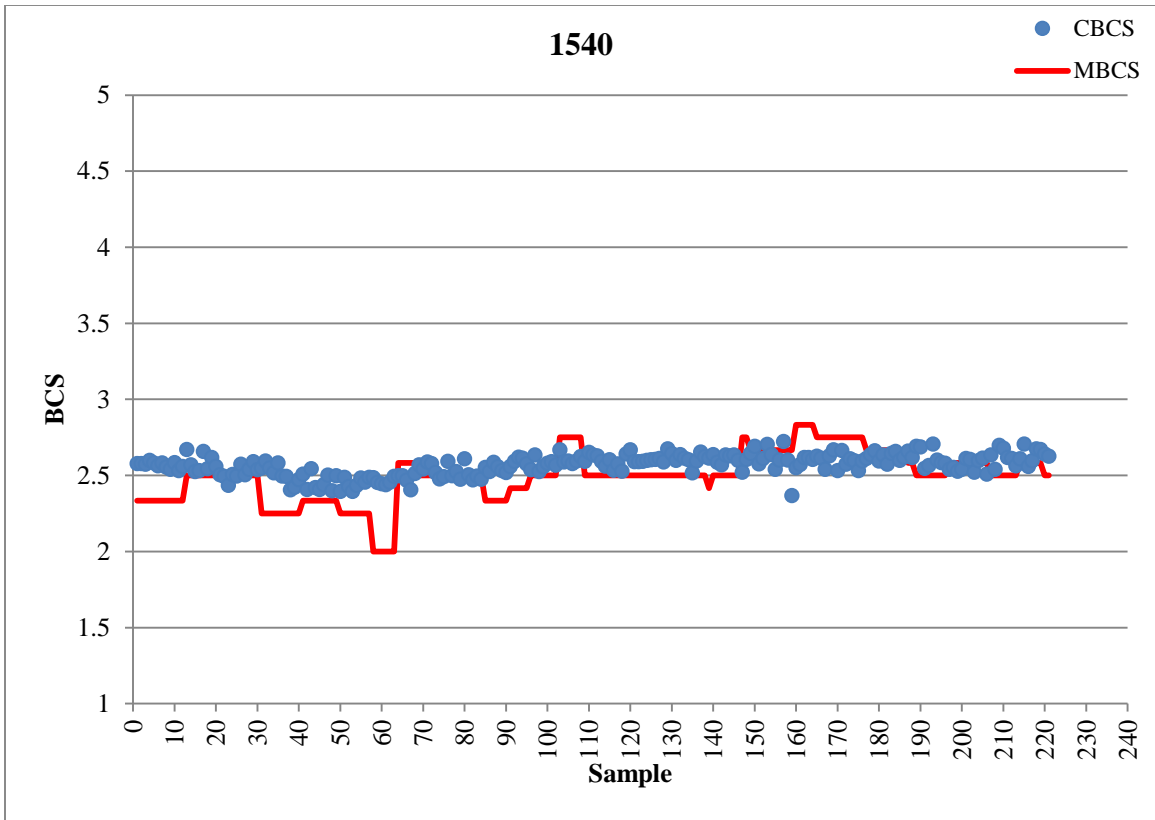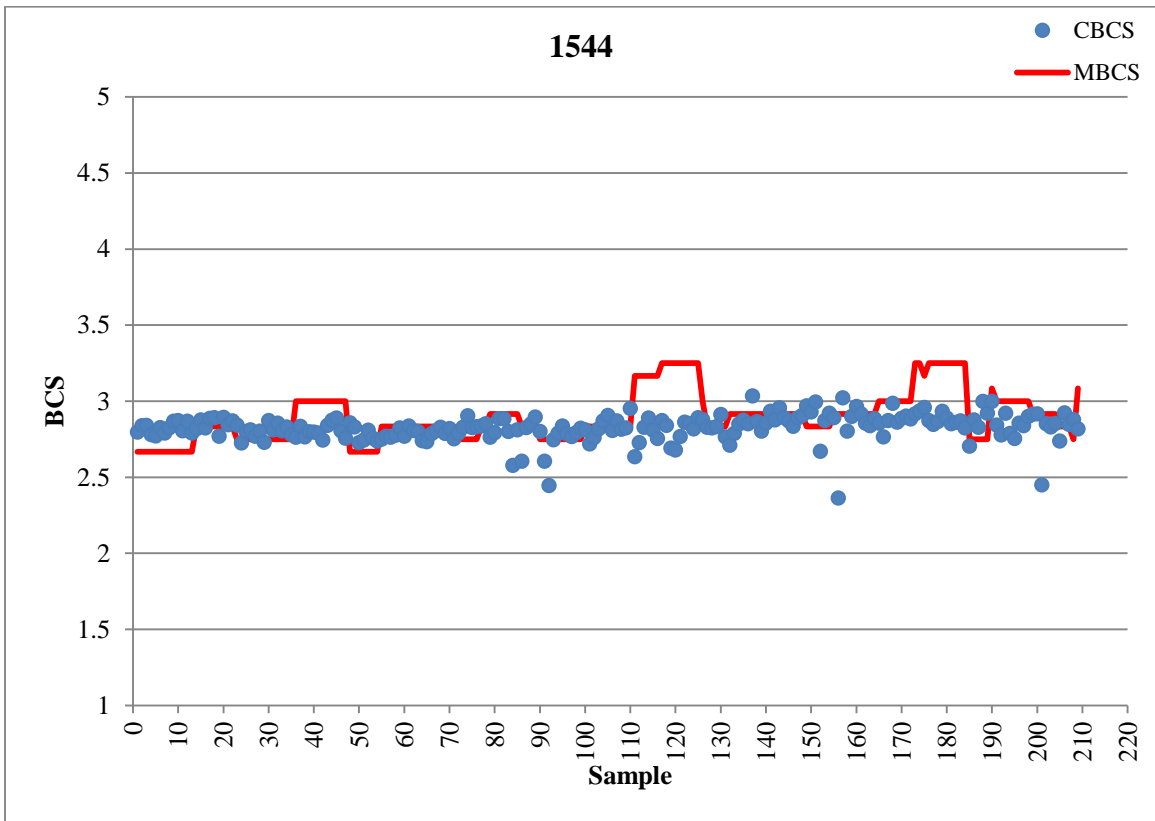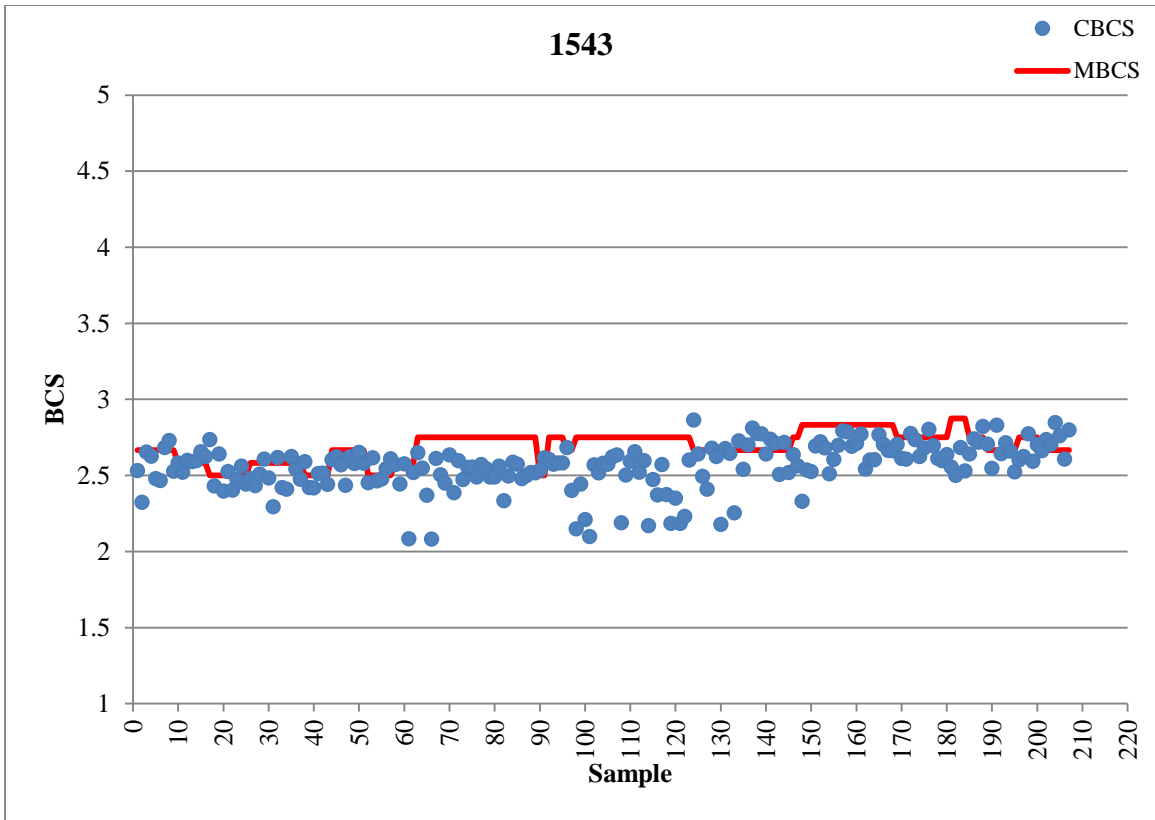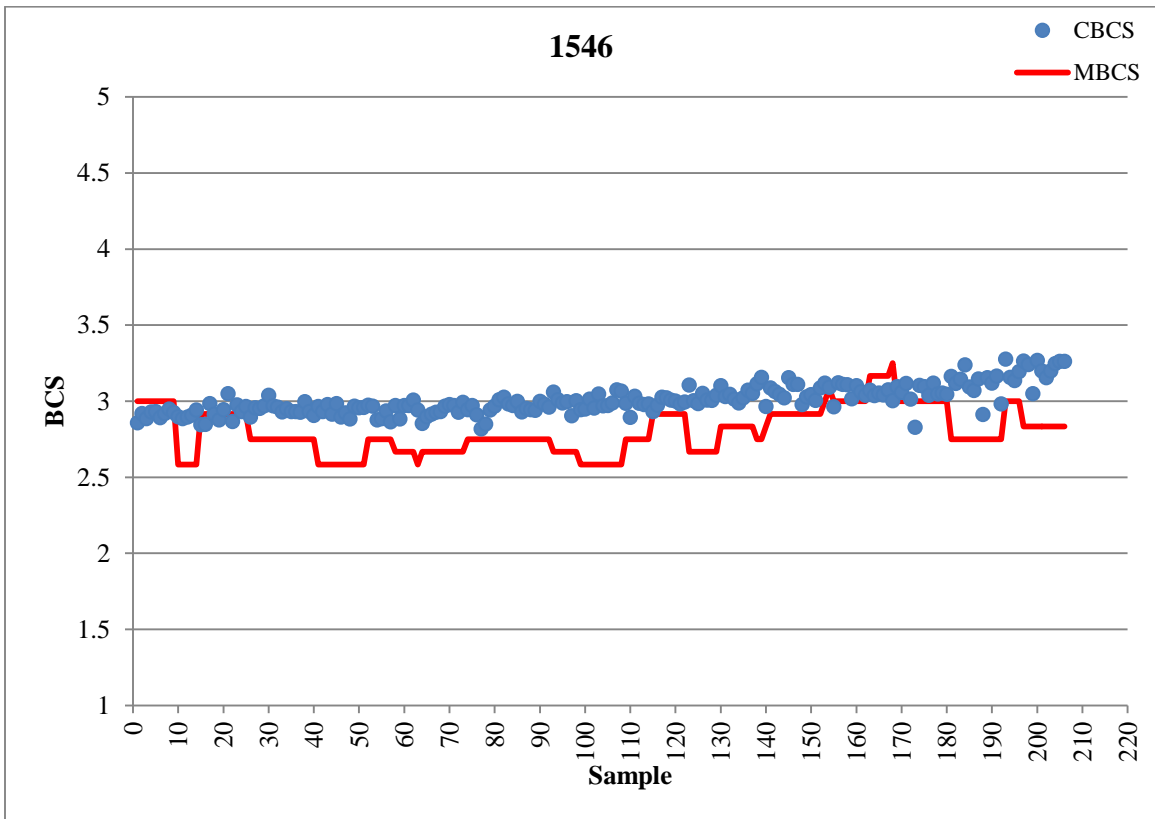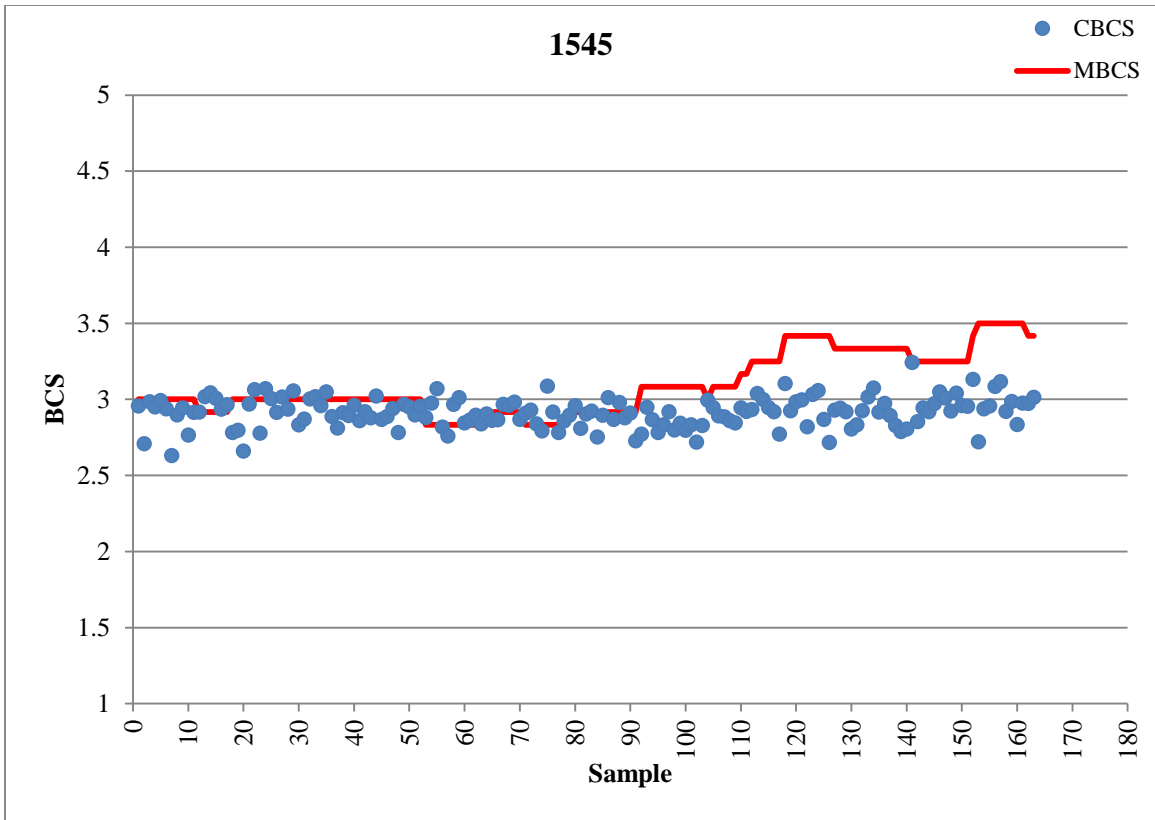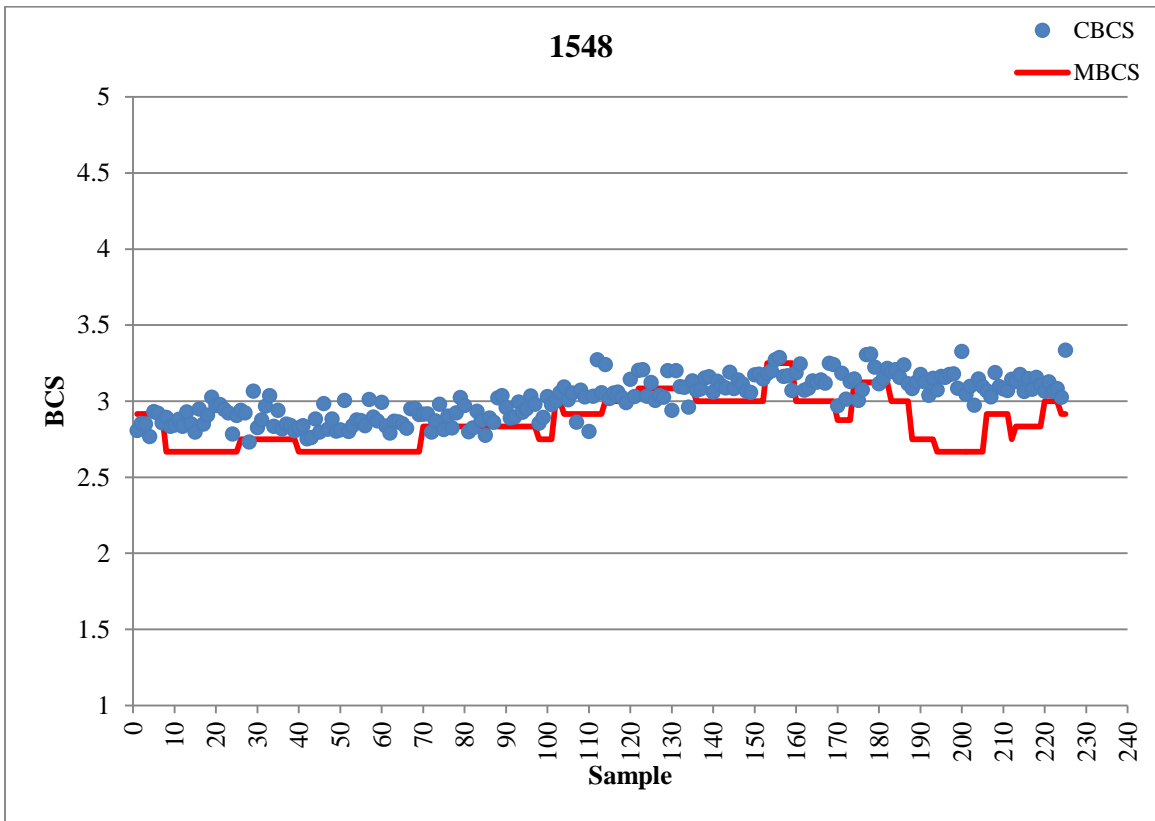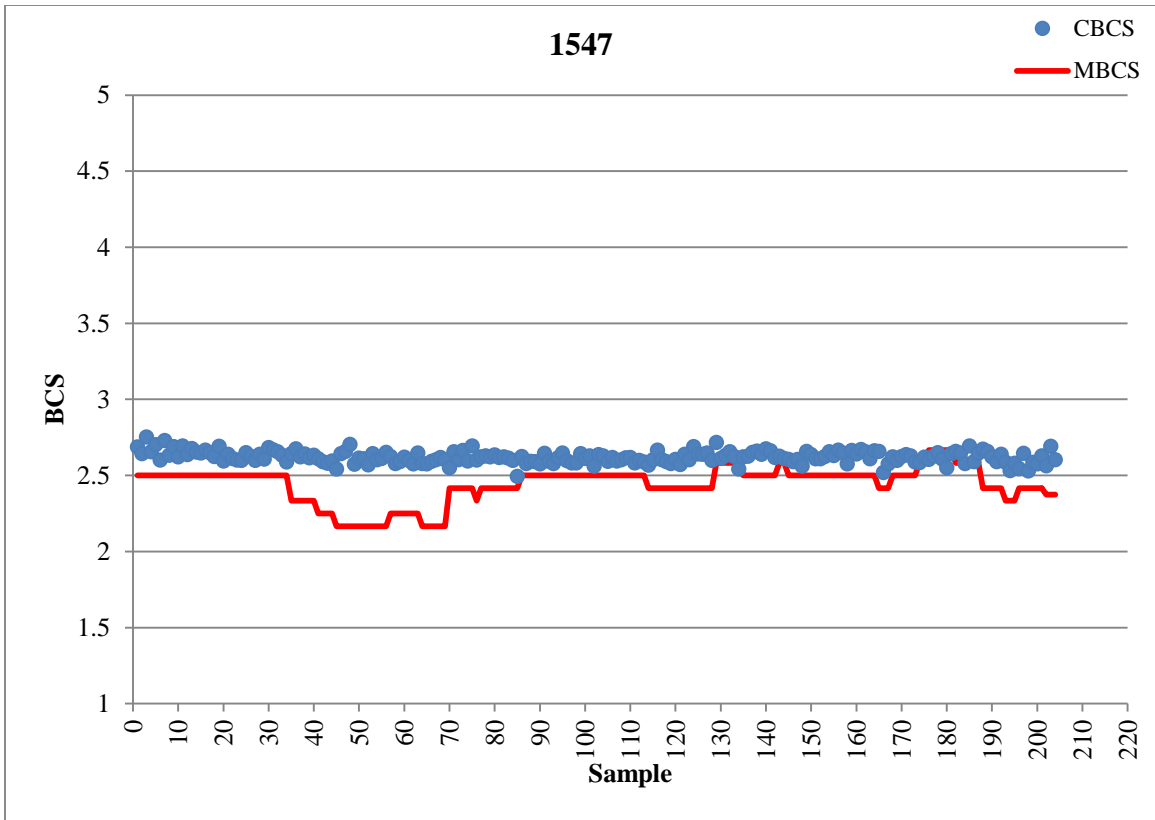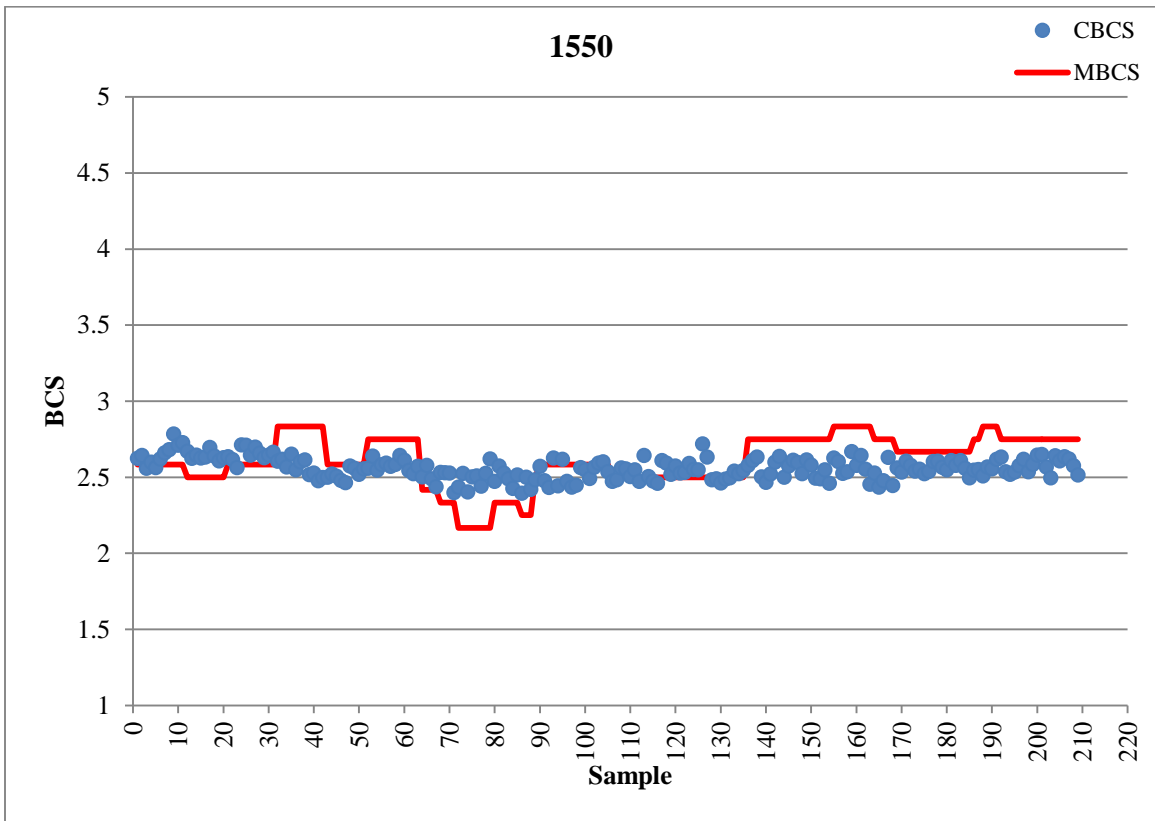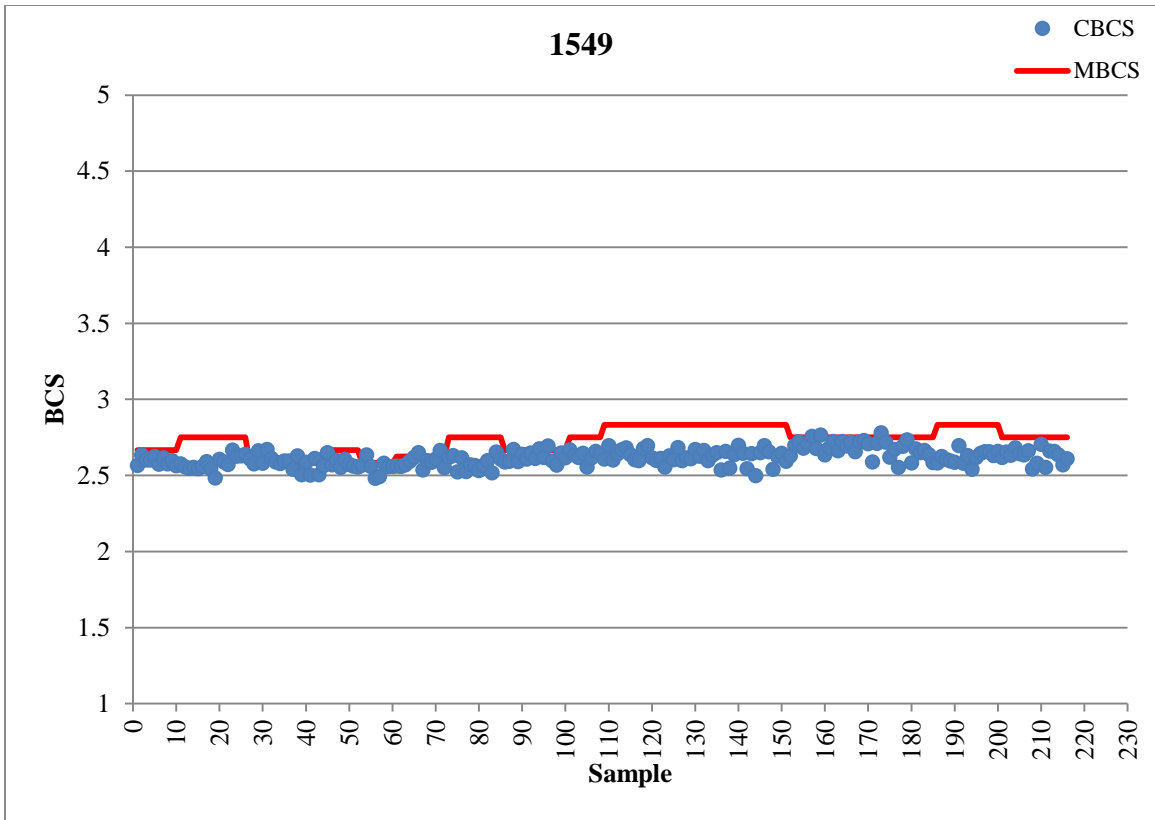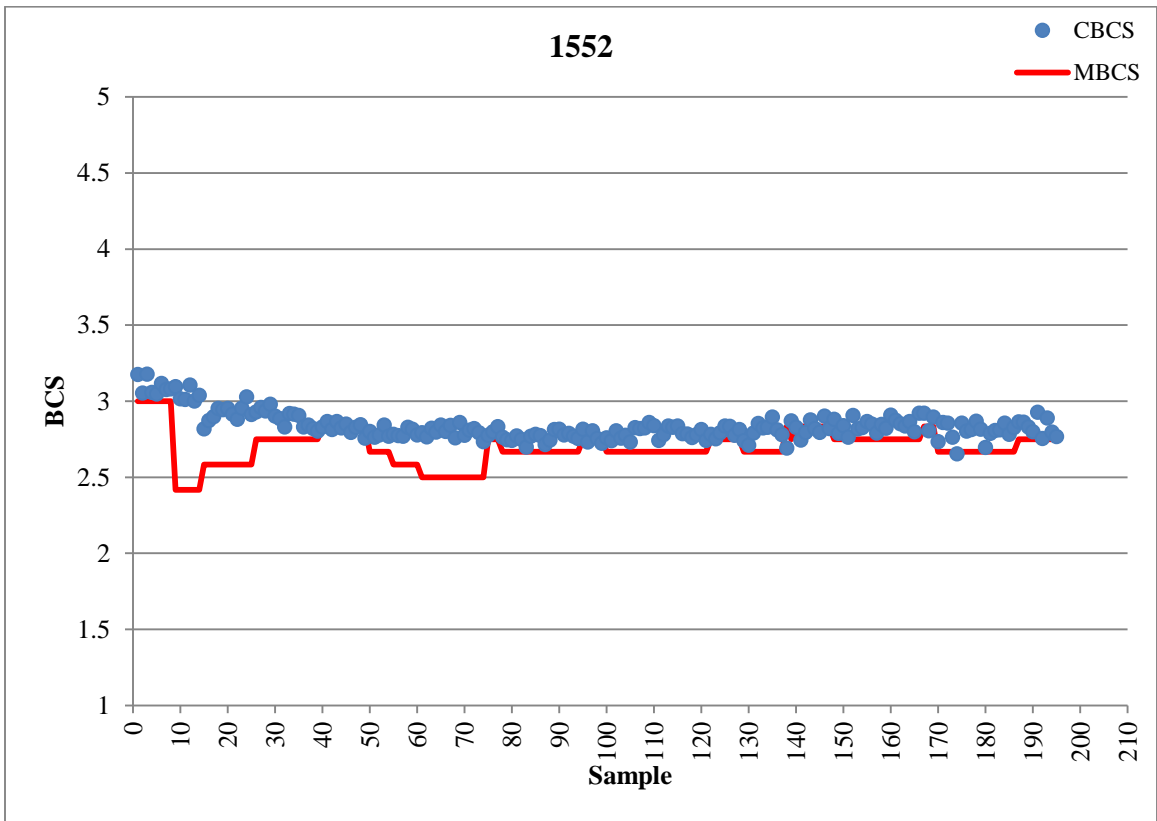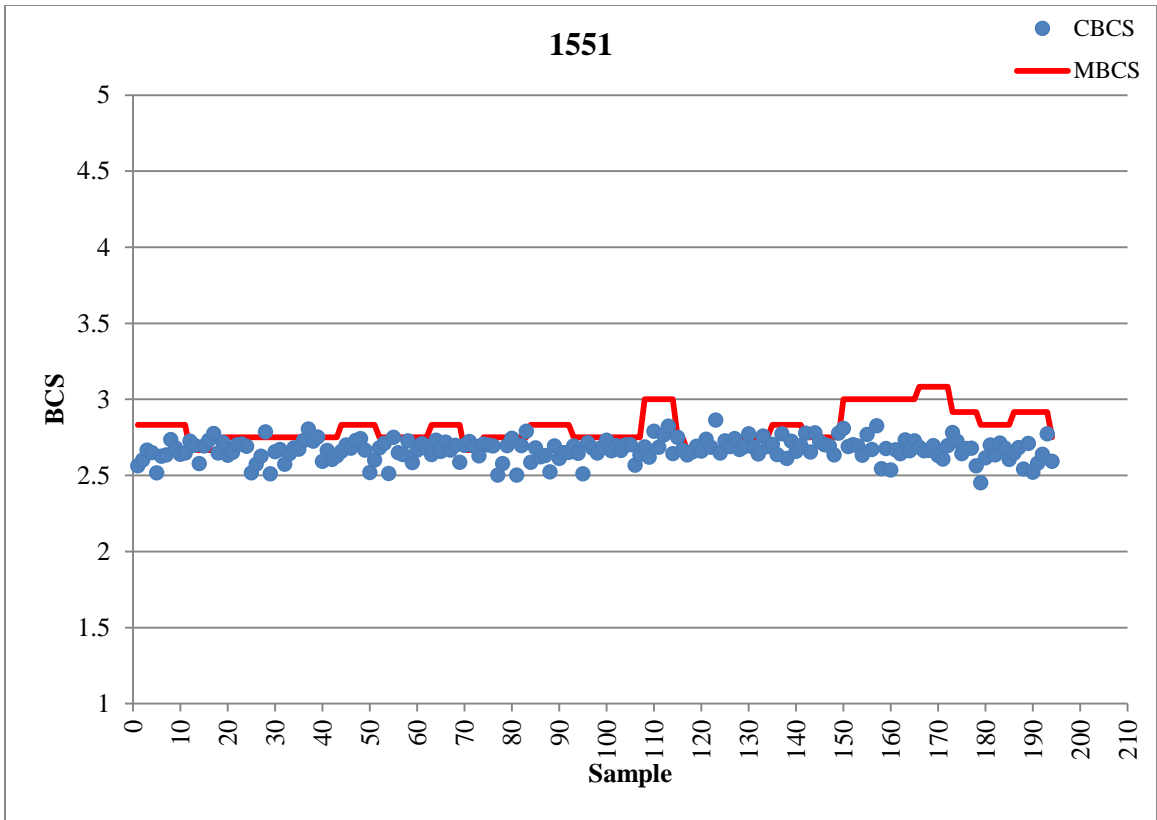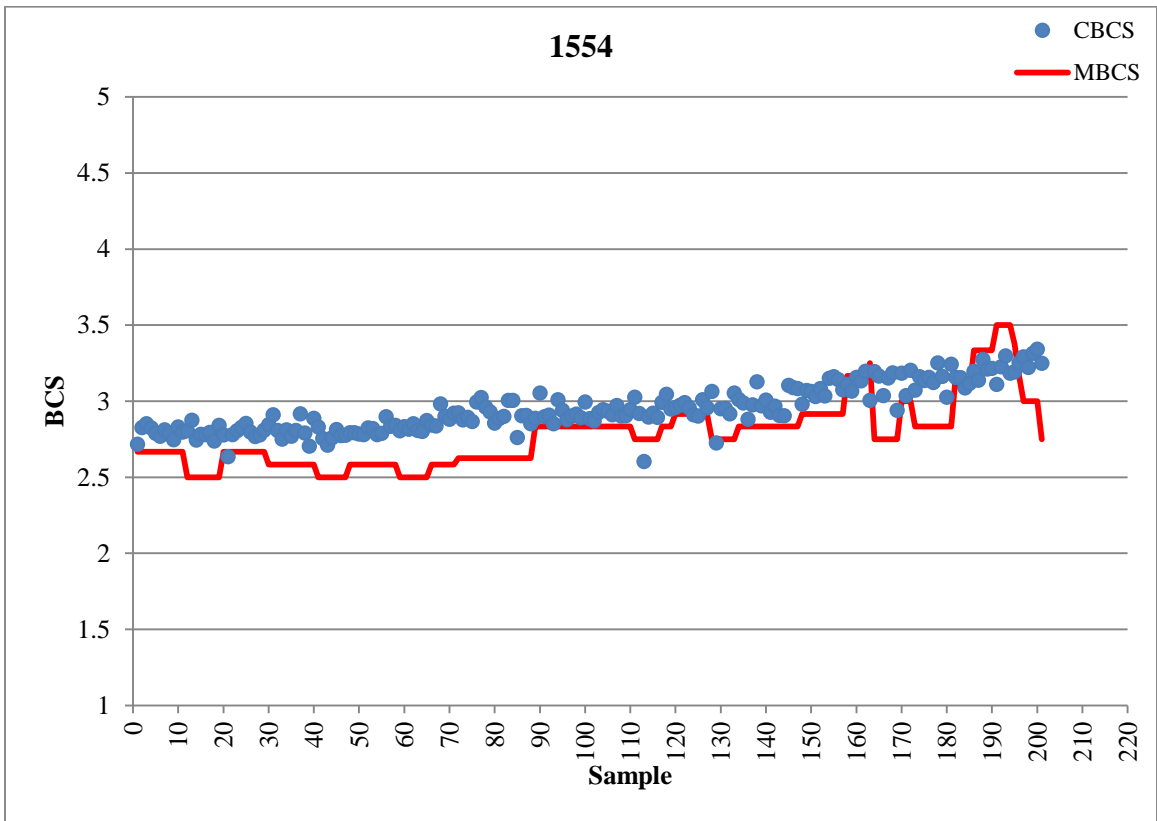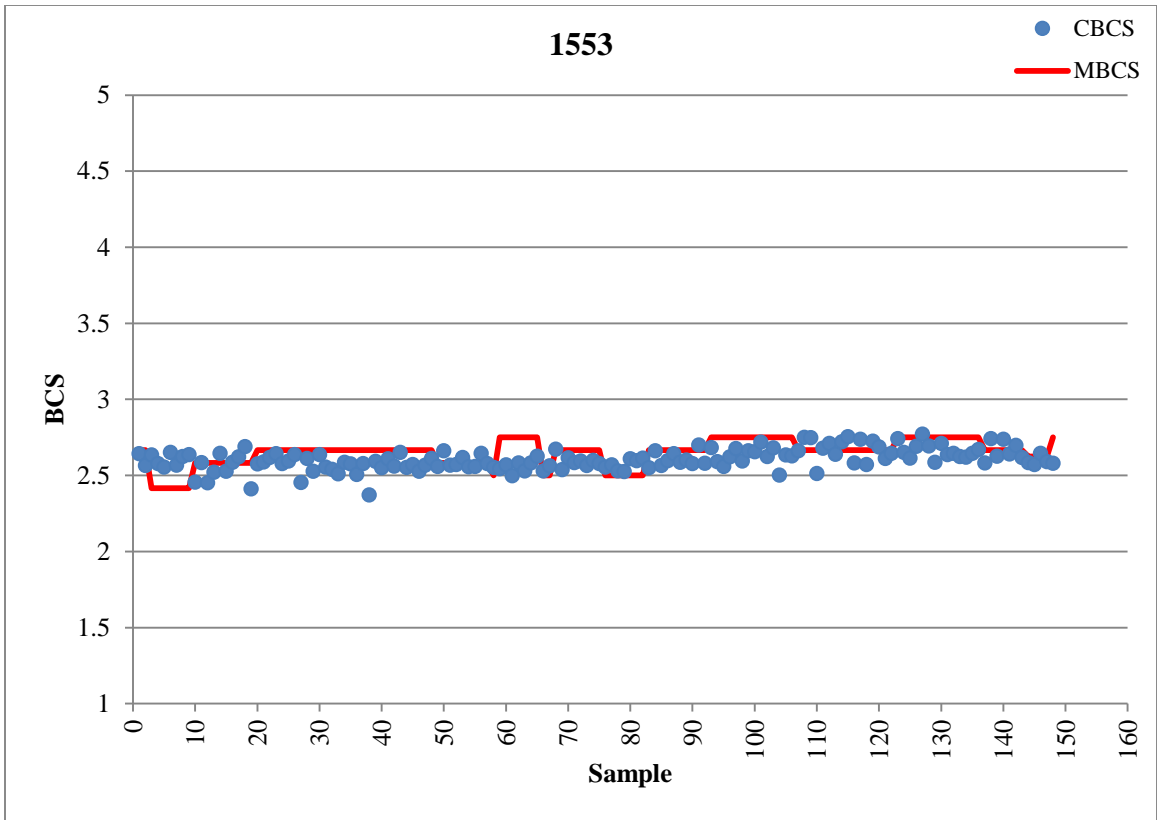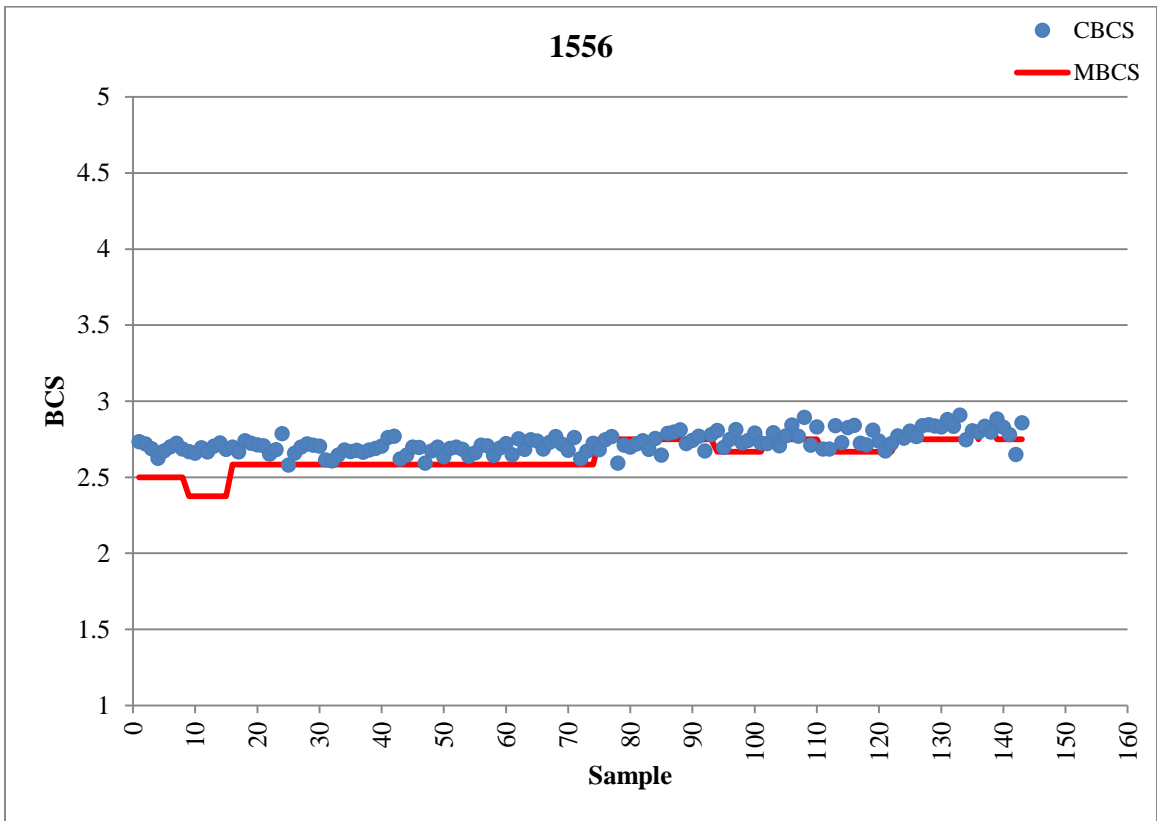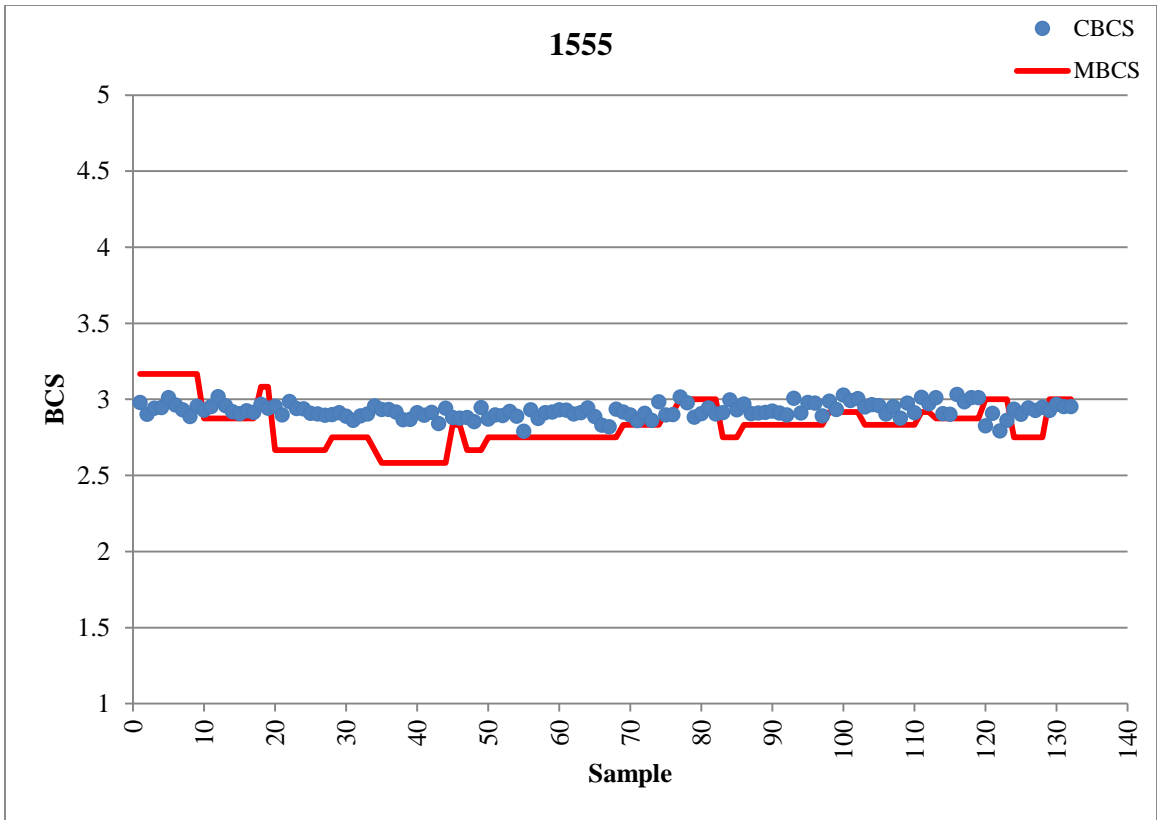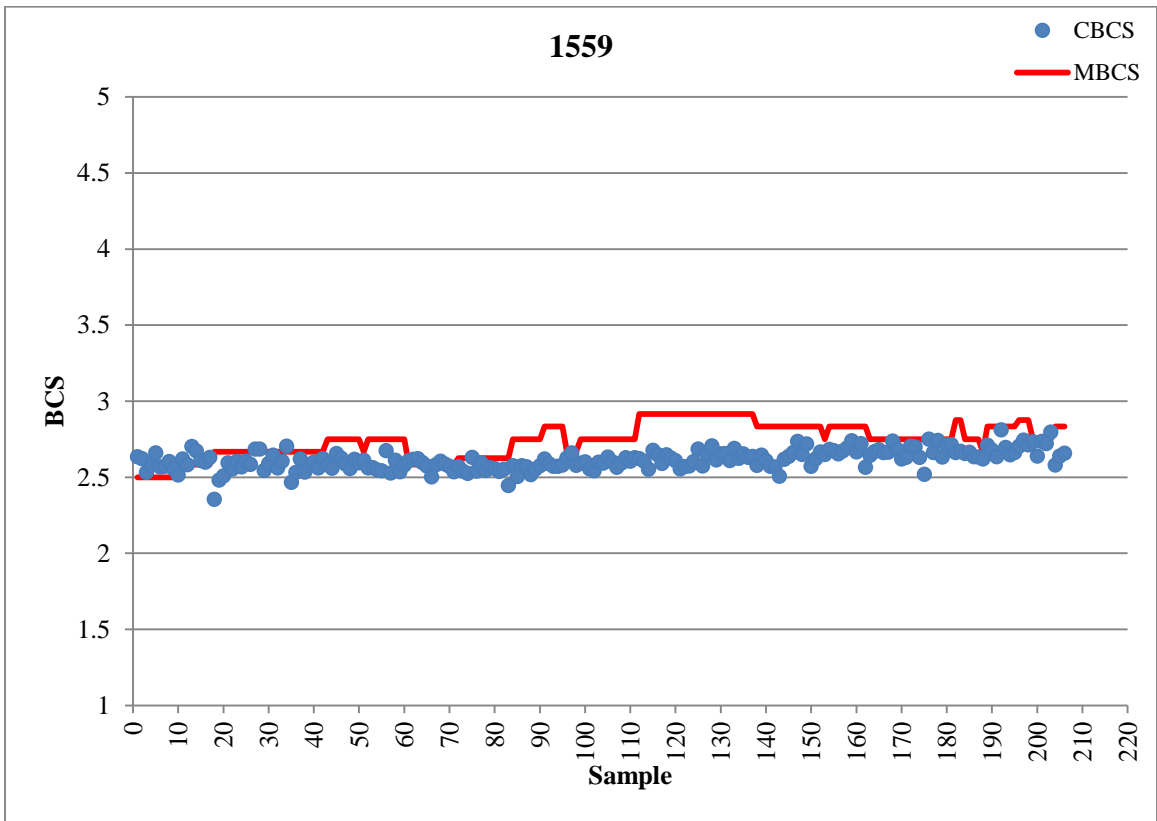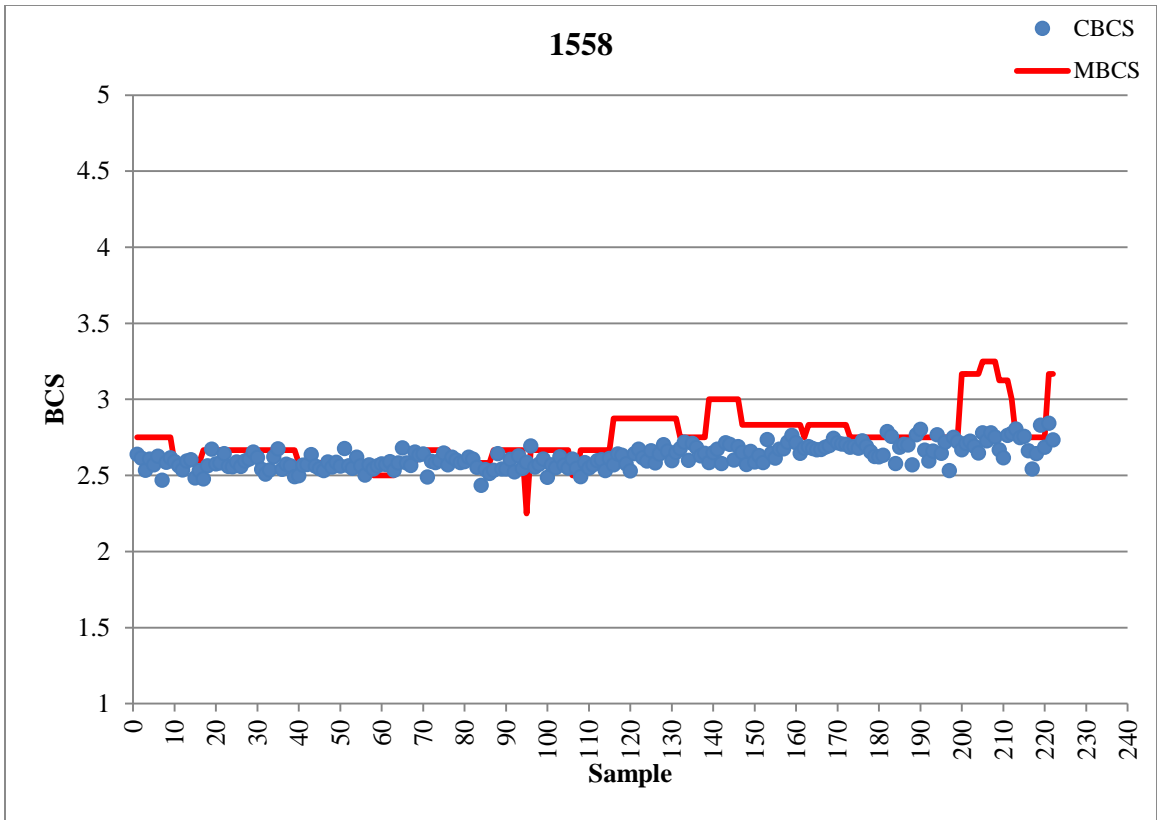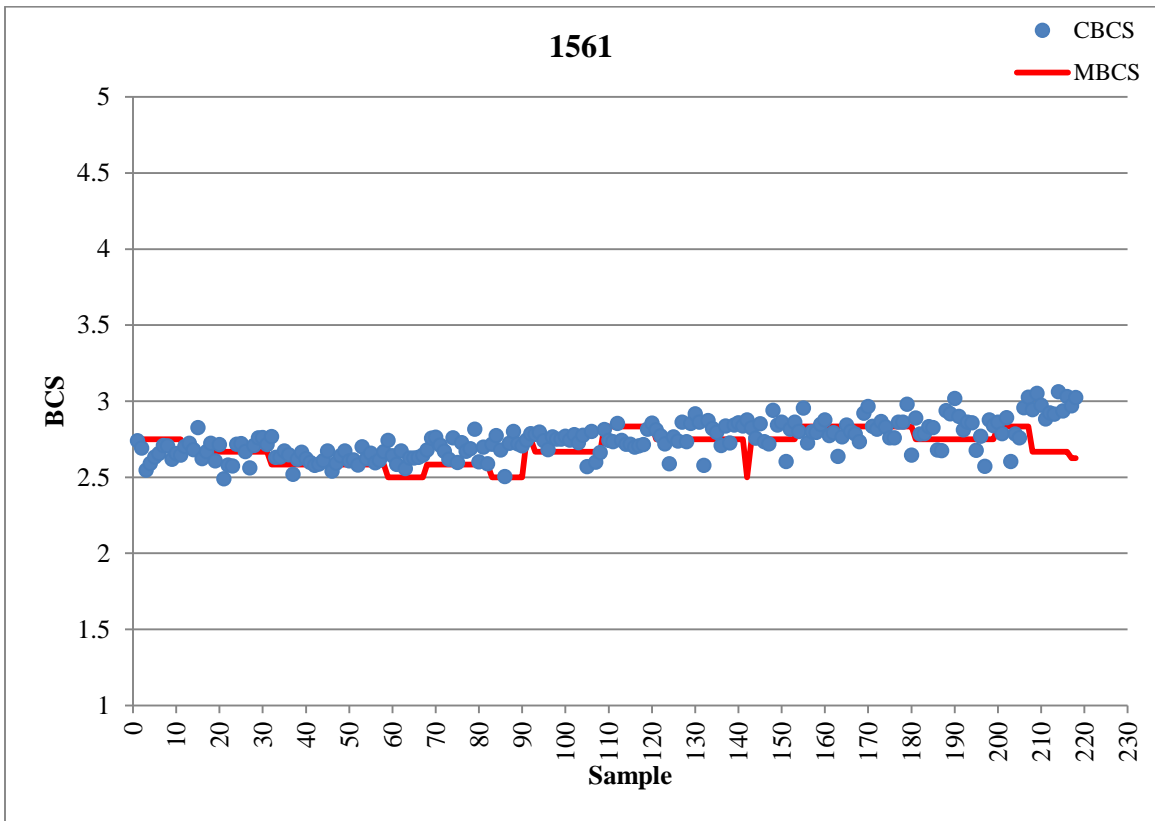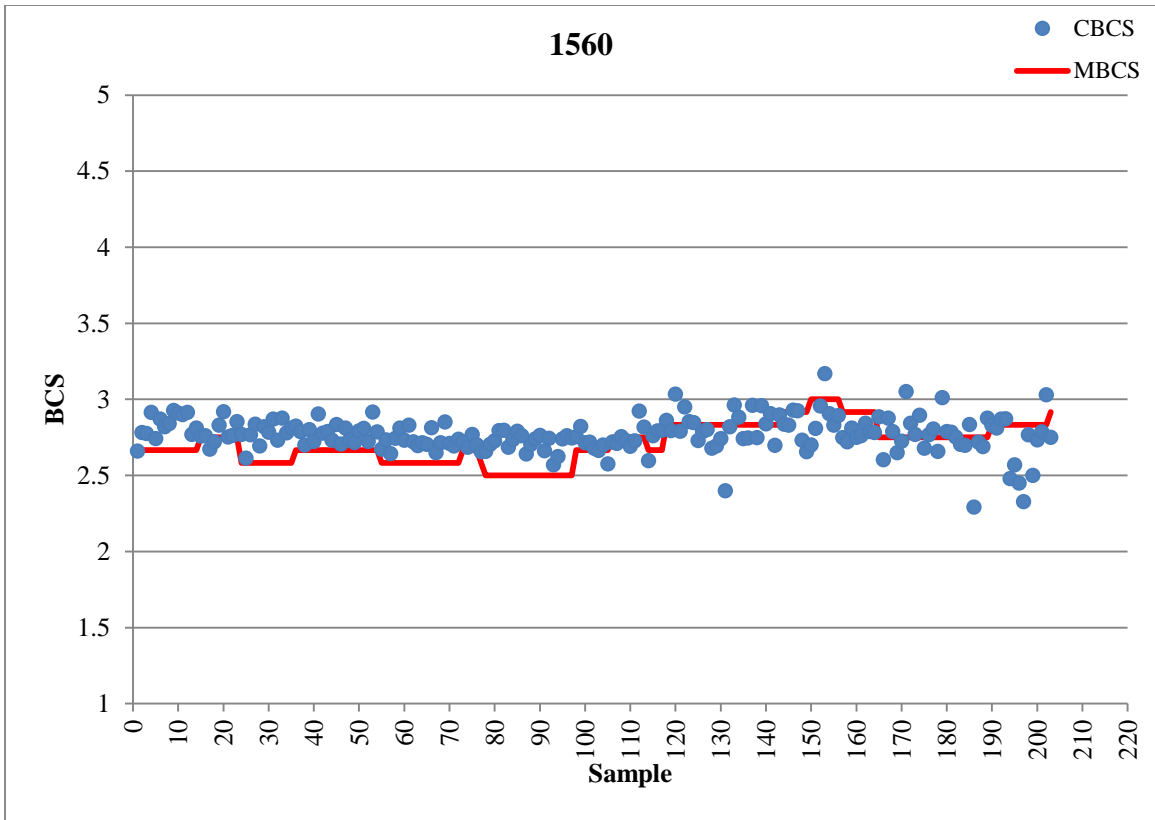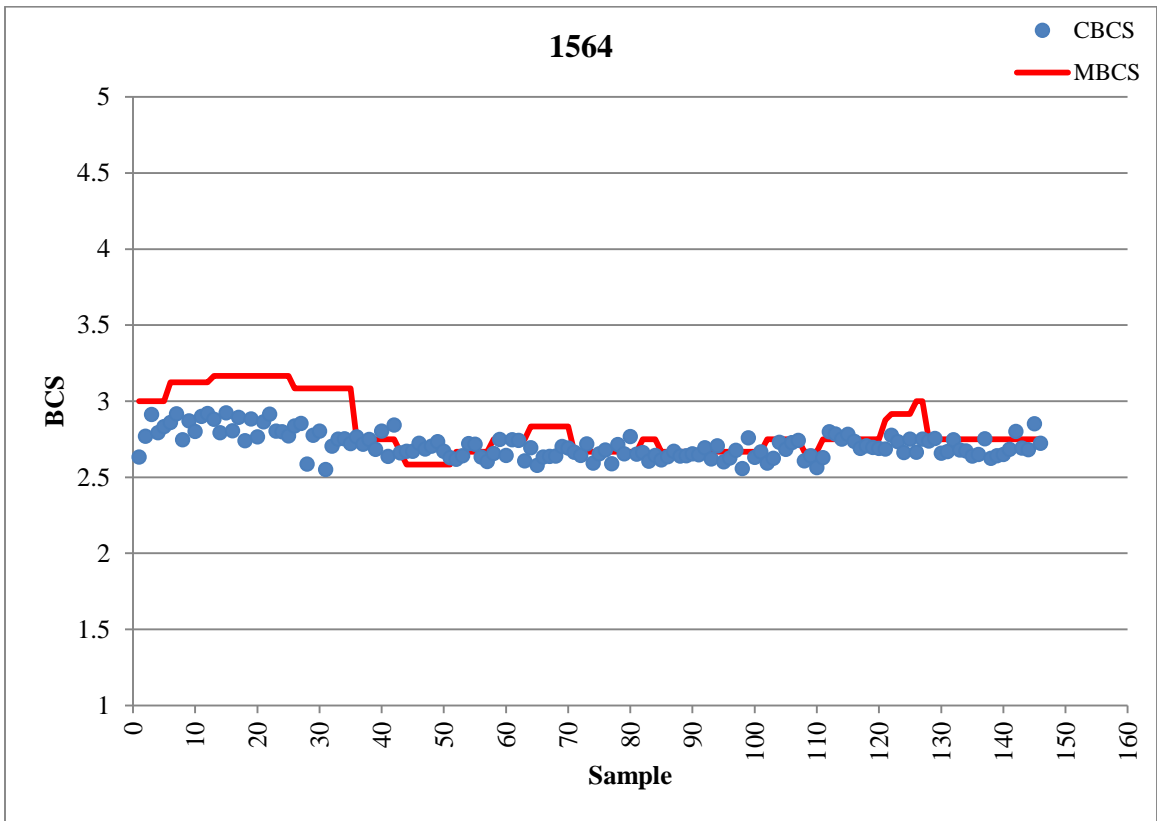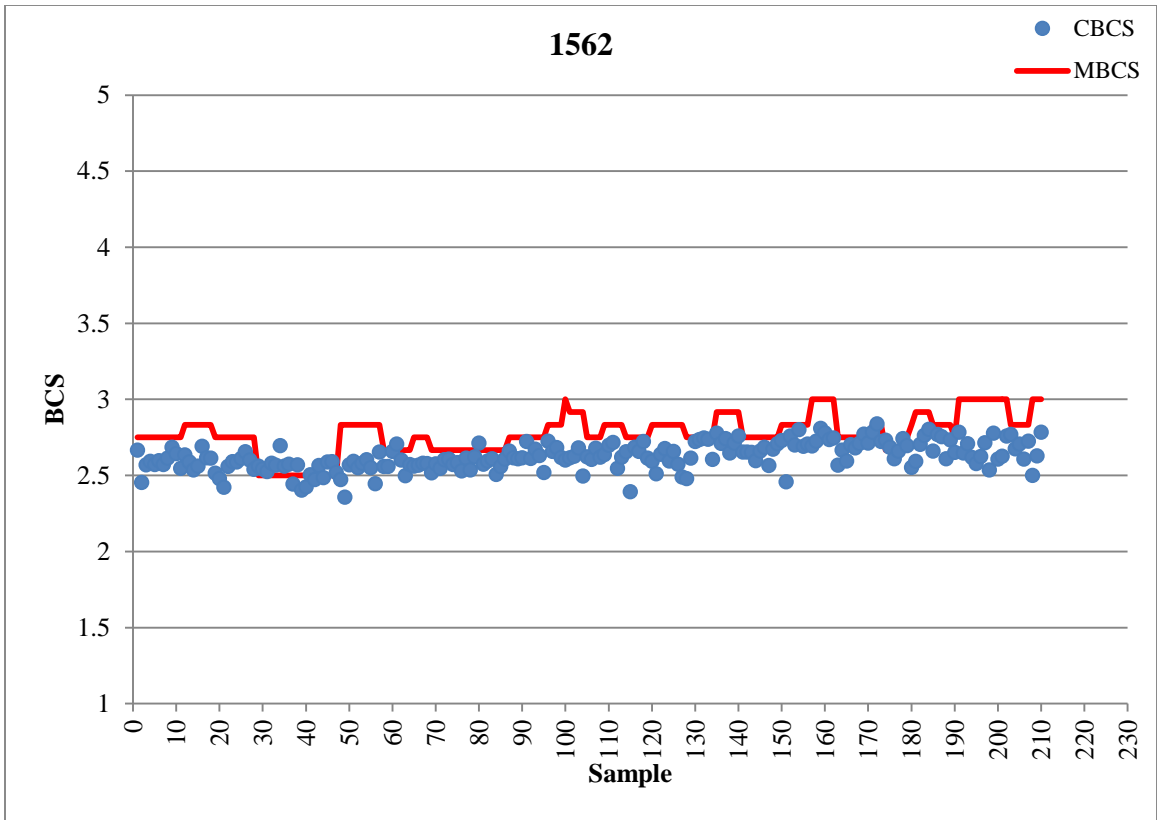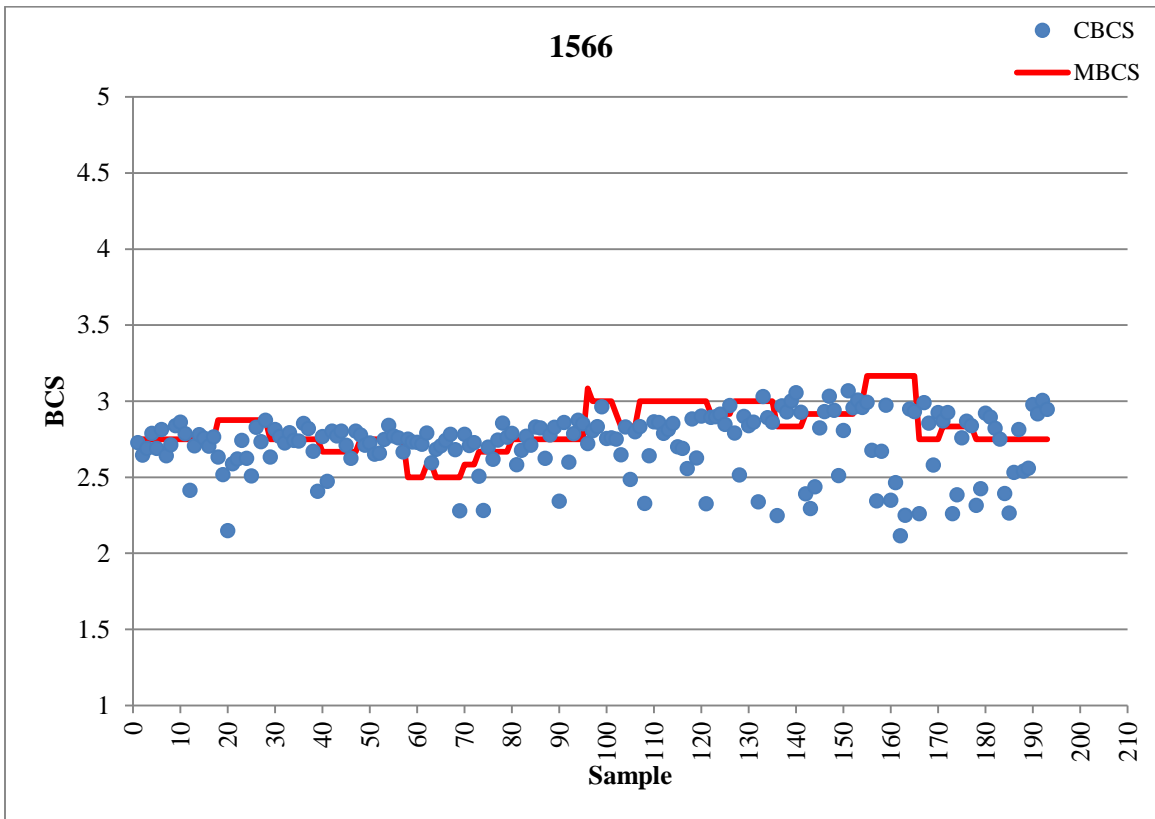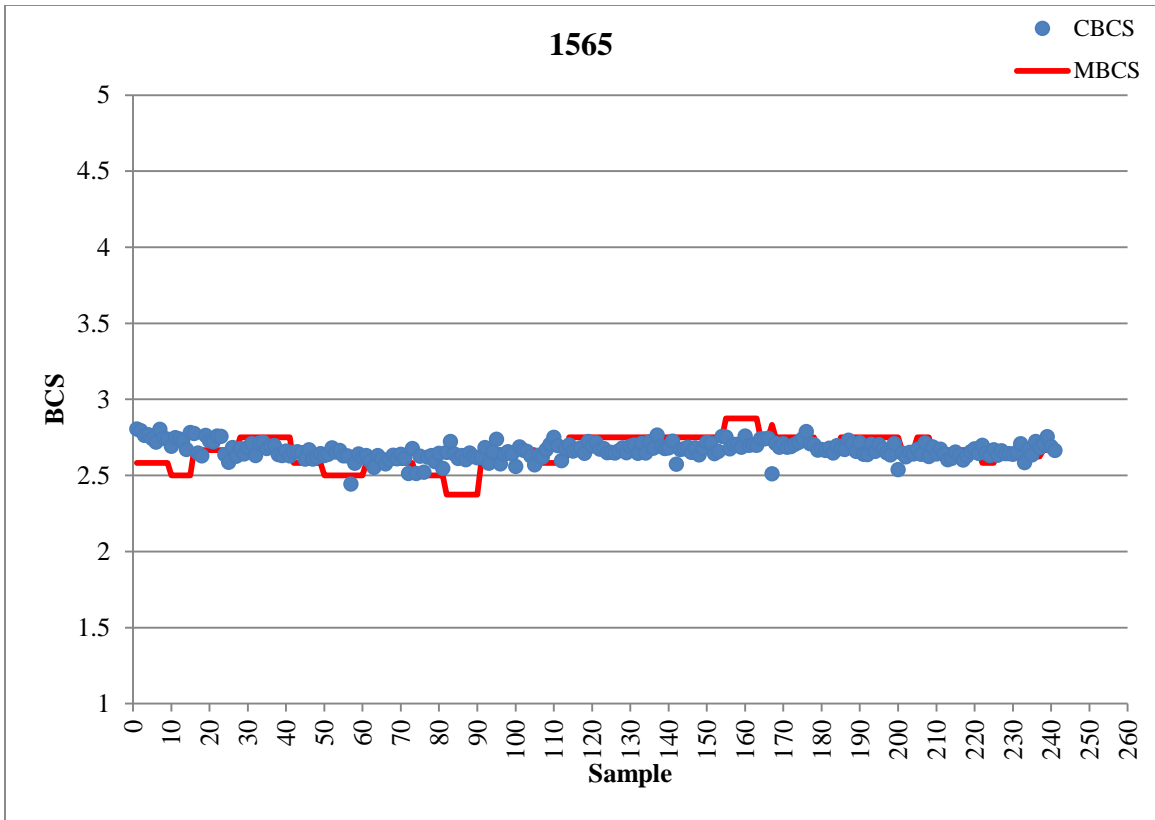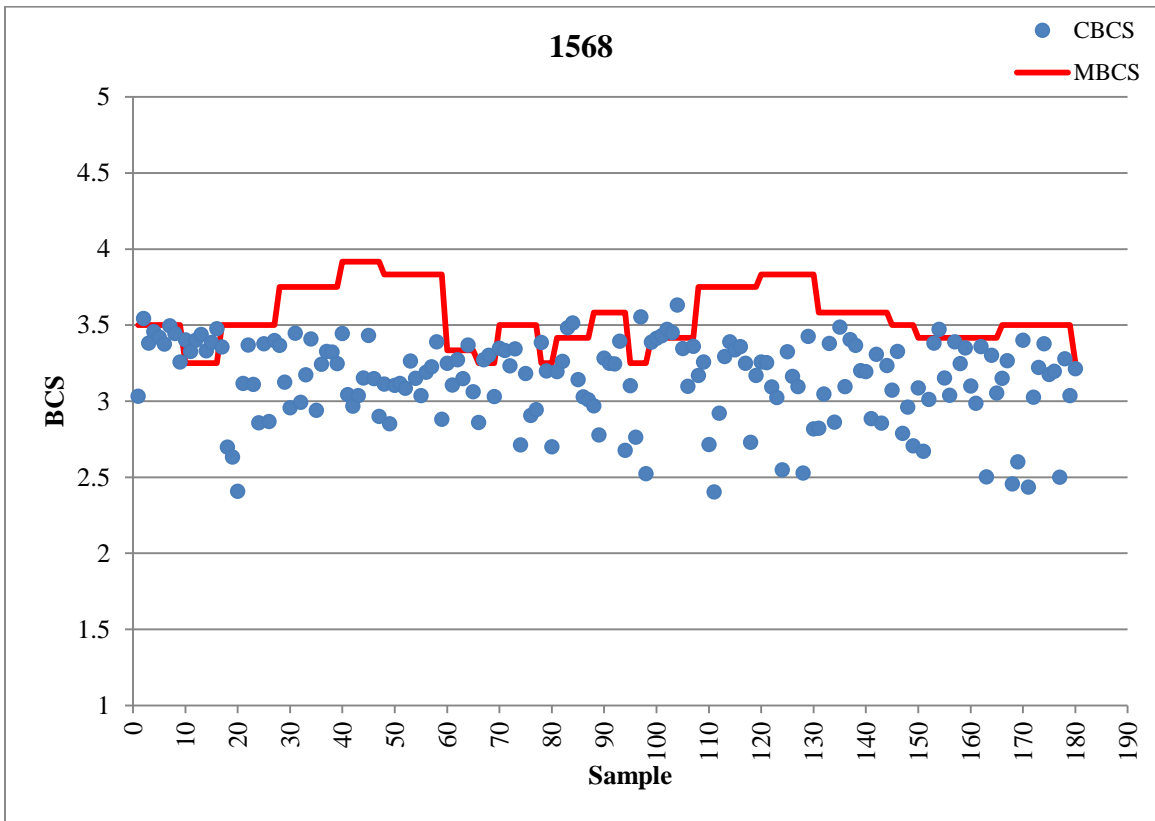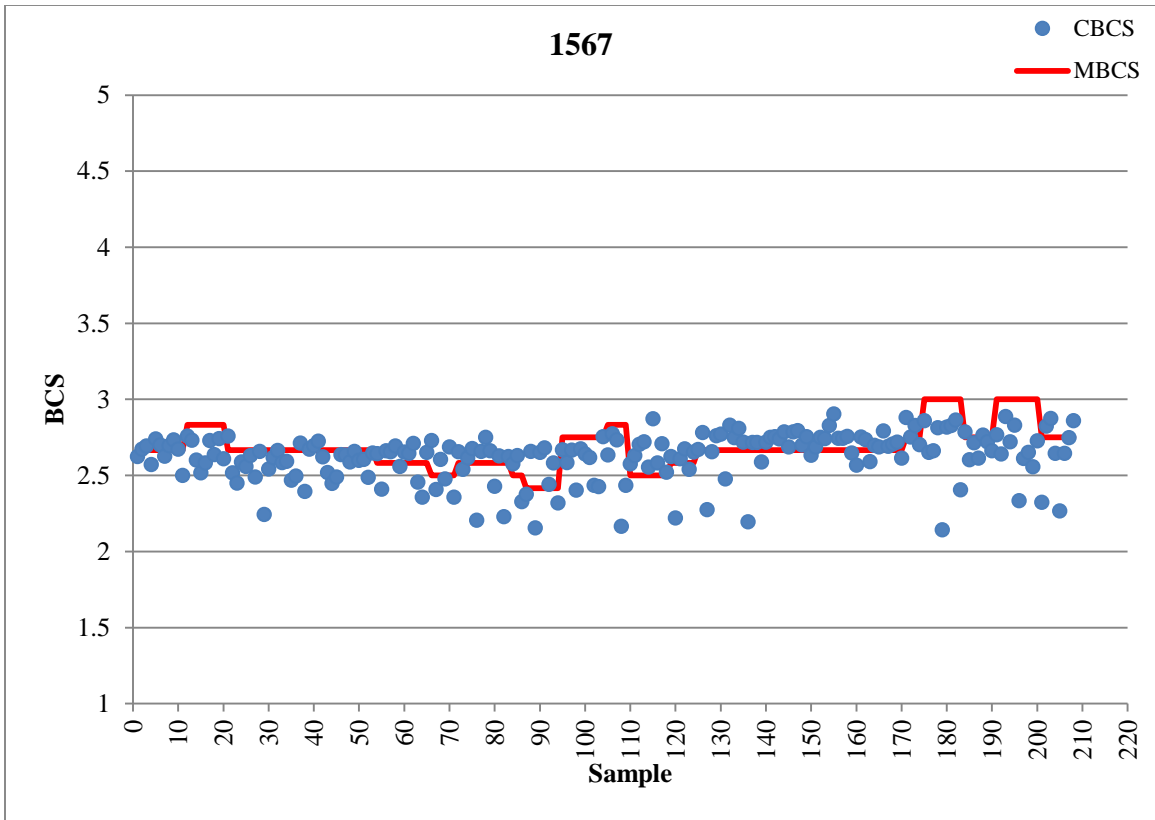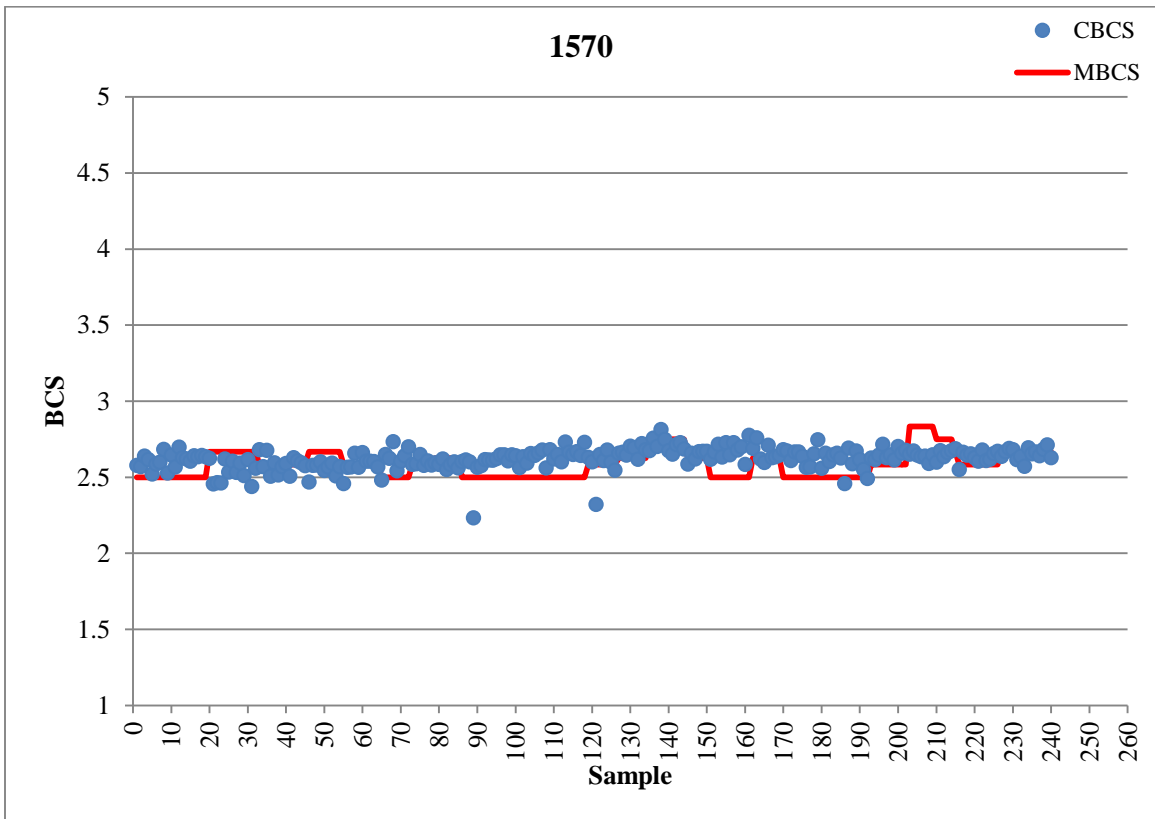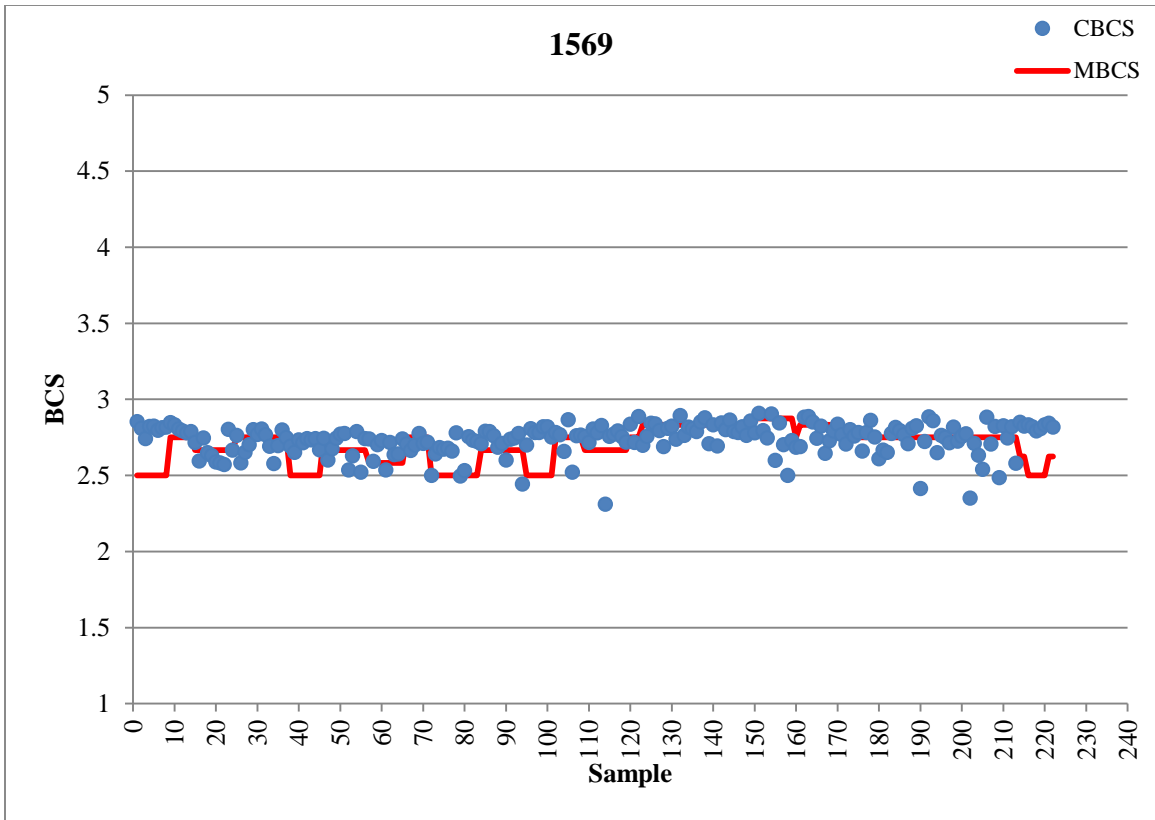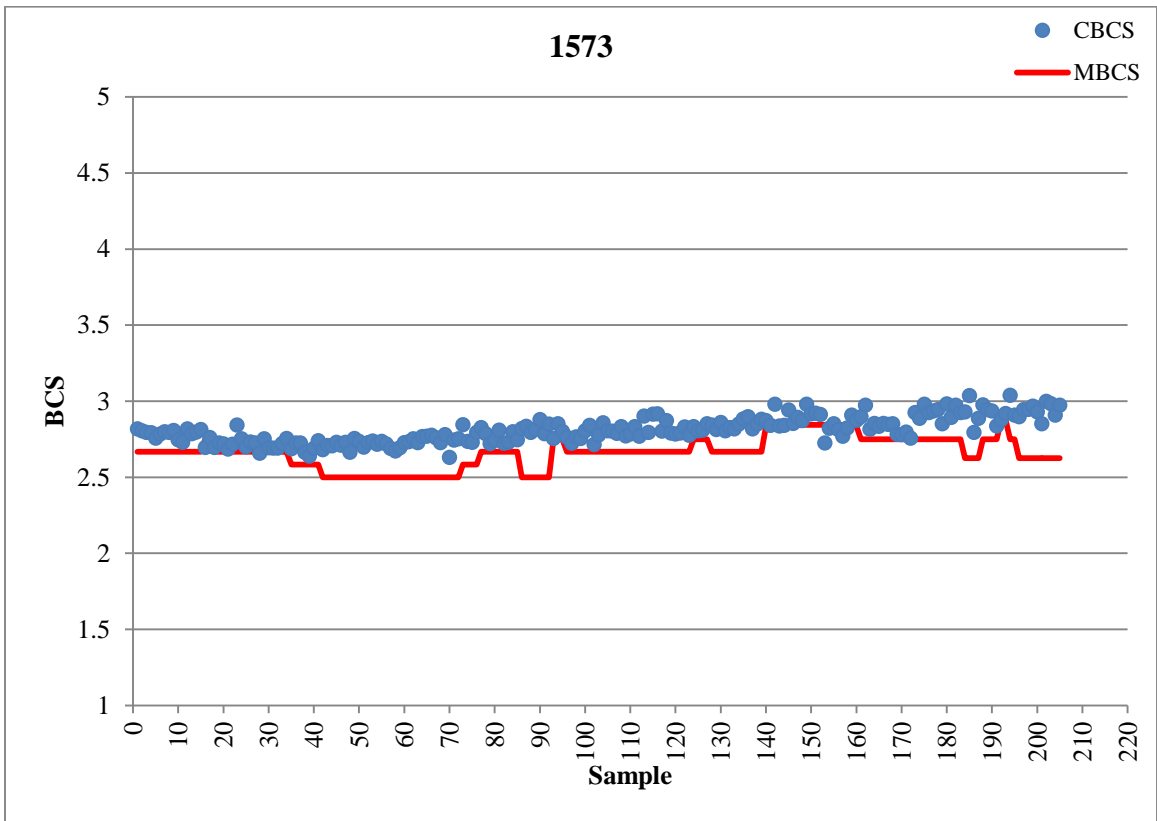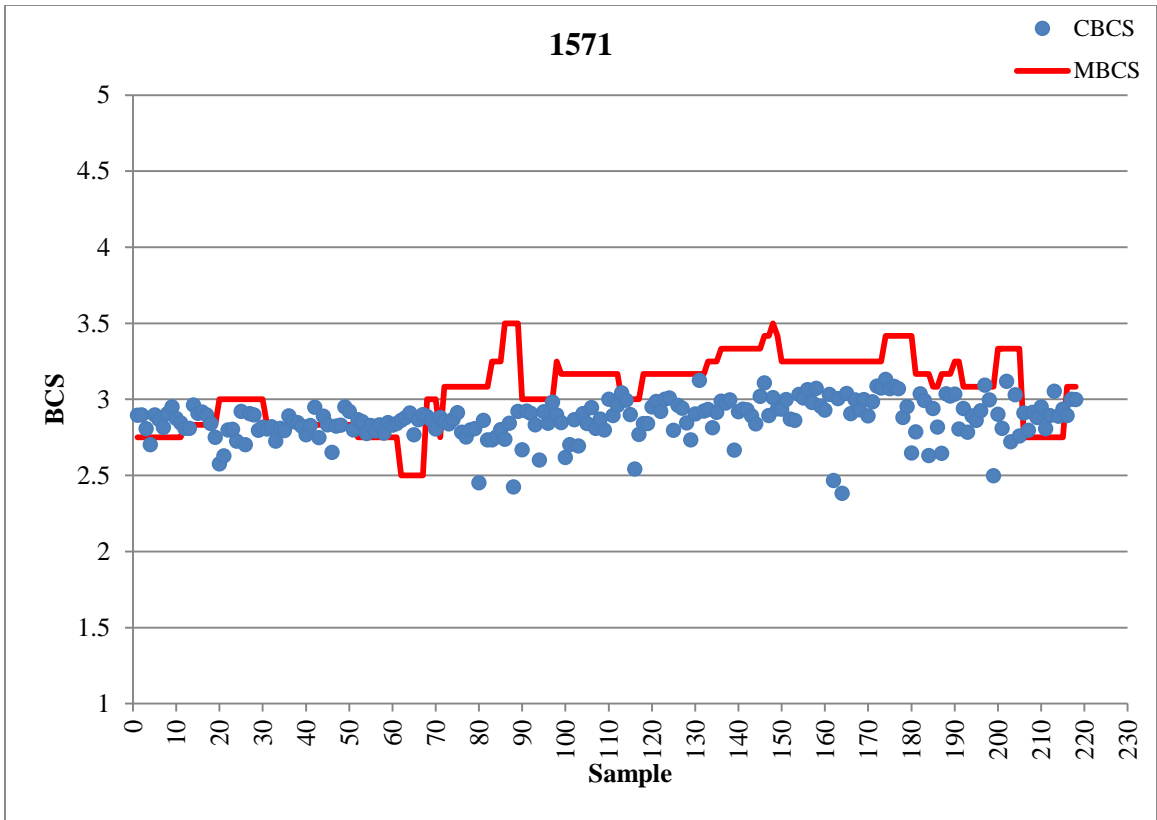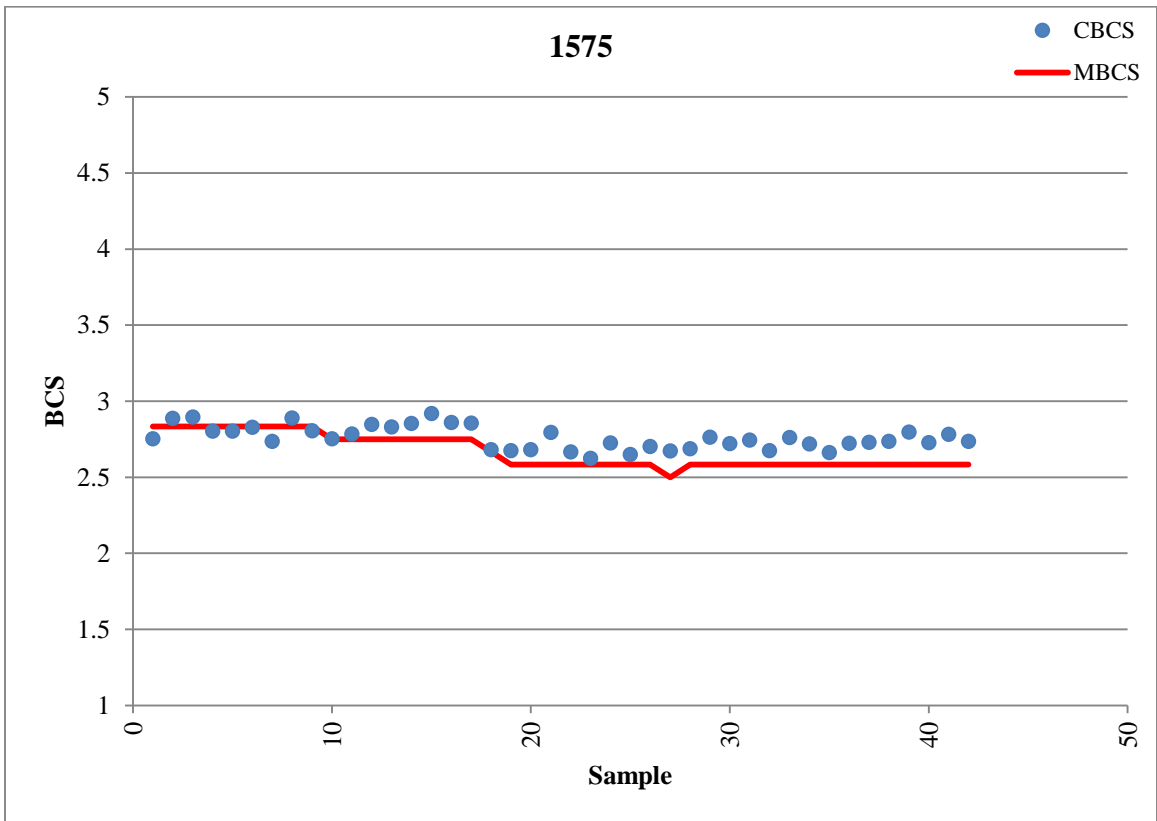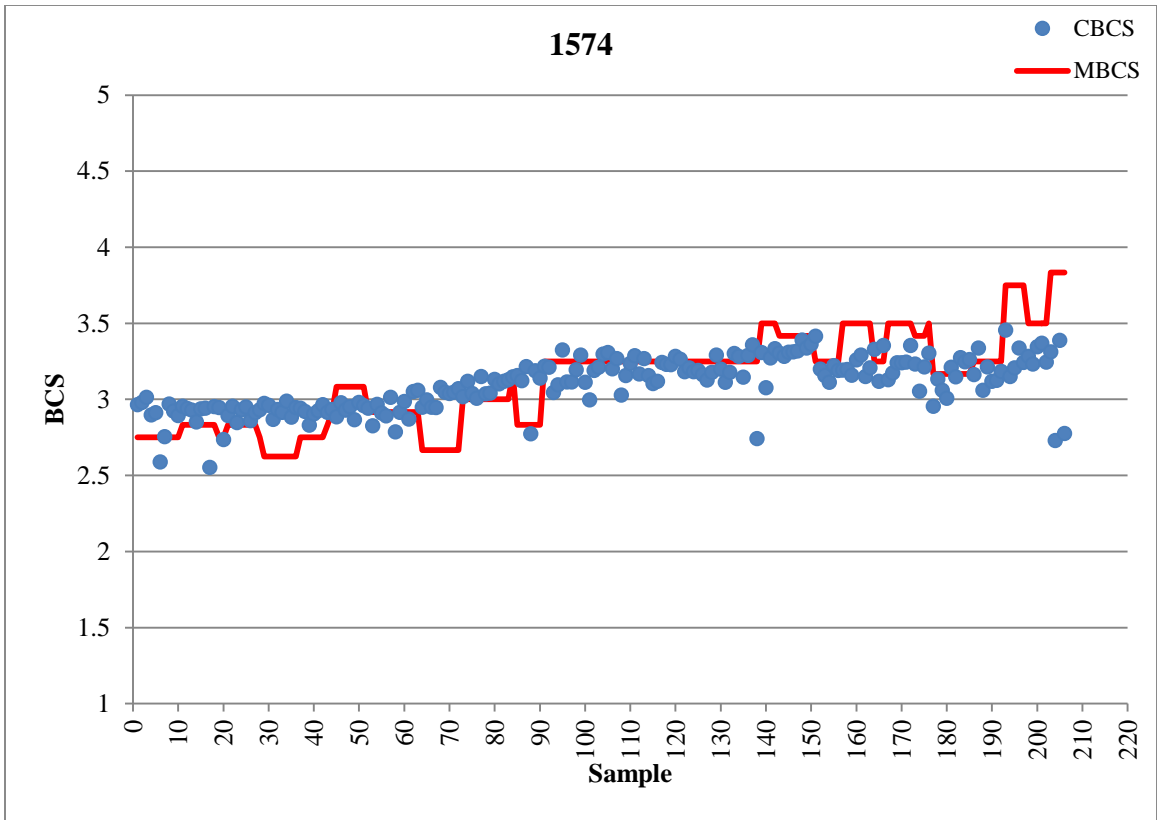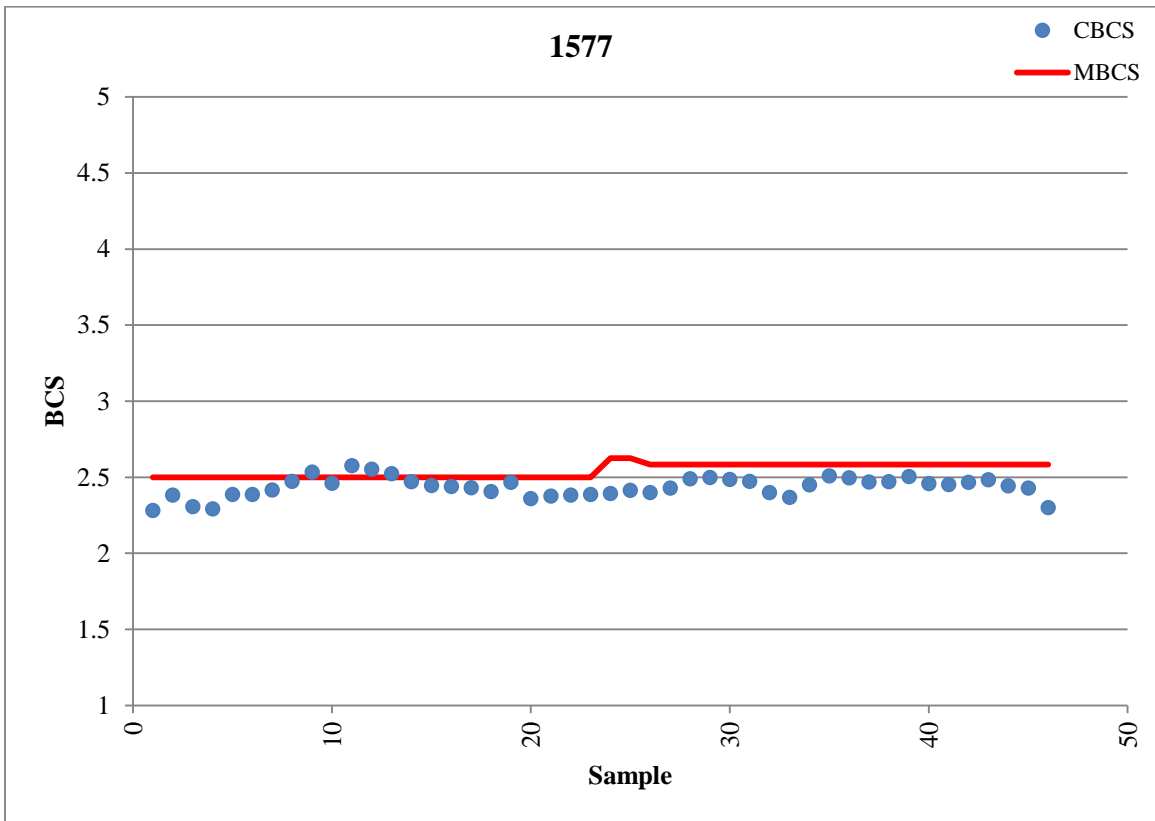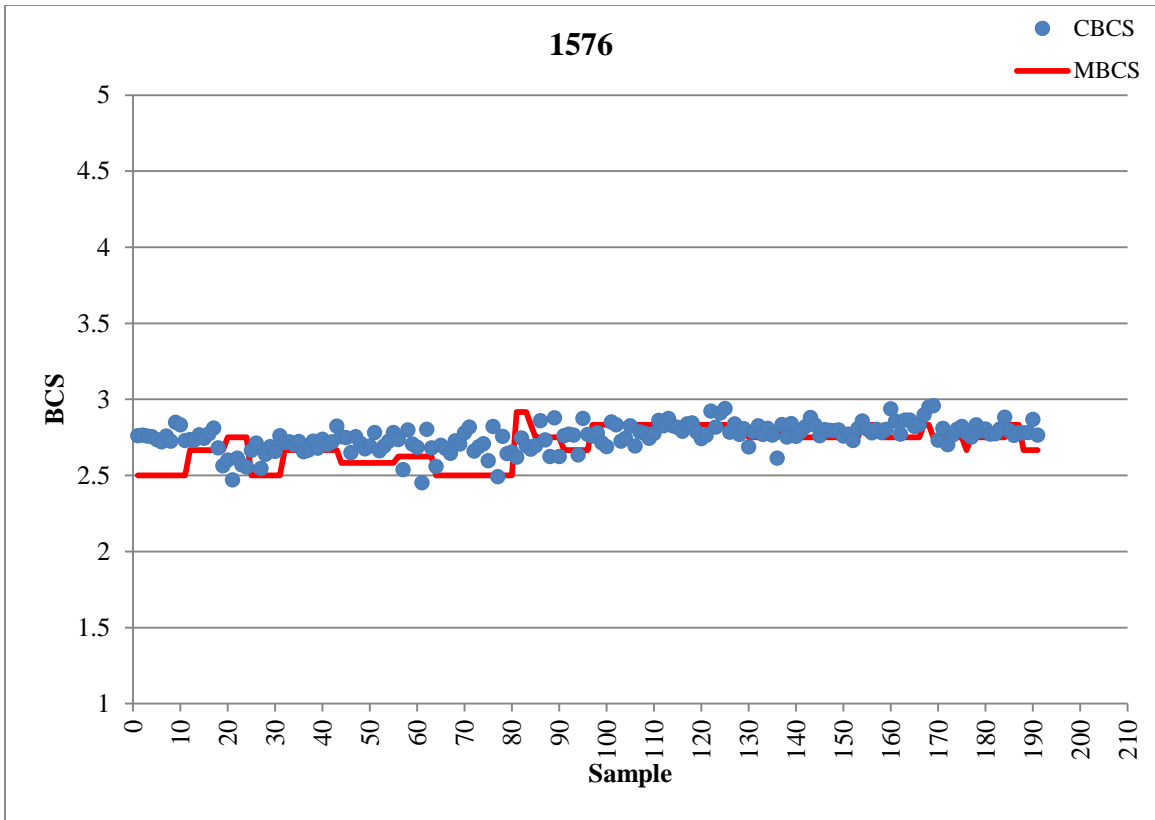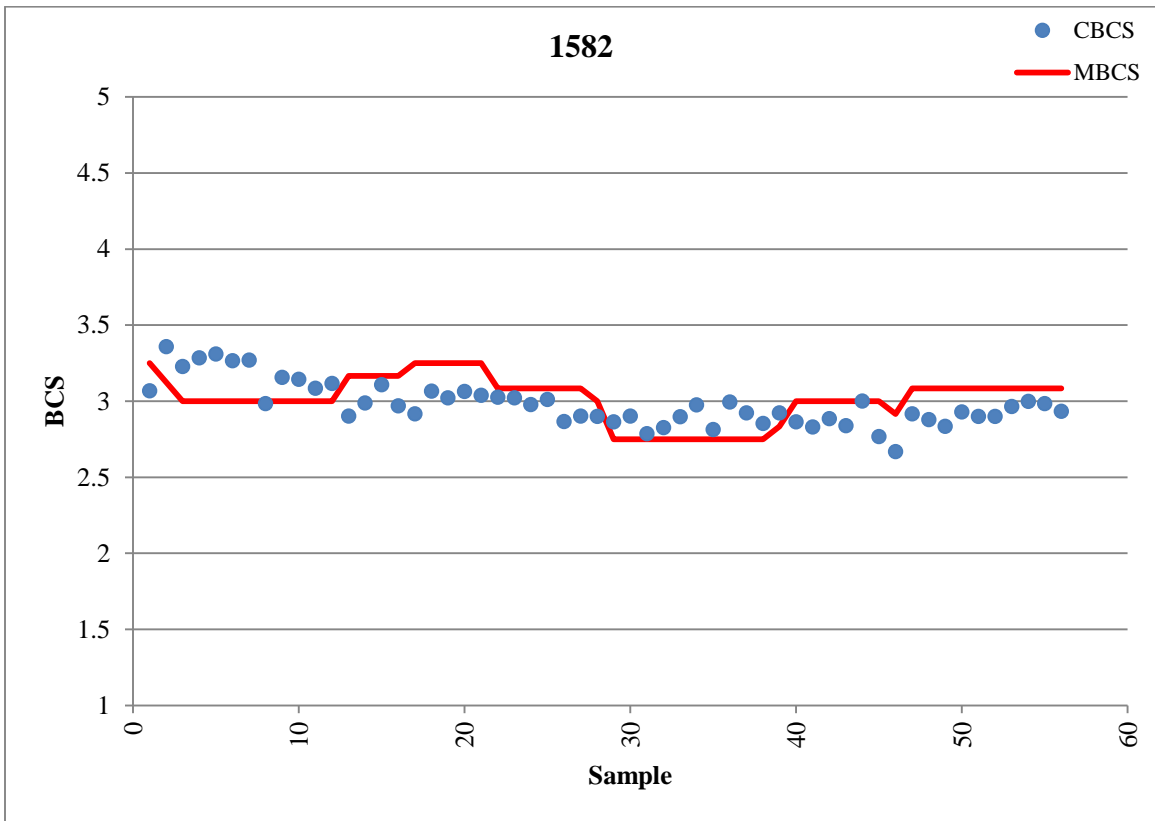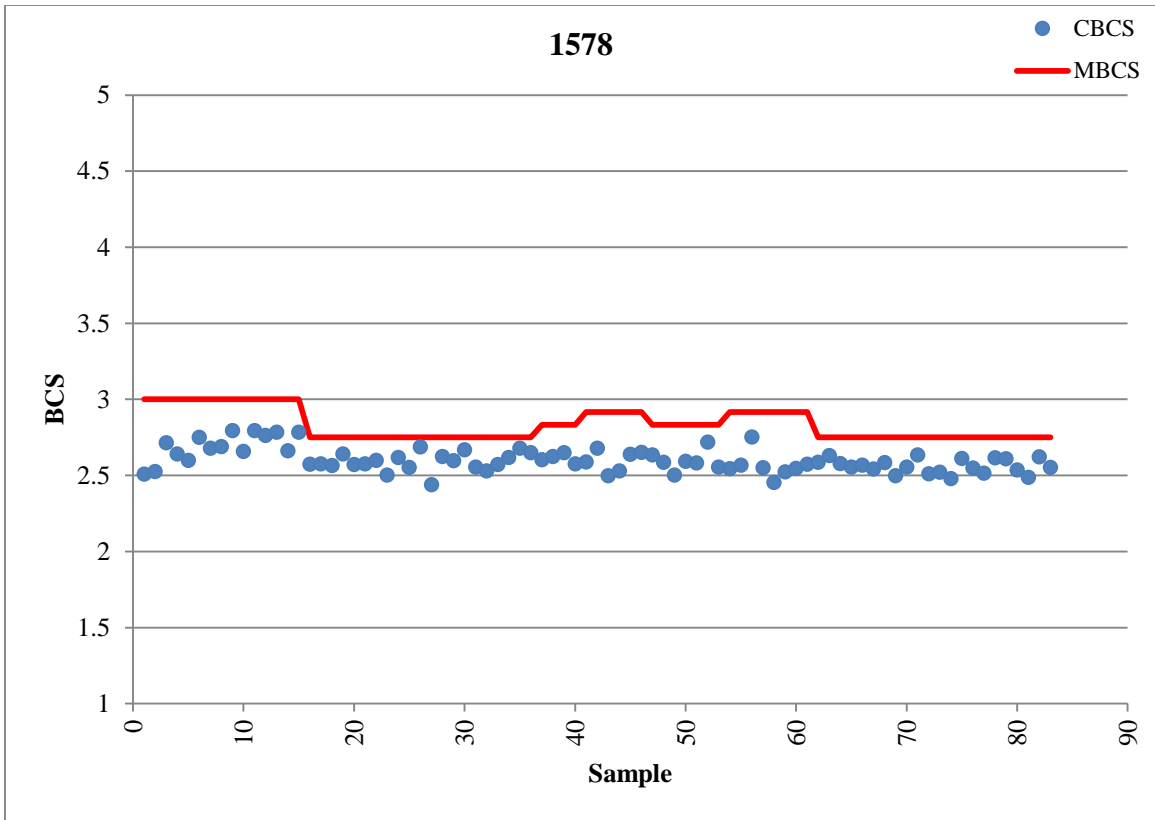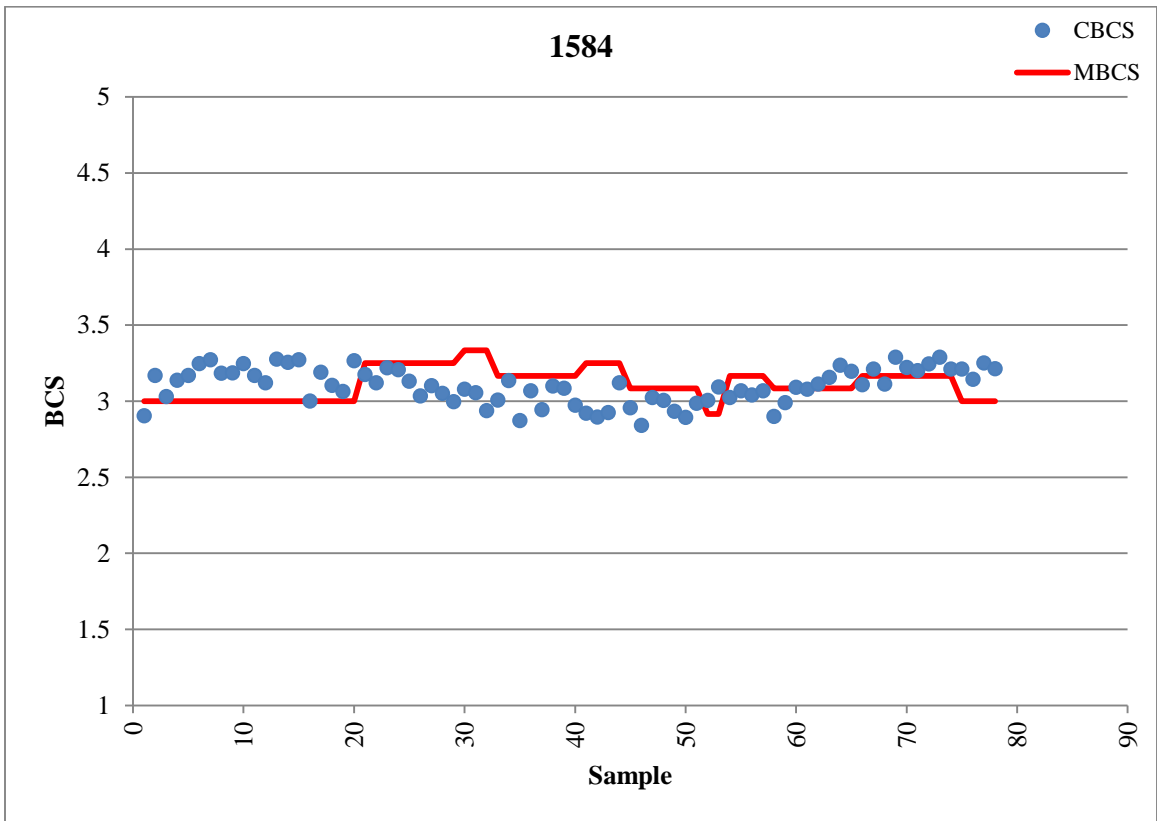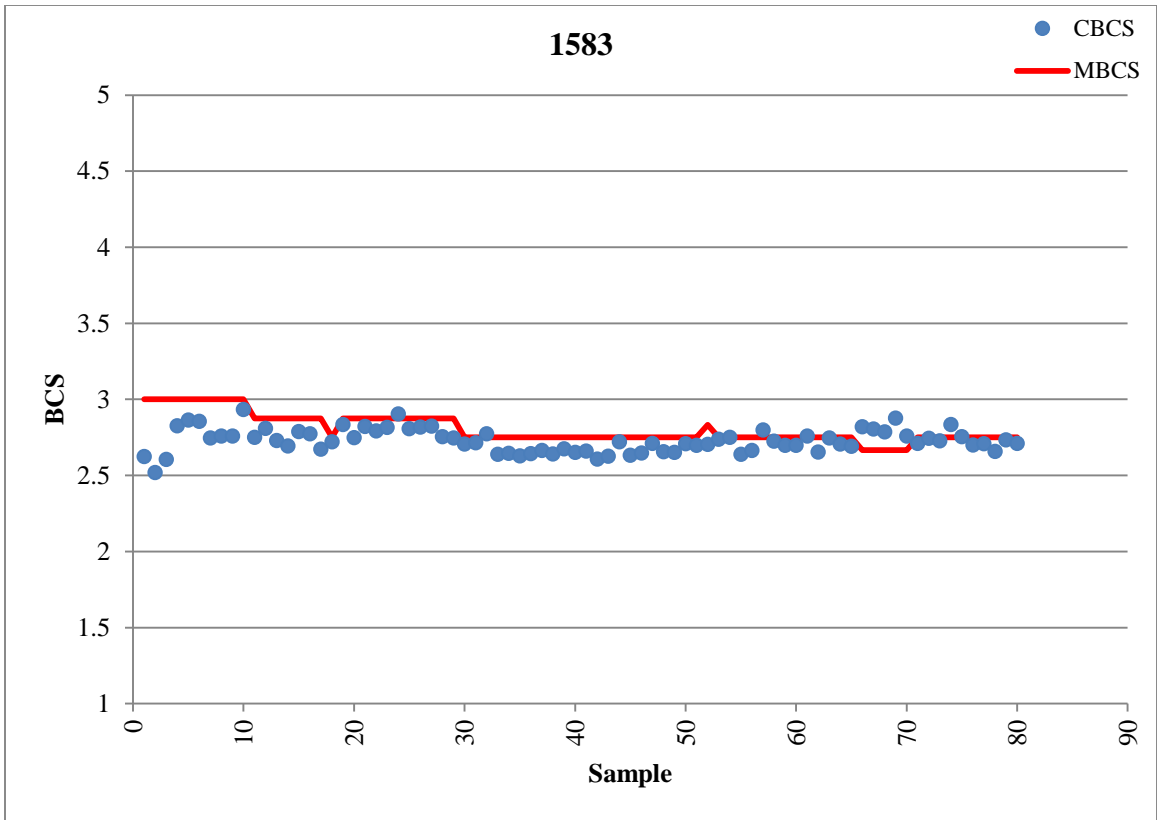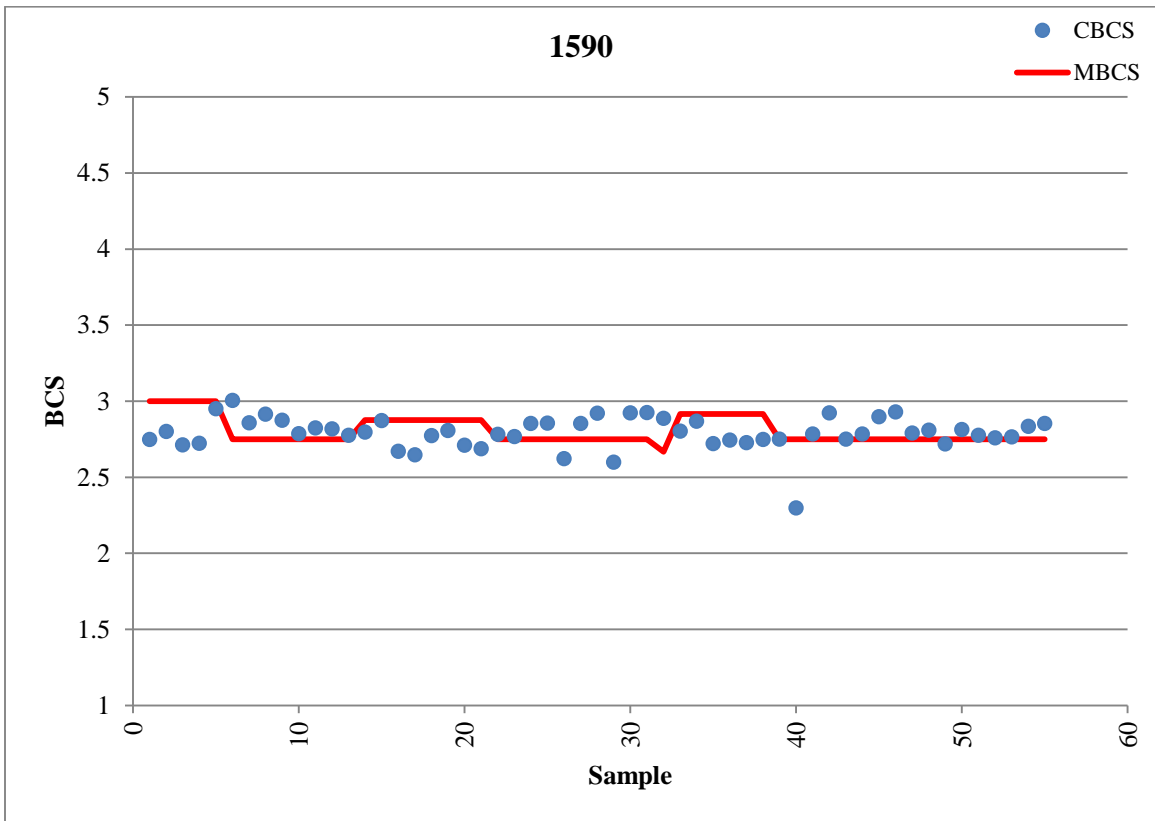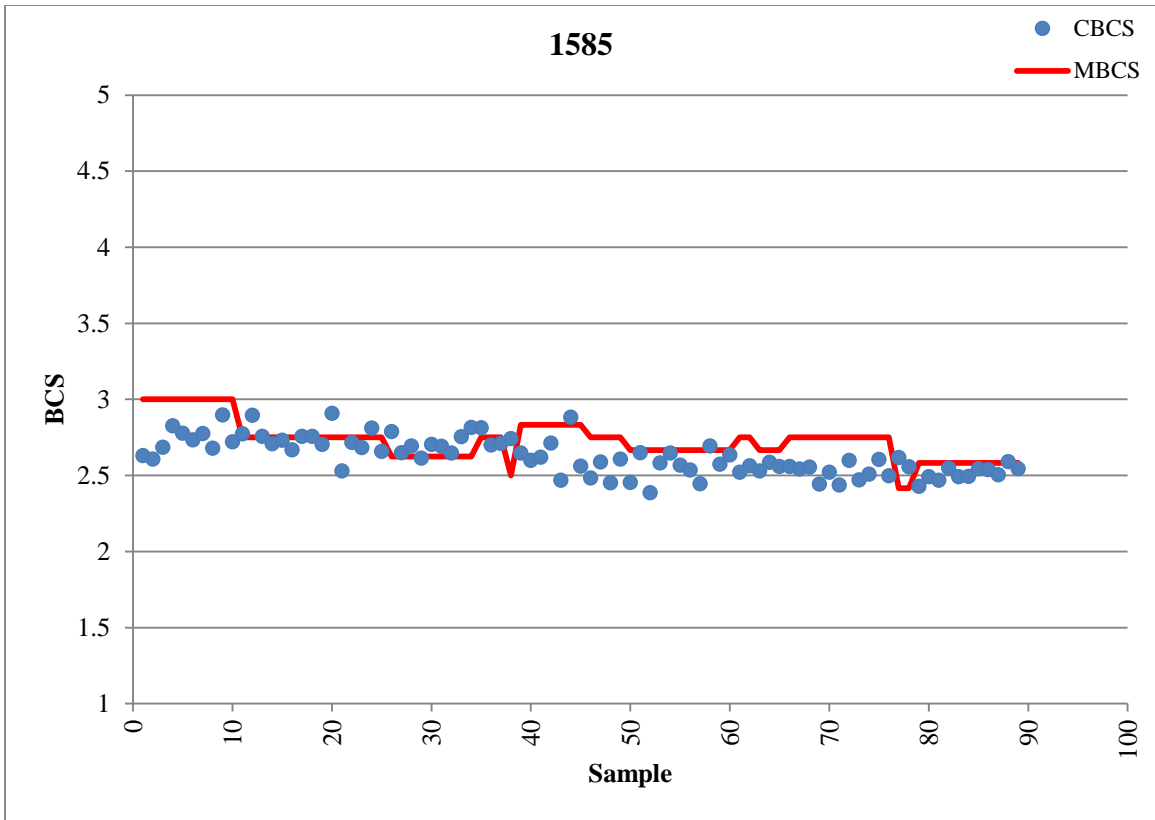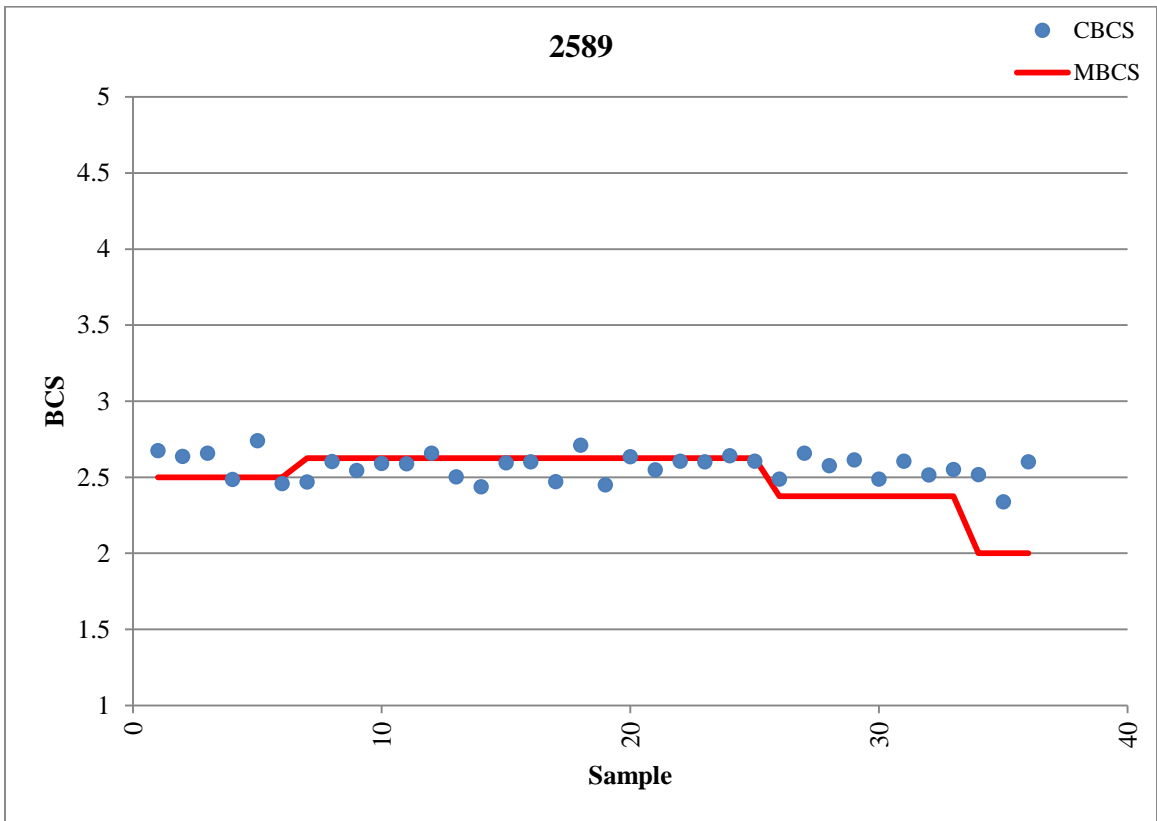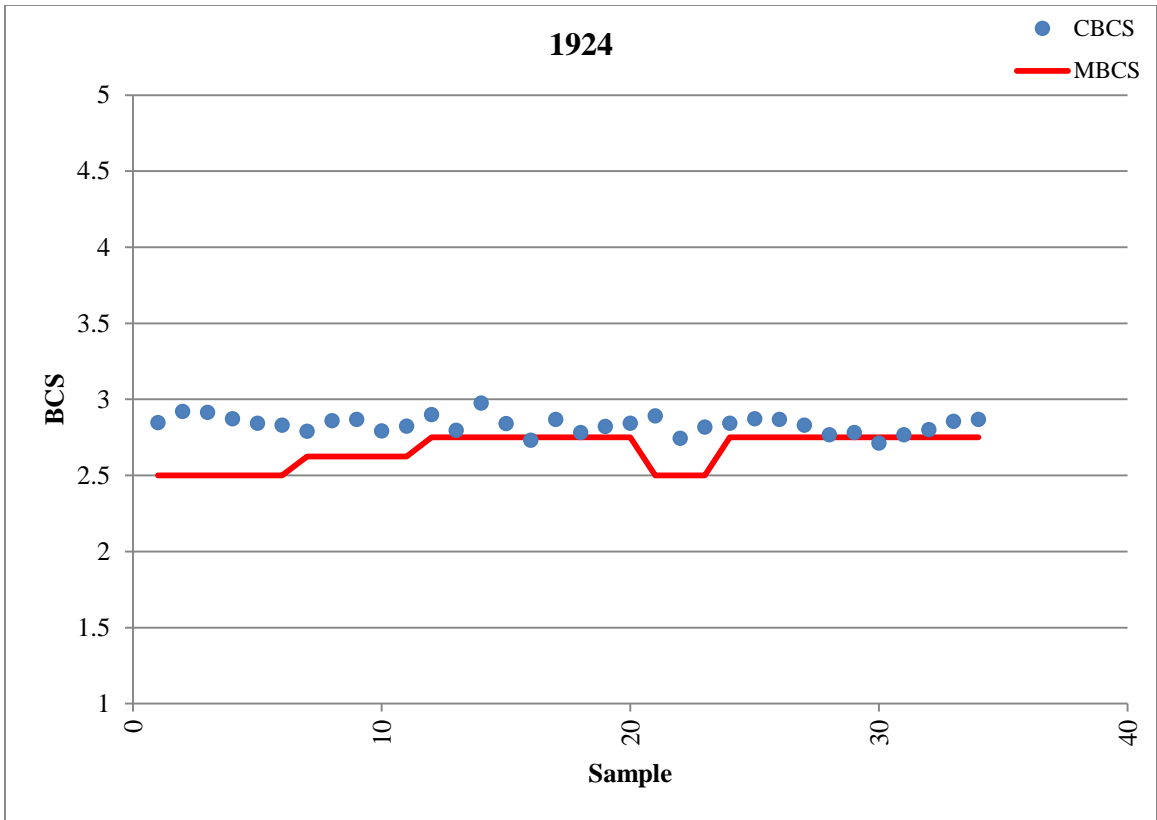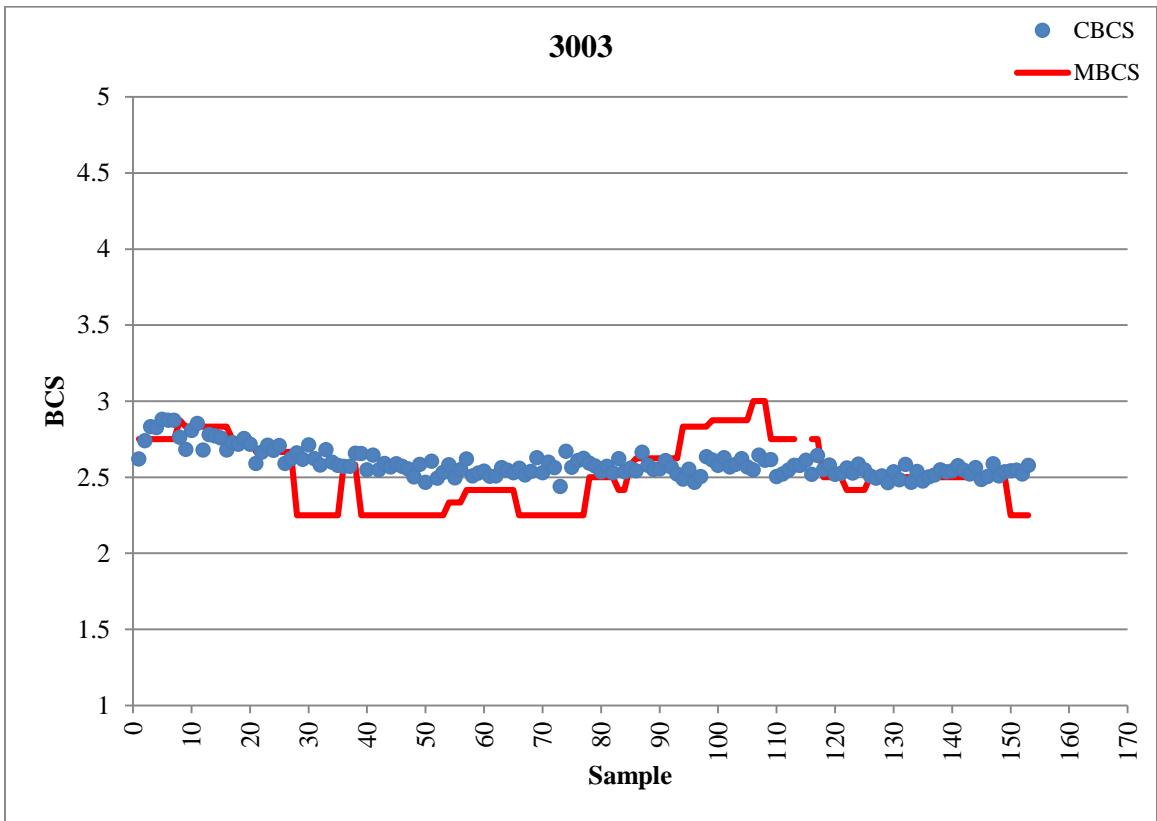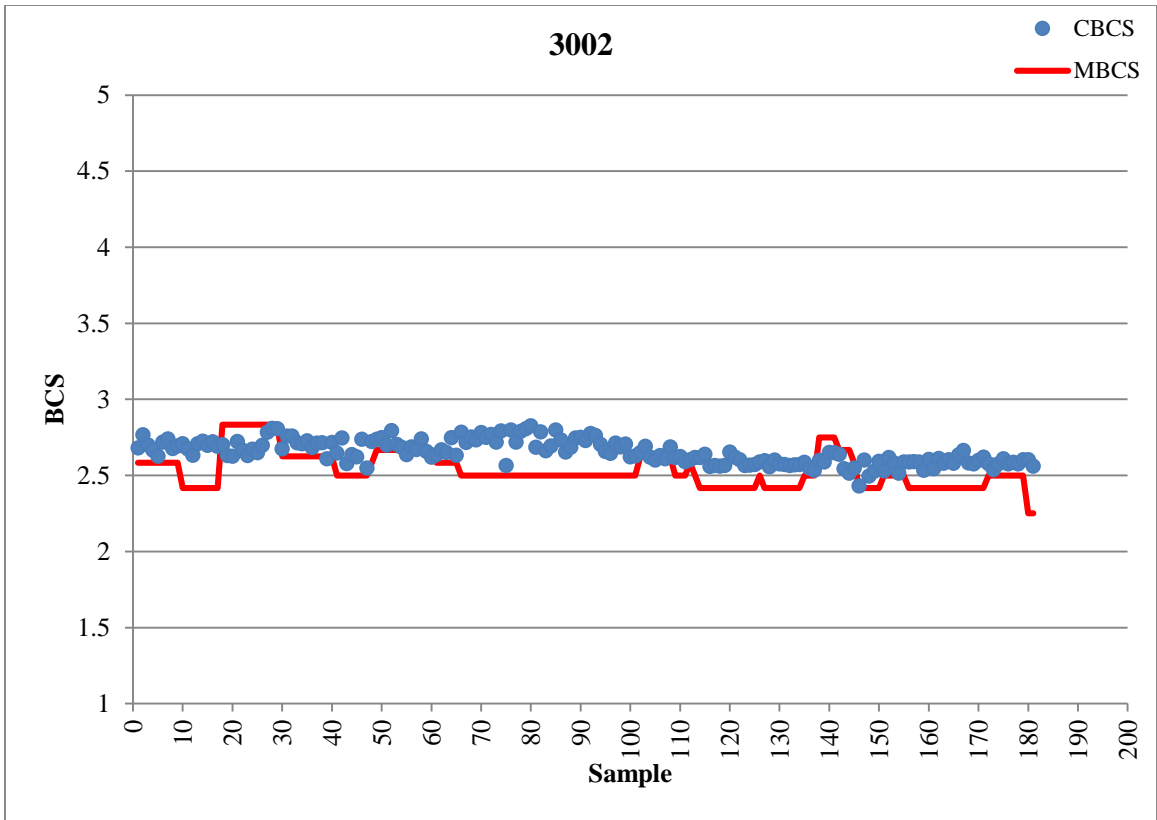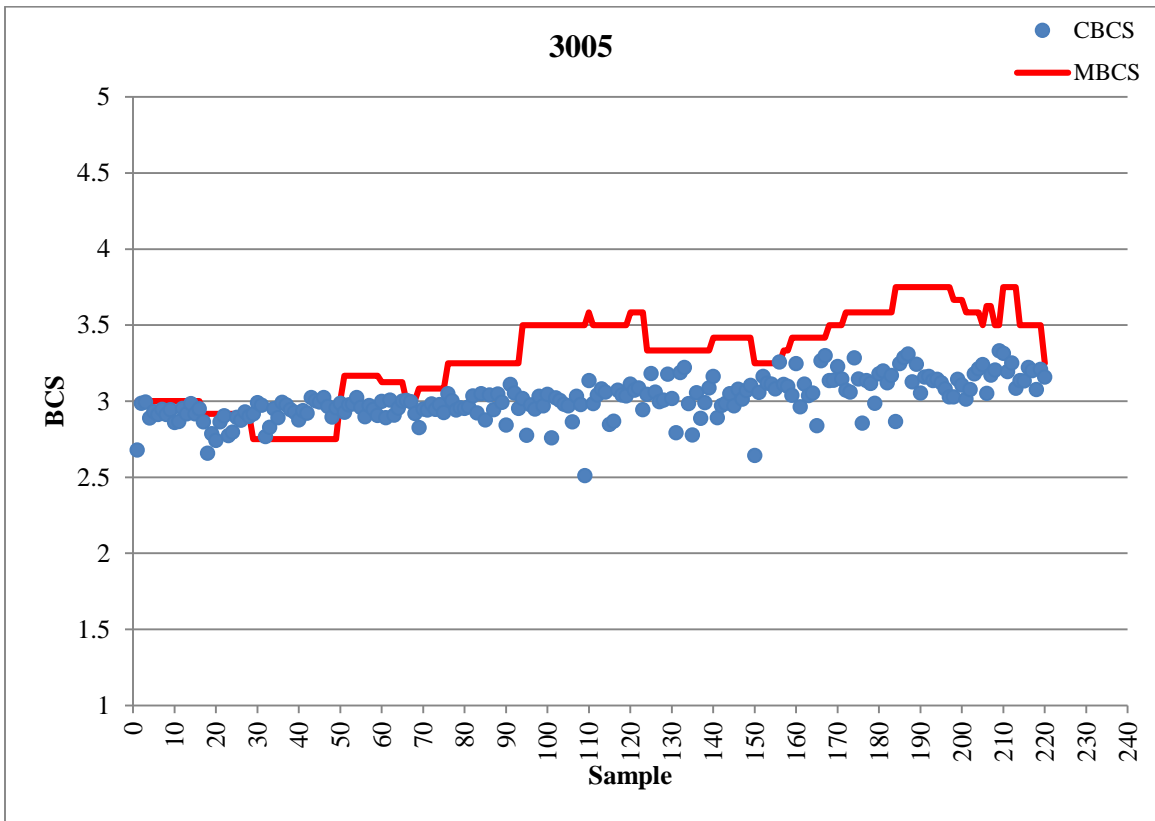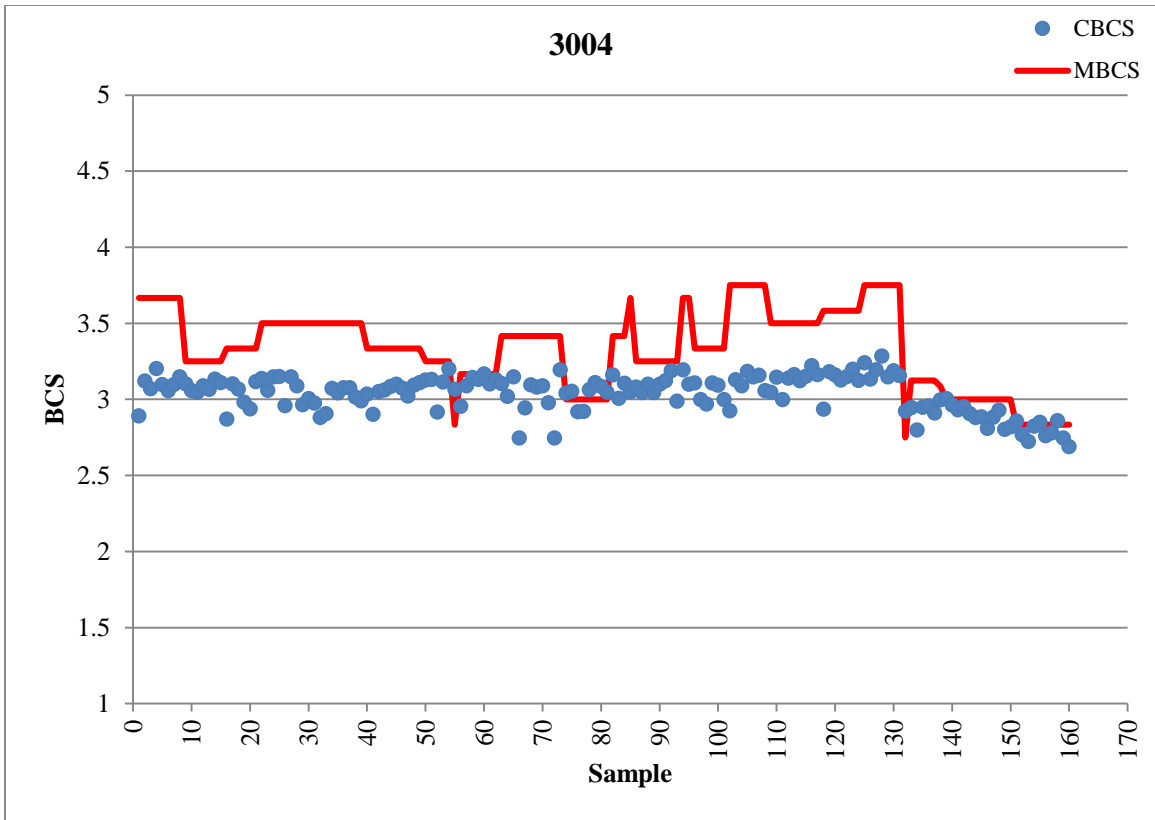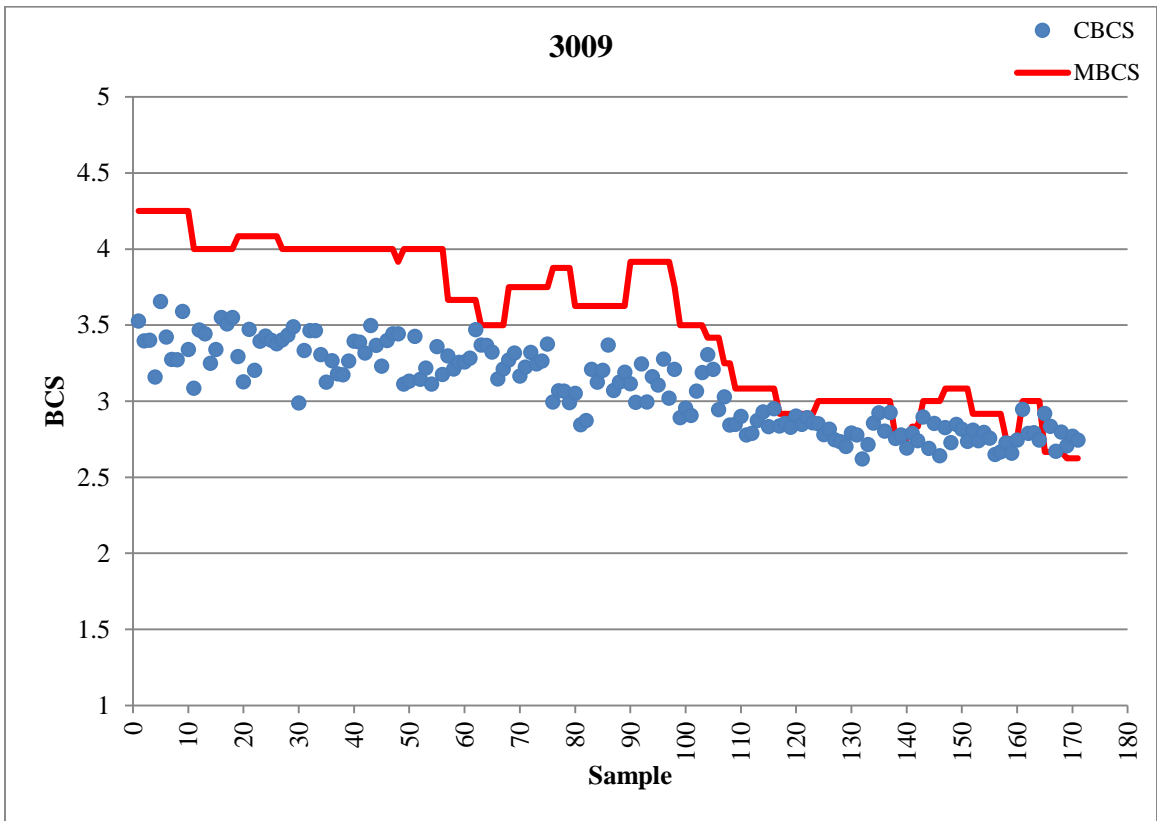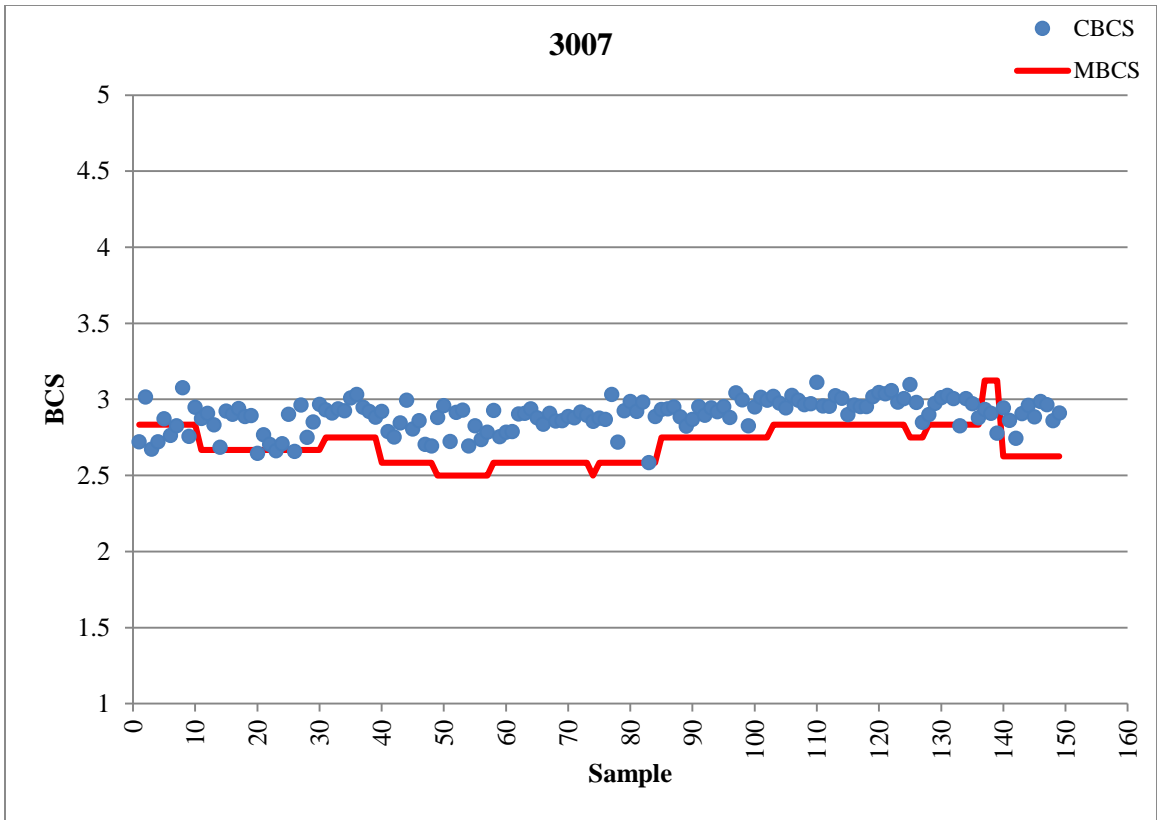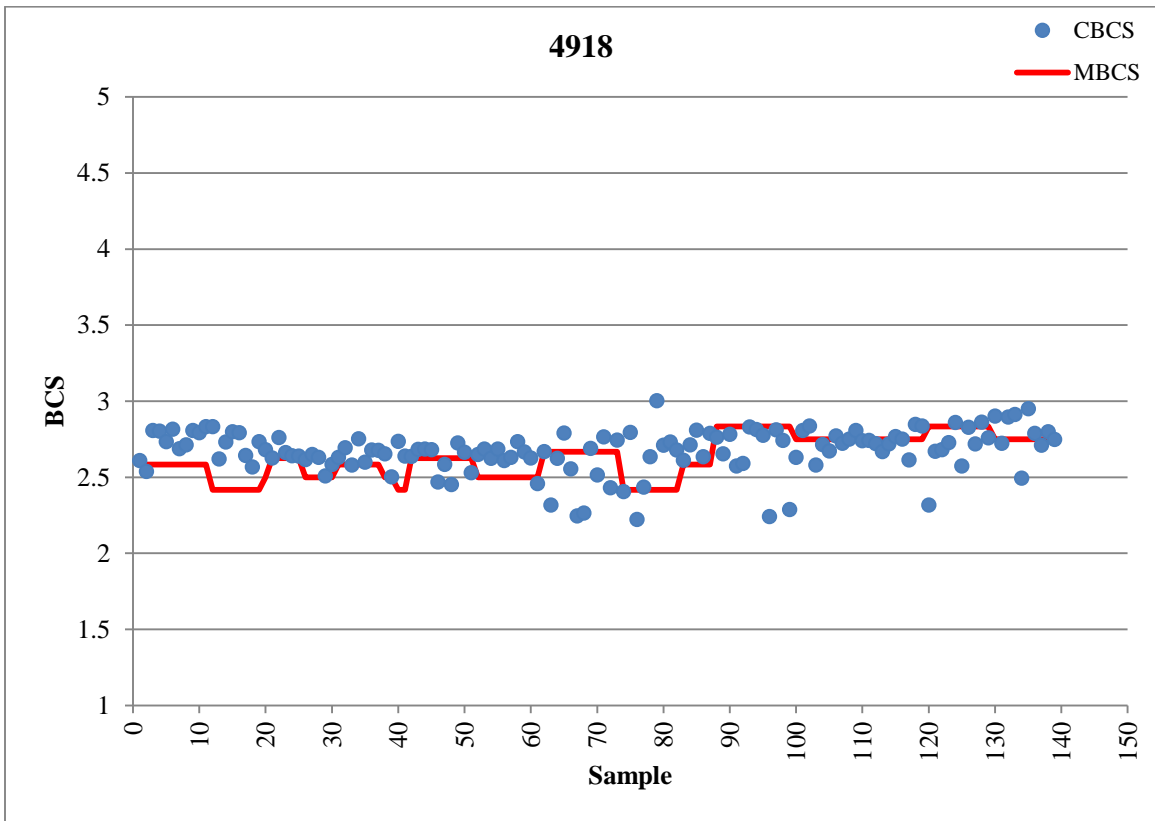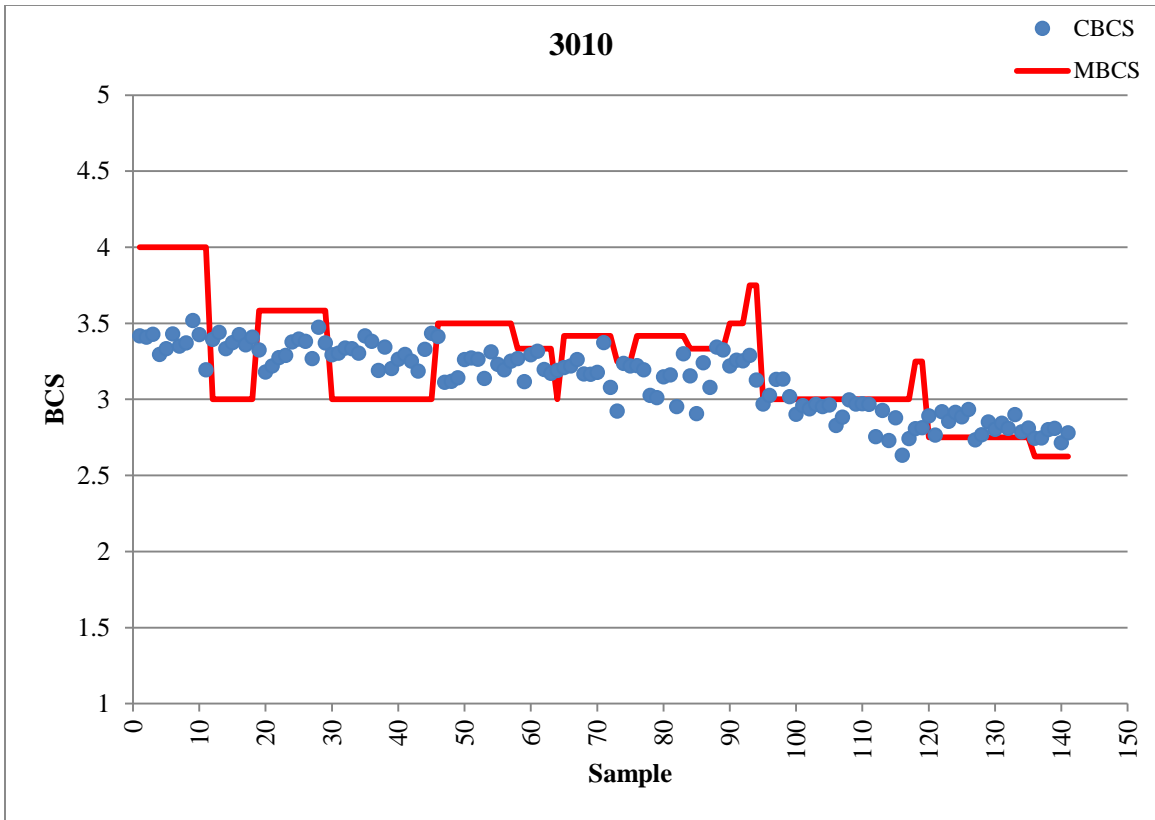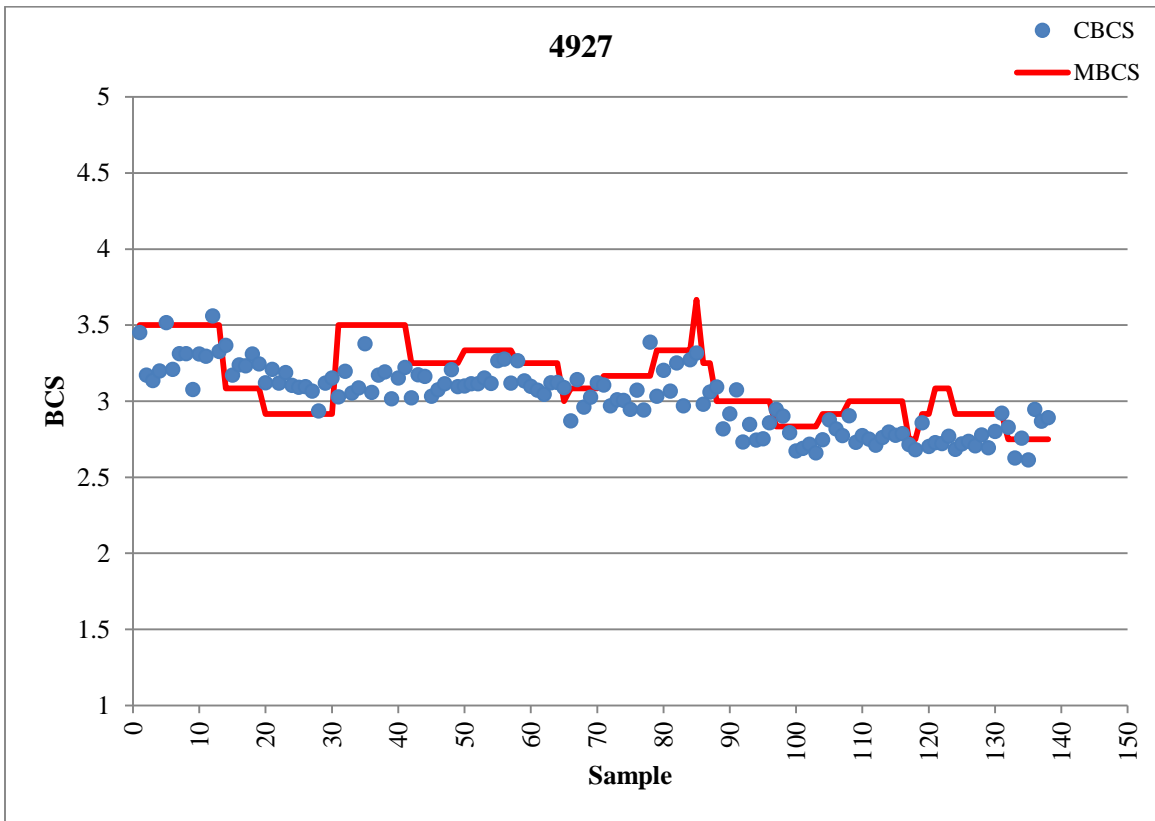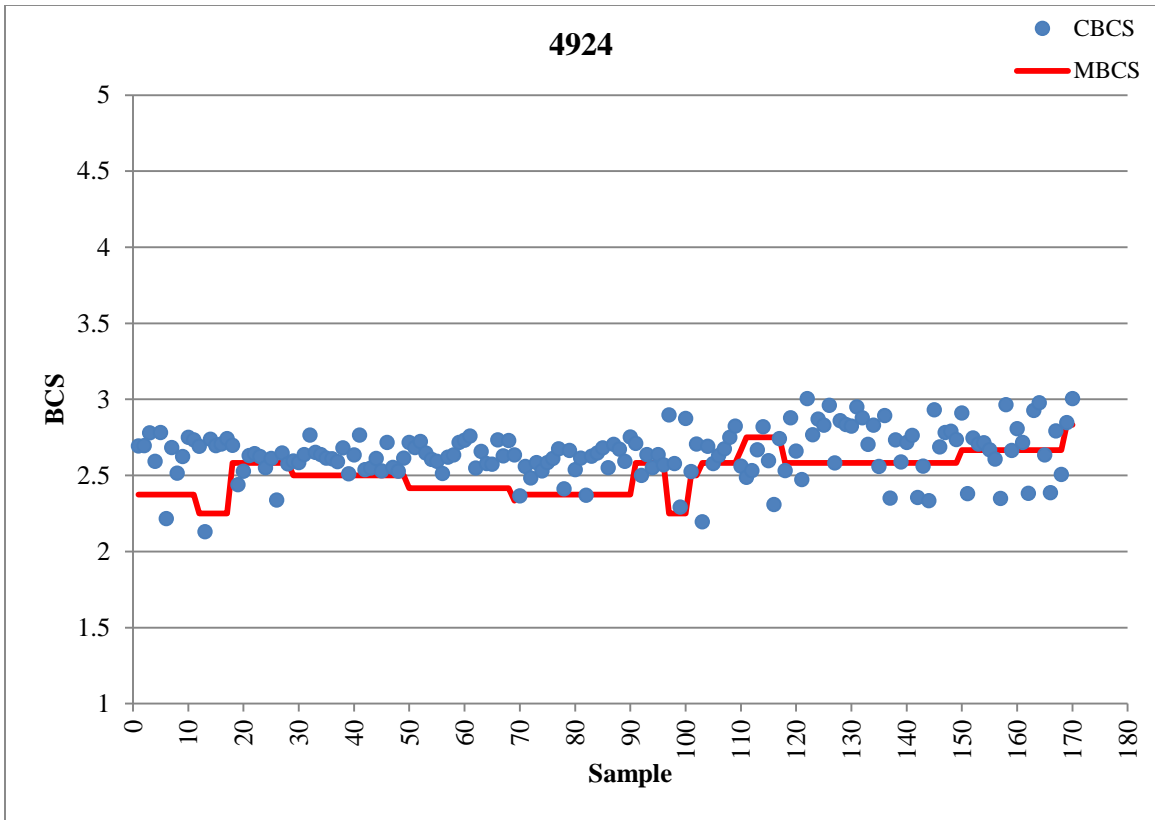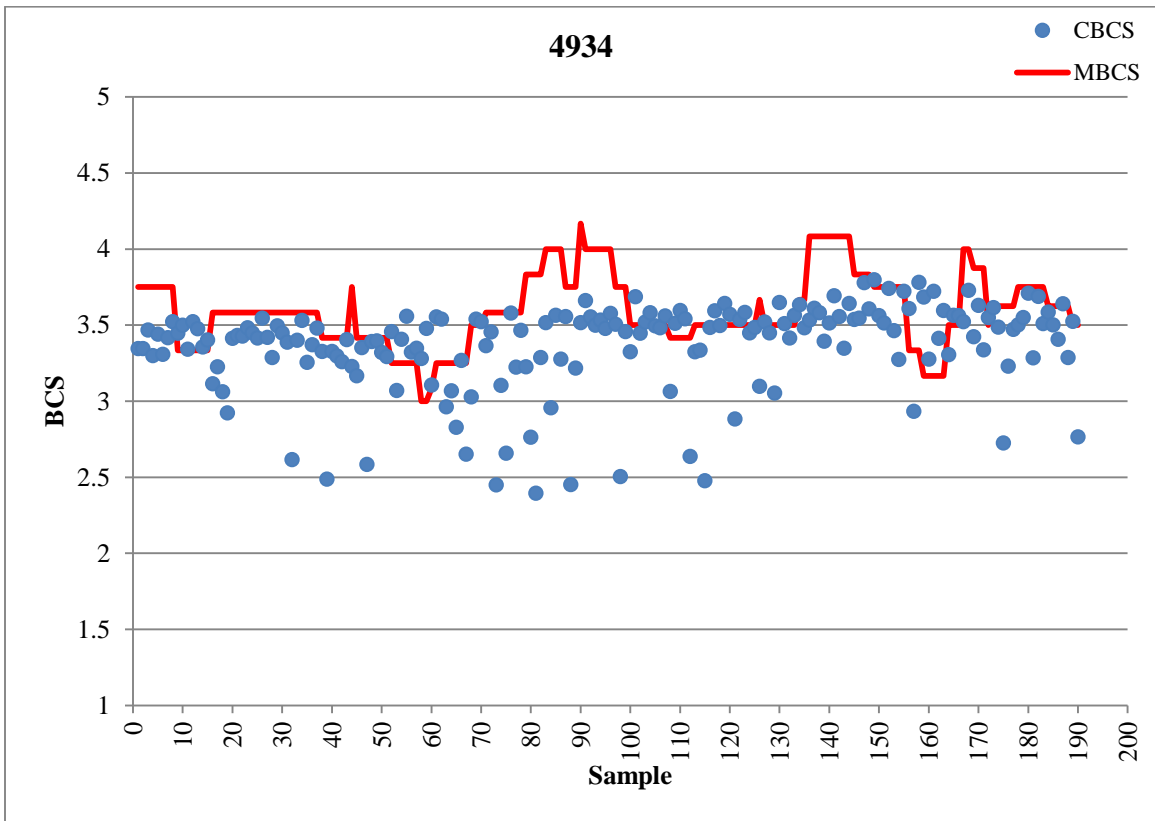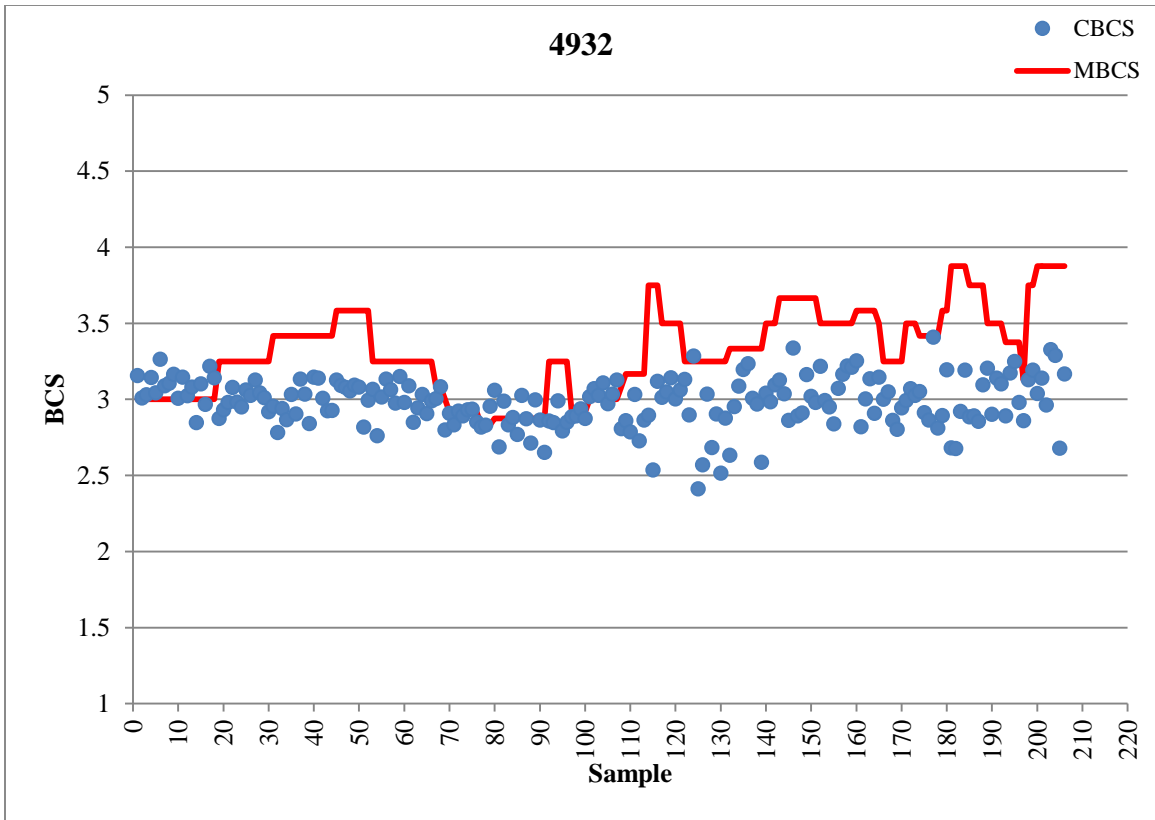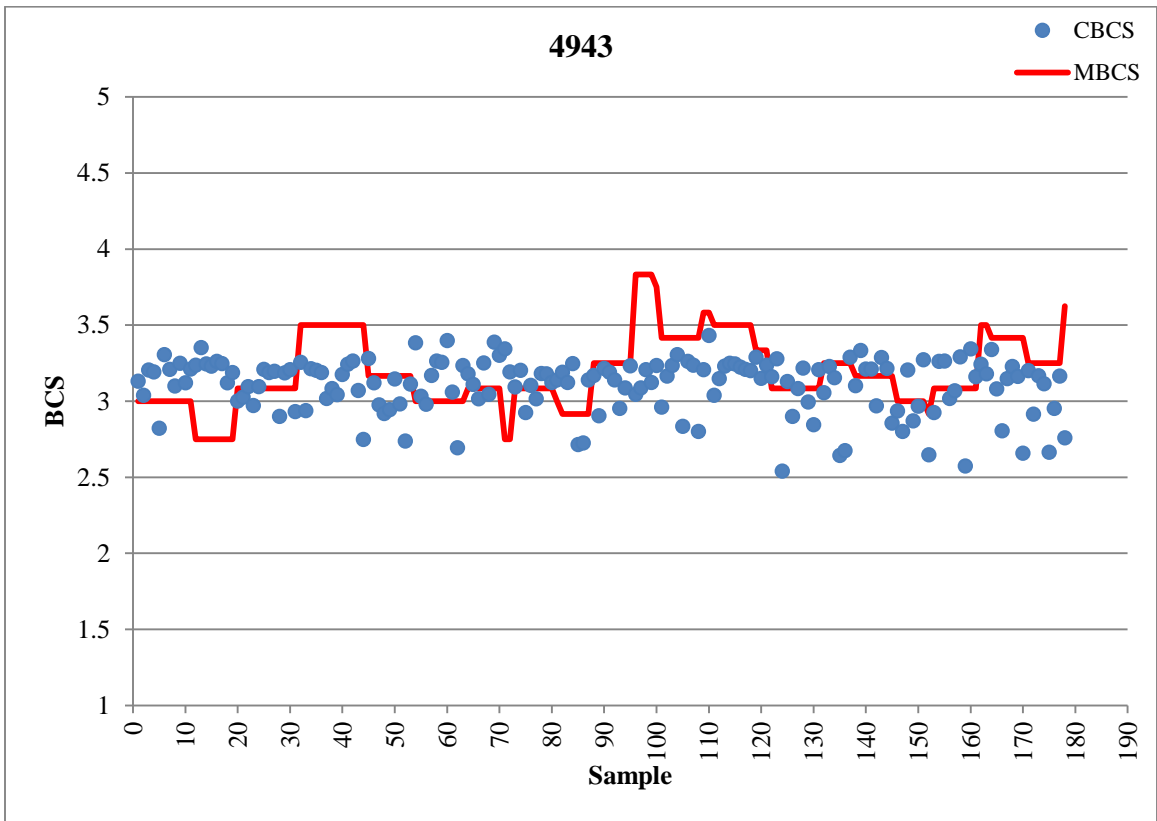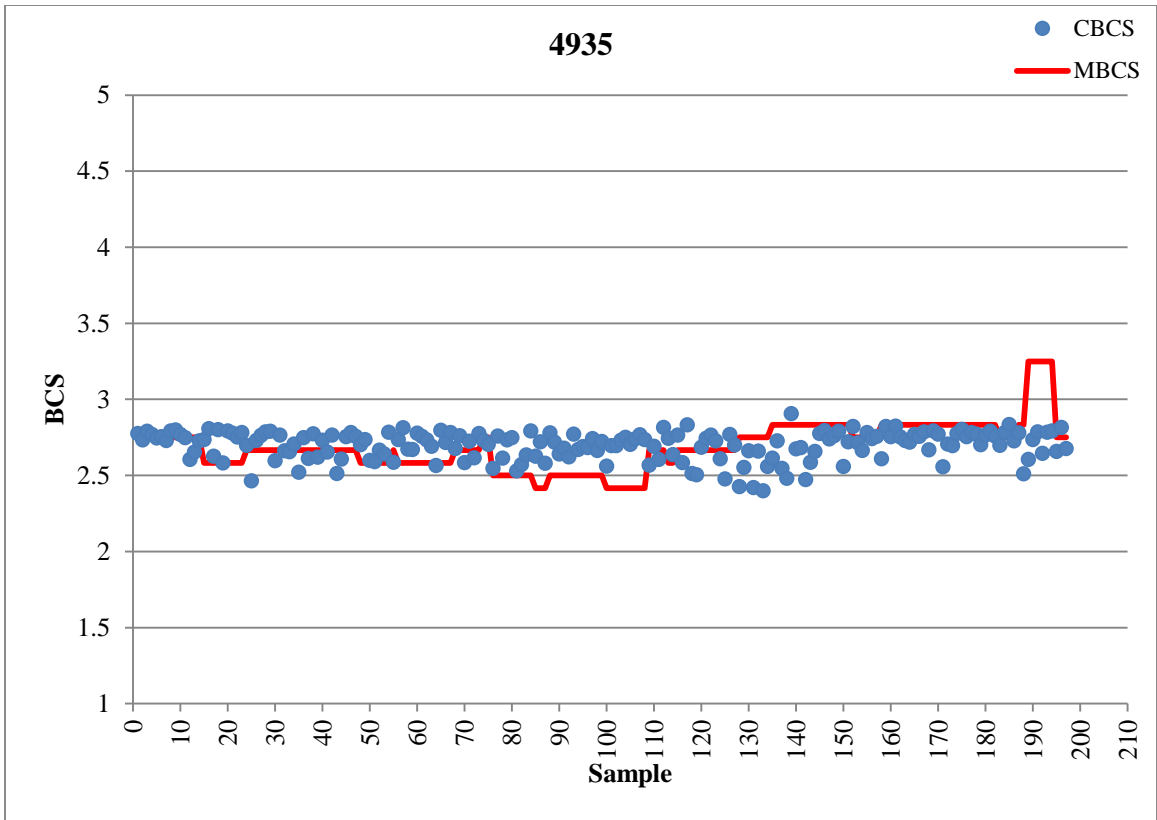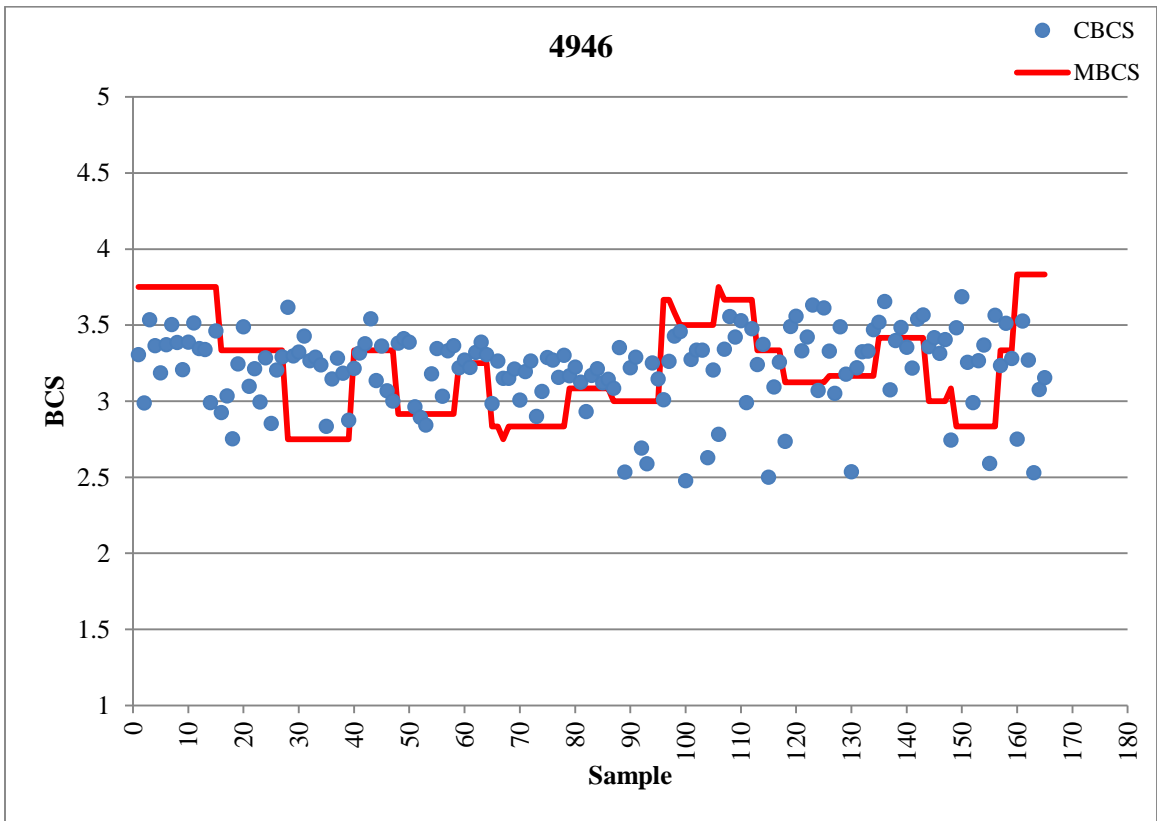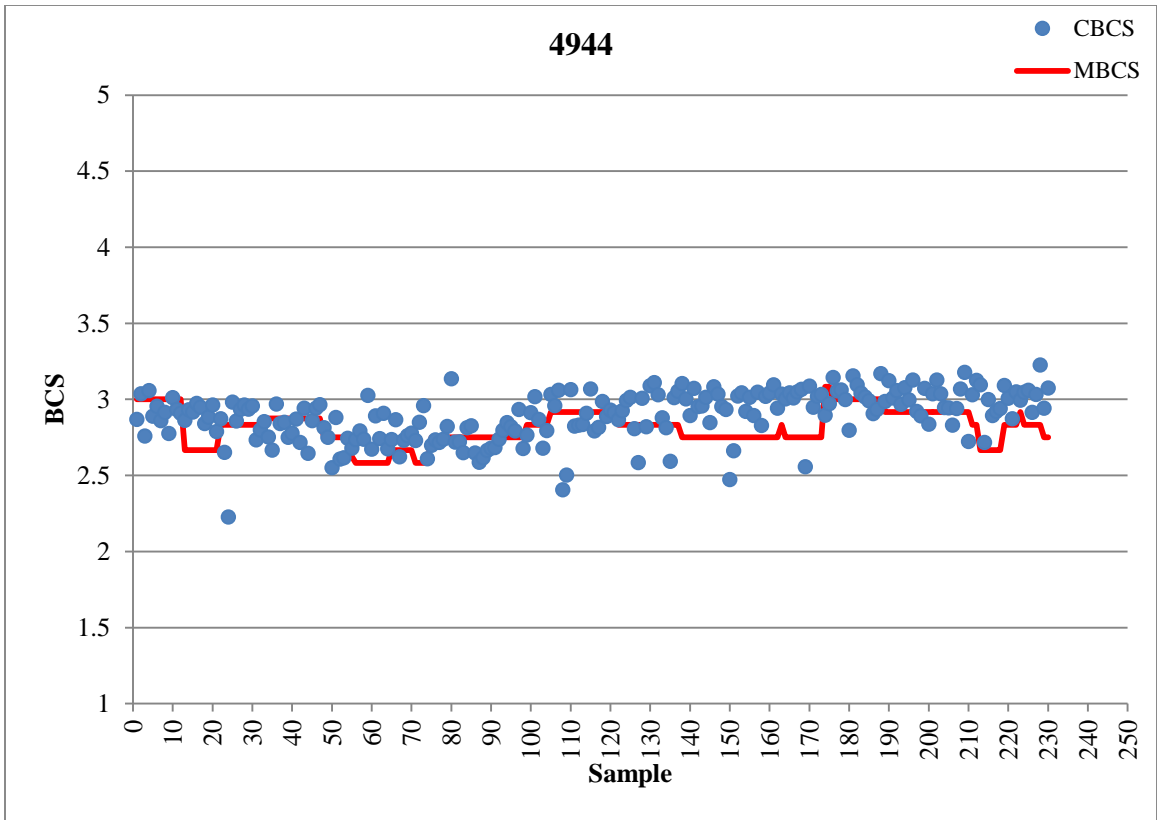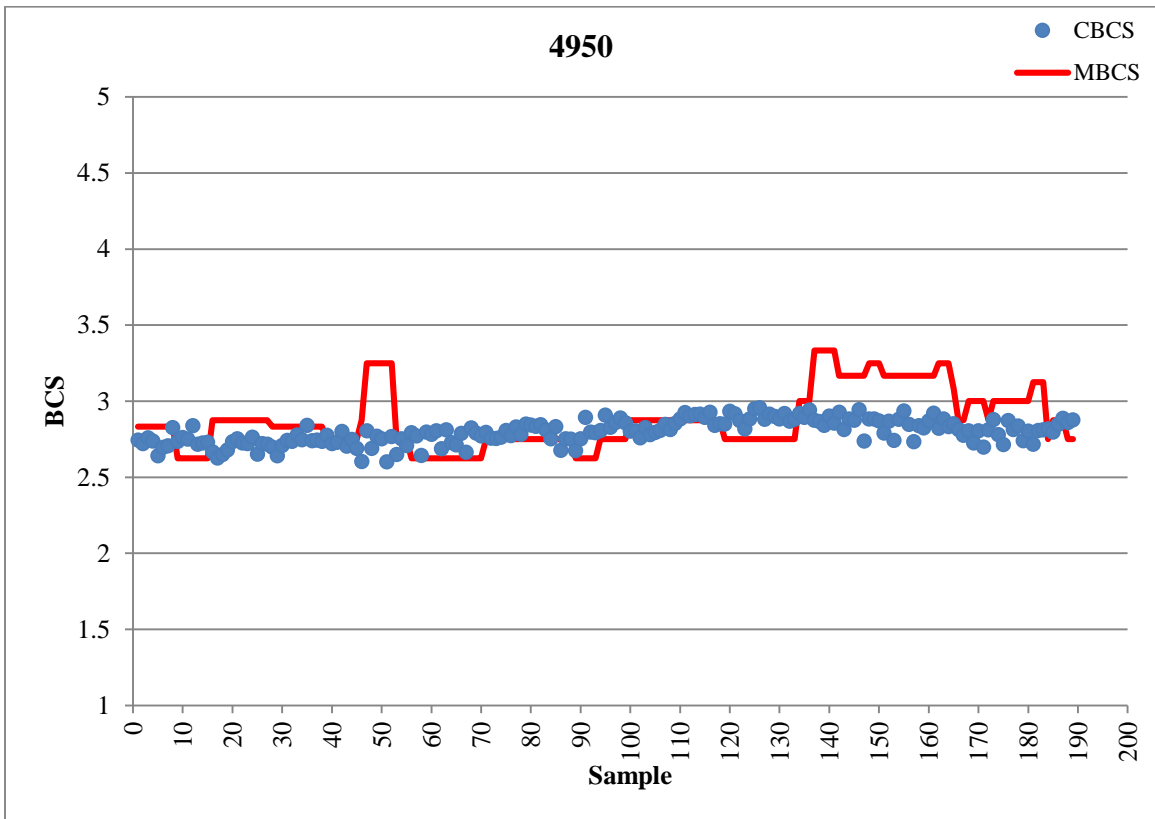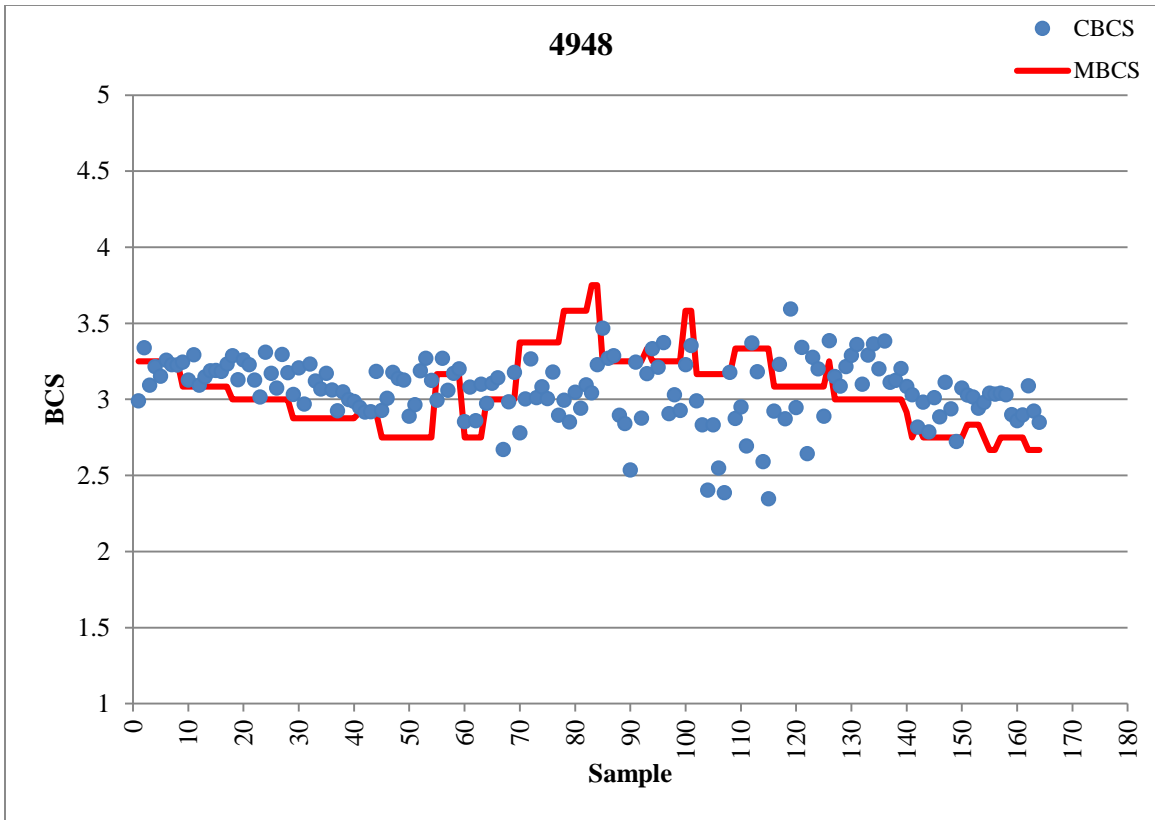
REFERENCES

[1] *Overview of the United States Dairy Industry*. Rep. National Agricultural Statistics Service (NASS), Agricultural Statistics Board, United States Department of Agriculture (USDA), 22 Sept. 2010. Web. <http://usda.mannlib.cornell.edu/usda/current/USDairyIndus/USDairyIndus-09-22-2010.pdf>.

[2] Mathews, K., & Haley, M. (2016). Livestock, Dairy, and Poultry Outlook. Available at: http://www.ers.usda.gov/media/2009937/ldp-m-260.pdf. Accessed February 25, 2016.

[3] Poulton, C., Dorward, A., & Kydd, J. (2010). The future of small farms: New directions for services, institutions, and intermediation. *World Development*, *38*(10), 1413-1428. http://dx.doi.org/10.1016/j.worlddev.2009.06.009

[4] Winsten, J. R., Kerchner, C. D., Richardson, A., Lichau, A., & Hyman, J. M. (2010). Trends in the Northeast dairy industry: Large-scale modern confinement feeding and management-intensive grazing. *Journal of Dairy Science*, *93*(4), 1759-1769. http://dx.doi.org/10.3168/jds.2008-1831

[5] Tauer, L. W. (2001). Efficiency and competitiveness of the small New York dairy farm. *Journal of dairy science*, *84*(11), 2573-2576. http://dx.doi.org/10.3168/jds.S0022-0302(01)74710-8

[6] Hadley, G. L., Harsh, S. B., & Wolf, C. A. (2002). Managerial and financial implications of major dairy farm expansions in Michigan and Wisconsin. *Journal of Dairy Science*, *85*(8), 2053-2064. http://dx.doi.org/10.3168/jds.S0022-0302(02)74283-5

[7] Bewley, J., Palmer, R. W., & Jackson-Smith, D. B. (2001). An overview of experiences of Wisconsin dairy farmers who modernized their operations. *Journal of Dairy Science*, *84*(3), 717-729. http://dx.doi.org/10.3168/jds.S0022-0302(01)74526-2

[8] VandeHaar, M. J., & St-Pierre, N. (2006). Major advances in nutrition: Relevance to the sustainability of the dairy industry. *Journal of Dairy Science*, *89*(4), 1280-1291. http://dx.doi.org/10.3168/jds.S0022-0302(06)72196-8

[9] College of Agriculture, Food, and Environment. University of Kentucky. n.d. Web. 25 February 2016. <http://afsdairy.ca.uky.edu/research>

[10] Bewley, J. M. (2008). Automated body condition scoring of dairy cattle: Technical and economic feasibility.

[11] Oltenacu, P. A., & Broom, D. M. (2010). The impact of genetic selection for increased milk yield on the welfare of dairy cows. *Animal welfare*, *19*(1), 39-49.

[12] Dobson, H., Smith, R. F., Royal, M. D., Knight, C. H., & Sheldon, I. M. (2007). The High-producing Dairy Cow and its Reproductive Performance. *Reproduction in domestic animals*, *42*(s2), 17-23. http://dx.doi.org/10.1111/j.1439-0531.2007.00906.x

[13] Dekkers, J. C. M., & Gibson, J. P. (1998). Applying breeding objectives to dairy cattle improvement. *Journal of Dairy Science*, *81*, 19-35. http://dx.doi.org/doi:10.3168/jds.S0022-0302(98)70151-1

[14] Goddard, M. E. (1998). Consensus and debate in the definition of breeding objectives. *Journal of Dairy Science*, *81*, 6-18. http://dx.doi.org/10.3168/jds.S0022-0302(98)70150-X

[15] Groen, A. F., Steine, T., Colleau, J. J., Pedersen, J., Pribyl, J., & Reinsch, N. (1997). Economic values in dairy cattle breeding, with special reference to functional traits. Report of an EAAP-working group. *Livestock Production Science*, *49*(1), 1-21. http://dx.doi.org/10.1016/S0301-6226%2897%2900041-9

[16] Kossaibati, M. A., & Esslemont, R. J. (1997). The costs of production diseases in dairy herds in England. *The Veterinary Journal*, *154*(1), 41-51. http://dx.doi.org/10.1016/S1090-0233(05)80007-3

[17] Knight-Jones, T. J. D., & Rushton, J. (2013). The economic impacts of foot and mouth disease–What are they, how big are they and where do they occur?. *Preventive veterinary medicine*, *112*(3), 161-173. http://dx.doi.org/10.1016/j.prevetmed.2013.07.013

[18] Alvåsen, K., Mörk, M. J., Sandgren, C. H., Thomsen, P. T., & Emanuelson, U. (2012). Herd-level risk factors associated with cow mortality in Swedish dairy herds. *Journal of dairy science*, *95*(8), 4352-4362. http://dx.doi.org/10.3168/jds.2011-5085

[19] Raboisson, D., Cahuzac, E., Sans, P., & Allaire, G. (2011). Herd-level and contextual factors influencing dairy cow mortality in France in 2005 and 2006. *Journal of dairy science*, *94*(4), 1790-1803. http://dx.doi.org/10.3168/jds.2010-3634

[20] De Rensis, F., Garcia-Ispierto, I., & López-Gatius, F. (2015). Seasonal heat stress: Clinical implications and hormone treatments for the fertility of dairy cows. *Theriogenology*, *84*(5), 659-666. http://dx.doi.org/10.1016/j.theriogenology.2015.04.021

[21] Borchers, M. R., & Bewley, J. M. (2015). An assessment of producer precision dairy farming technology use, prepurchase considerations, and usefulness. *Journal of dairy science*, *98*(6), 4198-4205. http://dx.doi.org/10.3168/jds.2014-8963

[22] Yule, I., Lawrence, H., Mackenzie, C., Hedley, C., Grafton, M., & Pullanagari, R. (2013). Case studies which demonstrate the financial viability of precision dairy farming. *Magnesium*, *9*(6), 1-16.

[23] Maatje, K., De Mol, R. M., & Rossing, W. (1997). Cow status monitoring (health and oestrus) using detection sensors. *Computers and electronics in agriculture*, *16*(3), 245-254. http://dx.doi.org/doi:10.1016/S0168-1699(96)00052-X

[24] McArt, J. A. A., Nydam, D. V., & Overton, M. W. (2015). Hyperketonemia in early lactation dairy cattle: A deterministic estimate of component and total cost per case. *Journal of dairy science*, *98*(3), 2043-2054. http://dx.doi.org/10.3168/jds.2014-8740

[25] Ott, S. L., Wells, S. J., & Wagner, B. A. (1999). Herd-level economic losses associated with Johne's disease on US dairy operations. *Preventive veterinary medicine*, *40*(3), 179-192. http://dx.doi.org/10.1016/S0167-5877(99)00037-9

[26] Tauer, L. W. (2016). The effect of bovine somatotropin on the cost of producing milk: Estimates using propensity scores. *Journal of dairy science*. http://dx.doi.org/10.3168/jds.2015-9942

[27] Rollin, E., Dhuyvetter, K. C., & Overton, M. W. (2015). The cost of clinical mastitis in the first 30 days of lactation: An economic modeling tool. *Preventive veterinary medicine*, *122*(3), 257-264. http://dx.doi.org/10.1016/j.prevetmed.2015.11.006

[28] Holland, J. K., Hadrich, J. C., Wolf, C. A., & Lombard, J. (2015). Economics of
Measuring Costs Due to Mastitis-Related Milk Loss. In *2015 AAEA & WAEA
Joint Annual Meeting, July 26-28, San Francisco, California* (No. 205638).
Agricultural and Applied Economics Association & Western Agricultural
Economics Association.

[29] Enting, H., Kooij, D., Dijkhuizen, A. A., Huirne, R. B. M., & Noordhuizen-Stassen,
E. N. (1997). Economic losses due to clinical lameness in dairy cattle. *Livestock
production science*, *49*(3), 259-267. http://dx.doi.org/10.1016/S0301-
6226(97)00051-1

[30] Seegers, H., Fourichon, C., & Beaudeau, F. (2003). Production effects related to
mastitis and mastitis economics in dairy cattle herds. *Veterinary research*, *34*(5),
475-491. http://dx.doi.org/10.1051/vetres:2003027

[31] Rutten, C. J., Velthuis, A. G. J., Steeneveld, W., & Hogeveen, H. (2013). Invited
review: Sensors to support health management on dairy farms. *Journal of dairy
science*, *96*(4), 1928-1952. http://dx.doi.org/10.3168/jds.2012-6107

[32] Flett, R., Alpass, F., Humphries, S., Massey, C., Morriss, S., & Long, N. (2004). The
technology acceptance model and use of technology in New Zealand dairy
farming. *Agricultural Systems*, *80*(2), 199-211.
http://dx.doi.org/10.1016/j.agsy.2003.08.002

[33] Trevarthen, A. (2007). The national livestock identification system: the importance
of traceability in e-business. *Journal of Theoretical and Applied Electronic
Commerce Research*, *2*(1), 49.

[34] Trevarthen, A., & Michael, K. (2008, July). The RFID-enabled dairy farm: towards total farm management. In *Mobile Business, 2008. ICMB'08. 7th International Conference on* (pp. 241-250). IEEE. http://dx.doi.org/10.1109/ICMB.2008.39

[35] Dufaux, F., Pesquet-Popescu, B., & Cagnazzo, M. (2013). *Emerging technologies for 3D video: creation, coding, transmission and rendering*. John Wiley & Sons.

[36] Trussell, H. J., & Vrhel, M. J. (2008). *Fundamentals of digital imaging*. Cambridge University Press.

[37] Geng, J. (2011). Structured-light 3D surface imaging: a tutorial. *Advances in Optics and Photonics*, *3*(2), 128-160. http://dx.doi.org/10.1364/AOP.3.000128

[38] Mallick, T., Das, P. P., & Majumdar, A. K. (2014). Characterizations of noise in Kinect depth images: a review. *Sensors Journal, IEEE*, *14*(6), 1731-1740. http://dx.doi.org/10.1109/JSEN.2014.2309987

[39] Breuer, T., Bodensteiner, C., & Arens, M. (2014, October). Low-cost commodity depth sensor comparison and accuracy analysis. In *SPIE Security+ Defence* (pp. 92500G-92500G). International Society for Optics and Photonics. http://dx.doi.org/10.1117/12.2067155

[40] Sarbolandi, H., Lefloch, D., & Kolb, A. (2015). Kinect range sensing: Structured-light versus Time-of-Flight Kinect. *Computer Vision and Image Understanding*, *139*, 1-20. http://dx.doi.org/10.1016/j.cviu.2015.05.006

[41] Xu, Z., Perry, T., & Hills, G. (2013). *U.S. Patent No. 8,587,771*. Washington, DC: U.S. Patent and Trademark Office.

[42] Buza, M. H., Holden, L. A., White, R. A., & Ishler, V. A. (2014). Evaluating the
    effect of ration composition on income over feed cost and milk yield. *Journal of
    dairy science*, *97*(5), 3073-3080. http://dx.doi.org/10.3168/jds.2013-7622

[43] VandeHaar, M. J., & St-Pierre, N. (2006). Major advances in nutrition: Relevance to
    the sustainability of the dairy industry. *Journal of Dairy Science*, *89*(4), 1280-
    1291. http://dx.doi.org/10.3168/jds.S0022-0302%2806%2972196-8

[44] Bernard, J.K. & M.J. Montgomery. The University of Tennessee Agricultural
    Extension Service (1997, October). PB1598-Managing Intake of Lactating Dairy
    Cows. Retrieved from
    https://utextension.tennessee.edu/publications/Documents/pb1598.pdf

[45] Bach, A., Iglesias, C., & Busto, I. (2004). Technical note: A computerized system
    for monitoring feeding behavior and individual feed intake of dairy cattle. *Journal
    of dairy science*, *87*(12), 4207-4209. http://dx.doi.org/10.3168/jds.S0022-
    0302(04)73565-1

[46] Friggens, N. C., Nielsen, B. L., Kyriazakis, I., Tolkamp, B. J., & Emmans, G. C.
    (1998). Effects of feed composition and stage of lactation on the short-term
    feeding behavior of dairy cows. *Journal of dairy science*, *81*(12), 3268-3277.
    http://dx.doi.org/10.3168/jds.S0022-0302(98)75891-6

[47] Vandehaar, M. J. (1998). Efficiency of nutrient use and relationship to profitability
    on dairy farms. *Journal of Dairy Science*, *81*(1), 272-282.
    http://dx.doi.org/10.3168/jds.S0022-0302(98)75576-6

[48] Rim, J. S., Lee, S. R., Cho, Y. S., Kim, E. J., Kim, J. S., & Ha, J. K. (2008).
    Prediction of dry matter intake in lactating Holstein dairy cows offered high levels

of concentrate. *ASIAN AUSTRALASIAN JOURNAL OF ANIMAL SCIENCES*, *21*(5), 677.

[49] Nielsen, B. L. (1999). On the interpretation of feeding behaviour measures and the use of feeding rate as an indicator of social constraint. *Applied Animal Behaviour Science*, *63*(1), 79-91. http://dx.doi.org/10.1016/S0168-1591(99)00003-9

[50] DeVries, T. J., Von Keyserlingk, M. A. G., Weary, D. M., & Beauchemin, K. A. (2003). Technical note: Validation of a system for monitoring feeding behavior of dairy cows. *Journal of dairy science*, *86*(11), 3571-3574. http://dx.doi.org/10.3168/jds.S0022-0302(03)73962-9

[51] Chapinal, N., Veira, D. M., Weary, D. M., & Von Keyserlingk, M. A. G. (2007). Technical note: Validation of a system for monitoring individual feeding and drinking behavior and intake in group-housed cattle. *Journal of dairy science*, *90*(12), 5732-5736. http://dx.doi.org/10.3168/jds.2007-0331

[52] Mendes, E. D. M., Carstens, G. E., Tedeschi, L. O., Pinchak, W. E., & Friend, T. H. (2011). Validation of a system for monitoring feeding behavior in beef cattle. *Journal of animal science*, *89*(9), 2904-2910. http://dx.doi.org/10.2527/jas.2010-3489

[53] Krawczel, P. D., Klaiber, L. M., Thibeau, S. S., & Dann, H. M. (2012). Technical note: Data loggers are a valid method for assessing the feeding behavior of dairy cows using the Calan Broadbent Feeding System. *Journal of dairy science*, *95*(8), 4452-4456. http://dx.doi.org/10.3168/jds.2011-4999

[54] Ferris, C. P., Keady, T. W. J., Gordon, F. J., & Kilpatrick, D. J. (2006). Comparison of a Calan gate and a conventional feed barrier system for dairy cows: feed intake

and cow behaviour. *Irish journal of agricultural and food research*, 149-156. http://www.jstor.org/stable/25562573

[55] Halachmi, I., Edan, Y., Maltz, E., Peiper, U. M., Moallem, U., & Brukental, I. (1998). A real-time control system for individual dairy cow food intake. *Computers and Electronics in Agriculture*, *20*(2), 131-144. http://dx.doi.org/10.1016/S0168-1699(98)00013-1

[56] Shelley, A. N. (2013). Monitoring Dairy Cow Feed Intake Using Machine Vision.

[57] Koster, E. C. (1976). *U.S. Patent No. 3,994,156*. Washington, DC: U.S. Patent and Trademark Office.

[58] "PB1598-Managing Intake of Lactating Dairy Cows," The University of Tennessee Agricultural Extension Service, PB1598-500-10/97 E12-2015-00-078-098, http://trace.tennessee.edu/utk_agexani/8

[59] Nguyen, C. V., Izadi, S., & Lovell, D. (2012, October). Modeling kinect sensor noise for improved 3d reconstruction and tracking. In *3D Imaging, Modeling, Processing, Visualization and Transmission (3DIMPVT), 2012 Second International Conference on* (pp. 524-530). IEEE. http://dx.doi.org/10.1109/3DIMPVT.2012.84

[60] Wildman, E. E., Jones, G. M., Wagner, P. E., Boman, R. L., Troutt, H. F., & Lesch, T. N. (1982). A dairy cow body condition scoring system and its relationship to selected production characteristics. *Journal of Dairy Science*, *65*(3), 495-501. http://dx.doi.org/10.3168/jds.S0022-0302(82)82223-6

[61] Kellogg, Wayne. "FSA4008-Body Condition Scoring With Dairy Cattle," University of Arkansas Cooperative Extension Service, https://www.uaex.edu/publications/PDF/FSA-4008.pdf

[62] Krukowski, M. (2009). *Automatic determination of body condition score of dairy cows from 3D images*. Skolan för datavetenskap och kommunikation, Kungliga Tekniska högskolan.

[63] Halachmi, I., Klopčič, M., Polak, P., Roberts, D. J., & Bewley, J. M. (2013). Automatic assessment of dairy cattle body condition score using thermal imaging. *Computers and electronics in agriculture*, *99*, 35-40. http://dx.doi.org/10.1016/j.compag.2013.08.012

[64] Azzaro, G., Caccamo, M., Ferguson, J. D., Battiato, S., Farinella, G. M., Guarnera, G. C., ... & Licitra, G. (2011). Objective estimation of body condition score by modeling cow body shape from digital images. *Journal of dairy science*, *94*(4), 2126-2137. http://dx.doi.org/10.3168/jds.2010-3467

[65] Salau, J., Haas, J., Junge, W., Bauer, U., Harms, J., & Bieletzki, S. (2014). Feasibility of automated body trait determination using the SR4K time-of-flight camera in cow barns. *Springer Plus*, *3*, 225.

[66] Son, J. Y., Javidi, B., Yano, S., & Choi, K. H. (2010). Recent developments in 3-D imaging technologies. *Display Technology, Journal of*, *6*(10), 394-403. http://dx.doi.org/10.1109/JDT.2010.2045636

[67] Stoykova, E., Alatan, A. A., Benzie, P., Grammalidis, N., Malassiotis, S., Ostermann, J., ... & Zabulis, X. (2007). 3-D time-varying scene capture technologies—A survey. *Circuits and Systems for Video Technology, IEEE*

Transactions on, *17*(11), 1568-1586.

http://dx.doi.org/10.1109/TCSVT.2007.909975

[68] Ehara, Y., Fujimoto, H., Miyazaki, S., Tanaka, S., & Yamamoto, S. (1995).

Comparison of the performance of 3D camera systems. *Gait & Posture*, *3*(3),

166-169. http://dx.doi.org/10.1016/0966-6362(95)99067-U

[69] Ehara, Y., Fujimoto, H., Miyazaki, S., Mochimaru, M., Tanaka, S., & Yamamoto, S.

(1997). Comparison of the performance of 3D camera systems II. *Gait & Posture*,

5(3), 251-255. http://dx.doi.org/10.1016/S0966-6362(96)01093-4

[70] Viazzi, S., Bahr, C., Van Hertem, T., Schlageter-Tello, A., Romanini, C. E. B.,

Halachmi, I., ... & Berckmans, D. (2014). Comparison of a three-dimensional and

two-dimensional camera system for automated measurement of back posture in

dairy cows. *Computers and Electronics in Agriculture*, *100*, 139-147.

http://dx.doi.org/10.1016/j.compag.2013.11.005

[71] Blais, F. (2004). Review of 20 years of range sensor development. *Journal of

Electronic Imaging*, *13*(1).

[72] Smith, G. C., Pendell, D. L., Tatum, J. D., Belk, K. E., & Sofos, J. N. (2008). Post-

slaughter traceability. *Meat Science*, *80*(1), 66-74.

http://dx.doi.org/10.1016/j.meatsci.2008.05.024

[73] Barcos, L. O. (2001). Recent developments in animal identification and the

traceability of animal products in international trade. *Revue scientifique et

technique (International Office of Epizootics)*, *20*(2), 640-651.

[74] Barge, P., Gay, P., Merlino, V., & Tortia, C. (2013). Radio frequency identification

technologies for livestock management and meat supply chain traceability.

Canadian Journal of Animal Science, *93*(1), 23-33.

http://dx.doi.org/10.4141/cjas2012-029

[75] Stankovski, S., Ostojic, G., Senk, I., Rakic-Skokovic, M., Trivunovic, S., & Kucevic, D. (2012). Dairy cow monitoring by RFID. *Scientia Agricola*, *69*(1), 75-80. http://dx.doi.org/10.1590/S0103-90162012000100011

[76] Fosso Wamba, S., & Wicks, A. (2010, June). RFID deployment and use in the dairy value chain: applications, current issues and future research directions. In *Technology and Society (ISTAS), 2010 IEEE International Symposium* (pp. 172-179). http://dx.doi.org/10.2139/ssrn.1663682

[77] Ruiz-Garcia, L., & Lunadei, L. (2011). The role of RFID in agriculture: Applications, limitations and challenges. *Computers and Electronics in Agriculture*, *79*(1), 42-50. http://dx.doi.org/10.1016/j.compag.2011.08.010

[78] Voulodimos, A. S., Patrikakis, C. Z., Sideridis, A. B., Ntafis, V. A., & Xylouri, E. M. (2010). A complete farm management system based on animal identification using RFID technology. *Computers and Electronics in Agriculture*, *70*(2), 380-388. http://dx.doi.org/10.1016/j.compag.2009.07.009

[79] Ng, M. L., Leong, K. S., Hall, D., & Cole, P. H. (2005, August). A small passive UHF RFID tag for livestock identification. In *Microwave, Antenna, Propagation and EMC Technologies for Wireless Communications, 2005. MAPE 2005. IEEE International Symposium on* (Vol. 1, pp. 67-70). IEEE. http://dx.doi.org/10.1109/MAPE.2005.1617849

[80] Leong, K. S., Ng, M. L., & Cole, P. H. (2007, June). Investigation on the deployment of HF and UHF RFID tag in livestock identification. In *Antennas and*

Propagation Society International Symposium, 2007 IEEE (pp. 2773-2776).

IEEE. http://dx.doi.org/10.1109/APS.2007.4396110

[81] Ruiz-Garcia, L., & Lunadei, L. (2011). The role of RFID in agriculture:

Applications, limitations and challenges. *Computers and Electronics in*

Agriculture, *79*(1), 42-50. http:dx.doi.org/10.1016/j.compag.2011.08.010

[82] Samad, A., Murdeshwar, P., & Hameed, Z. (2010). High-credibility RFID-based

animal data recording system suitable for small-holding rural dairy farmers.

Computers and electronics in agriculture, *73*(2), 213-218.

http://dx.doi.org/10.1016/j.compag.2010.05.001

[83] Schwartzkopf-Genswein, K. S., Huisma, C., & McAllister, T. A. (1999). Validation

of a radio frequency identification system for monitoring the feeding patterns of

feedlot cattle. *Livestock production science*, *60*(1), 27-31.

http://dx.doi.org/10.1016/S0301-6226(99)00047-0

[84] Cheong, C., Han, T. D., Kim, J. Y., Kim, T. J., Lee, K., Lee, S. Y., ... & Craney, C.

(2007, March). Pictorial image code: A color vision-based automatic

identification interface for mobile computing environments. In *Mobile Computing*

Systems and Applications, 2007. HotMobile 2007. Eighth IEEE Workshop on (pp.

23-28). IEEE. http://dx.doi.org/10.1109/HotMobile.2007.8

[85] Hetzel, G., Leibe, B., Levi, P., & Schiele, B. (2001). 3D object recognition from

range images using local feature histograms. In *Computer Vision and Pattern*

Recognition, 2001. CVPR 2001. Proceedings of the 2001 IEEE Computer Society

Conference on (Vol. 2, pp. II-394). IEEE.

http://dx.doi.org/10.1109/CVPR.2001.990988

[86] Belongie, S., Malik, J., & Puzicha, J. (2002). Shape matching and object recognition using shape contexts. *Pattern Analysis and Machine Intelligence, IEEE Transactions on*, *24*(4), 509-522. http://dx.doi.org/10.1109/34.993558

[87] Ahonen, T., Hadid, A., & Pietikäinen, M. (2004). Face recognition with local binary patterns. In *Computer vision-eccv 2004* (pp. 469-481). Springer Berlin Heidelberg. http://dx.doi.org/10.1007/978-3-540-24670-1_36

[88] Fergus, R., Perona, P., & Zisserman, A. (2003, June). Object class recognition by unsupervised scale-invariant learning. In *Computer Vision and Pattern Recognition, 2003. Proceedings. 2003 IEEE Computer Society Conference on* (Vol. 2, pp. II-264). IEEE. http://dx.doi.org/10.1109/CVPR.2003.1211479

[89] LeCun, Y., Huang, F. J., & Bottou, L. (2004, June). Learning methods for generic object recognition with invariance to pose and lighting. In *Computer Vision and Pattern Recognition, 2004. CVPR 2004. Proceedings of the 2004 IEEE Computer Society Conference on* (Vol. 2, pp. II-97). IEEE. http://dx.doi.org/10.1109/CVPR.2004.1315150

[90] Wathes, C. M., Kristensen, H. H., Aerts, J. M., & Berckmans, D. (2008). Is precision livestock farming an engineer's daydream or nightmare, an animal's friend or foe, and a farmer's panacea or pitfall?. *Computers and Electronics in Agriculture*, *64*(1), 2-10. http://dx.doi.org/10.1016/j.compag.2008.05.005

[91] Shelley, A. N., Lau, D. L., Stone, A. E., & Bewley, J. M. (2016). Short communication: Measuring feed volume and weight by machine vision. *Journal of dairy science*, *99*(1), 386-391. http://dx.doi.org/10.3168/jds.2014-8964

[92] Poursaberi, A., Bahr, C., Pluk, A., Van Nuffel, A., & Berckmans, D. (2010). Real-time automatic lameness detection based on back posture extraction in dairy cattle: Shape analysis of cow with image processing techniques. *Computers and Electronics in Agriculture*, *74*(1), 110-119. http://dx.doi.org/10.1016/j.compag.2010.07.004

[93] Mohan, A., Papageorgiou, C., & Poggio, T. (2001). Example-based object detection in images by components. *Pattern Analysis and Machine Intelligence, IEEE Transactions on*, *23*(4), 349-361. http://dx.doi.org/10.1109/34.917571

[94] Xu, F., & Fujimura, K. (2003, July). Human detection using depth and gray images. In *Advanced Video and Signal Based Surveillance, 2003. Proceedings. IEEE Conference on* (pp. 115-121). IEEE. http://dx.doi.org/10.1109/AVSS.2003.1217910

[95] Fujimura, K., & Liu, X. (2006, April). Sign recognition using depth image streams. In *Automatic Face and Gesture Recognition, 2006. FGR 2006. 7th International Conference on* (pp. 381-386). IEEE. http://dx.doi.org/10.1109/FGR.2006.101

[96] Wilson, P. I., & Fernandez, J. (2006). Facial feature detection using Haar classifiers. *Journal of Computing Sciences in Colleges*, *21*(4), 127-133.

[97] Castrillón, M., Déniz, O., Hernández, D., & Lorenzo, J. (2011). A comparison of face and facial feature detectors based on the Viola–Jones general object detection framework. *Machine Vision and Applications*, *22*(3), 481-494. http://dx.doi.org/10.1007/s00138-010-0250-7

[98] Pflug, A., & Busch, C. (2012). Ear biometrics: a survey of detection, feature
extraction and recognition methods. *Biometrics, IET*, *1*(2), 114-129.
http://dx.doi.org/10.1049/iet-bmt.2011.0003

[99] Hjelmås, E., & Low, B. K. (2001). Face detection: A survey. *Computer vision and
image understanding*, *83*(3), 236-274. http://dx.doi.org/10.1006/cviu.2001.0921

[100] Newman, T. S., & Jain, A. K. (1995). A survey of automated visual inspection.
Computer vision and image understanding, *61*(2), 231-262.
http://dx.doi.org/10.1006/cviu.1995.1017

[101] Chin, R. T., & Harlow, C. A. (1982). Automated visual inspection: A survey.
Pattern Analysis and Machine Intelligence, IEEE Transactions on, (6), 557-573.
http://dx.doi.org/10.1109/TPAMI.1982.4767309

[102] Lin, C. (2007). Face detection in complicated backgrounds and different
illumination conditions by using YCbCr color space and neural network. *Pattern
Recognition Letters*, *28*(16), 2190-2200.
http://dx.doi.org/10.1016/j.patrec.2007.07.003

[103] Abate, A. F., Nappi, M., Riccio, D., & Sabatino, G. (2007). 2D and 3D face
recognition: A survey. *Pattern Recognition Letters*, *28*(14), 1885-1906.
http://dx.doi.org/10.1016/j.patrec.2006.12.018

[104] Tan, X., Chen, S., Zhou, Z. H., & Zhang, F. (2006). Face recognition from a single
image per person: A survey. *Pattern recognition*, *39*(9), 1725-1745.
http://dx.doi.org/10.1016/j.patcog.2006.03.013

[105] Bowyer, K. W., Chang, K., & Flynn, P. (2006). A survey of approaches and challenges in 3D and multi-modal 3D+ 2D face recognition. *Computer vision and image understanding*, *101*(1), 1-15. http://dx.doi.org/10.1016/j.cviu.2005.05.005

[106] Kakumanu, P., Makrogiannis, S., & Bourbakis, N. (2007). A survey of skin-color modeling and detection methods. *Pattern recognition*, *40*(3), 1106-1122. http://dx.doi.org/10.1016/j.patcog.2006.06.010

[107] Yang, M. H., Kriegman, D. J., & Ahuja, N. (2002). Detecting faces in images: A survey. *Pattern Analysis and Machine Intelligence, IEEE Transactions on*, *24*(1), 34-58. http://dx.doi.org/10.1109/34.982883

[108] Johnson, A. E., & Hebert, M. (1999). Using spin images for efficient object recognition in cluttered 3D scenes. *Pattern Analysis and Machine Intelligence, IEEE Transactions on*, *21*(5), 433-449. http://dx.doi.org/10.1109/34.765655

[109] Kim, H. T., Choi, H. L., Lee, D. W., & Yong, C. Y. (2005). Recognition of individual Holstein cattle by imaging body patterns. *ASIAN AUSTRALASIAN JOURNAL OF ANIMAL SCIENCES*, *18*(8), 1194.

[110] Guo, Y., Bennamoun, M., Sohel, F., Lu, M., & Wan, J. (2014). 3D object recognition in cluttered scenes with local surface features: a survey. *Pattern Analysis and Machine Intelligence, IEEE Transactions on*, *36*(11), 2270-2287. http://dx.doi.org/10.1109/TPAMI.2014.2316828

[111] Viola, P., & Jones, M. (2001). Rapid object detection using a boosted cascade of simple features. In *Computer Vision and Pattern Recognition, 2001. CVPR 2001. Proceedings of the 2001 IEEE Computer Society Conference on* (Vol. 1, pp. I-511). IEEE. http://dx.doi.org/10.1109/CVPR.2001.990517

[112] Haar, A. (1910). On the theory of orthogonal function systems. *Math. Ann*, *69*(3), 331-371.

[113] Stanković, R. S., & Falkowski, B. J. (2003). The Haar wavelet transform: its status and achievements. *Computers & Electrical Engineering*, *29*(1), 25-44. http://dx.doi.org/10.1016/S0045-7906(01)00011-8

[114] Lienhart, R., & Maydt, J. (2002). An extended set of haar-like features for rapid object detection. In *Image Processing. 2002. Proceedings. 2002 International Conference on* (Vol. 1, pp. I-900). IEEE. http://dx.doi.org/10.1109/ICIP.2002.1038171

[115] Hiromoto, M., Sugano, H., & Miyamoto, R. (2009). Partially parallel architecture for adaboost-based detection with haar-like features. *Circuits and Systems for Video Technology, IEEE Transactions on*, *19*(1), 41-52. http://dx.doi.org/10.1109/TCSVT.2008.2009253

[116] Bradski, G., Kaehler, A., & Pisarevsky, V. (2005). Learning-Based Computer Vision with Intel's Open Source Computer Vision Library. *Intel Technology Journal*, *9*(2).

[117] Lienhart, R., Kuranov, A., & Pisarevsky, V. (2003). Empirical analysis of detection cascades of boosted classifiers for rapid object detection. In *Pattern Recognition* (pp. 297-304). Springer Berlin Heidelberg. http://dx.doi.org/10.1007/978-3-540-45243-0_39

[118] Pulli, K., Tico, M., & Xiong, Y. (2010, June). Mobile panoramic imaging system. In *Computer Vision and Pattern Recognition Workshops (CVPRW), 2010 IEEE*

Computer Society Conference on (pp. 108-115). IEEE.

http://dx.doi.org/10.1109/CVPRW.2010.5543792

[119] Po, L. M., & Ma, W. C. (1996). A novel four-step search algorithm for fast block

motion estimation. *Circuits and Systems for Video Technology, IEEE*

Transactions on, 6(3), 313-317. http://dx.doi.org/10.1109/76.499840

[120] Ardizzone, E., La Cascia, M., Avanzato, A., & Bruna, A. (1999, July). Video

indexing using MPEG motion compensation vectors. In *Multimedia Computing*

and Systems, 1999. IEEE International Conference on (Vol. 2, pp. 725-729).

IEEE. http://dx.doi.org/10.1109/MMCS.1999.778574

[121] Meng, J., Juan, Y., & Chang, S. F. (1995, April). Scene change detection in an

MPEG-compressed video sequence. In *IS&T/SPIE's Symposium on Electronic*

Imaging: Science & Technology (pp. 14-25). International Society for Optics and

Photonics. http://dx.doi.org/10.1117/12.206359

[122] Watanabe, H., & Singhal, S. (1991, November). Windowed motion compensation.

In *Visual Communications,'91, Boston, MA* (pp. 582-589). International Society

for Optics and Photonics. http://dx.doi.org/10.1117/12.50301

[123] Guizar-Sicairos, M., Thurman, S. T., & Fienup, J. R. (2008). Efficient subpixel

image registration algorithms. *Optics letters*, 33(2), 156-158.

http://dx.doi.org/10.1364/OL.33.000156

ANTHONY NEAL SHELLEY
Morehead, Kentucky

Education

University of Kentucky

M.S., Electrical Engineering (3.1 GPA)
University of Kentucky, Lexington, KY (January 2011 – May 2013)
Power & Energy Institute of Kentucky (PEIK) Graduate Certificate Program completed
      & certificate awarded.
Thesis: "MONITORING DAIRY COW FEED INTAKE USING MACHINE VISION"
Thesis Committee: Daniel Lau (Advisor), Ph.D., Jeffrey Bewley, Ph.D., & Janet Lumpp,
      Ph.D.

Post-Baccalaureate, Electrical Engineering (3.5 GPA)
University of Kentucky, Lexington, KY (January 2010 - May 2010)

Morehead State University

M.S., Engineering Technology (3.8 GPA)
Morehead State University, Morehead, KY (August 2009 - December 2010)
Thesis: "A 24FT/7.3M PARABOLIC REFLECTOR ANTENNA PERFORMANCE &
      FEED DESIGN ANALYSIS"
Thesis Committee: Ahmad Zargari (Advisor), Ph.D., Hans Chapman, Ph.D., & Capp
      Yess, Ph.D.

B.S., Space Science (3.1 GPA)
Minor, International Studies
Morehead State University, Morehead, KY (August 2004 - May 2009)
Senior Research: "Implementation of A Secondary Space Tracking Antenna
      at Morehead State University"
Undergraduate Advisor: Benjamin Malphrus, Ph.D.

Research & Teaching Experience

- Graduate Teaching Assistant: August 2015 – May 2016
  Department of Electrical Engineering
  University of Kentucky, Lexington, KY

- Graduate Research Assistant: August 2012 – June 2014
  Department of Electrical Engineering
  University of Kentucky, Lexington, KY

- Graduate Assistant: January 2010 – December 2010
  Department of Applied Engineering & Technology
  Morehead State University, Morehead, KY

- Undergraduate Fellowship: August 2008 – May 2009
  Space Science Center
  Morehead State University, Morehead, KY

- Work-Study: August 2004 – May 2008
  Space Science Center
  Morehead State University, Morehead, KY

Publications, Presentations, & Awards

- Shelley, A.N., D. L. Lau, A. E. Stone, and J. M. Bewley. 2016. Short communication: Measuring feed volume and weight by machine vision. J. Dairy Sci., 99:386-391. http://dx.doi.org/10.3168/jds.2014-8964.

- Paola Bargagna-Mohan, Ling Lei, Anthony Shelley, Eric C Mohan, Cindy Caruk, Daniel L Lau, Royce Mohan; Role of Vimentin in Regulation of Cell Spreading during Early Stages of Corneal Fibrosis. *Invest. Ophthalmol. Vis. Sci.* 2014;55(13):4703.

- Dean's Scholarship recipient, 2014.

- Shelley, A.N, Lau, D.L., Sterrett, A.E., & Bewley, J.M., "Machine Vision For Precision Dairy Farming," 9th Kentucky Innovation & Entrepreneurship Conference (KIEC), Lexington, KY, August 29, 2013. (Won poster presentation 1st place overall).

- Power & Energy Institute of Kentucky (PEIK) Scholarship recipient, 2012-2013.

- Bewley, J.M., Lau, D.L., Shelley, A.N, & Sterrett, A.E., Kentucky Science & Engineering Foundation (KSEF) Research & Development Excellence Award recipient, 2012. KSEF-2670-RDE-015.

- Shelley, A. N., "A 24ft/7.3m Parabolic Reflector Antenna Performance & Feed Design Analysis," 2010 Kentucky Academy of Science (KAS) Annual Meeting, Bowling Green, KY, 13-14 November 2010. (Won 1st place for Engineering).

- Shelley, A.N., Midden, D.P., and Arabmakki, E., "Digital Signal Processing and Medical Imaging," International Association of Journals and Conferences – American Society for Engineering Education (IAJC – ASEE) 2011 Joint International Conference, University of Hartford, CT, 15-16 April 2011.

- Outstanding Senior in Space Science, May 2009.